UNIVERSIDAD DE LAS PALMAS
DE GRAN CANARIA

INSTITUTO UNIVERSITARIO
SIANI
INGENIERIA COMPUTACIONAL

Advances in preventive monitoring of machinery through audio and vibration signals

Avances en monitorización preventiva de maquinaria a través de señales de audio y vibración

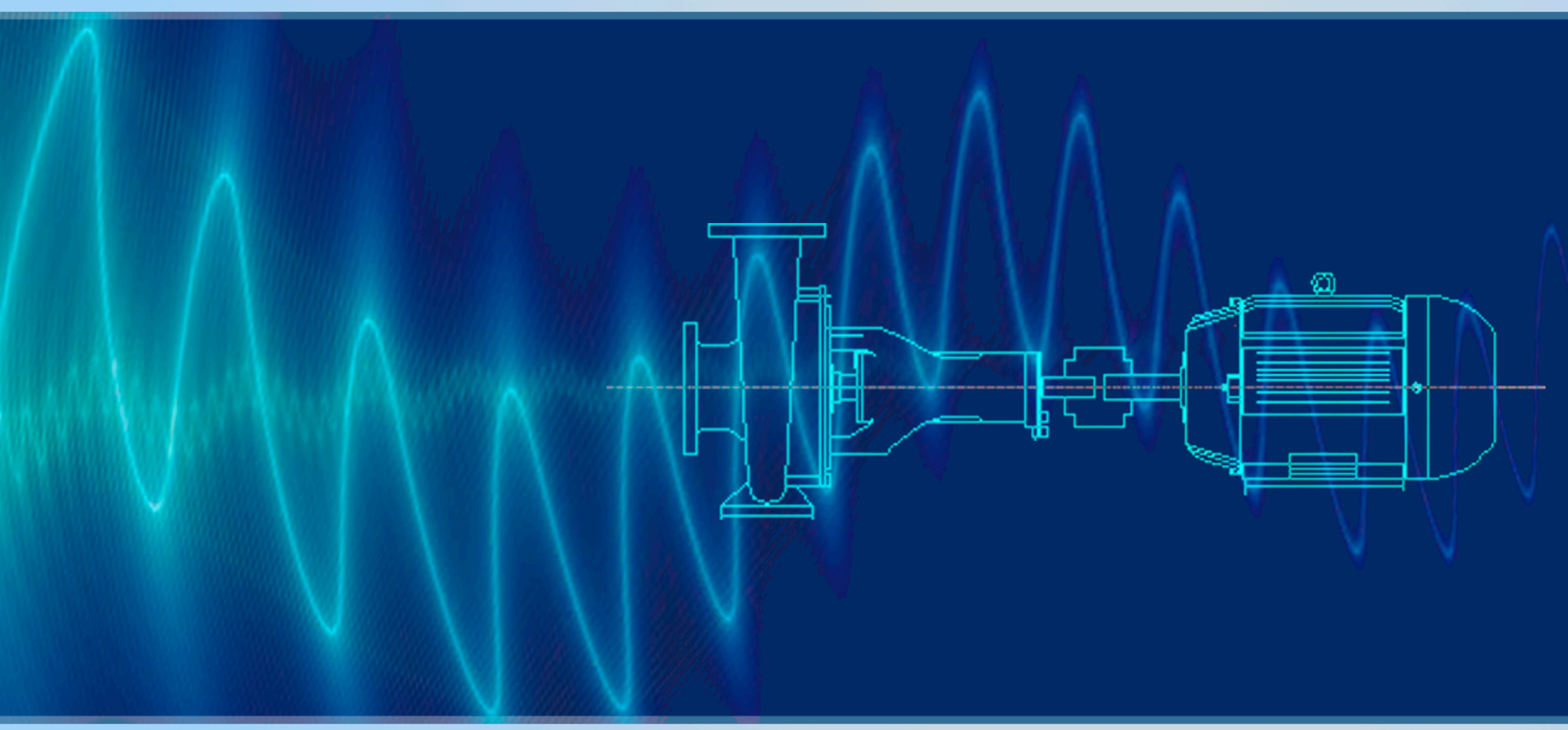

Patricia Henríquez Rodríguez

Las Palmas de Gran Canaria, Octubre 2015

UNIVERSIDAD DE LAS PALMAS DE GRAN CANARIA
Instituto Universitario de Sistemas Inteligentes
y Aplicaciones Numéricas en Ingeniería

EDUARDO M. RODRÍGUEZ BARRERA, SECRETARIO DEL INSTITUTO UNIVERSITARIO DE SISTEMAS INTELIGENTES Y APLICACIONES NUMÉRICAS EN INGENIERÍA (SIANI) DE LA UNIVERSIDAD DE LAS PALMAS DE GRAN CANARIA,

CERTIFICA

Que el Consejo de Doctores del Instituto Universitario de Sistemas Inteligentes y Aplicaciones Numéricas en Ingeniería (SIANI), en su sesión de fecha 26 de octubre de 2015, tomó el acuerdo de dar el consentimiento para la tramitación de la Tesis Doctoral titulada "Avances en Monitorización Preventiva de Maquinaria a través de señales de audio y vibración / Advances in preventive monitoring of machinery through audio and vibration signals", presentada por el doctorando **D. Patricia Henríquez Rodríguez**, dirigida por el Dr. D. Miguel Ángel Ferrer Ballester y el Dr. D. Jesús Bernardino Alonso Hernández, propuesta para acceder a la mención de doctor europeo, a la vista de la idoneidad y calidad de su contenido, interés y relevancia del tema a nivel internacional, y la realización de una estancia de más de un trimestre en un centro de investigación europeo fuera de España.

Para que así conste, y a los efectos oportunos se expide el correspondiente certificado a 26 de octubre de 2015.

UNIVERSIDAD DE LAS PALMAS DE GRAN CANARIA

INSTITUTO UNIVERSITARIO DE SISTEMAS INTELIGENTES Y APLICACIONES NUMÉRICAS EN INGENIERÍA

PROGRAMA DE DOCTORADO
SISTEMAS INTELIGENTES Y APLICACIONES NUMÉRICAS EN INGENIERÍA

TÍTULO DE LA TESIS

Avances en Monitorización Preventiva de Maquinaria a tráves de Señales de Audio y Vibración

Tesis Doctoral presentada por Patricia Henríquez Rodríguez

Dirigida por el Dr. D. Miguel Ángel Ferrer Ballester

Codirigida por el Dr. D. Jesús Bernardino Alonso Hernández

El Director **El Codirector** **La Doctoranda,**

Las Palmas de Gran Canaria, a 22 de Octubre de 2015

A mi familia.

ACKNOWLEDGEMENTS

This Thesis summarizes the work I have carried out during my Ph.D. studies with the División de Procesado Digital de la Señal (DPDS) -Digital Signal Processing Division- of the Instituto para el Desarrollo Tecnológico y la Innovación en Comunicaciones (IDeTIC)-Institute for Technological Development and the Innovation in Communications- since 2009. This research group is with the Department of Señales y Comunicaciones of the Universidad de Las Palmas de Gran Canaria. IDeTIC started in 2010 from the CeTIC (Technological Centre for the Innovation in Communications). The CeTIC was founded in 2006 from the three different Research Groups, including the Digital Signal Processing Group with was founded in 1990. This Thesis has been mainly supported by a Ph.D. scholarship granted to the author by Gobierno de Canarias and Social European Fund (ESF), which covered the period between March 2009 and March 2013, and also by the Spanish government MICNN TEC2009-14123-C04 and TEC2012-38630-C04-02 research projects.

Foremost, I would like to thank my supervisors **Prof. Jesús B. Alonso Hernández** and **Prof. Miguel A. Ferrer Ballester** for their guidance and support over the past six years. During this period I have benefited from their wise advices, intelligent efforts and courage which have shaped my thinking and working attitude. They also were the responsible of my first steps in research world when I first took at their door for pursuing my MsC. Project about laryngeal pathology detection through voice signal. They introduced me to the signal processing and pattern recognition world. In the framework of DPDS I have also received support from Prof. Carlos M. Travieso González.

After finishing my MsC. Project, they gave me the great opportunity of working in a national project of homeland security (*Hesperia*) founded by the office of the

industrial technological development (CDTI) (attached to the Ministriy of Industry and Trade) of the Spanish government in the frame of CENIT projects. In the framework of this work, I learned about condition monitoring in industrial scenarios and I could benefit from the knownledge of many experts in industrial security involved in the project. Thanks to this work, I decided to focus my PhD on condition monitoring implementing fault diagnosis.

During my Ph. D. studies I had the great opportunity of visiting two foreign institutions. The first 4-month stay was in 2011 at the Institute of Sound and Vibration Research (ISVR) of the University of Southampton (Southampton, England) with Prof. Paul R. White. During those four months I could benefit from his mastery in the field of signal processing. I also had the fortune to meet Prof. Ling Wang from who I could benefit from her expertise in pump fault diagnosis.

The second 3-month stay was in 2012 at the Reliability Research Lab of the University of Alberta (Edmonton, Canada) with Prof. Ming J. Zuo. I have met a fantastic group of people there. I would like to specially thank Dr. Funda Akdere Iscioglu for her care during my visit. I have also would like to thank Mayank Pandey for our discussions about the pump installation and condition monitoring techniques.

From such research stays there is a huge number of colleagues and friends who I want to thank: Alberto Baldelli, Pierre Rosado, Vianey Landeros, Kiran Konde, Rami Saba, Dao Duc Cuong, Luis Espitia and his wife Jessica Espitia.

I want to thank to my MsC. student Garoé Gómez for his valuable help with the pump installation and data acquisition process.

I also want to thank all the work mates at IDeTIC who with I have shared lunch and discussions: Himar, Javier, Laura, Jaime, Daniel, Pedro, Ayaya, Manolo, Víctor and all IDeTIC human group. Thank you guys!

Quiero también darle las gracias a mis amigos de Las Palmas, los cuales han aguantado durante todos estos años mis dudas, mis ausencias, mis nervios y con los cuales he compartido mis logros y mis alegrías. Muchas gracias a Eli, Paco, Raquel, Davinia, Rosalva, Silvia, Gema, Mónica y Octavio. Y en especial gracias a Briseida, por estar siempre a mi lado.

Gracias a mi familia.

PROLOGUE

"Does the Flap of a Butterfly's Wings in Brazil Set Off a Tornado in Texas?"

Edward Lorenz

CONTENTS

LIST OF FIGURES

LIST OF TABLES

CHAPTER 1
Introduction

Engineering systems, industrial products and/or equipments deteriorate over time due to the stress they suffer during their operational lives in real environments. An unexpected failure can result in a devastating accident and in financial losses for the company. Early detection prevents failures from growing and eventually turning into serious problems. Consequently, condition monitoring of a physical asset (a machine, a part of a machine or a system) in industrial scenarios is of paramount importance to early fault detection and has a great influence on the operational continuity of many industrial processes. It helps to reduce maintenance costs and increase security and reliability. The advantages of a monitoring system and their expected percentages of improvement are shown in Table 1-1 [1].

TABLE 1-1: IMPROVEMENTS IN RELIABILITY USING A MONITORING SYSTEM [1]

Maintenance costs	Reduction of 50% to 80%
Equipment damages	Reduction of 50% to 60%
Extra hours expenses	Reduction of 20% to 50%
Machine life expectancy	Increase of 50% to 60%
Total productivity	Increase of 20% to 30%

Humankind has used different maintenance techniques to the control and the monitoring of the machine condition. Earlier maintenance techniques include over-current protection relays or ground failure protection, while the latest developments introduce signal processing techniques together with artificial intelligence.

The increasing interest of condition monitoring (including fault detection, fault diagnosis and fault degradation) in research and also in industry is evident by the great amount of papers published in the field and by efforts focused on standard organizations (ISO, SAE, etc), and the organization of different conferences in the fault diagnosis field such as *COMADEM* (*Condition Monitoring and Diagnostic Engineering Management*) and *Surveillance* conferences.

This introductory chapter presents the basics of condition monitoring. We also outline the topic of audio and vibration based fault diagnosis in bearings and pumps, from which the motivation of the Thesis is also derived. We finish the chapter by stating the Thesis, describing the methodology of the Thesis, giving an outline of the Dissertation, and summarizing the research contributions originated from this work.

Although no special background is required for this chapter, the reader will benefit from introductory reading in condition monitoring as [2]. A deeper reference is [3]. In Chapter 2 of this Thesis, we provide a state of the art of audio- and vibration-based diagnosis especially focused on the latest developments from 2006 up to nowadays [4].

1.1 Maintenance techniques

Maintenance techniques aim to monitoring the machine condition. Generally, maintenance techniques can be divided into corrective maintenance and preventive maintenance (PM). In corrective maintenance, actions are carried out after a fault or breakdown has occurred. These actions lead to fixing the fault or to postponing the repair according to the judgment of specialized personnel.

PM was introduced in the 1950s and can be divided into pre-determined preventive maintenance (pdPM) and condition-based maintenance (CBM). In pdPM, scheduled maintenance activities are performed in periodical intervals in order to prevent components from degrading. The machine is repaired or a part is changed before the fault occurs. Corrective and pdPM approaches have shown to be costly in many applications for several reasons (e.g. lost production, cost of keeping spare parts, quality deficiencies). For this reason, some industries started performing CBM in the 1980s. CBM refers to machine condition monitoring in which information is continuously collected on parameters that indicate the condition of a machine. The parameters' deviation from the normal condition indicates the development of a failure. CBM takes maintenance action only when there is evidence of abnormal behaviour. For this reason, CBM reduces the number of scheduled PM activities [3].

1.2 Stages of a Condition-based monitoring system

An automatic CM system usually includes four stages (see Figure 1-1).

1) **Data Acquisition** deals with the collection of relevant data or information about the machine condition. The acquired data may vary from the kind of machine to the nature of the failure. The information collected can include several kinds of data: *value type data* such as pressure, temperature, oil analysis data, *waveform data* (i.e. *signals*) such as vibration signal, audio signal or acoustic emission signal, and *multidimensional data* such as images [2]. The complete set of extracted signals is called the machine's signature. In this Thesis, we focus on audio and vibration signals.

2) **Data Processing**: the data obtained in the previous stage are analyzed to extract information about a possible fault. In this Thesis, as the collected data are signals (waveform data), signal processing techniques are used to analyse the data and extract valuable information. This process is called feature extraction.

3) **Decision Support System** or the classification of the previously analyzed data into different condition states. In this Thesis, pattern recognition approach is used in the decision support system.

4) **Fault diagnosis/prediction**. The aim of a condition monitoring system is to perform fault diagnosis and fault identification. Fault diagnosis comprises fault detection (indicating if there is a fault) and fault isolation (determining where the fault is) based on the previous stages. Fault identification comprises the determination of the size of the fault (i.e. the severity of the fault) and sometimes also the determination of the time of onset of the fault (or fault prediction). In this Thesis, fault diagnosis and fault identification is performed.

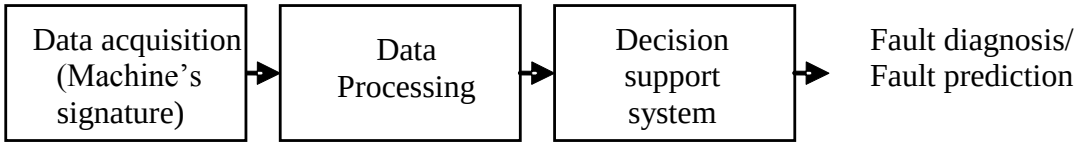

Figure 1-1: Stages in a condition-based montioring system.

Due to the complexity of vibration and audio signals in fault diagnosis, mathematical transformations, signal processing and pattern recognition techniques are widely used to extract useful features from these signals to discriminate between different machine conditions and to follow the machine degradation process.

1.3 Vibration and audio based fault diagnosis in bearings and centrifugal pumps

As explained in the stages of a condition monitoring system, the information collected in the data acquisition stage can include several kinds of data. In this Thesis, we focus on vibration and audio signals and we have driven our research into two applications: bearings and centrifugal pumps.

Bearings are vital components in rotating machines since they support the machine structures facilitating their rotation. An undetected fault in a bearing can cause the halt of the machine. Examples of rotating machines are motors and generators. Rotating machines are widely used in several industries. For that reason, the condition monitoring of bearings is very useful to early fault detection and diagnosis.

Centrifugal pumps are important elements in several systems because they transport fluids. They are used in several industries such as power stations, chemical industry, water depuration systems, oil extraction, cooling and heating systems and even in spas and swimming pools. So, the condition monitoring of pumps is also very important for the operational continuity.

Vibration signals are widely used as source of information in condition monitoring of different machines and component of machines. Bearings and centrifugal pumps are not an exception. Vibration-based fault diagnosis refers to fault diagnosis using vibration as information source. Vibration-based fault diagnosis is a well-established field that includes a wide range of techniques which have rapidly evolved during the last decades. In condition monitoring, vibration based fault diagnosis techniques have been widely used due to the easiness to acquire the vibration of the machine. That is why most research papers in fault diagnosis literature is devoted to vibation fault diagnosis [1].

Audio-based or airborne-based fault diagnosis refers to fault diagnosis using audio as information source. Audio-based fault diagnosis using microphones in the audible range (0-20kHz) is an emerging field with a great potential in fault diagnosis since microphones are non-invasive sensors and with greater location possibilities. For this reason, we think audio-based techniques need further research efforts.

In short, we focus our efforts in this Ph.D. Thesis on improvements in both audio-based and vibration-based fault diagnosis in condition monitoring in bearings and centrifugal pumps. In each application area we have mainly focused on the processing stage of a condition monitoring squeme (see Figure 1-1), specifically in feature extraction. In general, time, frequency and time-frequency domains are frequenctly used for feature extraction. Recently, nonlinear techniques such as nonlinear dynamics applied to time series and complexity measures have appeared in fault diagnosis of certain machines. We think that the study of such features in condition moniroting can improve the performance of a condition monitoring system.

There exist a vast literature of different methods to bearing fault diagnosis and fault identification and in bearing degradation assessment. There are also some available

public databases of bearing vibration signals in normal (free-fault) and fault conditions. For this reason, in bearing fault diagnosis we have used only vibration signal from the public available databases. We have proposed improvements in nonlinear features aiming at detecting different bearing faults and also at the identification of faults. So, we have made contributions in the signal processing (feature extraction) stage.

In pump fault diagnosis we have recorded our own database using audio and vibration signals simultenously acquired with the aim of comparing and combining vibration and audio signals as source of information because there are no public available databases of centrifugal pumps. As we stated before, most condition monitoring is carried out using vibration signals and pump condition monitoring is not an exception. Most research in centrifugal pump condition moniroting is focused in energy and statistical features extracted from time and frequency domain of vibration signals as well as pression signals. In this Thesis, we explore the use of audio signals in pump fault diagnosis, propose new features and study the combination of information from audio and vibration signals. Specifically, we have proposed three improvements not previously addressed in the literature: i) the application of features originally used with vibration signals to audio signal, ii) the proposal of new features extracted from frequency, cepstrum, time-frequency domains as well as complexity features and features related to nonlinear dynamics applied to time series in vibration and audio pump fault diagnosis and iii) a study of the combination features extracted from vibration signals and features extracted from audio signals. So, we have made contributions to the acquisition stage, only in the way there is no public audio database of centrifugal pumps available and to the processing stage (feature extraction) applying vibration features to audio signals, proposing a set of new features in pump fault diagnosis and combining information from audio and vibration signals.

1.4 Motivation of the Thesis

This Thesis is focused on two aspects of condition monitoring: the signal used to extract the information about the condition of the machine and the feature extraction with signal processing techniques. The aim is fault diagnosis and fault identification (fault degradation). The two application areas are: bearings and pumps. In bearings only

vibration signal is used and in centrifugal pumps audio and vibration signals are used as source of information. The research carried out in this Thesis is motivated by the following observations from the state-of-the art:

.Vibration-based monitoring is a consolidated field in CBM due to the easiness to acquire the vibration of the machine [2]-[4]. In bearing fault diagnosis, there are multiple signal processing techniques to extract features in order to discriminate between different bearing conditions and to follow the degradation of a bearing fault [5]. The early detection of a fault is very important in condition monitoring to prevent the fault develops. Moreover, nonlinear features extracted from the machine's signature can reveal new understanding of the signal under consideration and the application of nonlinear features can improve the task of fault diagnosis and fault degration [8]. For this reason, we have proposed improvements in nonlinear features aiming at detecting different bearing faults (fault diagnosis) and also at following the degradation of bearings at early stages.

.Audio-based monitoring (also called airborne-based monitoring) is a less developed field than vibration-based monitoring. The main reason is that audio signal can be affected by surrounding noise. However, microphones have more possibilities of location and are not mounted on the machine [6], [7]. For this reason, we aim to explore audio-based fault diagnosis. In order to study audio signals and to compare them with vibration signals, audio and vibration signals are acquired from an experimental set of a centrifugal pump.

.There is a lack of public available databases of audio signals acquired from machines for audio-based fault diagnosis. Moreover, there are only few works related to audio and vibration signals acquired together. These are more reasons for recording the database of audio and vibration signals acquired simoultaneously from an experimental set of a centrifugal pump.

.As audio signals are less used in fault diagnosis literature, most features extracted from vibration signals have not previously used in audio signals. In this Thesis, we address this issue applying state-of-the-art vibration features into audio

signals in the centrifugal pump application in order to study their discrimination ability between different condition of the centrifugal pump (normal and fault conditions).

.In pump fault diagnosis literature, most features are extracted from time, frequency and time-frequency domain [9], [10]. In this Thesis, a set of new features extracted from frequency, cepstrum, time-frequency domains as well as complexity features and features based on nonlinear dynamics applied to time series are extracted from both vibration and audio signals. These features along with the state-of-the-art features are evaluated in order to study their discrimination ability between different pump conditions using two classifiers.

.There are few works in literature using vibration and audio signals acquired simoulstaneously [11], [12]. For this reason, in this Thesis the fusion of both vibration and audio signals at feature level, score level and decision level is carried out in order to evaluate whether the fusion improves the performance of the system.

These observations will be discussed in Chapter 2, in which the Thesis problem is analized in depth.

1.5 The Thesis

The thesis developed in this Dissertation can be stated as follows:

The use of audio signals as source of information and the application of nonlinear techniques improves condition monitoring performance.

1.6 Objectives of the Thesis

This PhD Thesis seeks to improve the performance of condition monitoring systems in fault diagnosis and fault identification using vibration and audio signals in two applications (bearings and pumps) with special emphasis in the feature extraction stage and in the use of audio signals as source of information.

The main objetives of the PhD Thesis are as follows:

1. To review signal processing techniques and pattern recognition techniques in audio-based and vibration-based fault diagnosis.

2. To obtain vibration bearing databases of free-fault bearings and bearings with faults.

3. To study nonlinear techniques for bearing fault diagnosis and bearing fault identification.

4. To create a database of audio and vibration signals simultaneously recorded from a centrifugal circulating pump with normal (free-fault) and fault conditions.

5. To apply features extracted from vibration signals in pump fault diagnosis to audio signals obtained from a centrifugal pump.

6. To generate new features to discriminate between different pump conditions in pump fault diagnosis.

7. To compare vibration and audio features performances in the centrifucal pump application.

8. To study the combination of audio and vibration signals in the centrifugal pump application.

1.7 Methodology of the Thesis

The methodology of this Thesis is divided in the following steps:

Provided there are no available public audio databases, we record our own audio database acquiring at the same time vibration signals. We record simultaneously audio and vibration signals from a centrifugal pump in a closed loop. Normal and different

faults conditions were recorded. We also collect bearing vibration databases publicly available from different internet repositories.

Once the bearing vibration databases are collected and the audio and vibration database from the centrifugal pump is acquired in our laboratory, we carry out different experiments for bearing application and for pump application.

For bearing application, two new proposed methods based on nonlinear features are applied to the vibration signals from the bearings for fault diagnosis and fault identification. The proposed methods are compared with methods in the literature. The ability of the proposed features for bearing fault diagnosis is quantyfied using two classifiers: a neural network classifier and a Least-Square Support Vector Machine (LS-SVM) classifier. In the case of bearing identification, an index to follow the degradation of bearings with outer race fault and different severities is proposed.

For centrifugal pump application, features from the state of the art of pump fault diagnosis are implemented and extracted from vibration signals of the centrifugal pump. Then, these features are applied to the audio acquired from the centrifugal pump. Features in frequency domain, cepstrum domain, time-frequency domain and nonlinear features are proposed for pump condition monitoring. Feature selection is implemented for select relevant features in pump fault diagnosis. We study the relevance of the selected features and the performance of vibration and audio signals using two standard classifiers (LS-SVM and neural networks). Finally we analyze how the fusion of audio signals to vibration signals affects the monitoring performance.

1.8 Outline of the Dissertation

The Dissertation is structured according to a traditional complex type [13] with literature review and two different applications in which methods are explained and applied to experimental studies. The chapter structure is as follows:

.Chapter 1 introduces the topic of condition monitoring and gives the motivation, outline, methodology and contribution of this PhD Thesis.

.Chapter 2 summarizes related works which have given rise to the motivation of the Thesis and details the motivation of this Thesis based on these previous works. The state of the art is a contribution of this Thesis. The writing of Chapter 2 is based on a paper published by the author of this Thesis.

.Chapter 3 is devoted to the application areas of this Thesis, namely bearings and centrifugal pumps. A brief description of bearings basics followed by a description of the public bearing vibration databases used in this Thesis is carried out in the first part of the chapter. The second part is focused on centrifugal pump application. Pump basics and the acquisition process of the audio and vibration database are described. We contribute with the recording of an audio and vibration database of a centrifugal pump.

.Chapter 4 shows the contributions in bearing fault diagnosis and fault identification using vibration signals. Two methods based on nonlinear techniques are proposed and the results of the application of each method are shown. The contributions of this Chapter are the proposed new methods based on nonlinear features for bearing fault diagnosis and identification. The writing of Chapter 4 is based on three publications by the author of this Thesis.

.Chapter 5 is devoted to the contributions in the centrifugal pump application for fault diagnosis using audio and vibration signals. The features used in pump fault diagnosis literature are described as well as the features proposed in this Thesis for pump fault diagnosis. We contribuite with the application of vibration features to audio signals and with the proposal of a set of new features in frequency, cepstrum, time-frequency and nonlinear domains for pump fault diagnosis. The results of the feature evaluation with two classifiers are also shown. Part of the writing of Chapter 5 is based on two publications of the author of this Thesis.

.Chapter 6 shows the results of audio and vibration fusion at feature level, score level and decision level in the pump application. We contribute with a study of the combination of audio and vibration signals in pump fault diagnosis.

.Chapter 7 concludes the Dissertation summarizing the main results obtained and outlining future research lines.

Chapters 5, 6 and 7 have an introductory part in which the methodology is explained, a second parte in which the methodology is applied to the databases and a third part with the results and conclusions.

.The Appendix of the Thesis is an extra chapter that shows a summary of the work carried out in voice pathology detection and in the discrimination between emotional states in speech during the Thesis. As the background of the PhD candidate is voice characterization using nonlinear featres, during the Thesis she continued this research line.

The dependence among the chapters is illustrated in Figure 1-2. For example, before reading any of the Chapters 4, 5, and 6, one should read first Chapters 3 and 41 Before Chapter 3 one should start with the introduction in Chapter 1, and it is recommended to read also Chapter 2.

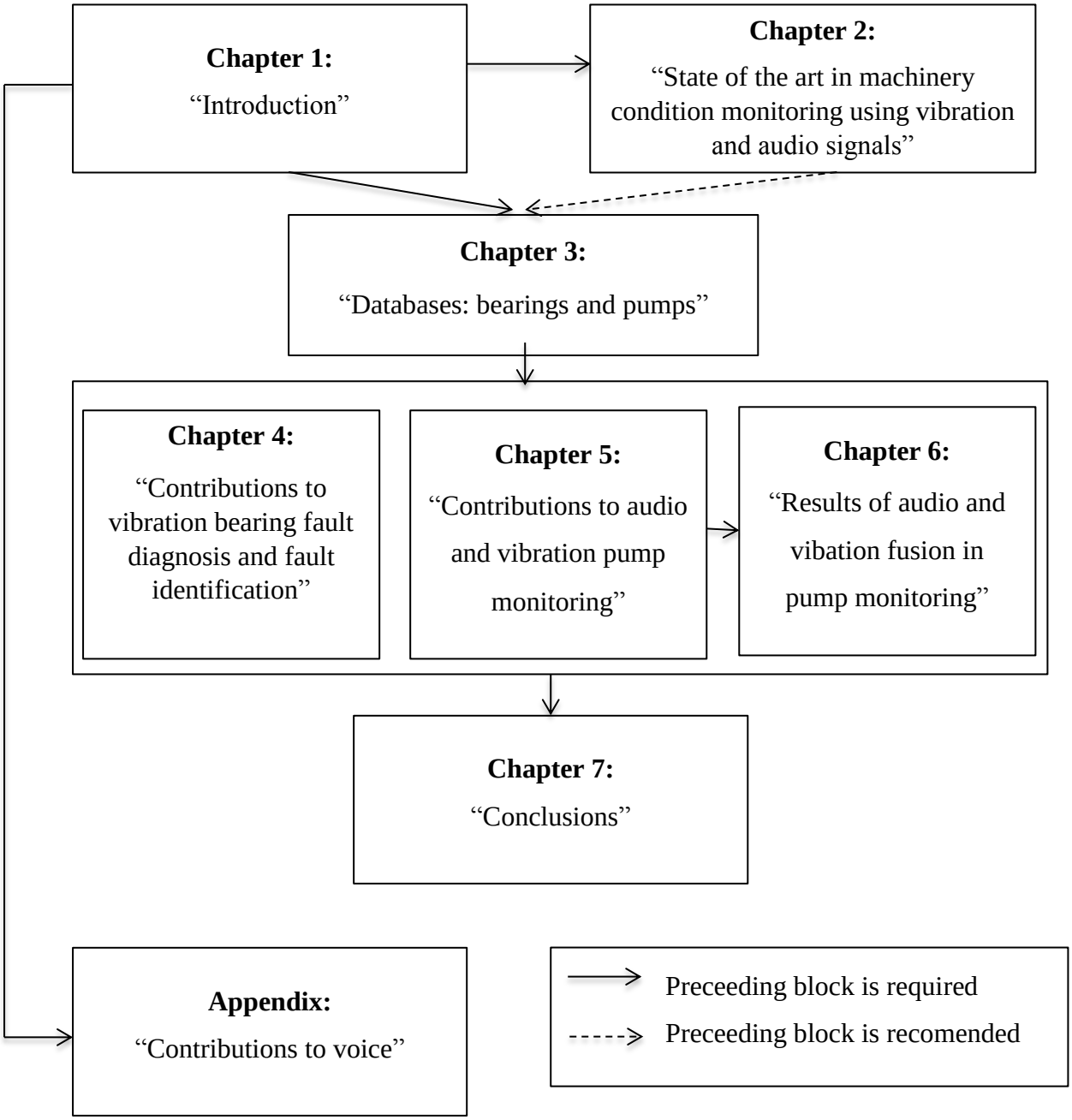

Figure 1-2: Dependence among Dissertation chapters.

1.9 Research contributions

The research contributions of this PhD Thesis are divided into condition monitoring contributions and voice contributions. Provided that the research background of the PhD candidate is voice characterization and she kept working on this subject during her PhD, the publications in voice are also presente here. Journal papers included in ISI JCR appear in bold.

1.9.1 Research contributions in condition monitoring

1. Literature review in audio and vibration fault diagnosis techniques focusing on feature extraction and pattern recognition techniques.

Henríquez, P., Alonso, J. B., Ferrer, M., & Travieso, C. M. (2014). Review of automatic fault diagnosis systems using audio and vibration signals. *Systems, Man, and Cybernetics: Systems, IEEE Transactions on*, *44*(5), 642-652.

2. A method based on Teager-Kaiser energy operator and statistic and energy features for bearing fault diagnosis and application of the proposal to bearing degradation in a helicopter.

Henríquez, P., Alonso, J. B., Ferrer, M. A., & Travieso, C. M. (2013). Application of the Teager–Kaiser energy operator in bearing fault diagnosis.*ISA transactions*, *52*(2), 278-284.

Henríquez, P., White, P., Alonso, J. B., Ferrer. M. A. (2011, October). Application of Teager-Kaiser Energy Operator to the Analysis of Degradation of a Helicopter Input Pinion Bearing. In *Proc. of the International Conference Surveillance 6* (pp. 265-274), University of Technology of Compiègne, France.

Henríquez, P., Alonso, J. B., Ferrer, M. A., Travieso, C. M. (2011, May-June). Application of Higher Order Statistics of Teager-Kaiser Energy Transformed Vibration Signal for Bearing Fault Diagnosis. In *Proc. of the 24th Int. Congress on Condition Monitoring and Diagnostics Engineering Management* (pp. 265-274), Stavanger, Norway.

3. A method based on wavelet packet transform and Lempel-Ziv complexity for bearing fault identification.

Henríquez, P., Alonso, J. B., Ferrer, M. A., Travieso, C. M. (2014, September). Degradation assessment in bearings with outer race fault. In *27th International Congress of Condition Monitoring and Diagnostic Engineering Management (COMADEM 2014)*, Brisbane, Australia.

4. Proposal of energy features from wavelet packet transform for pump monitoring using vibration and audio signals.

Henríquez, P.; Alonso, J. B.; Ferrer, M. A.; Travieso, C. M.; Gómez, G. (2012, June). Fault diagnosis using audio and vibration signals in a circulating pump. *Journal of Physics: Conference Series 25th Int.Congress on Condition Monitoring and Diagnostic Engineering (COMADEM 2012)* (Vol. 364, No. 1, p. 012135), Huddersfiled, England.

5. Proposal of Lempel-Ziv complexity and Hurst exponent for pump monitoring.

Henríquez, P., Alonso, J. B., Ferrer, M. A., Travieso, C. M. (2014, September). Application of complexity measures to pump fault diagnosist. In *27th International Congress of Condition Monitoring and Diagnostic Engineering Management (COMADEM 2014)*, Brisbane, Australia.

Other contributions so far related to the problem developed in this Thesis in condition monitoring but not presented in this Dissertation include:

1. Proposal of nonlinear features to audio signals from electric machines.

Henríquez, P., Alonso, J.B., Travieso, C.M., Ferrer, M.A. (2007, August). Advances in automatic detection of failures in electric machines using audio signals. In *Proc. of the 11th IASTED Int. Conference on Artificial Intelligence and Soft Computing*, (pp. 114-119), Palma de Mallorca, Spain.

2. Method for bearing fault detection based on dynamic time warping and direct matching point techniques.

Díaz-Cabrera, M., Henríquez, P., Ferrer, M.A., Pirlo, G. , Alonso, J.B., Impedovo, D. (2015, September). Novel Method for Early Bearing Fault Detection based on Dynamic Stability Measure. In *Proc. of IEEE 49th Annual Int. Conf. on Security Technology*, Taipei, Taiwan.

1.9.2 Research contributions in voice

Research contributions in voice pathology detection and voice emotion detection are listed. The Appendix (Extension to voice) of this Dissertation is based on the following four publications.

1. Proposal of measures based on nonlinear dynamics for characterization of healthy and pathological voice.

Henríquez, P., Alonso, J. B., Ferrer, M., Travieso, C. M., Godino-Llorente, J., & Díaz-de-María, F. (2009). Characterization of healthy and pathological voice through measures based on nonlinear dynamics. *Audio, Speech, and Language Processing, IEEE Transactions on*, *17*(6), 1186-1195.

2. Proposal of measures based on nonlinear dynamics and complexity measures for discriminating between emotional states through speech.

Henríquez, P., Alonso, J. B., Ferrer, M. A., Travieso, C. M., Orozo-Arroyave, J. R. (2014). Nonlinear Dynamics Characterization of Emotional Speech. *Neurocomputing*, *132*, 126-135.

Henríquez, P., Alonso, J. B., Ferrer, M. A., Travieso, C. M., & Orozco-Arroyave, J. R. (2013). Global Selection of Features for Nonlinear Dynamics Characterization of Emotional Speech. *Cognitive Computation*, *5*(4), 517-525.

Henríquez, P., Alonso, J. B., Ferrer, M. A., Travieso, C. M., & Orozco-Arroyave, J. R. (2011). Application of Nonlinear Dynamics Characterization to Emotional Speech. In *Advances in Nonlinear Speech Processing* (pp. 127-136). Springer Berlin Heidelberg.

1.10 References

[1] Vilela, R. M., Metrôlho, J. C., & Cardoso, J. C. (2004, May). Machine and industrial monitorization system by analysis of acoustic signatures. In *Electrotechnical Conference, 2004. MELECON 2004. Proceedings of the 12th IEEE Mediterranean* (Vol. 1, pp. 277-279). IEEE.

[2] Jardine, A. K., Lin, D., & Banjevic, D. (2006). A review on machinery diagnostics and prognostics implementing condition-based maintenance.*Mechanical systems and signal processing*, *20*(7), 1483-1510.

[3] Vachtsevanos, G., Lewis, F. L., Roemer, M., Hess, A., & Wu, B. (2006) Intelligent Fault Diagnosis and Prognosis for Engineering Systems, 1st ed. Hoboken, New Jersey: John Wiley & Sons, Inc.

[4] Henríquez, P., Alonso, J. B., Ferrer, M., & Travieso, C. M. (2014). Review of automatic fault diagnosis systems using audio and vibration signals. *Systems, Man, and Cybernetics: Systems, IEEE Transactions on*, *44*(5), 642-652.

[5] Yang, H., Mathew, J., & Ma, L. (2003, Nov). Vibration feature extraction techniques for fault diagnosis of rotating machinery: a literature survey.In *Asia-Pacific Vibration Conference, 2003* (pp. 277-279).

[6] Baydar, N., & Ball, A. (2003). Detection of gear failures via vibration and acoustic signals using wavelet transform. *Mechanical Systems and Signal Processing*, *17*(4), 787-804.

[7] Al-Hashmi, S.A. (2012, September 23-26). Spectrum Analysis of Acoustic Signals for Cavitation Detection. In *2012 IEEE Symposium on Industrial Electronics and Applications (ISIEA2012)*, Bandung, Indonesia.

[8] Janjarasjitt, S., Ocak, H., Loparo, K. A. (2008). Bearing condition diagnosis and prognosis using applied nonlinear dynamical analysis of machine vibration signal. *J. of Sound and Vibration, 317*, 112-126.

[9] Zhao, X. M., Hu, Q. H., Lei, Y. G., & Zuo, M. J. (2010). Vibration-based fault diagnosis of slurry pump impellers using neighbourhood rough set models.*Proceedings of the Institution of Mechanical Engineers, Part C: Journal of Mechanical Engineering Science*, *224*(4), 995-1006.

[10] Farokhzad, S. (2013). Vibration based fault detection of centrifugal pump by fast fourier transform and adaptive neuro-fuzzy inference system. *Journal of Mechanical Engineering and Technology 1*(3), 82-87.

[11] Wu, J. -D., Chuang, C. -Q. (2005). Fault diagnosis of internal combustion engines using visual dot patterns of acoustic and vibration signals. *NDT&E Int.*, *38*, 605-614.

[12] Al Thobiani, A., Gu, F., & Ball, A. (2010 June 22-24). The monitoring of cavitation in centrifugal pumps based on the analysis of vibro-acoustic measurements. In *CM 2010 and MFPT 2010*, UK.

[13] Paltridge, B. (2002). Thesis and dissertation writing: an examination of published advice and actual practice. *English for Scientific Purposes*, *21*(2), 125–143.

CHAPTER 2
State of the art in machinery condition monitoring using vibration and audio signals

2.1 Introduction

The objective of this chapter is to provide a review of automatic vibration-based and audio-based fault diagnosis in machinery using condition monitoring strategies. Based on the analysis of the state of the art, we focus our Thesis on both vibration and audio-based fault diagnosis and fault identification. This Chapter is based on a review paper published by the autor of this Theis [1].

We repeat for convenience the steps of an automatic condition monitoring system. Then, we will describe the state of the art focusing on each stage.

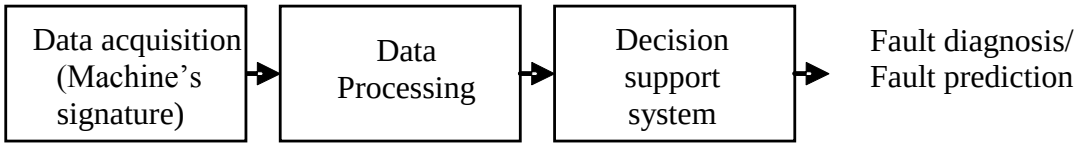

Figure 2-1: Stages in a condition-based montioring system

Due to the complexity of vibration and audio signals in fault diagnosis, mathematical transformations, signal processing and pattern recognition techniques are widely used to extract useful features from these signals to discriminate between different machine conditions and to follow the machine degradation process. Some reviews up to 2006 using different kinds of machine signature are available in the literature [3]-[6] and some works are focused only on vibration-based fault diagnosis [7]-[9]. In this review, we focus specially on works from 2006 up to 2015.

The most referenced papers in this review belong to vibration-based diagnosis and were published from 2000 up to 2015 (see Figure 2-2). Several kinds of faults can be detected using vibration and audio signals. Figure 2-2 (bottom pie charts) shows the fault distribution of the referenced papers when vibration-based and audio-based fault diagnosis are used. In the case of vibration-based papers, most references are related to bearing faults, followed by rotor/stator faults and gears. In the case of audio-based papers, most references are related to combustion engine faults (C. Eng). Most of these faults occur in motors, pumps, fans, helicopters, end-milling machines, on load tap chargers (OLTC) of power transformers and in bearing, gear and rotor test-rigs.

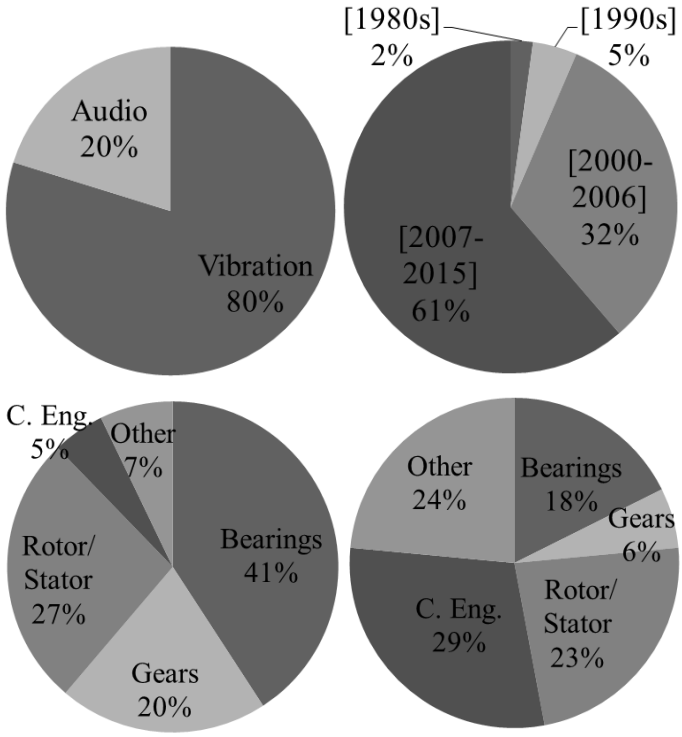

Figure 2-2: Distributions of referenced papers: Audio-based and vibration-based fault diagnosis distribution (upper left). Publishing years distribution (upper right).Distribution of faults in vibration-based diagnosis (bottom left) and in audio-based diagnosis (bottom right).

The remainder of this chapter is divided into five subsections. The second, third and fourth subsections focus on the steps of a CM system (acquisition, data processing and decision stage). Subsection 2.5 reports on some examples of CM systems. Finally, an analysis of the gaps of the state of the arte is carried out.

2.2 Acquisition Stage

Good quality and precision of the signal in the acquisition stage is essential for posterior analysis and feature extraction. In this Thesis, we focus on vibration and audio signals acquired by accelerometers and microphones, respectively.

The dynamic forces within a machine produce compression and bending waves. This vibration pattern changes when an incipient failure starts to evolve. Thus, the analysis of vibration signals is a useful tool for establishing the machine's condition. In

order to detect these signals, vibration sensors are mounted directly onto the machine. There are different kinds of sensors depending on the frequency range: position sensors (0Hz-10kHz), velocity sensors (10Hz-1kHz) and accelerometers (8Hz-15kHz). Piezoelectric accelerometers are popular because of their higher dynamic range of frequencies, reliability, robustness and smaller dimensions. The number and location of vibration sensors is an important issue discussed in [8].

The acoustic characteristics of a machine change when a fault evolves. Consequently, the sound of a machine carries information about its condition. Extracting the sound signature of the machine is a useful tool in fault diagnosis [1]. We focus our review on audio signals obtained with microphones. They usually acquire sounds in the 0Hz-20kHz range. Some microphones can even acquire signals above 100kHz. Microphones are not mounted directly onto the machine. As a result, they are less intrusive than vibration sensors but they are more sensitive to environmental noise. For this reason, microphones must be pointed to the machine or system under consideration and should be placed from 2 cm to 10 cm from the wanted source [1], [12].

2.3 Processing Stage

Signal processing transforms original signals into useful features to accomplish fault diagnosis. These features should be independent of the normal machine operating conditions (variations of load and speed) and extraneous noise and be sensitive only to machinery faults. This section is divided into vibration and audio signals analysis. Table 2-1 shows some of the most common vibration and audio features discussed in the literature since 2000 up to 2015.

2.3.1 Vibration signal processing

The main processing techniques applied to vibration signals are based on: time analysis, frequency and cepstral analysis, time-frequency analysis and non-linear analysis.

Time domain analysis

Signal processing in the time domain extracts information from the vibration signal as a function of time. Conventional techniques include several time features such as root mean square, crest factor [35], variance, skewness, kurtosis and higher order moments [68],[93]. Some features, such as crest factor, kurtosis, impulse and clearance factors, do not vary with load and speed variations and are good indicators for impulsive faults [35], [60] especially in bearings. Other conventional techniques are time averaging methods, including time synchronous average (TSA), residual signal and difference signal, all of which are powerful tools in the detection of gear faults [36], [37], [102]. TSA removes background noise and periodic events that are not synchronous with the gear of interest. The resulting signal is used for posterior advanced analysis [80]. Autoregressive (AR) modelling [30] and autoregressive moving average (ARMA) modelling [38] have also proven to be efficient tools in modelling transients in the vibration signal. Novel approaches include a modification of the time-varying AR and ARMA models in which the coefficients are updated with the incoming vibration signal [37]. These models are robust to variations in load and speed. Another novel AR approach [102] proposes the load information as an exogenous input.

Frequency and cepstral domain analysis

Frequency analysis gives information about the periodicity of the signal in the peaks of the frequency and detects harmonics and side-bands. Conventional frequency features, such as the mean and standard deviation of the frequency, the root mean square frequency, peak magnitude, energies and ratios of spectral energies are used in fault diagnosis in pumps, motors and gearboxes [35], [63], [67]. Another conventional technique is envelope analysis (EnA) or the amplitude demodulation technique, used especially in bearings [7], [16], [63] to identify the bearing defect characteristic frequency and also in gears [76]. EnA improves the signal to noise ratio (SNR) and makes the spectral analysis more effective. For a good review of EnA see [16]. EnA is usually applied using the Hilbert transform (HT) [16]. Recently, the skewness information wave (SIW) has been proposed to compute EnA without using the HT [103]. The skewness is computed in small regions of the signal, resulting in a skewness wave. The skewness information wave (SIW) is obtained using the Kullback-Leibler

divergence information from the skewness wave of the reference signal (measured far from the diagnostic location) and the diagnosis signal (measured in the diagnostic location). Then the envelope SIW is obtained from their absolute values and the spectrum is computed. This method is shown to be superior to the conventional EnA and more robust to strong background noise. Another novel EnA method is the Teager Energy Operator (TEO) [50], [100]. TEO is a nonlinear operator with higher demodulation precision and needs less calculation than HT.

Cepstral analysis, which gives information from the vibration signal as a function of quefrency has, since the nineties, been shown to be effective in fault diagnosis [83]. Power cepstrum gives information about the periodicity of the spectrum and detects harmonics and sideband patterns in the power spectrum. The application of Mel-Frequency Cepstral Coefficients (MFCC), a technique from speech processing, to vibration fault diagnosis [40] was proposed in 2006. MFCC contain both time and frequency information of the signal which makes them more useful for feature extraction in vibration signals. In 2007, a method called minimum variance cepstrum was proposed to detect faulty periodic impulses in bearings in noisy environments [19]. It minimizes the variance of the signal power in its cepstrum representation.

Another family of techniques is based on higher order statistics (HOS) in the frequency domain: bispectrum, summed bispectrum and bicoherence have, since the late nineties, been shown to be effective in fault diagnosis in the bearings of induction motors, gearboxes and in flexible rotor systems [17], [18], [39]. These provide more information than the power spectra, in the case of non-Gaussian signals, can detect nonlinear couplings and can explain the origin of certain peaks in the power spectra. For instance, [96] proposed in 2009 the use of HOS in the cepstral domain (bicepstrum) to detect failures in gears. This technique eliminated noise and modulation effects caused in gears.

Conventional frequency techniques assume stationarity and linearity and are usually applied in machines working at fixed speeds. However, most machine processes presents non-stationary components in speed-up, speed-down and in several faults. Cyclostationary analysis (a 2nd-order technique in the frequency domain), and time-frequency techniques are more appropriate for non-stationary processes. The periodic

variation of statistical moments of rotating machinery makes cyclostationarity techniques suitable for early fault detection [84], [98].

Time-Frequency domain analysis

Time-frequency analysis extracts information from the vibration signal as a function of time and frequency and overcomes the problems encountered in frequency analysis when analyzing non-stationary events. Some conventional time-frequency techniques include Short time Fourier transform (STFT) (Koo et Kim, 2000) [41], Wigner-Ville distribution (WVD) (Koo et Kim, 2000; Li et Mechefske, 2006) [41], [56] and the directional Choi-Williams distribution [42]. Techniques from the late nineties include Empirical Mode Decomposition (EMD) [35], [43], the Hilbert-Huang transform (HHT) [21], [35], and the Wavelet Transform (WT) [12], [81]. The WT has adjustable window size through the choice of the mother wavelet and different approximation scales. This flexibility makes it suitable for the analysis of non-stationary signals. Multiple features, such as singularity points [20], Lipschitz exponents [13], scalogram [36], energies, statistics and entropies [44], [81], are extracted from continuous WT (CWT), discrete WT (DWT) and Wavelet Packet Transforms (WPT). These are used to detect imbalance, misalignment, spalling, pitting in gears, faulty bearings and OLTC [97]. Contrary to WT, EMD is a self-adaptive method, applied to fault diagnosis for the first time in 1998. EMD decomposes the signal into a sum of intrinsic mode functions (IMFs). The frequency components in each IMF are related to the sampling frequency and to the signal itself, whereas WT is related only to the sampling frequency. However, the number of IMFs cannot be controlled [35], [63], [91], [117]. The HHT uses the EMD to obtain IMFs [21], [35] and then EnA is applied to each IMF using the HT.

Many new techniques have, in the last years, been proposed in time-frequency analysis. Most of them are related to the decomposition of the signal into mono-component AM-FM signals (amplitude modulated and frequency modulated signals) which are then analyzed using EnA techniques, and to the improvements in WT and EMD techniques. These techniques allow a finer analysis of the signal and more accuracy to detect single and compound faults, essential in fault diagnosis. They are discussed next.

Spectral Kurtosis (SK) is a spectral statistic reformulated in 2006 for non-stationary signals [104]. SK provides a robust way of detecting incipient faults that produce impulse-like signals, even in the presence of strong noise. SK also offers a way of designing optimal filters for filtering out the mechanical signature of faults using the kurtogram or the fast kurtogram (ways to compute the SK) as a prelude to EnA [105]. Recently, an enhanced kurtogram has been proposed for bearing fault diagnosis in combination with wavelet packet transform [114]. Local mean decomposition (LMD) and improved LMD are also proposed for fault diagnosis [110]. Contrary to the HHT, LMD does not use HT to estimate the envelope but uses the moving average. Product functions are obtained by multiplying the envelope estimates and the FM signal. Generalized demodulation time frequency (GDTF) also decomposes the signal into mono-component AM-FM signals, transforming the original signal into a new space where WT can be applied, therefore obtaining frequencies with physical meaning. GDTF was first proposed for analyzing biomedical signals. The envelope order spectrum technique, which blends GDTF and the spectrum, has also been proposed for fault diagnosis [99]. Iterated Hilbert transform (ItHT) analyzes AM-FM signals using the iterated application of the HT to a filtered version of the amplitude envelope. Amplitude envelopes and instantaneous frequencies are then extracted. ItHT has higher demodulation accuracy and lower complexity than EMD. The combination of ItHT and a smoothed instantaneous frequency estimation has been recently applied to fault diagnosis [106]. Ensemble EMD (EEMD) is a novel technique (2009) that eliminates the mode mixing problem in EMD. In the mode mixing problem the physical meaning of each IMF is unclear and EMD fails to represent the fault characteristics of a signal accurately. EEMD uses a noise-assisted technique to eliminate the mode mixing problem. EEMD and EMD are applied to a rotor fault and in a heavy oil catalytic cracking machine set [43]. Results show that EEMD can extract the fault characteristic information better than EMD. The multi-scale enveloping spectrogram (MuSEnS) [46] algorithm was developed in 2009 using time, scale, and frequency domain information contained in the signal. It decomposes the signal into different wavelet scales and the envelope signal in each scale is calculated, resulting in an ‘‘envelope spectrum’’ [46].

TABLE 2-1: FEATURES FOR VIBRATION AND AUDIO SIGNALS

Evolution

Methods		2000-2006	2007-2015
Time	Statistics	(2004)[59] (A)	(2009)[37] (V)
	TSA	-	(2010)[36] (V)
	AR,ARMA models	(2002)[30], (2006)[38] (V)	(2010)[102] (V)
Frequency	Statistics	(2004) [59] , (2005) [58], (2006) [56] (A)	(2010)[35], (2009)[54], (2006)[63], (2008)[67](V), (2007)[52] (A)
	EnA (HT)	(2000)[26] (A) ; (2007)[77](V)	(2008)[63] (V)
	SIW	-	(2010)[103] (V)
	TEO	(2007)[100] (V)	(2009)[50] (V)
	Cyclostationarity	(2001)[84] (V)	(2010)[98] (V)
	Polyspectrum (HOS)	-	(2007)[39] (V)
Cepstral	Cepstrum	-	(2007)[19] (V)
	MFCC	(2006) [40] (V)	(2009)[54] (A)
Time-Frequency	STFT, WVD, Choi dist.	(2000)[41], (2001)[42] (V), (2006)[56] (A)	(2009)[54], (2010)[86](A)
	WT (CWT, DWT, WPT)	(2003)[12] (V, A) (2007)[13], (2007)[20], (2007)[39] (V)	(2010)[36], (2009)[47](V) (2009)[57](A)
	SGWT (IWPT)	(2007)[44] (V)	(2009) [68] (V)
	RSGWT	-	(2010) [108] (V)
	dtcWT	-	(2010)[94] (V)
	Generalized S transform	-	(2011)[107] (V)
	MuSEnS	-	(2009)[46](V)
	EMD, HHT, EEMD	(2005)[21] (V)	(2010)[35], (2009) [43], (2015)[117] (V)
	ItHT	-	(2008)[106] (V)
	LMD	-	(2009)[110] (V)
	GDTF	-	(2010)[99] (V)
	SK	-	(2009)[104], (2009)[105] (2013)[114] (V)
Non-linear	Phase portrait, dot pattern	(2000)[10] (A), (2003)[11] (V)	- -
	Lyapunov Exponents, CD, fractals	(2001)[18], (2000)[23] (V)	(2007)[24], (2007)[52], (2008)[51], (2010)[95] (V), (2005)[55] (A,V), (2007)[25] (A)
	ApEn, Multi-Scale PermEn		(2007)[48], (2007)[49], (2015)[116](V)
	Multiple manifold	-	(2009)[109] (V)

V: Vibration, A: Audio.

Second generation WT (SGWT) [111] was proposed in 2006 and overcomes the main shortcoming of the WT (the proper selection of the mother wavelet) because SGWT is realized by a lifting scheme in the time domain (which is not based on the Fourier transform). The improved WPT (IWPT) is also based on SGWT and it is shown to be superior to WPT in extracting the fault characteristics in bearings [44], [68]. An approach that improves the SGWT is the redundant SGWT (RSGWT) proposed in 2009 [108], [111]. RSGWT is time-invariant, contrary to SGWT, which allows capturing more useful fault information. RSGWT outperforms SGWT in extracting transient components in gearbox vibration signals [111]. The dual-tree complex WT (dtcWT) was proposed in 2010 [94] in fault diagnosis. In [94], the authors show that dtcWT outperforms SGWT, fast kurtogram and DWT because dtcWT enhances noise reduction, is approximate time-invariant and can detect multiple fault features simultaneously Another application of the WT includes a novel growth index [47], insensitive to different mother wavelets and levels of decomposition. Finally, the generalized S transform was proposed in 2011 for fault diagnosis. It unifies STFT and WT so as to obtain more satisfactory time-frequency representations than other similar techniques such as STFT, WVD and the S transform. This allows more accurate detection of the bearing fault characteristic [107].

Nonlinear analysis

Evidence of a complex and non-linear vibratory system has been found in stator-rotor rub, loose pedestal and unstable oil film faults [18]. Conventional non-linear methods include pseudo-phase portrait, singular spectrum analysis, correlation dimension (CD) [22], [23], fractal dimensions, approximate entropy (ApEn), information entropy [92], mutual information [25] and Lyapunov exponents [14], [109]. CD quantifies the complexity of a time series and has successfully proven to detect rotor-stator rub, loose pedestal faults [23] and bearing faults [22]. Phase portrait shows qualitative differences in a normal gear and in a gear with an early fatigue cracked tooth [10]. ApEn quantifies the regularity of a time series and can effectively indicate the condition in fans [48] and bearings with speed and load variations [49].

A new technique is proposed in [24] to select a proper fractal dimension spectrum less affected by noise. In a more recent paper (2008) [51], a modification of

the correlation integral is introduced to the real-time fault diagnosis of bearings. Multiple manifold analysis is a novel nonlinear approach [109] (2009) that extracts manifold information from the vibration signals and outperforms conventional nonlinear techniques. A paper of 2010 proposes to compute the fractal dimension using DWT [95]. Fractal features are estimated from the slope of the variances of the DWT in different scales. The multiscale permutation entropy (Multi-Scale PermEn) has recently applied to bearing fault diagnosis [116]. Multi-Scale PermEn computes the permutation entropy across different scales.

2.3.2 Audio signal processing

Most research in machinery diagnosis is oriented towards the analysis of vibration signals. Audio-based CM has, however, not developed at the same rate**.** This is due to the contamination of the sound signal by unwanted sources such as other machines, noisy environments and the structural vibration of the machine itself [2]. This situation makes it difficult to acquire the machine's signature. Two main options are used to improve the low SNR in audio signals: the use of partial or full enclosure using an anechoic chamber [15], [17], which is an unrealistic approach for real industrial scenarios, or the use of pre-processing de-noising methods, such as wavelet [12] or blind source separation [2], [15], [26]. These techniques can affect the feature extraction stage. The choice of certain parameters, such as the threshold in wavelet techniques, is important for the extraction of the purified signal with the smallest distortion and the highest SNR. Audio-based techniques are useful in certain cases, especially when it is impossible to access the machine. Audio measurements can be performed at a distance from the machine so the use of sensors mounted directly on the machine is avoided.

The same processing techniques for vibrations are applied to extract features in audio signals obtained from machines. Statistical time domain features and energy features in the frequency domain [59] are used to detect wear in internal combustion engines and mass unbalance faults in rotary disks. EnA is used in a heavy sizing-press [26] and in the end-test of vacuum cleaner production [58], where the use of vibration and current analysis did not prove useful. As in vibration-based techniques, the audio spectrum is used when the machine is working at constant speeds [10], [56]. Some papers compare the use of Fourier analysis in audio and vibration signals, [10], [87].

These works claim that Fourier analysis is less effective in sound signals because of the low SNR. As in the case of vibration analysis, time-frequency techniques are more appropriate. For example, STFT is applied to identify engine fault frequencies [54]. However, WVD [86] and pseudo WVD [56] are shown to have better results in extracting non-stationary signatures in the bearings of induction motors. Continuous WT, WPT and MFCC are successfully applied to fault diagnosis of engines [15], [52], [57] working at different speeds and run-up conditions.

The symmetrised dot pattern technique is based on the visualization of changes in amplitude and frequency of the audio signal. It has been applied to distinguish between normal and faulty fans [10] and in the fault identification of an internal combustion engine working at different speeds [55]. Some papers have focused on the analysis of a group of chaotic measures extracted from audio signals of different machines. Asynchronous changes in audio signals can be detected with chaotic measures [25]. The spectral entropy of audio signals has shown to be more effective than vibration signals in the diagnostic of cavitation [88].

The development of techniques to improve SNR and the use of the same tool, i.e. wavelets, in the de-noising and extraction stages can put audio-based techniques at an advantageous position in CM systems since they are less intrusive than vibration-based techniques.

Multiple features are extracted from vibration and audio signals in CM techniques. However, a unique feature capable of representing the machine condition does not exist. A good characterization requires the extraction of different features from different domains. Thus we need to find, using feature selection, the most suitable ones for the application under consideration. The selection of well-suited features providing fault-related information and the discarding or weakening of irrelevant or redundant features is an important stage in machine CM to improving system performance.

2.4 Decision Stage

The decision support stage of CM systems helps take maintenance actions when a fault is impending or already detected. The decision stage can be performed by a qualified person or an expert system. This paper focuses on pattern recognition techniques applied to machine CM. Automatic pattern recognition techniques can be accomplished using supervised or unsupervised learning. In supervised learning, the machine should be forced to work in different conditions, including faulty states, to train the pattern recognition system. Alternatively, unsupervised learning methods (or novelty detection), only require normal data and it is not necessary to damage the machine.

However, novelty methods can only distinguish between normal and faulty conditions. Noise and the changing environment must also be taken into account to avoid incorrect interpretations. In the next paragraphs, pattern recognition techniques used in fault diagnosis are discussed. Table 2-2 presents some of the most common classification methods used in the literature from 2000 up to 2015.

TABLE 2-2: CLASSIFICATION METHODS FOR VIBRATION AND AUDIO

	Evolution	
Methods	2000-2006	2007-2015
SPC	(2001)[27] (V, U)	-
Distances	(2002)[66] (V, S)	(2008)[67] (V,U); (2010) [35] (V, S)
SVM, SVDD, PSVM	(2005)[70] (V, U)	(2007)[44], (2007)[52], (2007)[101], (2009)[91], (2011)[93], (2014)[118] (V,S) (2009)[68] (V, U)
HMM	(2005)[29] (V, U)	(2007)[24] (V, S)
Hyp. test, GMM	(2004)[65] (V) (2006)[40] (V)	(2009)[37] (V)
NN	-	(2007)[69], (2009)[61] (V, U) (2010)[35], (2009)[45], (2008)[63], (2008)[64] (V, S) (2009)[57] (A, S)
Fuzzy-logic	-	(2007)[13], (2010)[60] (V, S)
Evolutionary alg.	-	(2007)[39], (2010)[35] (V, S)
Expert systems	(2004)[59] (A, S)	(2007)[90], (2008)[63], (2012)[112], (2015)[115] (V, S)

V: Vibration, A: Audio, S: Supervised, U: Unsupervised.

Statistical Process Control (SPC) is a conventional unsupervised method that measures the deviation of the current signals from a reference signal (which represents

the normal condition) to determine whether the current signal is inside the control limits [27], [82]. Cluster analysis groups signals into different fault categories according to the similarity of the features. The objective is to minimize the variance inside the same group and to maximize it between different groups. Conventional distances used to achieve this objective are: Mahalanobis distance [66], Euclidean distance [35], [66] and Bayesian distance [66]. In 2008, [67] proposed a novel clustering algorithm using a compensation distance evaluation technique in unsupervised clustering. The Support Vector Machine (SVM) is a cluster-based technique widely used in machinery diagnosis [44], [52], [93]. It maximizes the distance of the closest point to the boundary curve that separates two data classes. The original SVM performs bi-class classification but multiclass SVMs have been developed to classify different kinds of faults [44]. Proximal SVM (PSVM) has also been proposed in fault diagnosis [101]. PSVM is modeled as a system of linear equations which produces results similar to SVM but with less computational effort. In 2005, the application of one-class SVM was proposed in fault diagnosis. One-class SVM is an unsupervised technique [70] based on the Support Vector Data Description (SVDD). It fits a tight hypersphere around the feature vector extracted from normal signals. This method has been used in bearing degradation experiments [68]. SVDD for multiclass classification was proposed in 2009 [91]. It uses the centers of a set of hyperspheres and models the decision boundaries via a combination of linear discriminant analysis and the nearest-neighbor rule.

HMM is a conventional method used to perform fault classification by analysing the time series. The hidden states of the Markov model represent “healthy” and “faulty” states [28], although in the latest developments the relationship between hidden states and physical meaning is not established [29]. The factorial HMM classifier has a strong capability for classification of non-stationary signals. For this reason, factorial HMM was applied in 2006 for the speed-up and speed-down process [62]. In 2007, an HMM was used in unsupervised learning mode for fault detection [24].

Statistical hypothesis tests such as the Kolmogorov-Smirnov test [37], [65] and Student’s t-test [65] have been conducted to statistically compare signatures of normal and faulty machinery. Density estimation techniques are also popular in fault detection. These are unsupervised methods that model the underlying distribution of the data. The Gaussian mixture model (GMM) analyzes features extracted from a signal using a

weighted sum of Gaussians. The success of GMM in the classification of dynamic data makes GMM especially suitable in modelling vibration data from machinery. GMM was applied for the first time to fault diagnosis in 2006 [40].

Neural networks (NN), fuzzy-logic (FL), expert systems and evolutionary algorithms are pattern recognition techniques widely used in fault diagnosis. They are usually utilized in a blended way to obtain better performance. Because of their high learning and generalizing capabilities, NN are used to classify different machinery faults [85], [93]. The NN is a conventional classification method and multiple NN models such as multilayer perceptron [35], [63], radial basis functions [35], [64], back-propagation NN [57], probabilistic NN [45], generalized regression NN [57] and wavelet NN [64] have been used in fault diagnosis. Auto-associative NN [69] and self-organizing maps [61] are unsupervised conventional NN techniques applied in diagnosis. FL and decision trees have been combined to generate rules from the feature set automatically [60]. The combination of NN and FL improves the learning capabilities at the self-adaption and self-learning stages [13], [89]. The neuro-fuzzy approach aims at automating the design of a fuzzy system using NN. An extended neuro-fuzzy system was proposed in 2008 for condition monitoring [113]. NN, FL and a decision tree algorithm are used together in [60].

Expert systems use the knowledge of an expert in a computer program. The knowledge base contains domain knowledge while the inference mechanism manipulates the knowledge to produce solutions [90]. When the expert knowledge is inexact, FL obtains uncertainty measures [13]. An NN inference mechanism is used in an expert system to diagnose unbalances using acoustic signals [59]. Recent papers have focused on a new adaptive neuro-fuzzy inference system (ANFIS) that combines the FL approach and the adaptive NN capability [63], [115]. Recently, the soft set theory, a mathematical tool used to deal with uncertainties, has been applied for the first time in fault diagnosis (2012) [112].

Finally, in artificial techniques, evolutionary algorithms have been used to reproduce the natural process of the evolution of a population. The most frequently used are genetic algorithms which are applied to fault diagnostics to select the more adequate

and competitive features and to combine different classifiers to obtain better performance [35], [39].

2.5 Systems & Performance

This subsection discusses the performance evaluation techniques in diagnostic technologies and shows examples of the application of CM systems. The use of performance metrics allows different algorithms and techniques to be compared so as to evaluate the entire CBM system. The creation of a common performance evaluation framework is a challenging task for researchers and standards institutions and organizations; ISO 17359 outlines the CM metrics and the Society of Automotive Engineers (SAE) (SAE, 2007) [31] addresses all aspects of metrics. The NASA Ames Research Center proposes an annual international Diagnostic Competition (http://dx-competition.org/) to discuss the latest developments.

The metrics used in diagnostic/prognostic technologies can be divided into performance metrics and effectiveness metrics. Performance metrics assess technical performance such as algorithm performance while effectiveness metrics measure the capability of the global system to achieve operational goals. Most metrics used in the literature include classification accuracy, true positive (TP, percentage of correct classification), false positive (FP, percentage of incorrect classification), false negative (FN, number of misses), true negative (TN number of correct rejections), the confusion matrix (a representation of TP, FP, FN and TN) [60], [61] and the Receiving Operating Curve (ROC) [61]. ROC gives a comprehensive overview of the trade-off between FP and FN.

Some authors and institutions have developed test beds to assess the performance and effectiveness of the proposed metrics for diagnostic systems [32]-[34]. The NASA Ames Research Center developed a real-world electrical power system test bed [32] and the US Navy [33] developed a CBM test bench with data provided by the State ARL Mechanical Diagnostics Test Bed (MDTB) [73].

The fault diagnosis techniques proposed in the literature cannot be easily compared because of the lack of common and public machinery databases. Some efforts have been made to develop public databases, although there is only a limited number of them: Case Western Reserve University (Case Western) [71] provides bearing vibration signals, Ypma provides normal and faulty samples of gears and pumps [74], the NASA Prognostics Data Repository includes a collection of donated data sets (NASA) [75], the Naval Systems Command provides vibration signals of an UH-60 helicopter (UH-60) [72] and the MDTB data [73] of gears, shaft and bearings can be obtained under previous petition.

Table 2-3 summarizes the characteristics of some CM systems based on vibration or audio analysis. Performance evaluation of most of these systems is made using classification accuracy. Y. Lei et al. [63] and G. Yu et al. [45] use the Case Western University bearing vibration dataset (Case Western) [71]. A 100% accuracy is obtained by Y. Lei et al. [63] using a set of selected features from time, frequency and time-frequency domain. The improved distance evaluation technique is used to select the most suitable features that feed the ANFIS. G. Yu et al. [45] use an unsupervised procedure based on cluster-based feature extraction from DWT and probabilistic NN. Different scales of WT decomposition are used and the classification accuracy is computed for each scale. J. Sanz et al. [69] apply WT and unsupervised auto-associative NN in a gearbox of a pump station [74] with the data collected by Ypma. S. Cho et al. [78] and W. Wang et al. [76] propose automatic fault diagnosis systems applied to real industrial scenarios. S. Cho et al. [78] propose a CM system in an end milling machine. Multiple sensors, including vibration sensors, are used and features from the frequency domain are extracted. Fusion at feature and decision levels is performed. W. Wang et al. [76] proposes a real-time CM system for gears in printing machines. J.-D. Wu et al. [57] use audio signals in the development of an expert system for internal combustion engines. Shannon entropy is extracted from WPT. Back propagation NN and generalized regression NN were used as classification methods achieving a success rate of 95%.

Most CM products on the market are directed to specific applications so the results of using a prototype are not generally reproducible for other applications. For this reason, the use of standards is recommended. Two standards and two

standardization proposals can be found in: IEEE 1451 and IEEE 1232, MIMOSA and OSA-CBM [77].

TABLE 2-3: SYSTEMS PERFORMANCE

Author	Main Features	Database	Approach	Results
(Y. Lei et al., 2008,[63]) (V)	Time and Frequency domains, EMD	Bearing vibration data set [71] (N, OR, IR, B faults)	ANFIS	100% Training: 140, Test: 70
(G. Yu et al., 2009,[45] (V)	DWT (cluster-based feature extraction)	Bearing vibration data set [71] (N, OR, IR, B faults)	Probabilistic NN	98.2 % (maximum accuracy) Training: 168, Test: 60
(J. Sanz et al., 2007,[69]) (V)	Discrete Wavelet Transform	Pump vibration database [74] (gears) (N and Damage pump), (Two loads)	Auto-associative NN (unsupervised mode)	100%, Training: 650 (N); Test: 160 (N), 810 (damage)
(S. Cho et al., 2010,[78]) (V)	Time and Frequency domain; Parameters: speed, feed and depth of cut.	OKUMA ES 3016 CNC vertical machining center (N, Breakage, Chipping, wear), (Different speeds)	SVM, Multilayer Perceptron, Radial Basis Function	97.67% (maximum accuracy with three-sensor combination)
(W. Wang et al., 2009,[76]) (V)	Wavelet energy function, Phase demodulation, kurt.	Gears (N, Cracked and Chipped)	Neural Fuzzy scheme	97.6 %
(J.-D. Wu et al., 2009,[57]) (A)	Shannon Entropy of Wavelet Package Transform coefficients	Internal combustion engine (N, 5 faulty conditions) (2 fixed speeds and a run-up experiment)	Generalized Regression NN	> 95% in all experiments Training: 30 for each condition Test: 120 for each condition

V: Vibration, A: Audio, N: normal condition, OR: outer race fault, IR: inner race fault, B: Ball fault.

2.6 Analysis of the state of the art

Nowadays, machinery diagnosis implementing CBM is a field of intensive research. A good CBM policy leads to the detection and prevention of faults. Companies can save millions of dollars per year and human lives with a well-implemented CM system. The need for increasing security in industrial scenarios and the rapid development of signal processing techniques and communication technologies have helped scientific and technological advancements in this field. This chapter summarizes a review of

vibration-based and audio-based automatic fault diagnosis in machinery implementing the stages of a CBM system (data acquisition, signal processing and decision-making). We have paid special attention to recent advancements in signal processing techniques and classification methods. Finally, some examples of CM systems have been presented.

Vibration-based monitoring is a well-established technique widely used in CBM [2], [3]. According to Figure 2-2, most research papers consulted for this state of the art are related to vibration-based fault diagnosis. This fact seems reasonable due to two aspects: the easiness to acquire the vibration signal from a machine and the transmission path between the machine or a component of the machine and the sensor is less affected by interferences than in the case of audio-based diagnosis. We can extract another conclusion from Figure 2-2. Most faults are related to bearings. In fact a large motor reliability survey [119] reports that 42% of the faults in large motors (more than 200 horsepower) are related to bearing faults. In small motor the percentage of faults related to faults is 90% [120]. For this reason, research efforts in condition monitoring are focused on bearing fault diagnosis. Most bearing fault diagnosis is done using vibration signal and current signal as source of information. In Figure 2-2 it is also observed that most referenced papers related to bearings use vibration signal for monitoring. Moreover, in the elaboration of this review, we carried out a search of public available databases. We have found three vibration databases public available. For all these reasons, in this Thesis, we focus the first part of our research in methods for bearing fault diagnosis and bearing fault identification using vibration signals.

Signal processing techniques have evolved from conventional time and frequency analysis, which assume stationarity and linearity, to more developed techniques that exploit the non-stationary and non-linear nature of faulty signals and of speed-up and speed down processes. These provide a more realistic description of the real condition of the machine. For this reason, in bearing application, our research aims at fault diagnosis and fault degradation using nonlinear techniques.

Audio-based monitoring has not been applied to CBM systems to the same degree as vibration-based monitoring (see Figure 2-2), even though microphones are not mounted on the machine and have greater location possibilities. The main reason is the

difficulty of recovering the machine's signature because the signal can be immersed in noise. Some authors have proposed to locate the microphone at a distance from the machine between 2cm and 20cm to avoid unwanted interferences [12]. The application of audio-fault diagnosis techniques in an extensive way will improve greatly the inspection of certain industrial environments in which a permanent CM system is expensive or the mounting of vibration sensors is difficult. For this reason, we think audio-based techniques need further research efforts and we have focused the second part of our research on audio-based fault diagnosis.

Provided the fact that there is a lack of large publicly available databases in fault diagnosis and audio signals are not an exception, we have built an experimental set in our laboratory to acquire simultaneously vibration and audio signals from a centrifugal pump working in normal condition and in different fault conditions. In this way, we obtain vibration and audio signals for different machine conditions that we use in different fault diagnosis experiments. Moreover, this database can be made public so other researchers can benefit from it. Public databases provide common data to comparatively evaluate fault diagnosis techniques and CM systems.

In this chapter, multiple features from vibration-based diagnosis are described. Most of them are not used in audio-based diagnosis. In this Thesis, we address this issue. We apply vibration features to audio signals and we make a comparison of the performance in both cases. Moreover, in the literature there are only few works related to audio and vibration signals acquired together. In this Thesis, we focus on a study of audio and vibration signals acquired simultaneously from a centrifugal pump. A set of features are extracted from both signals and classifiers are used to discriminate between different machine conditions (normal and faulty conditions).

Data fusion of multiple data is a clear research line in fault diagnosis. Multiple signals can be fusioned to obtain a more reliable diagnosis. In this Thesis, fusion of audio and vibration signals from a centrifugal pump is carried out.

2.7 References

[1] Henriquez, P., Alonso, J. B., Ferrer, M., & Travieso, C. M. (2014). Review of automatic fault diagnosis systems using audio and vibration signals. *Systems, Man, and Cybernetics: Systems, IEEE Transactions on*, *44*(5), 642-652.

[2] Vilela, R. M., Metrôlho, J. C., & Cardoso, J. C. (2004, May). Machine and industrial monitorization system by analysis of acoustic signatures. In *Electrotechnical Conference, 2004. MELECON 2004. Proceedings of the 12th IEEE Mediterranean* (Vol. 1, pp. 277-279). IEEE.

[3] Basak, D., Tiwari, A., & Das, S. P. (2006, December). Fault diagnosis and condition monitoring of electrical machines-A Review. In *Industrial Technology, 2006. ICIT 2006. IEEE International Conference on* (pp. 3061-3066). IEEE.

[4] Jardine, A. K., Lin, D., & Banjevic, D. (2006). A review on machinery diagnostics and prognostics implementing condition-based maintenance.*Mechanical systems and signal processing*, *20*(7), 1483-1510.

[5] Nandi, S., Toliyat, H., & Li, X. (2005). Condition monitoring and fault diagnosis of electrical motors-a review. *Energy Conversion, IEEE Transactions on*, *20*(4), 719-729.

[6] Vachtsevanos, G., Lewis, F. L., Roemer, M., Hess, A., and Wu, B. (2006). Intelligent Fault Diagnosis and Prognosis for Engineering Systems, 1st ed. Hoboken, New Jersey: John Wiley & Sons, Inc.

[7] Tandon, N., & Choudhury, A. (1999). A review of vibration and acoustic measurement methods for the detection of defects in rolling element bearings.*Tribology international*, *32*(8), 469-480.

[8] Doebling, S. W., Farrar, C. R., & Prime, M. B. (1998). A summary review of vibration-based damage identification methods. *Shock and vibration digest*, *30*(2), 91-105.

[9] Yang, H., Mathew, J., & Ma, L. (2003, Nov). Vibration feature extraction techniques for fault diagnosis of rotating machinery: a literature survey.In *Asia-Pacific Vibration Conference, 2003* (pp. 277-279).

[10] Shibata, K., Takahashi, A., & Shirai, T. (2000). Fault diagnosis of rotating machinery through visualisation of sound signals. *Mechanical Systems and Signal Processing*, *14*(2), 229-241.

[11] Wang, W. J., & Lin, R. M. (2003). The application of pseudo-phase portrait in machine condition monitoring. *Journal of sound and vibration*, *259*(1), 1-16.

[12] Baydar, N., & Ball, A. (2003). Detection of gear failures via vibration and acoustic signals using wavelet transform. *Mechanical Systems and Signal Processing*, *17*(4), 787-804.

[13] Shanlin, K., Peilin, P., Feng, F., & Guangbin, D. (2007, July). Feature extraction method in fault diagnosis based on wavelet fuzzy network for power system rotating machinery. In *Control Conference, 2007. CCC 2007. Chinese*(pp. 437-441). IEEE.

[14] Müller, P. C., Bajkowski, J., & Söffker, D. (1994). Chaotic motions and fault detection in a cracked rotor. *Nonlinear Dynamics*, *5*(2), 233-254.

[15] Zhong, Z. M., Chen, J., Zhong, P., & Wu, J. B. (2006). Application of the blind source separation method to feature extraction of machine sound signals. *The International Journal of Advanced Manufacturing Technology*, *28*(9-10), 855-862.

[16] McFadden, P. D., & Smith, J. D. (1984). Vibration monitoring of rolling element bearings by the high-frequency resonance technique—a review. *Tribology international*, *17*(1), 3-10.

[17] Yang, D. M., Stronach, A. F., MacConnell, P., & Penman, J. (2002). Third-order spectral techniques for the diagnosis of motor bearing condition using artificial neural networks. *Mechanical systems and signal processing*, *16*(2), 391-411.
[18] Wang, W. J., Wu, Z. T., & Chen, J. (2001). Fault identification in rotating machinery using the correlation dimension and bispectra. *Nonlinear Dynamics*,*25*(4), 383-393.
[19] Choi, Y. C., & Kim, Y. H. (2007). Fault detection in a ball bearing system using minimum variance cepstrum. *Measurement Science and Technology*, *18*(5), 1433.
[20] Peng, Z. K., Chu, F. L., & Peter, W. T. (2007). Singularity analysis of the vibration signals by means of wavelet modulus maximal method. *Mechanical Systems and Signal Processing*, *21*(2), 780-794.
[21] Peng, Z. K., Peter, W. T., & Chu, F. L. (2005). A comparison study of improved Hilbert–Huang transform and wavelet transform: application to fault diagnosis for rolling bearing. *Mechanical systems and signal processing*, *19*(5), 974-988.
[22] Logan, D. B., & Mathew, J. (1996). Using the correlation dimension for vibration fault diagnosis of rolling element bearings—II. Selection of experimental parameters. *Mechanical Systems and Signal Processing*, *10*(3), 251-264.
[23] Wang, W., Chen, J., & Wu, Z. (2000). The application of a correlation dimension in large rotating machinery fault diagnosis. *Proceedings of the Institution of Mechanical Engineers, Part C: Journal of Mechanical Engineering Science*, *214*(7), 921-930.
[24] Xinmin, T., Baoxiang, D., & Yong, X. (2007, August). Bearings fault diagnosis based on HMM and fractal dimensions spectrum. In *Mechatronics and Automation, 2007. ICMA 2007. International Conference on* (pp. 1671-1676). IEEE.
[25] Henríquez, P., Alonso, J. B., Travieso, C. M., & Ferrer, M. A. (2007, August). Advances in automatic detection of failures in electric machines using audio signals. In *Proc. of 11th IASTED Int. Conf. on Artificial Intell. and Soft Computing* (pp. 114-119).
[26] Li, L., & Qu, L. (2002, December). Machine diagnosis with independent component analysis and envelope analysis. In *Industrial Technology, 2002. IEEE ICIT'02. 2002 IEEE International Conference on* (Vol. 2, pp. 1360-1364). IEEE.
[27] Fugate, M. L., Sohn, H., Farrar, C. R. (2001). Vibration-based damage detection using statistical process control. *Mechanical Syst. and Signal Process., 15*, 707-721.
[28] Bunks, C., McCarthy, D., Al-Ani, T. (2000). Condition-based maintenance of machines using hidden Markov models. *Mechanical Syst. and Signal Process., 14*, 597-612.
[29] Li, Z., Wu, Z. , He, Y., Fulei, C. (2005). Hidden Markov model-based fault diagnostics method in speed-up and speed-down process for rotating machinery. *Mechanical Syst. and Signal Process., 19*, 329-339.
[30] Wang, W., & Wong, A. K. (2002). Autoregressive Model-Based Gear Fault Diagnosis. *J. of Vibration and Acoustics, 124*, 172-179.
[31] SAE (Society of Automotive Engineers) E-32, 2007, "Health and Usage Monitoring Metrics, Monitoring the Monitor", SAE ARP 5783-DRAFT, Feb. 14, 2007.
[32] Kurtoglu, T., Mengshoel, O., Poll, S. (2008, October). A Framework for Systematic Benchmarking of Monitoring and Diagnostic Systems. In *Int. Conf. on Prognostics and Health Management,* (pp. 1-13), Denver.
[33] Kurtoglu, T., Narasimhan, S., Poll, S., Garcia, D., Kuhn, L., de Kleer, J., Van Gemund, A., & Feldman, A. (2009). Towards a Framework for Evaluating and Comparing Diagnosis Algorithms. In *Proc. of the 20th Int. Workshop on Principles of Diagnosis (DX'09)*, Stockholm.

[34] Roemer, M. J., Dzakowic, J., Orsagh, R. F., Byington, C. S., & Vachtsevanos, G. (2005, March). Validation and Verification of Prognostic Health Management Technologies. In *IEEE Conf. Proc.*(pp. 3941-3947).
[35] Lei, Y., Zuo, M. J., He, Z., Zi, Y. (2010). A multidimensional hybrid intelligent method for gear fault diagnosis. *Expert Syst. with Appl.*, *37*, 1419-1430.
[36] Wang, X., Makis, V., Yang, M. (2010). A wavelet approach to fault diagnosis of a gearbox under varying load conditions. *J. of Sound and Vibration*, *329*, 1570–1585.
[37] Shao, Y., Mechefske, C. K. (2009). Gearbox vibration monitoring using extended Kalman filters and hypothesis tests. *J. of Sound and Vibration*, *325*, 629–648.
[38] Wang, F. L., Mechefske, C. K. (2006). Adaptive modelling of transient vibration signals. *Mechanical Syst. and Signal Process.*, *20*, 825-842.
[39] Dou, W., Liu, Z.-S., Wang, D.-H. (2007, August). Combination Diagnosis Based on Genetic Algorithm for Rotating Machinery. In *Proc. of the 3rd Int. Conf. on Natural Computation* (vol. 4, pp. 307-313). IEEE.
[40] Nelwamondo, F. V., & Marwala, T. (2006, October). Faults Detection Using Gaussian Mixture Models, Mel-Frequency Cepstral Coefficients and Kurtosis. In *IEEE Int. Conf. on Syst., Man, and Cybern.* (vol. 1, pp. 290-295), Taiwan. IEEE.
[41] Koo, I. S., Kim, W. W. (2000). The development of reactor coolant pump vibration monitoring and a diagnostic system in the nuclear power plant. *ISA Trans.*, *39*, 309-316.
[42] Lee, S. U., Robb, D., Besant, C. (2001) .The Direction Choi-Williams Distribution for the analysis of Rotor-Vibration Signals. *Mechanical Syst. and Signal Process.*, *15*(4), 789-811.
[43] Lei, Y., He, Z., Zi, Y. (2009).Application of the EEMD method to rotor fault diagnosis of rotating machinery. *Mechanical Syst. and Signal Process.*, *23*, 1327–1338.
[44] Hu, Q., He, Z., Zhang, Z., Zi, Y. (2007). Fault diagnosis of rotating machinery based on improved wavelet package transform and SVMs ensemble. *Mechanical Syst. and Signal Process.*, *21*, 688-705.
[45] Yu, G., Li, C., Kamarthi, S. (2009). Machine fault diagnosis using a cluster-based wavelet feature extraction and probabilistic neural networks. *Int. J. Adv. Manuf. Technol.*, *42*, 145–151.
[46] Yan, R. Gao, R. X. (2009). Multi-scale enveloping spectrogram for vibration analysis in bearing defect diagnosis. *Tribology Int.*, *42*, 293-302.
[47] Wang, D., Miao, Q., Kang, R. (2009). Robust health evaluation of gearbox subject to tooth failure with wavelet decomposition. *J. of Sound and Vibration*, *324*, 1141-1157.
[48] Tan, J., Gu, J. -J., Peng, X. -Z., Qin, Z. -M. (2007, August). A fault diagnosis method based on wavelet approximate entropy for fan. In *Proc. of the 6th Int. Conf. on Machine Learning and Cybern.* (pp. 519-523), Hong Kong.
[49] Yan, R., Gao, R. X. (2007). Approximate Entropy as a diagnostic tool for machine health monitoring. *Mechanical Syst. and Signal Process.*, *21*, 824-839.
[50] Li, H., Fu, L., Zhang, Y. (2009, April). Bearing Faults Diagnosis Based on Teager Energy Operator Demodulation Technique. *Int. Conf. on Meas. Technol. and Mechatronics Automation*, (pp. 594-597), Zhangjiajie, China.
[51] Janjarasjitt, S., Ocak, H., Loparo, K. A. (2008). Bearing condition diagnosis and prognosis using applied nonlinear dynamical analysis of machine vibration signal. *J. of Sound and Vibration*, *317*, 112-126.
[52] Yang, J., Zhang, Y., Zhu, Y. (2007). Intelligent fault diagnosis of rolling element bearing based on SVMs and fractal dimension. *Mechanical Syst. and Signal Process.*, *21*, 2012-2024.

[53] Singh, V., Meena, N. (2009, January). Engine Fault Diagnosis using DTW, MFCC and FFT. In *Proc. of the 1st Int. Conf. on Intelligent Human Computer Interaction*, (pp. 83-94).
[54] Mansoor, A. B., Ahmed, H., Mahmood, Z. (2009, February). Design and Development of an Automated Acoustic based Jet Engine Performance Evaluator. In *Proc. of the IEEE Int. Conf. on Industrial Technol.* (pp. 1-4).
[55] Wu, J. -D., Chuang, C. -Q. (2005). Fault diagnosis of internal combustion engines using visual dot patterns of acoustic and vibration signals. *NDT&E Int.*, *38*, 605-614.
[56] Li, W., Mechefske, C. K. (2006). Detection of Induction Motor Faults: A Comparison of Stator Current, Vibration and Acoustic Methods. *J. of Vibration and Control*, *12*(2), 165-188.
[57] Wu, J. -D., Liu, C. -H. (2009). An expert system for fault diagnosis in internal combustion engines using wavelet packet transform and neural network. *Expert Syst. with Appl.*, *36*, 4278-4286.
[58] Benko, U., Petrovcic, J., Juricic, D., Tavcar, J., Rejec, J. (2005). An approach to fault diagnosis of vacuum cleaner motors based on sound analysis. *Mechanical Syst. and Signal Process.*, *19*, 427-445.
[59] Li, W., Tsai, Y. P., Chiu, C. L. (2004). The experimental study of the expert system for diagnosing unbalances by ANN and acoustic signals. *J. of Sound and Vibration*, *272*, 69–83.
[60] Sakthivel, N. R., Sugumaran, V., & Nair, B. B. (2010). Comparison of decision tree-fuzzy and rough set-fuzzy methods for fault categorization of mono-block centrifugal pump. *Mechanical Syst. and Signal Process.*, *24*, 1887-1906.
[61] Ballal, P., Ramani, A., Middelton, M., McMurrough, C., Athamneh, A., Lee, W., & Lewis, F. (2009, March). Mechanical Fault Diagnosis using Wireless Sensor Networks and a Two-Stage Neural Network Classifier. In *IEEE Aerosp. Conf*, (pp. 1-10). IEEE.
[62] Li, Z., He, Y., Chu, F., Han, J., Hao, W. (2006). Fault recognition method for speed-up and speed-down process of rotating machinery based on independent component analysis and Factorial Hidden Markov Model. *J. of Sound and Vibration*, *291*, 60-71.
[63] Lei, Y., He, Z., Yi, Y. (2008). A new approach to intelligent fault diagnosis of rotating machinery. *Expert Syst. with Appl.*, *35*, 1593-1600.
[64] Wei, L., Pu, H. (2008, July) .Wavelet Neural Network Aided On-Line Detection and Diagnosis of Rotating Machine Fault. In *Chinese Control and Decision Conf., 2008* (pp.1868-1871). IEEE.
[65] Kar, C., Mohanty, A. R. (2004). Application of KS test in ball bearing fault diagnosis. *J. of Sound and Vibration*, *269*, 439-454.
[66] Goumas, S. K., Zervakis, M. E., & Stavrakakis, G. S. (2002). Classification of Washing Machines Vibration Signals Using Discrete Wavelet Analysis for Feature Extraction. *IEEE Trans. on Instrumentation and Meas.*, *51*(3), 497-508.
[67] Lei, Y., He, Z., Zi, Y., Chen, X. (2008). New clustering algorithm-based fault diagnosis using compensation distance evaluation technique. *Mechanical Syst. and Signal Process.*, *22*, 419-435.
[68] Pan, Y., Chen, J., Guo, L. (2009). Robust bearing performance degradation assessment method based on improved wavelet packet– support vector data description. *Mechanical Syst. and Signal Process.*, *23*, 669-681.

[69] Sanz, J., Perera, R., Huerta, C. (2007). Fault diagnosis of rotating machinery based on auto-associative neural networks and wavelet transforms. *J. of Sound and Vibration*, *302*, 981–999.
[70] Shina, H. J., Eomb, D. -H., Kim, S. -S. (2005). One-class support vector machines—an application in machine fault detection and classification. *Computers & Industrial Eng.*, *48*, 395-408.
[71] Case Western Reserve University Bearing Test Data Center. http://www.eecs.case.edu/laboratory/bearing/ (Last visited: Jan. 2014).
[72] http://qsun.eng.ua.edu/cpw_web_new/intro.htm (Last visited: Jan. 2014)
[73] MDTB Test-run Data CDs, Condition-based Maintenance Department, Applied Research Laboratory, The Pennsylvania State University.
[74] Ypma A., Ligteringen, R.P.W., Duin, E.E.E., Frietman, E.E.E. (1999). Pump vibration datasets, Pattern recognition group, Delf University of Technology.
[75] http://ti.arc.nasa.gov/tech/dash/pcoe/prognostic-data-repository/ (Last visited: Jan. 2012)
[76] Wang, W., Kanneg, D. (2009). An integrated classifier for gear system monitoring. *Mechanical Syst. and Signal Process.*, *23*, 1298-1312.
[77] Zhang, L., Yan, R., Gao, R. X., Lee, K. (2007, March). Design of a Real-time Spindle Health Monitoring and Diagnosis System Based on Open Systems Architecture. In *Int. Smart Machining Syst. Conf., France* (pp. 373-378).
[78] Cho, S., Binsaeid, S., Asfour, S. (2010). Design of multisensor fusion-based tool condition monitoring system in end milling. *Int. J. Adv. Manuf. Technol.*, *46*, 681-694.
[79] Hitchcock, L. (2006). *ISO Standards for Condition Monitoring*. *Engineering Asset Management*. Springer London, pp. 606-613.
[80] Lebold, M., McClintic, K., Campbell, R., Byington, C., Maynard, K. (2000, May). Review of Vibration Analysis Methods for Gearbox Diagnostics and Prognostics. In *Proc. of the 54th Meeting of the Society for Machinery Failure Prevention Technol.*(Vol. 643, p. 16).
[81] Rafiee, J., Rafiee, M. A., Tse, P. W. (2010). Application of mother wavelet functions for automatic gear and bearing fault diagnosis. *Expert Syst. with Appl.*, *37*, 4568-4579.
[82] Farrar, C. R., Duffey, T. A., Doebling, S. W., Nix, D. A. (1999, September). A Statistical Pattern Recognition Paradigm for Vibration-Based Structural Health Monitoring. *Structural Health Monitoring*, *2000*, 764-773.
[83] Tandon, N. (1994). A comparison of some vibration parameters for the condition monitoring of rolling element bearings. *Meas.*, *12*, 285-289.
[84] Bouillaut, L., Sidahmed, M. (2001).Cyclostationary approach and bilinear approach: Comparison, applications to early diagnosis for helicopter gearbox and classification method based on hocs. *Mechanical Syst. and Signal Process.*, *15*, 923-943.
[85] Wu, S.-j., Gebraeel, N., Lawley, M. A. & Yih, Y. (2007). A Neural Network Integrated Decision Support System for Condition-Based Optimal Predictive Maintenance Policy. *IEEE Trans. On Syst., Man and Cybern.-Part A: Syst. and Humans*, *37*, 226-236.
[86] Albarbar, A., Gu, F., Ball, A. D. (2010). Diesel engine fuel injection monitoring using acoustic measurements and independent component analysis. *Meas.*, *43*(10), 1376-1386.
[87] Devi S., Siva Kumar, Dr. L., Shanker N. R., & Prabakaran, K. (2010). A Comparative Study between Vibration and Acoustic Signals in HTC Cooling Pump and Chilling Pump. *Int. J. of Eng. and Technol.*, *2*.

[88] Al Thobiani, A., Gu, F. , & Ball, A. (2010, June). The monitoring of cavitation in centrifugal pumps based on the analysis of vibro-acoustic measurements. In *CM 2010 and MFPT 2010*, UK.
[89] Wang, W. (2008). An Enhanced Diagnostic System for Gear System Monitoring. *IEEE Trans. on Syst., Man, and Cybern.-Part B: Cybern.*, vol. *38*(1), 102-112.
[90] Todd, M., McArthur, S. D. J., McDonald, J. R., & Shaw, S. J. (2007). A Semiautomatic Approach to Deriving Turbine Generator Diagnostic Knowledge. *IEEE Trans. on Syst., Man, and Cybern.-Part C: Appl. and Reviews*, *37*(5).
[91] Mu, T., & Nandi, A. K. (2009). Multiclass Classification Based on Extended Support Vector Data Description. *IEEE Trans. on Syst., Man, and Cybern.-Part B: Cybern.*, *39*(5), 1206-1216.
[92] Chen, Z. (2010, May). Fault Diagnosis of Gear Box Based on Information Entropy. *Control and Decision Conference* (pp. 1239-1242).
[93] Kankar, P. K., Sharma, S. C., Harsha, S. P. (2011). Fault diagnosis of ball bearings using machine learning methods. *Expert Syst. with Appl., 38*, 1876-1886.
[94] Wang, Y. , He, Z., Zi, Y. (2010). Enhancement of signal denoising and multiple fault signatures detecting in rotating machinery using dual-tree complex wavelet transform. *Mechanical Syst. and Signal Process., 24*, 119-137.
[95] Li, P., He, Q., & Kong, F. (2010, June). An Approach for Fault Diagnosis of Bearings Using Wavelet-Based Fractal Analysis. In *Proc. of the IEEE Int. Conf. on Information and Automation* (pp. 2338-2343). IEEE.
[96] Fu, L., Li, H., Wang, Y. (2009, April). Application of Bi-cepstrum Analysis to Gear Fault Detection and Diagnosis. In *2009 Int. Conf. on Meas. Technol. and Mechatronics Automation* (pp. 590-593).
[97] Rivas, E., Burgos, J. C., & García-Prada, J. C. (2010). Vibration Analysis Using Envelope Wavelet for Detecting Faults in the OLTC Tap Selector. *IEEE Trans. on Power Delivery*, *25*(3) 3,1629-1636.
[98] Delvecchio, S., D'Elia, G., Mucchi, E., Dalpiaz, G. (2010). Advanced Signal Processing Tools for the Vibratory Surveillance of Assembly Faults in Diesel Engine Cold Tests. *J. of Vibration and Acoustics*, *132*(2), 021008.
[99] Cheng, J., Yang, Y., Yu, D. (2010). The envelope order spectrum based on generalized demodulation time–frequency analysis and its application to gear fault diagnosis. *Mechanical Syst. and Signal Process., 24*, 508-521.
[100] Junsheng, C., Dejie, Y., & Yu, Y.(2007). The application of energy operator demodulation approach based on EMD in machinery fault diagnosis. *Mechanical Syst. and Signal Process., 21*, 668-677.
[101] Sugumaran, V., Muralidharan, V., Ramachandran, K.I. (2007). Feature selection using Decision Tree and classification through Proximal Support Vector Machine for fault diagnostics of roller bearing. *Mechanical Syst. and Signal Process., 21*, 930-942.
[102] Yang, M., Makis, V. (2010). ARX model-based gearbox fault detection and localization under varying load conditions. *J. of Sound and Vibration*, *329*, 5209-5221.
[103] Wang, H., Chen, P., Fujioka, S., Wang, S., Li, K. (2010, March). Diagnosis Method Based on Skewness Wave and Information Divergence for a Diesel Engine. In *Asia-Pacific Conf. of Power and Energy Eng.*(pp. 1-4), Chengdu, China.
[104] Antoni, J., Randall, R. B. (2006). The spectral kurtosis: application to the vibratory surveillance and diagnostics of rotating machines. *Mechanical Syst. and Signal Process., 20*, 308-331.

[105] Barszcz, T., Randall, R. B. (2009). Application of spectral kurtosis for detection of a tooth crack in the planetary gear of a wind turbine. *Mechanical Syst. and Signal Process.*, *23*, 1352-1365.
[106] Qin, Y., Qin, S., & Mao, Y. (2008). Research on iterated Hilbert transform and its application in mechanical fault diagnosis. *Mechanical Systems and Signal Processing*, *22*(8), 1967-1980.
[107] Li, B., Zhang, P. L., Liu, D. S., Mi, S. S., Ren, G. Q., & Tian, H. (2011). Feature extraction for rolling element bearing fault diagnosis utilizing generalized S transform and two-dimensional non-negative matrix factorization. *Journal of Sound and Vibration*, *330*(10), 2388-2399.
[108] Zhou, R., Bao, W., Li, N., Huang, X., & Yu, D. (2010). Mechanical equipment fault diagnosis based on redundant second generation wavelet packet transform. *Digital signal processing*, *20*(1), 276-288.
[109] Li, M., Xu, J., Yang, J., Yang, D., & Wang, D. (2009). Multiple manifolds analysis and its application to fault diagnosis. *Mechanical systems and signal processing*, *23*(8), 2500-2509.
[110] Wang, Y., He, Z., & Zi, Y. (2009). A demodulation method based on improved local mean decomposition and its application in rub-impact fault diagnosis.*Measurement Science and Technology*, *20*(2), 025704.
[111] Hongkai, J., Zhengjia, H., Chendong, D., & Peng, C. (2006). Gearbox fault diagnosis using adaptive redundant lifting scheme. *Mechanical Systems and Signal Processing*, *20*(8), 1992-2006.
[112] Sun, X. L. (2012, February). A new method of fault diagnosis with soft set theory. In *Advanced Materials Research* (Vol. 383, pp. 7470-7474).
[113] Wang, W. (2008). An intelligent system for machinery condition monitoring.*Fuzzy Systems, IEEE Transactions on*, *16*(1), 110-122.
[114] Wang, D., Peter, W. T., & Tsui, K. L. (2013). An enhanced Kurtogram method for fault diagnosis of rolling element bearings. *Mechanical Systems and Signal Processing*, 35(1), 176-199.
[115] Moosavian, A., Khazaee, M., Ahmadi, H., Khazaee, M., & Najafi, G. (2015). Fault diagnosis and classification of water pump using adaptive neuro-fuzzy inference system based on vibration signals. *Structural Health Monitoring*,14(5), 402-410.
[116] Tiwari, R., Gupta, V. K., & Kankar, P. K. (2015). Bearing fault diagnosis based on multi-scale permutation entropy and adaptive neuro fuzzy classifier. *Journal of Vibration and Control*, 21(3), 461-467.
[117] Ali, J. B., Fnaiech, N., Saidi, L., Chebel-Morello, B., & Fnaiech, F. (2015). Application of empirical mode decomposition and artificial neural network for automatic bearing fault diagnosis based on vibration signals. *Applied Acoustics*, 89, 16-27.
[118] Muralidharan, V., Sugumaran, V., & Indira, V. (2014). Fault diagnosis of monoblock centrifugal pump using SVM. *Engineering Science and Technology, an International Journal*, *17*(3), 152-157.
[119] Bell, R.N., McWilliams, D.W., O'Donnell, P., Singh, C., & Wells, S. J. (1985). Report of large motor reliability survey of industrial and commercial installations Part I and II. *IEEE Transactions on Industry Applications*, *21*(4), 853-872.
[120] Immovilli, F., Bellini, A., Rubini, R., & Tassoni, C. (2010). Diagnosis of bearing faults in induction machines by vibration or current signals: A critical comparison. *IEEE Transactions on Industry Applications*, *46*(4), 1350-1359.

CHAPTER 3
Databases: bearings and pumps

This Chapter focuses on the databases collected and generated in this Thesis for bearing and pump condition monitoring. The Chapter is divided into two subsections. The first one is devoted to public vibration bearing databases and the second one to the audio and vibration pump database generated in this Thesis. The basic concepts of bearings and centrifugal pumps are also explained in each respective subsection.

3.1 Bearing Vibration Data

The Oxford English Dictionary defines a bearing ‘‘as a part of a machine that allows one part to rotate or move in contact with another part with as little friction as possible’’. Additional functions include the transmission of loads and enabling the accurate location of components [21].

Bearings are vital components in a great range of machinery since they support the rotating structures and facilitate their rotation. They dominate the performance of the machine and maintenance programs are usually timed according to the bearings. Bearing problems can result in costly downtime, equipment damage and breakdowns.

Establishing and following a preventive maintenance program is a key factor in guaranteeing long bearing service hours and minimizing equipment downtime.

3.1.1 Faults in Rolling Bearing

A rolling-element bearing consists of four components: an outer ring, an inner ring, the rolling elements (balls or rollers) and a cage. The rings form the raceway. The rolling elements are several balls or rollers contained in the space between the outer race and the inner race and the cage is used to fix the position of the rolling elements. In most applications, the outer race is generally stationary and the inner race is attached to the rotating assembly such as a shaft. As one of the bearing races rotates it causes the rolling elements to rotate as well with low resistance. Because the balls are rolling they have a much lower coefficient of friction than if two flat surfaces were sliding against each other. Figure 3-1 shows the components of a rolling-element bearing with balls (a ball bearing).

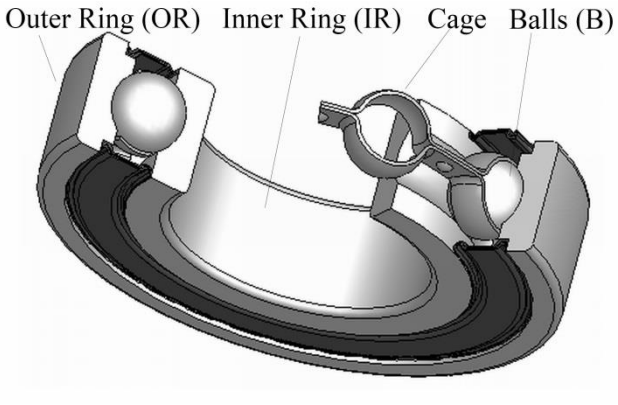

Figure 3-1: Components of a ball bearing

Bearing defects can be divided into distributed and discrete defects [24]. Distributed defects are due to the progressive growing of surface wear or to low-quality manufacturing process [25]. Discrete defects, localized defects or single-point defects are localized areas of damages in the rolling surfaces of the bearing. They are characterised by sharp discontinuities in the rolling surface producing impulsive-like vibrations [24]. The presence of a discrete defect in a bearing can be indicative of incipient failure. As such, bearing research and vibration monitoring programmes for rolling element bearings are concerned principally with the detection of discrete faults.

The main discrete defects in bearings are the outer-race fault (OR), inner-race fault (IR) and ball fault (B), which are faults located in the outer-race, in the inner-race and in the balls (or rollers) respectively. All bearings, even free-fault bearings, produce noise as the rolling-elements roll over the races. This noise is generated at high frequency and low amplitude. The bearing housing amplifies the noise and a transducer such an accelerometer can acquire the signal produced by the bearing transformed by the transmission path. Vibration signals generated by bearings with discrete faults produce a distinct bearing signature. As the rolling element strikes a discrete fault on the inner or outer race or when a fault on a rolling element strikes the inner or outer race an impulse is produced, which excites the supporting structure between the bearing and the transducer. These impulses appear as a very sharp rise that corresponds to the impact between a roller and the defect. Then, the impulse decays with an approximately exponential envelope as the energy is dissipated by the internal damping. The impact frequencies are called characteristic bearing frequencies and can be determined by the geometry of the bearing and the rotation frequency of the shaft [22]. During bearing running, the impulses are further modulated in amplitude by two factors: i) the transfer function of the transmission path varies due to the fault position change in relation to the position of the transducer; ii) the strengths of the impulses change due to a non-homegeneous load distribution. The bearing components support load as they pass the lower half of the bearing, i.e. the load zone. The strength of the impulses will be higher in the load zone and lower in the non-load zone [26]. Therefore, a low-frequency envelope is generated. See Figure 3-2, extracted from [26], where the typical acceleration signals produced by discrete faults in the different components of the bearing are shown. The dotted line is the low-frequency envelope. This phenomenom appears in the case of inner-race or ball faults. The inner-race fault pass through the load zone at the shaft frequency and the rolling elements pass through the load zone at the fundamental cage frequency, i.e. the cage frequency. Usually, the outer race of the bearing is fixed and it is not affected by the non-homogeneous load distribution. In the vibration bearing signal acquired by the transducer there is also noise.

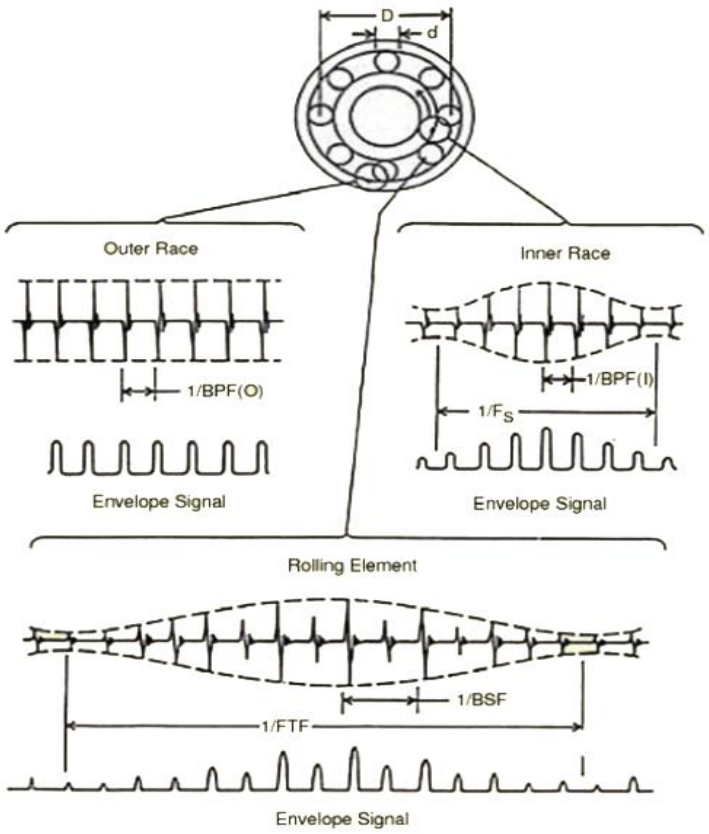

Figure 3-2: Bearing vibration signals of bearings with discrete faults at outer race, inner race and ball. BPFO = ball pass frequency, outer race, BPFI = ball pass frequency, inner race, BSF = ball spin frequency, FTF: fundamental train frequency (cage frequency). Source: [26].

Therefore, a model for a faulty bearing comprises the pulse sequence generated by the interaction of the fault with the surface ($x_{ps}(t)$), the non-homegeneous load distribution causing a low-amplitude modulation to the pulses ($x_l(t)$), then the natural frequencies excited by the pulses ($x_{tp}(t)$) and noise ($n(t)$).

$$x(t) = [x_{ps}(t)x_l(t)] * x_{tp}(t) + n(t) \qquad \text{[Eq. 3-1]}$$

For the fault-free bearing with no pulse sequence generated by faults, the natural frequencies are not excited. The spectrum of bearing vibration signal can have peaks at the rotation frequency and some harmonics. A free-fault bearing vibration signal can be considerer as a random sequence with low amplitude.

As a simplification, vibration signal from a bearing with a discrete fault can be considered as an amplitude modulated signal in which the carrier is the resonance frequency excited and the fundamental frequency of the modulating signal (the envelope) is the bearing characteristic frequency of the faulty bearing. In figure 3-2 the amplitude demodulated signals (the envelope) of each kind of fault is shown.

In Figure 3-3 real vibration signals of a bearing in normal condition (free-fault bearing), a bearing with inner-race defect, a bearing with outer-race defect and a bearing with ball defect are shown. The signals are from the Case Bearing Database [1]. The impulsive characteristic of the vibration signals for bearings with single point defects can be clearly seen in the figure.

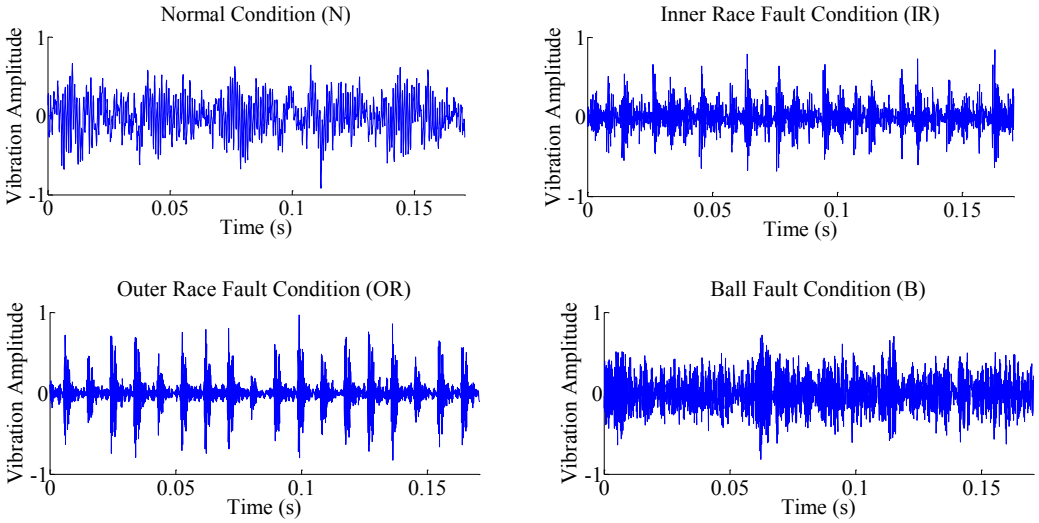

Figure 3-3: Time bearing vibration signal of 0.17 seconds (sample frequency is 12kHz) for different bearing conditions: Normal condition (upper-left), Inner race fault condition (upper-right), Outer race fault condition (bottom-left) and Ball fault condition (bottom-right).

As stated in Chapter 2, time and frequency techniques are conventional techniques to extract features from the bearing vibration signal aim to fault diagnosis or to find an index for fault evolution or for severity assessment. Features that are good indicators for impulsive faults are kurtosis, crest factor, impulse factor. In frequency domain, the popular technique of envelope analysis is used to amplitude demodulate the bearing vibration signal and obtain the bearing defect characteristic frequency. An alternative demodulation technique is based on the Teager-Kaiser energy operator. In

this Thesis, we propose to use the TEO over the raw vibration signal and to feature the result signal with time features. We also propose a methodology to assess the severity degree of a bearing with inner race fault and outer race fault. The methodology is based on wavelet packet transform and a complexity measure called Lempel-Ziv complexity. In Chapter 4 the methodology, experiments and results are shown for both proposals.

In order to evaluate the proposals in bearing fault diagnosis and bearing fault evolution, public available bearing vibration databases were collected. In the next subsection, the bearing vibration databases are described.

3.1.2 Bearing Vibration databases publicly available

The three publicly available databases collected in this Thesis in chronological order are: the Case Western Bearing Vibration Database [1] with samples of bearing vibration data in normal condition and in outer-race, inner-race and ball fault conditions; the UH-60 Blackhawk Helicopter Vibration Database [2] with vibration samples from an endurance test of an helicopter and the bearing vibration database of the Intelligent Maintenance Systems (IMS) with bearing vibration samples of a run-to-failure experiment [3].

Case Western Bearing Vibration Database

The bearing vibration data from the Case Western Reserve University [1] were collected from an accelerometer mounted on an induction motor housing at the drive-end bearing. The drive-end bearing are located at the drive-end part of the motor and supports the motor shaft.

The test stand is shown in figure 3-3. The 2 hp three-phase induction motor (left in the figure) was connected to a dynamometer (right in the figure) and a torque sensor/encoder (center in the figure) by a self-aligning coupling. The dynamometer is controlled so that desired torque load levels can be achieved. It is important to mention that the load supported by the motor affects only the rotational speed of the shaft. It does not affect the load supported by the bearing.

Faults were introduced into the drive-end 6205-2RS JEM SKF, deep groove ball bearing using the electro-discharge machining method. Faults of diameter 0.007, 0.014 and 0.021 inch (7 mills, 14 mills and 21 mills respectively) are considered, corresponding to 0.01778 cm, 0.03556 cm and 0.05334 cm respectively. The deep of the fault is 0.011 inch/ 0.02794 cm.

Vibration data was collected with an accelerometer attached to the housing with magnetic bases placed at the 12 o'clock position at the drive end. The sample frequency was 12 kHz. Speed and horsepower data were collected using the torque sensor/encoder and recorded by hand. Vibration data was recorded at four different conditions: normal (N), inner race fault (IR), outer race fault (OR) and ball fault (B). Each signal is 10 seconds. Experiments were repeated for motor loads of 0 to 3 horsepower (motor speeds varying from 1797 to 1720 RPM. The higher the load is the lower the speed). The shaft rotating frequency is about 30 Hz. Data consisted of 4 vibration signals for N condition and 12 vibration signals for each fault condition (12 IR, 12 OR and 12 B). In total there are 40 vibration signals.

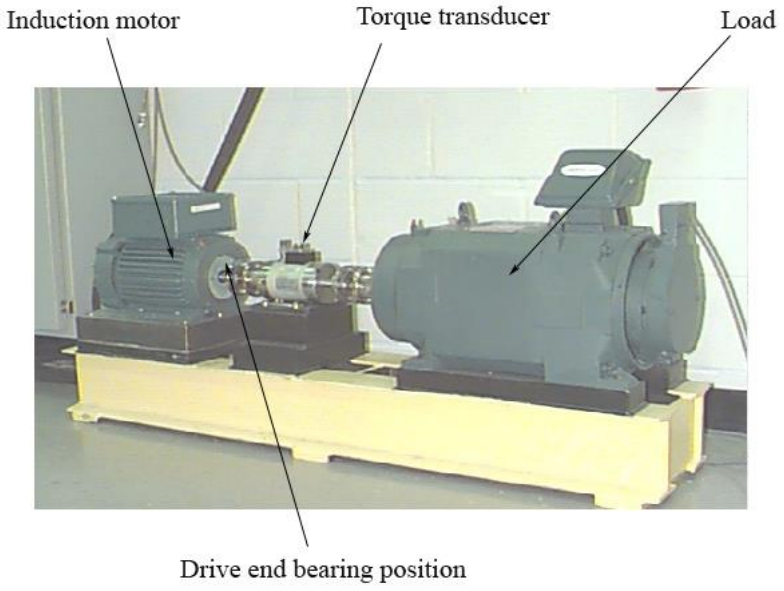

Figure 3-4: Test stand for the acquisition of bearing vibration data. Source [1].

The Case bearing vibration database was used in this Thesis for the evaluation of the following proposals: the proposal of using Teager-Kaiser energy operator to extract

statistics, energy and higher order statistics features in order to detect between IR, OR, B and normal condition in bearing fault diagnosis and the proposal of a new methodology based on wavelet package transform and Lempel Ziv complexity to the assessment of bearing severity and degradation (see Chapter 4).

UH-60 Blackhawk Helicopter Vibration Database

The UH-60 Blackhawk helicopter vibration database was recorded during a component endurance test of an UH-60 Blackhawk helicopter at Patuxent River, M.D. [2]. Figure 3-5 shows the main gearbox transmission system of the UH-60 helicopter. The gearbox transmission system translates the energy from the two engines into the main rotor and it is a complicated system.

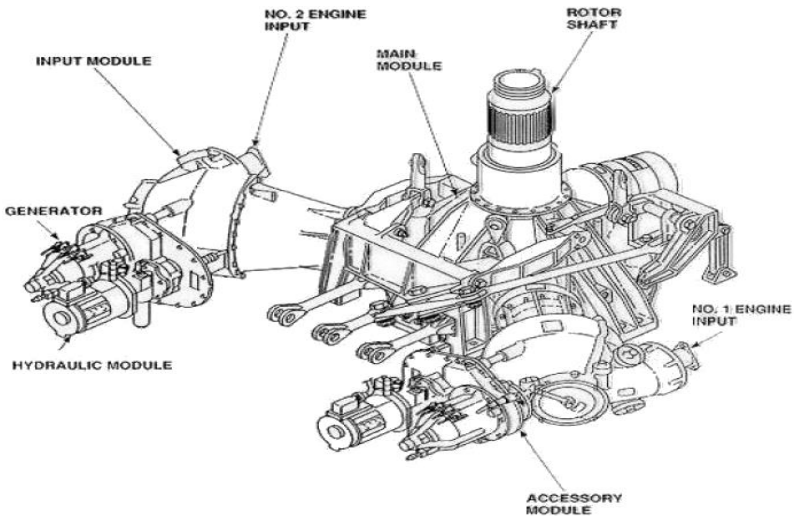

Figure 3-5: Main transmission of an UH-60 Backhawk helicopter. Source: [27].

The data sets were recorded at irregular intervals throughout the endurance tests with a sample frequency of 100kHz and only recordings at conditions within +/- 10% of full torque are used in the experiments. Vibration signals were acquired using Endevco 6259M31 accelerometers. The vibration database consists of 62 data sets of 10 seconds each.

Severe degradation of the inboard roller bearing SB-2205 occurred during the endurance test. The helicopter indicators showed chip lights (a chip light is an indicator

of the presence of metal chips or particles in the module) in the experiment. The first chip light occurred in the data set number 40, 10200 minutes after the recordings had begun. The position of bearing SB-2205, which supports the combining bevel pinion in one of the input modules, is shown in Figure 3-5 (left). As it can be seen from Figure 3-6 (left), the bearing is located deep inside the gearbox. In this position, the background noise is greater and the detection of a bearing fault is more difficult. The bearing condition at the end of the test is also shown in Figure 3-6 (right). From the figure, it can be seen a fault in the rolling element of the bearing.

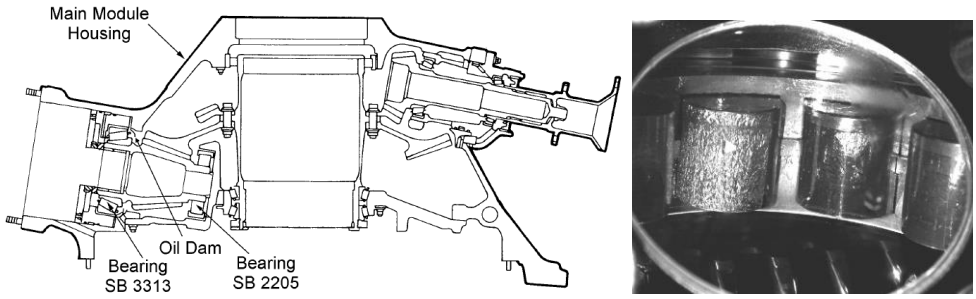

Figure 3-6: Position of the bearing SB-2205 in the transmission (left figure) and the fnal bearing condition (right figure). Source: [28].

The UH-60 Blackhawk helicopter vibration database was used in this Thesis for the evaluation of the following proposals: the proposal of using Teager-Kaiser energy operator to extract statistics, energy and higher order statistics features in order to detect between IR, OR, B and normal condition in bearing fault diagnosis and the proposal of a new methodology based on wavelet package transform and Lempel Ziv complexity to the assessment of bearing severity and degradation (see Chapter 4).

IMS Vibration Bearing Database

The IMS vibration bearing database is a bearing data set provided by the Center on Intelligent Maintenance Systems (IMS) [3]. Four bearings were installed on one shaft and two accelerometers were placed in each of them to register the vibration signals in two different spatial axes (see Figure 3-7). The shaft was driven by an AC motor and coupled by rub belts. The rotation speed was kept constant at 2000 rpm and a 6000 lb. radial load was added to the shaft and bearings by a spring mechanism. Vibration data

was collected every 10 min for 164 h with a sampling rate of 20 kHz. At the end of the test-to-failure experiment, an outer race defect was discovered on bearing 1. Captures obtained by the horizontal accelerometer of bearing 1 have been used in this Thesis for bearing degradation. According to [34], the first indication of fault is 89 hours after the beginning of the experiment.

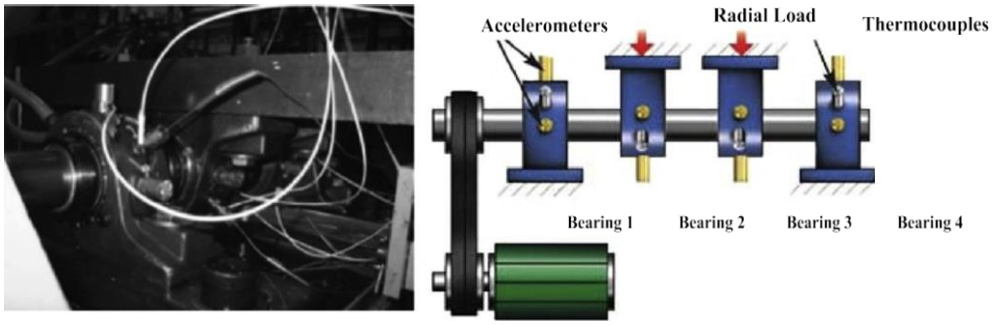

Figure 3-7: Position of the bearings in the IMS bearing database. Source: [3].

The IMS vibration bearing database was used in this Thesis for the evaluation of the following proposal: the proposal of a new methodology based on wavelet package transform and Lempel Ziv complexity to the assessment of bearing severity and degradation.

3.2 Centrifugal Pump Audio and Vibration Data

A pump is defined as a mechanical device that rotates or reciprocates to move fluid from one place to another [5]. There are multiples kinds of pumps with different applications. According to the Hydraulic Institute [6] pumps can be classified according to the manner in which the pump adds energy to the pumped fluid to generate movement into: kinetic pumps and positive displacement pumps. In this Thesis we focus on centrifugal pumps, a kind of kinetic pumps. They add energy by high-speed rotating wheels or impellers.

Pumps are important components in a wide range of technical processes such as power stations, chemical industry, cooling and heating systems, etc. The degradation of pump components such as impellers, bearings, seals or the presence of impurities or

strange objects in the fluid being pumped can reduce the pump performance and lead to faults. The overall reliability and safety of many systems depends on the health of pumps. Therefore, pump condition monitoring plays a key role in maintenance procedures.

3.2.1 Elements and working of a centrifugal pump

A centrifugal pump consists of two main components: 1) the rotary element or impeller and 2) the stationary element or casing (called volute). The impeller is the rotating part that converts driver energy (i.e. the energy of a motor) into the kinetic energy. Rotation of the impeller forces the fluid (usually liquid) to circulate through the pump from the axial to the radial direction while energy is transferred to the fluid [7]. The volute is the stationary part that converts the kinetic energy into pressure energy. Summing up, the impeller produces fluid velocity and the volute converts velocity to pressure.

Figure 3-8 shows the components of a centrifugal pump. The direction of the fluid in a centrifugal pump (left) and the zones of velocity and pressure of the fluid when passing through the centrifugal pump (right) are also shown. The fluid enters in the suction eye (attached to the inlet part or suction part of the pump) for the inlet side (suction side), then pass through the impeller and finally exits in the outlet (discharge) side of the pump.

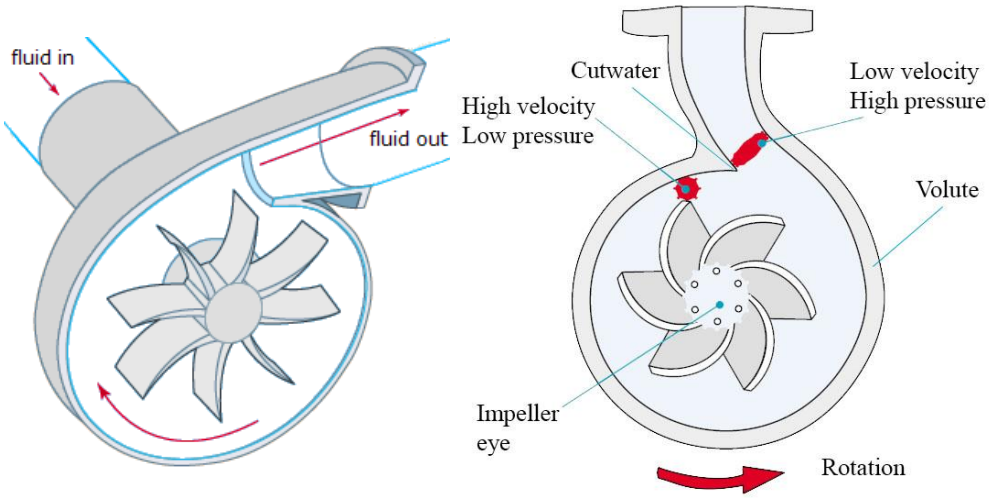

Figure 3-8: Left: Fluid direction in a centrifugal pump. Source: [6]. Right: velocity and pressure in a centrifugal pump. Modified from source: [5]. The inlet, outlet, volute and impeller are shown.

An impeller has a number of channels or vanes delimited by curved blades. A closed impeller (see Figure 3-9) has plates on both sides called hub plate and shroud plate that totally enclose the impeller from the suction eye to its edges. The hub plate is in the front of the impeller (where the impeller is connected to the rotor) and the shroud plate is in the rear of the impeller (in the impeller eye area). The impeller also has several blades (also called vanes) to impart the centrifugal force to the fluid. The center of the impeller is called the impeller eye. The region near the impeller eye is called vane leading edge (LED). The region at the tip of the vane is called vane trailing edge (TED) [14].

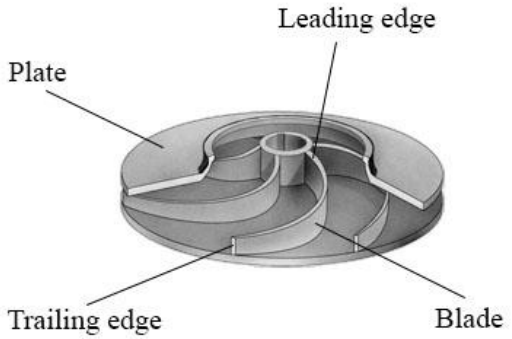

Figure 3-9: Closed impeller. Modified from source: [6].

A more detailed description of how the fluid passess through a centrifugal pump is described next [5].

1. Fluid flows through the pump by first entering the inlet side. Then the fluid enters the lowest pressure area in the pump, the impeller eye.

2. From here the fluid is picked up by the spinning impeller vanes. The fluid passes along the vanes where velocity and energy are added to it. The amount of energy given to the fluid is proportional to the velocity at the edge or vane tip of the impeller. The faster the impeller rotates or the bigger the impeller is, then the higher will be the velocity of the fluid at the vane tip and the greater the energy imparted to the fluid.

3. Through centrifugal force, the fluid is thrown to the outside tips of the impeller, against the volute and toward the discharge flange. At this point, because the fluid is confined by the volute, the velocity decreases thereby increasing the pressure. The fluid

velocity is decreasing because the volute is shaped in such a way that the impeller is not centered inside it. Rather, the impeller is offset from the center. This offset causes the impeller to volute clearance to increase from the cutwater to the discharge area. As the clearance increases the velocity decreases and the pressure increases.

4. Then the fluid moves through the inside edge of the volute to the discharge flange where it exits the pump at a higher pressure. The velocity of the fluid is converted to pressure according to Bernoulli's principle (Bernoulli's Principle states that as the speed of a moving fluid increases, the pressure within the fluid decreases).

Other parts of a centrifugal pump are the pump shaft, bearings, shaft seal, the wear rings, and the inlet and outlet. The shaft seal stops the fluid from leaking out of the casing. The wear rings separate the high and low pressure areas inside the casing. The bearings make the shaft turn easier. The inlet and outlet parts of the casing connect to the fluid piping system. The sealing device is placed inside the stuffing box to control or eliminate leakage from the pump casing.

3.2.2 Vibroacoustic mechanism in a centrifugal pump

The pump vibro-acoustics is generated by the following sources: hydraulics sources and mechanical sources [16], [18]. Both sources cause vibrations which make the pump structure vibrate. This vibration radiates airborne sound. Therefore, the acoustics of the pump has the same mechanism of production that the vibration mechanism [18].

Hydraulics sources are caused by the fluid-structure interaction with impeller vanes and volute (especially volute cutwater) and by flow perturbations.

Mechanical sources are caused by vibration of unbalanced rotating masses and friction in bearings, seals, impeller and shaft [16].

During the working process of a centrifugal pump non-steady fluid-dynamic forces may produce either discrete or broad-band frequencies in vibration and acoustic signals [8], [15], [16], [18]. The discrete frequencies are: the rotation frequency (RF), the vane-passing frequency (rotor frequency multiplied by the number of vanes or

blades of the impeller) and their harmonics. The rotation frequency is present due to pressure pulsation (fluctuations in the pressure being developed by the pump) caused by impeller imbalance [19] (when the impeller has an orbital motion coupled to the rotation [8]) and also by small manufacturing imperfections in the impeller [8]. The vane-passing frequency (VPF) is due to the finite thickness of the blades which causes flow disturbances associated with the passage of each blade near the cutwear or volute tongue [8]. A pressure pulse is developed as each vane passess the cutwater.

Broad-band fluid-dynamic excitation is due to pressure pulsations generated by flow turbulence, viscous forces, boundary layer vortex shedding, boundary layer interaction between a higher-velocity and lower velocity regions of the process fluid, and by vortices generated in the clearances between the rotor of the centrifugal pump and the adjacent stationary part of the casing [18]. Mechanical sources such as noise from the rotation of the pump shaft and bearings also contribute to broad-band vibration content. Broad-band content is always present due to turbulence [8].

Other perturbations not related directly with the pump itself can also exist, such as an obstacle or obstruction in the pump inlet, in the pump outlet or even inside the impeller [8]. Other frequencies generated may be related to fan frequency of the motor, motor frequencies or frequencies related to other part of the system in which the pump is operating.

In normal condition, the frequencies that dominate the spectrum are the discrete frequencies (RF and VPF and their harmonics). Although broadband noise is always present, in normal condition it has a minimum value. When some of the components of the centrifugal pump have a fault, other frequency components can appear, the previously mentioned frequency can increase, decrease in amplitude or even can dissapear. The broadband noise may also increase and dominate the spectra due to the presence of faults in the pump (such as cavitation for example).

3.2.3 Main faults in a centrifugal pump

The main faults in pumps are associated with impeller damages [9], [10], rotor faults, seals faults, cavitation [11] and bearing faults [11], [12]. A classification of the main

faults in a centrifugal pump might be done according to the component affected by the fault into electrical faults, mechanical faults and hydraulic faults. The electrical faults are associated with the pump motor, mechanical faults are associated with bearings and shaft and hydraulic faults are associated to hydraulic parts of the centrifugal pump. In this Thesis, we have focused on hydraulic faults. The hydraulic parts of the centrifugal pump are the impeller, the blades, the volute, the inlet and the outlet. The functionality of the hydraulic parts is to convert mechanical energy from the shaft to hydraulic energy induced into the liquid pumped by the pump [17].

The **hydraulics faults** are produced in the impeller, the blades and the volute. The hydraulics faults associated with them are: dry running, impurities fixed on the impeller (causing inbalance), wear of the impeller (leading edge fault, trailing edge fault), blocked or partial blocked flow field inside the impeller, blocked impeller rotation, wear of the sealing ring, missing sealing ring, loss of the impeller, cavitation, instability, rotating stall and pressure pulsations [13], [18], [19], [20]. The main effects of these faults are changes in the value of pressure and the load torque generated by the impeller at a given flow. Moreover some of the faults can induce pressure oscillations. These pressure oscillations can be either harmonics of the rotational frequency, or noise like signals covering a larger frequency span. Cavitation may produce the wear of impellers and piping system.

The inlet and the outlet part of the pump and the pump system can be considered apart. The faults in the inlet part of the pump are low pressure and obstruction at the inlet pump. The main effect of these faults is that the inlet pressure to the impeller becomes too low. The faults in the outlet part of the pump include leakage on the outlet pipe and obstruction of the outlet pipe. The main effects of these faults are leakages from the system and decreased pressure produced by the pump.

3.2.4 Considered Faults in a centrifugal pump in this Thesis

In this Thesis, we focus on impeller-related faults (leading edge damage, trailing edge damage and plate damage), system faults and seal fault.

Impeller-related faults were artificially created cutting the leading edge of all vanes for the leading edge fault and cutting the trailing edge of all vanes for the trailing edge fault [14]. The plate fault was created removing part of the plate. There are certain flow phenomena that occur in the fluid flow when it enters the inlet part of the pump, pass through the impeller and the volute up to the outlet part of the pump. The modification of the impeller geometry affects the flow patterns inside the centrifugal pump. When plate damage, trailing edge damage or leading edge damage occur flow pattern changes [13], [14], [19], [20]. These flow pattern changes affect mainly VPF and their harmonics [13]. They can also produce broadband noise due to the vortices generated in the clearances between the impeller and the volute [18]. The mechanism of production of flow patterns inside the pump is not very well understood yet [19] and this subject is outside the scope of this Thesis.

The system faults considered in this Thesis consist in the addition of strange obtjects and impurities to the fluid such as PVC (polyvinyl chloride) balls, sand, sand and paper. This can lead to partial obstruction of the piping system, producing low flow rate and the generation of turbulence (broadband) noise [8], [15]. The addition of impurities can produce degradation of the pump itself in long term.

3.2.5 Audio and Vibration Database acquisition from a centrifugal pump

In order to study audio and vibration signals simultaneously, we have recorded vibration and audio samples from a circulating centrifugal pump in an experimental test rig. This subsection describes the acquisition process of the database and the database generated.

A circulating centrifugal pump is a pump designed to circulate a fluid through a closed system. A closed system is one which runs in a loop, with the pump discharge line eventually returning back to the pump suction. The pump works like any centrifugal pump, except they only need to overcome the friction of the piping system. Circulation pumps are primarily used for circulation of water in closed systems e.g. heating, cooling and air conditioning systems as well as domestic hot water systems and in applications that require chemicals to be regularly mixed into the fluid, such as pool and spa pumps.

3.2.5.1 Acquisition system

A diagram of the acquisition system is shown in Figure 3-10.

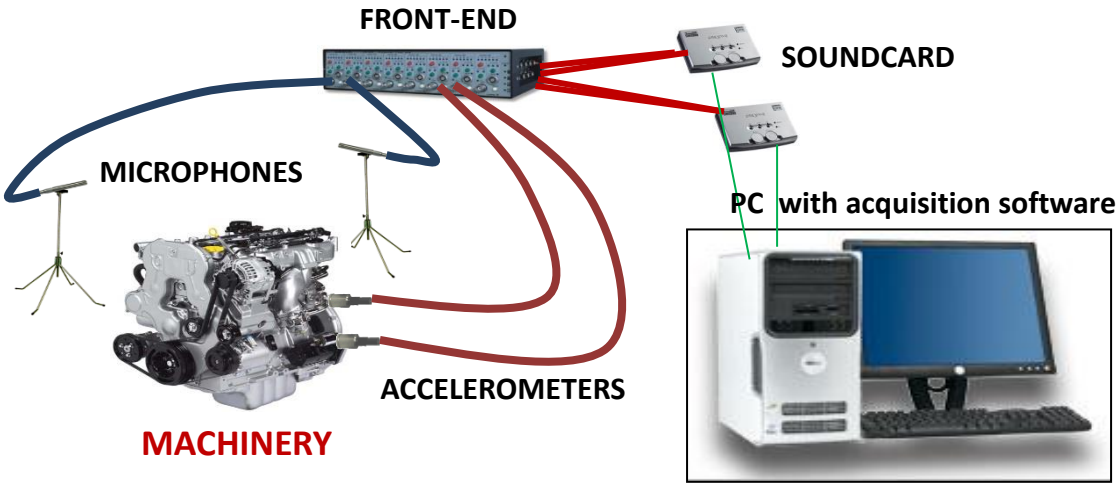

Figure 3-10: Diagram with the components of the acquisition system

The acquisition system consists of two microphones and two accelerometers connected to a front-end. The outputs of the front-end are connected to the Line-In input to two soundcards. The soundcards are connected to a PC with an acquisition software [23]. The characteristics of the sensors, the front-end and the soundcards are shown in Table 3-1 and Table 3-2.

TABLE 3-1: CHARACTERITICS OF AUDIO AND VIBRATION SENSORS

	Microphones	**Accelerometers**	
Model	CESVA PA25/C-250Preamplifier (PA-25) + ½" Prepolarised condenser microphone(C-250)	CESVA AC001	CESVA AC006
Frequency range	C-250 (re 1 kHz): 3.15Hz-20kHz (±2dB) (pressure or omnidirectional microphone)	0.7-10kHz (±10%)	0.35-2.6kHz (±10%)
Sensitivity	(1kHz): 50mV/Pa	100 mV/g	1000 mV/g

TABLE 3-2: CHARACTERITICS OF FRONT-END AND SOUND CARDS

	Front-end	**Sound Cards**
Model	CESVA FC-822	Sound Blaster Audigy 2NX
Characteristics	.8 input/output channels, .possibility of connecting microphone or accelerometers .adjustable gain .low-pass and high-pass filters .Inputs Band width: 0.3Hz–20kHz	.USB port .Line-in .Mic-in .Up to 96kHz (24-bits)

The audio and vibration samples were collected with a multichannel acquisition software. This system is able to record signals from different soundcards without cuts, in a continuous way and for large periods of time [23]. The sample frequency of the recording system was set to 44100 Hz.

3.2.5.2 Characteristics of the pump

A centrifugal circulating pump with in-line connections and dry rotor (ALP800, brand DAB) is used to acquire audio and vibration signals. The diagram of the pump is shown in Figure 3-11 and the measurements of the pump in Table 3-3. The main characteristics of the circulating pump are shown in Table 3-4.

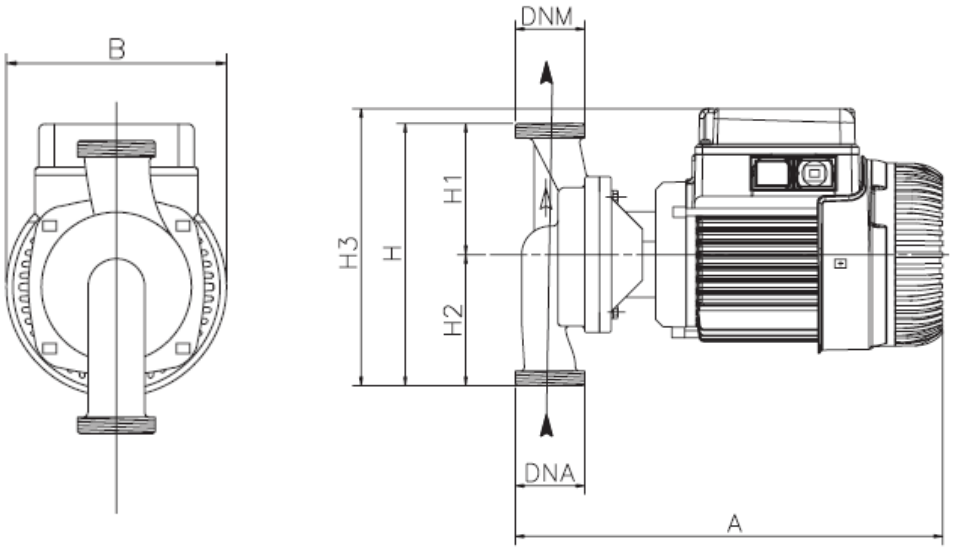

Figure 3-11: Diagram of the ALP800 pump

TABLE 3-3: MEASUREMENTS OF THE PUMP ALP800

PUMP MEASUREMENTS									
A	B	H	H1	H2	H3	DNA NPT*	DNM NPT*	Volume (m3)	Weight (Kg)
300	136	180	90	90	190	11/2" G-M (3.81 cm)	11/2" G-M (3.81 cm)	0.017	7.5

*NPT: American Standard Pipe Taper Thread.

TABLE 3-4: MAIN CHARACTERITICS OF THE PUMP ALP800

Type of motor	Induction motor, two-pole (single-phase)
RPM	**2925 (= 48.75 Hz)**
P2 Nominal Power (kW)	0.37 kW (0.5 HP)
Tension (50 Hz)	220-240 V
Current	1.4 A
Horse Power	0.5 HP
Pumped fluids	The machine has been designed and built for pumping water, clean, free from solids or abrasive substances, non viscous, non aggressive, non crystallized, chemically neutral, close to the characteristics of water
Maximum working pressure	10 Bar (1000 Kpa)
Liquid temperature range	-15ºC to +120ºC
Standard apertures	Unflanged, 1 1/2" M GAS
Maximum ambient temperature	+40 ºC
Relativity humidity of the air	Max. 95%
Insulation class	F
Working Range	From 0,6 to 8,4 m3/ with head up to 21 metres
Motor Protection	IP55
Installation	With motor in a horizontal position
Material of pump body and motor support	Bronze

The impeller and seal characteristics of the pump are also shown in Table 3-5 and Table 3-6 respectively.

TABLE 3-5: IMPELLER CHARACTERITICS OF PUMP ALP800

Impeller characteristics					
Material	Plate Diameter	Plate Circunference	Number of vanes	Vanes Length	Vane-passing frequency
Technopolymer	8 cm	25 cm	7	5 cm	341.25 Hz (7 vanes x 48.75 Hz)

TABLE 3-6: SEAL CHARACTERITICS OF PUMP ALP800

O-ring Seal characteristics			
Type	Material	Diameter	Height
O-ring	Carbon/Ceramics	2 cm	50 mm

Figure 3-12 shows two different views of the pump casing, the volute and the inlet and outlet part of the pump. In Figure 3-13 the casing is dissambled and the impeller mounted on the rotor is shown (left part of Figure 3-13). The right part of Figure 3-13 shows the volute with the inlet and outlet part of the pump. Figure 3-14 shows a different view of the impeller mounted on the rotor and two views of the impeller.

Figure 3-12: Two photos of the ALP 800 pump.

Figure 3-13: Photos of the pump ALP 800. Impeller mounted on the rotor (left). Volute, inlet and oulet pump (right).

Figure 3-14: Photos of the pump ALP 800. Impeller mounted on the rotor (left). Different views of the impeller (center and right).

3.2.5.3 Conditions recorded and Generation of faults

In this Thesis, we consider faults associated to the impellers (plate faults, leading edge fault and trailing edge fault), seal fault and system faults.

Four different impellers were used in the experiments. Table 3-7 shows the impellers used and the faults created in the impeller or in the pump system for each impeller.

For impeller 1, faults in the plates of impeller were created. Then, the impeller 1 was replaced by a free-fault impeller (impeller 2) and a spontaneous seal fault was detected. After detecting this fault, the seal was replaced. Then, a set of different objects and materials including sand, paper and PVC balls were added to the water in the tank in order to simulate system faults. For impeller 3, faults in the leading edge of the impeller were created. Finally, for impeller 4, faults in the trailing edge of the impeller were considered. For each impeller, normal (free-fault) condition was also recorded.

TABLE 3-7: IMPELLERS AND CONDITIONS

Impeller #	**Conditions Recorded**
Impeller 1	Normal/Plate Fault
Impeller 2	Normal/Seal Fault and System Fault
Impeller 3	Normal/Leading Edge fault
Impeller 4	Normal/Trailing Edge fault

The generation of each fault is described in this subsection: impeller-related faults, seal fault and system faults.

Plate Fault

Three different parts of the impeller plate were removed. The first part was removed from the hub plate (the plate of the impeller front, the plate facing the rotor). The second part was removed from the shroud plate in the opposite position from the first part. The third part was removed from the hub plate just side by side the second part removed. This fault simulates a broken impeller due to a crack present in the impeller.

Figure 3-15 shows the impeller in normal condition and the impeller with part of the plates removed.

Figure 3-15: Photos of the plate fault in impeller. Upper left: impeller in normal condition. Upper right: one part of the plate removed. Lower left: two parts of the plate are removed. Lower right: the third part of the impeller was removed.

Leading Edge Fault

The leading edge fault (LED) consists in removing part of the vane leading edge (the region near the impeller eye) of all vanes. Three different lenghts were used. Table 3-8 shows the original length of the vane and the millimeters of vane removed. This fault simulates the degradation of impellers along time due to particles or impurities that can

be in the water. Figure 3-16 shows the impeller used for LED fault with 5mm of vane leading edge removed from all vanes.

TABLE 3-8: SEVERITY OF LEADING EDGE FAULTS

Fault Severity	Length vane reduction	Length of the remaining vane
None	0	50 mm
Slight (LED5)	10% of the total length = 5mm	50mm - 5mm = 45 mm
Medium (LED10)	20% of the total length = 10mm	50mm - 10mm = 40 mm
Severe (LED15)	30% of the total length = 15mm	50mm - 15mm = 35 mm

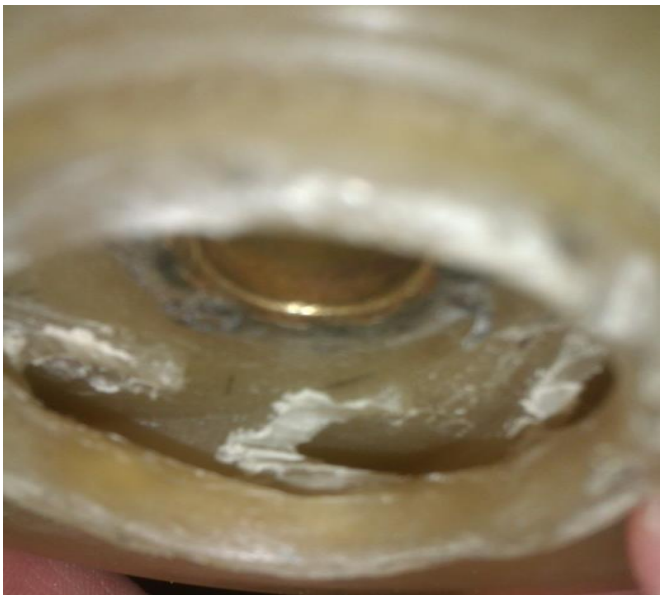

Figure 3-16: Photo of the impeller with leading edge fault. In this case, the slight fault (5mm from all vane leading edges were removed) is shown.

Trailing Edge Fault

The trailing edge fault (TED) consists in removing part of the vane trailing edge (the region at the tip of the vane) of all vanes. Three different lenghts were used. Table 3-9 shows the original length of the vane and the milimiters of vane removed. This fault simulates the degradation of impellers along time due to particles or impurities that can be present in the water. Figure 3-17 shows the impeller used for TED fault with 5mm of vane trailing edge removed from all vanes.

TABLE 3-9: SEVERITY OF TRAILING EDGE FAULTS

Fault Severity	Length vane reduction	Length of the remaining vane
None	0	50 mm
Slight	10% of the total length = 5mm	50mm - 5mm = 45 mm
Medium	20% of the total length = 10mm	50mm - 10mm = 40 mm
Severe	30% of the total length = 15mm	50mm - 15mm = 35 mm

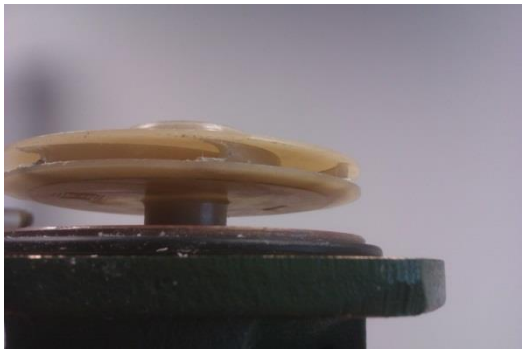

Figure 3-17: Photo of the impeller with trailing edge fault. In this case, the slight fault (5mm from all vane trailing edges were removed) is shown.

Seal rubber fault

The seal fault was produced spontaneously while impeller 2 was being recorded in normal condition. The sealing type of the pump is RS-1. The assembly of the impeller with the rotor is configured with a ceramic "O-ring" type stationary seat and is also equipped with a "set screw collar". The RS-1 type is an "Elastomer (or Rubber) bellows seal". When we open the pump, we discovered that the ceramic "O-ring" was displaced during the pump operation. This caused the friction between the O-ring and the impeller and a screech sound was audible. In Figure 3-18 the impeller with the O-ring is shown.

Figure 3-18: Photo of the o-ring of the impeller of the AL P800 pump.

System faults

The ALP800 pump is designed and built for pumping water, clean and free from solids. We have added different solids to the water to cause damage and partial obstruction to the pump. This causes a decrease of water flow.

The different solids added to the water are enumerated in Table 3-10. The characteristicas of the solids and their concentration in water are also shown in the table.

TABLE 3-10: CHARACTERISTICS OF SOLIDS ADDED TO THE PUMP

Conditions	Characteristics	Concentration
Sand	Fine sand from "Las Alcaravaneras" beach Grain diameter range: 0.0625-2 mm	2kg/50l
Sand + Paper	Standard paper A4 80gr	2kg/50l (sand), 2kg/50l(paper)
PVC balls (no sand anymore)	Polyvinyl chloride balls used for airsoft pellets Diameter: 6 mm Weight: 0.12 g	2000 balls / 50 l (240 g / 50 l)

Figure 3-19 shows the reservoir with sand and Figure 3-20 shows the PVC balls.

Figure 3-19: Photo of the reservoir with the sand added to simulate strange objects or particles in the system.

Figure 3-20: Kind of PVC balls (6 mm of diameter) used to simulate strange objects in the system [29].

3.2.5.4 Experimental set-up: sensor positions

The room where the experimental set-up is placed is shown in Figure 3-21. The room has a 29 dB of acoustic isolation respect aerial noise.

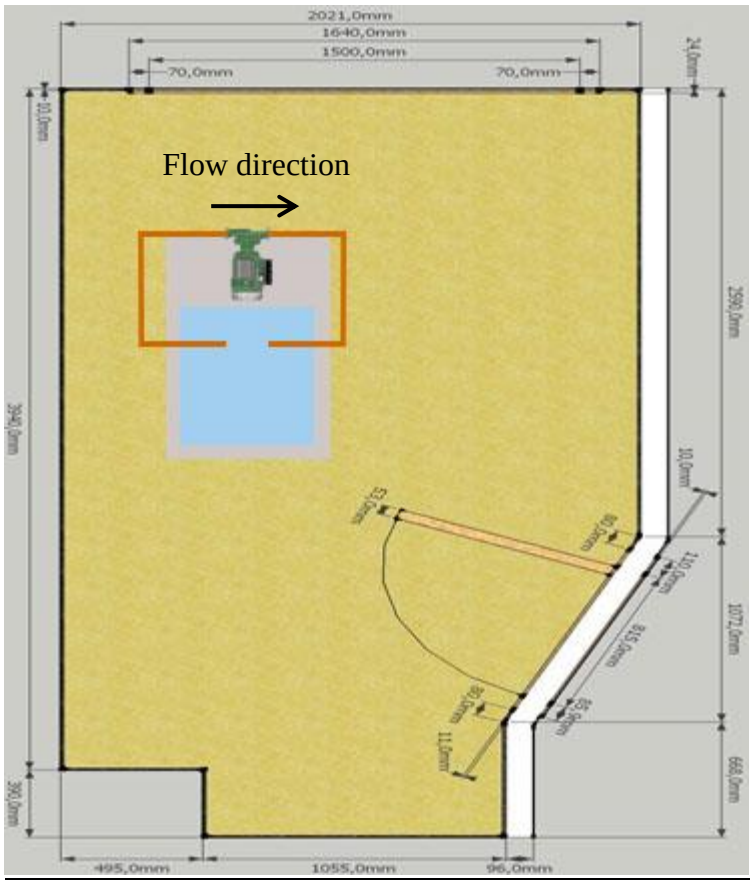

Figure 3-21: Drawing of the room for the experimental set-up with the measurements in mm. A squematic of the set-up is also shown.

A squematic of the experiment setup is also shown in Figure 3-21, where the pump (in green), the reservoir with water (in blue) and the pipes (in orange) are shown. The flow direction is also shown. A photograph of the experiment is shown in Figure 3-22, where the circulating pump and the sensors are shown. The elements of the experimental set-up are the following: a centrifugal pump, 4 meters of pipes of 3.81 cm (1.5 inches) of diameter connected to the inlet and outlet of the pump, a pressure gauge connected to the output of the pump, the reservoir and a trolley in which the reservoir and the pump are placed on. The reservoir is filled with 50 liters of water and a closed loop is formed with pipes. The pump is at the same height of the reservoir because is a circulating pump.

Two microphones were placed in the pump inlet and in the pump outlet. OutletMicro points the pump outlet and InletMicro points the pump inlet (see Figure 3-22). The microphones are expected to obtain information about the flow changes. The distance between the microphone and the pump used in different works in centrifugal

pumps varies from 5cm to 100cm [16],[18],[31],[32]. These works focus on detection of cavitation. Iniatially, the distance of the microphones from the pump was varied from 2cm to 100cm (in steps of 2cm from 2cm to 20cm and in steps of 5 cm from 20cm to 100cm) and audio signals were taken. Their spectra were visually inspected for searching peaks at the discrete frequencies (rotor frequency, vane passing frequency and their harmonics). The discrete frequencies were observed in all cases but from 50cm to 100cm the amplitude of the discrete frequencies vanished progressively. Taking into account that in industrial scenarios, the background noise is usually high, microphones should be located near the source [33]. For this reason, microphones were placed at 5 cm from the pump in this Thesis.

Accelerometers were placed in two orthogonal directions over the pump casing: accelerometer CESVA AC001 with sensitivity 100 ± 5 % mV/g (‘RadialInletAccel’ in Figure 3-22) and accelerometer CESVA AC006 with sensitivity 1000 ± 10 % mV/g (‘RadialAccel’ in Figure 3-22). 'RadialInletAccel' is placed on the volute in the radial plane (that is, the plane perpendicular to the rotor direction) and near the inlet, 'RadialAccel' is placed over the volute in the radial plane and perpendicular to “RadialInletAccel”. A third accelerometer was placed in axial direction (the rotor direction). However, this accelerometer is not considered in this Thesis. The accelerometers are expected to obtain information about the flows inside the volute.

Figure 3-22: Sensor Placement for the Experimental set-up.

3.2.5.5 Database Structure

The files of the database are in .mat format. The content of each file in the database is described in Table 3-11. The names of the variables stored in each file of the database are enumerated in the first column of Table 3-11. In the second column the possible values of the variables are enumerated and described.

The name of the files in database contains all the information to know the pump condition, the impeller used in the recording, the severity of the fault and the number of the file. The name of the files in the database has the following format:

*CON*_Im*I*_Sev*S*_*XX*.mat

CON is the condition. See variable *condition* in Table 3-11.

I is the number of the impeller. See variable *impeller* in Table 3-11.

S is degree of severity in a fault. See variable *severity* in Table 3-11.

XX is the number of the file.

For example, LED_Im3_Sev1_01.mat is a file with LED condition in impeller 3 with severity 1. The number of the file is 01.

TABLE 3-11: CONTENT OF A SAMPLE FROM THE DATABASE

condition	String with the name of the condition. Possible values are: .'nor': normal condition .'pla': plate fault condition. .'sea': plate fault condition. .'led': leading edge fault condition. .'ted': trailing edge fault condition. .'san': sand in water condition. .'sap': sand and paper in water condition. . 'pvc': balls of PVC in water
impeller	Contains the number of the impeller used in the recording. Possible values are: 1: impeller 1 2: impeller 2 3: impeller 3 4: impeller 4
multisigOriginal	Matrix that contains the audio and vibration signals of 59 seconds (with a sample frequency of 22050 Hz). Each row of the matrix corresponds to the signal acquired for a sensor.
Sensorposition	Type cell. Each cell contains the name of the sensors in the order that are stored in the matrix *multisigOriginal*. 'radialInletAccel' 'radialAccel' 'outletMicro' 'inletMicro' The data of 'ratialInletAccel' is stored in the first row of the *multisigOriginal* matrix. The data of 'radialAccel' is stored in the second row of the *multisigOriginal* matrix and so on.
severity	The severity of the fault. Possible values are: 0: no severity. 1: slight severity. 2: medium severity. 3: higher severity No severity means that the file corresponds to a normal condition or that the file corresponds to a fault with no severity associated (for example, seal fault). 1 can correspond to a plate fault with one part of plate removed, to a LED or TED fault of 5mm. 2 can correspond to a plate fault with two parts of the plate removed, to a LED or TED fault of 10 mm. 3 can correspond to a plate fault with three parts of the plate removed, to a LED or TED fault of 15 mm.
dateacq	String with the data of the data acquisition. Example: '21-Jul-2011' File recorded 11 July 201.

3.2.5.6 Numbers of samples for each condition

Table 3-12 shows the different conditions recorded for ALP800 pump. The first column of the table shows the impeller used, the second column shows the pump condition and the third column shows the number of samples acquired for each condition. Each sample has four signals of 59 seconds. Each sample was obtained in different recording sessions.

TABLE 3-12: RECORDED CONDITIONS FOR EACH IMPELLER

Impeller #	Condition	Number of samples per condition
1	Normal	20
1	1 Plate	20
1	2 Plates	20
1	3 Plates	18
2	Normal	20
2	Seal Ring	9
2	Sand	23
2	Sand and Paper	62
2	PVC balls	18
3	Normal	20
3	LED 5 mm	20
3	LED 10 mm	20
3	LED 15 mm	20
4	Normal	20
4	TED 5 mm	20
4	TED 10 mm	20
4	TED 15 mm	20

3.2.6 Pump Database Preprocessing and Baseline signals

Each original file of the database is 60 seconds at a sample frequency of 44.1kHz (more than twice the bandwidth of the microphones). As the amplitude in the spectra of the audio signals drops around 15kHz and the band-width of the accelerometers is up to 10kHz, each file of the database was decimated by 2. The new sample frequency is 22050Hz. To decimate the files a linear phase FIR (finite response) filter with order 30 is used. Finally, we remove the beginning of the signal and we obtain a signal of 59 seconds.

In the following figures, examples of spectra of vibration and audio signals from the centrifugal pump test rig in normal (free-fault) condition are shown.

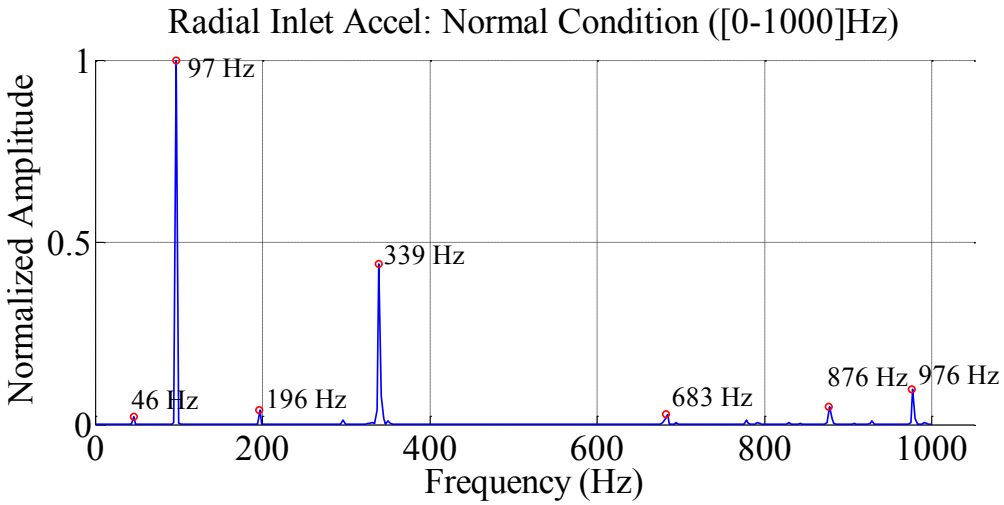

Figure 3-23: Spectrum in range [2.7-1000]Hz of a 8192 points vibration frame (371.5ms) from sensor RadialInletAccel. The higher peaks are marked with red circles and the frequency value is shown.

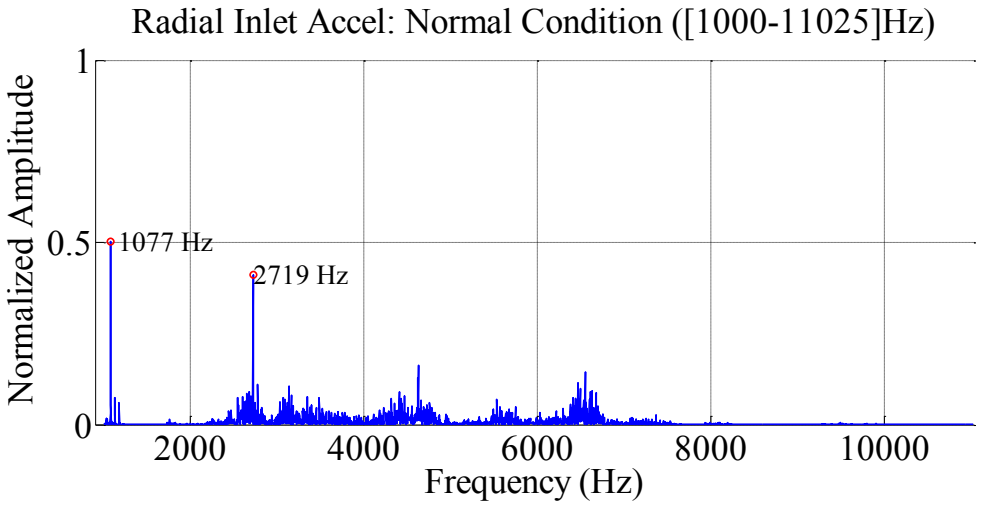

Figure 3-24: Spectrum in range [1000-11025]Hz of a 8192 points vibration frame (371.5ms) from sensor RadialInletAccel. The higher peaks are marked with red circles and the frequency value is shown.

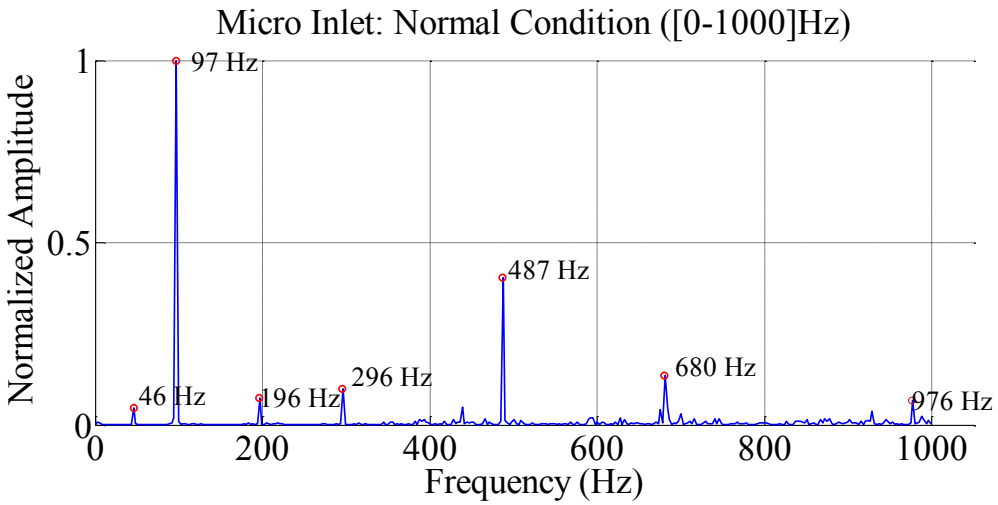

Figure 3-25: Spectrum in range [2.7-1000]Hz of a 8192 points audio frame (371.5ms) from sensor MicroInlet. The higher peaks are marked with red circles and the frequency value is shown.

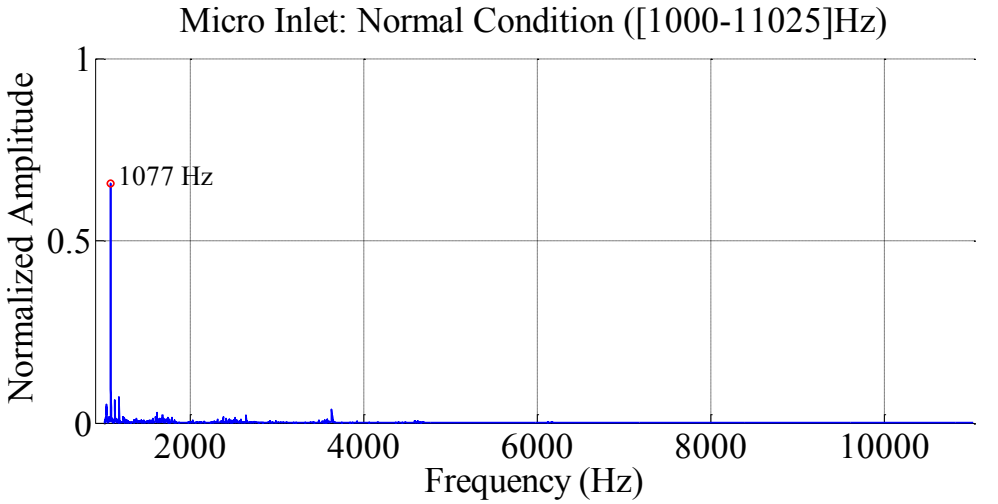

Figure 3-26: Spectrum in range [1000-11025]Hz of a 8192 points audio frame (371.5ms) from sensor MicroInlet. The higher peaks are marked with red circles and the frequency value is shown.

Figure 3-23 and Figure 3-24 show the normalized spectrum of a vibration signal from sensor Radial Inlet Accel in the frequency range [2.7-1000]Hz and [1000-11025]Hz respectively. Figure 3-25 and Figure 3-26 show the normalized spectrum of an audio signal from sensor Inlet Micro in the same frequency ranges. Both vibration and audio signals were acquired simultaneously. Focusing on the frequency range [2.7-1000]Hz in the case of the vibration spectrum, peaks appear at 46Hz, 97Hz, 196Hz, 339Hz, 683Hz, 876Hz, 976Hz corresponding at the rotor frequency (1X), 2X, 4X, vane-passing frequency (VPF), 2VPF, 18X and 20X respectively. In the case of the audio spectrum, peaks at 1X, 2X, 4X, 6X, 2VPF and 20X appear with different amplitudes at

those of the vibration spectrum. It can be observed another distinctive peak at 487Hz (10X frequency) in the audio spectrum. This peak is due to the fan of the pump, which has 10 blades. It can be observed that peaks at rotor frequency and vane-passing frequencies and their harmonics are present in both audio and vibration signals.

Regarding the frequency range [1000-11025]Hz, both the vibration spectrum and the audio spectrum show a peak at 1077Hz, a frequency multiple of the rotor frequency (22X). Low amplitude at this frequency (22X) would be expected. It is believed that this peak is due to structural resonances. The same observations were made in vibration and audio signals of a centrifugal pump in [30].

The rotor frequency and vane-passing frequency and their harmonics dominate in spectra for both vibration and audio signals. This confirms the vibroacustic mechanism in a centrifugal pump when operating without faults explained earlier in this Chapter.

3.3 Contributions of this Chapter

The first part of this Chapter contributes with the collection of different bearing vibration databases from different repositories in internet to form a corpus. The second part of this Chapter contributes with the acquisition of a vibration and audio database from a centrifugal pump in the DPDS.

3.4 References

[1] Case Western Bearing Data Center, http://csegroups.case.edu/bearingdatacenter/home Last visited: 25th November 2014.

[2] UH-60 database: http://qsun.eng.ua.edu/cpw_web_new/intro.htm. Last visited: Jan. 2014

[3] Lee, J., Qiu, H., Yu, G., Lin, J., & Rexnord Technical Services (2007). Bearing Data Set. IMS, University of Cincinnati. NASA Ames Prognostics Data Repository, [http://ti.arc.nasa.gov/project/prognostic-data-repository], NASA Ames, Moffett Field, CA."

[4] Webpage Explore the World of Piping http://www.wermac.org/equipment/pumps_general.html. Last visited: 19 November 2014

[5] "Pump Principles Manual: global training education and development program" eds. Chesterton.

[6] Hydraulic Institute http://www.pumps.org. Last visited: 19 November 2013

[7] Centrifugal Pumps: Basics Concepts of Operation, Maintenance, and Troubleshooting, Part I By: Mukesh Sahdev, Associate Content Writer Presented at The Chemical Engineers' Resource Page, www.cheresources.com

[8] Parrondo, J. L., Velarde, S., Pistono, J., & Ballesteros, R. (1999). Diagnosis based on condition monitoring of fluid-dynamic abnormal performance of centrifugal pumps. In *Proceedings of the Int. Seminar on Modal Analysis* (Vol. 3, pp. 1365-1372). Katholieke Universiteit Leuven.

[9] Patel, T., Moghaddas, R., Lipi, T., Zou, M. (2009, September). Review on Condition Monitoring of Hydraulic Pumps, Technnical Report, University of Alberta.

[10] Zhao, X. M., Hu, Q. H., Lei, Y. G., & Zuo, M. J. (2010). Vibration-based fault diagnosis of slurry pump impellers using neighbourhood rough set models.*Proceedings of the Institution of Mechanical Engineers, Part C: Journal of Mechanical Engineering Science*, *224*(4), 995-1006.

[11] Sakthivel, N. R., Sugumaran, V., & Babudevasenapati, S. (2010). Vibration based fault diagnosis of monoblock centrifugal pump using decision tree. *Expert Systems with Applications*, *37*(6), 4040-4049.

[12] Tian, Z., Wong, L., & Safaei, N. (2010). A neural network approach for remaining useful life prediction utilizing both failure and suspension histories.*Mechanical Systems and Signal Processing*, *24*(5), 1542-1555.

[13] Zhao, X., Zuo, M. J., & Patel, T. H. (2012). Generating an indicator for pump impeller damage using half and full spectra, fuzzy preference-based rough sets and PCA. *Measurement Science and Technology*, *23*(4), 045607.

[14] Zhao, X. M., Hu, Q. H., Lei, Y. G., & Zuo, M. J. (2010). Vibration-based fault diagnosis of slurry pump impellers using neighbourhood rough set models.*Proceedings of the Institution of Mechanical Engineers, Part C: Journal of Mechanical Engineering Science*, *224*(4), 995-1006.

[15] Parrondo, J. L., Velarde, S., & Santolaria, C. (1998). Development of a predictive maintenance system for a centrifugal pump. *Journal of Quality in Maintenance Engineering*, *4*(3), 198-211.

[16] Al-Hashmi, S. A. (2012, September). Spectrum analysis of acoustic signals for cavitation detection. In *2012 IEEE Symposium on Industrial Electronics and Applications (ISIEA)*, (pp. 321-325). IEEE.

[17] Kallesøe, C. S. (2005). *Fault Detection and Isolation in Centrifugal Pumps* (Doctoral Diessertation).

[18] Al Thobiani, F., Gu, F., & Ball, A. (2010, June). The monitoring of cavitation in centrifugal pumps based on the analysis of vibro-acoustic measurements. In: *CM 2010 and MFPT 2010 : The Seventh International Conference on Condition Monitoring and Machinery Failure Prevention Technologies*, 22-24 June 2010, Stratford-upon-Avon, UK, 2010.

[19] Dyson, G. (2005). Impeller rerate to reduce hydraulically generated vibration. In *Proceedings of the 22nd International Pump Users Symposium* (pp. 10-15).

[20] Schiavello, B., & Cicatelli, G. (2007). Vibration field problem resolved with analytical diagnostics approach and innovative impeller design. In *Proceedings of the 24th International Pump Users Symposium* (pp. 39-49).

[21] Bhadeshia, H. K. D. H. (2012). Steels for bearings. *Progress in materials Science*, *57*(2), 268-435.

[22] McFadden, P. D., & Smith, J. D. (1984). Model for the vibration produced by a single point defect in a rolling element bearing. *Journal of sound and vibration*, *96*(1), 69-82.

[23] Tejera, A., Herrera, A., Alonso, J. B., Travieso, C. M., Ferrer, M. A. (2007, June). Multichannel Audio Recording System. In *Proc. of 1er Workshop en Tecnologías de Audio Cognitivo para Aplicaciones en Seguridad y Acústica Forense* (p. 54-57) Gran Canaria.

[24] Epps, I. K. (1991). *An investigation into vibrations excited by discrete faults in rolling element bearings* (Doctoral Dissertation), University of Canterbury, New Zealand.

[25] D'Elia, G., Delvecchio, S., Cocconcelli, M., & Dalpiaz, G. (2013, August). Application of Cyclostationary Indicators for the Diagnostics of Distributed Faults in Ball Bearings. In *ASME 2013 International Design Engineering Technical Conferences and Computers and Information in Engineering Conference*. American Society of Mechanical Engineers.

[26] Randall, R. B. (2004). State of the art in monitoring rotating machinery-part 1. *Sound and vibration*, *38*(3), 14-21.

[27] Hardman, W., Hess, A., & Sheaffer, J. (1999). SH-60 helicopter integrated diagnostic system (HIDS) program-diagnostic and prognostic development experience. In *Aerospace Conference, 1999. Proceedings. 1999 IEEE* (Vol. 2, pp. 473-491). IEEE.

[28] Estupiñan, E., White, P., & San Martin, C. (2007). A cyclostationary analysis applied to detection and diagnosis of faults in helicopter gearboxes. In *Progress in Pattern Recognition, Image Analysis and Applications* (pp. 61-70). Springer Berlin Heidelberg.

[29] PVC balls: http://www.airgundepot.com/neonfire-uhc-py-p-267.html. Last visited: 3rd October 2015.

[30] Al Thobiani, Faisal (2011) The Non-intrusive Detection of Incipient Cavitation in Centrifugal Pumps. Doctoral thesis, University of Huddersfield.

[31] Cudina, M. (2003). Detection of cavitation phenomenon in a centrifugal pump using audible sound. *Mechanical Systems and Signal Processing 17*(6), 1335–1347.

[32] Cudina, M., Prezelj, J. (2009). Detection of cavitation in operation of kinetic pumps. Use of discrete frequency tone in audible spectra. *Applied Acoustics 70*, 540-546.

[33] Baydar, N., & Ball, A. (2003). Detection of gear failures via vibration and acoustic signals using wavelet transform. *Mechanical Systems and Signal Processing*, *17*(4), 787-804.

[34] Fernández-Francos, D., Martínez-Rego, D., Fontenla-Romero, O., Alonso-Betanzos, A. (2013). Automatic bearing fault diagnosis based on one-class *v*-SVM. *Computers and Industrial Engineering, 64*, 357-365.

CHAPTER 4
Contributions to vibration bearing fault diagnosis and fault identification

This Chapter focuses on vibration features in bearing fault diagnosis and bearing degradation. The contributions of this Thesis on bearing fault diagnosis are based on nonlinear measures. The nonlinear energy operator Teager-Kaiser is proposed as a preprocessing tool for bearing fault diagnosis followed by statistical and energy based feature extraction to diagnose between normal bearing condition, inner race fault, outer race fault and ball fault conditions. A new methodology to assess the severity of a fault in bearings (i.e.: the progression of the fault from an onset fault to a developed fault) for outer race fault and inner race fault using wavelet package transform and complexity measures Lempel-Ziv complexity is also proposed.

In this Chapter, we explain our proposals and the experimentation carried out. Finally, we show the results and the conclusions. The first part of the Chapter (section 4.1) is devoted to the experiment of the nonlinear energy operator Teager-Kaiser. The structure is based on papers published by the author of this Thesis [1]-[3]. The second

part of the Chapter is devoted to the degradation experiment. The structure is based on a published conference [4] and on an ongoing paper.

4.1 Proposal of nonlinear Teager-Kaiser energy operator for bearing fault diagnosis and bearing degradation assessment

As stated in Chapter 3, vibration signals generated by bearings with discrete faults located at the inner race, at outer race or at the rolling elements can be viewed as an amplitude modulated signal in which the carrier is the resonance frequency of the bearing (the frequency excited by the impacts of the discrete fault) and the fundamental frequency of the modulating signal (the envelope) is the bearing characteristic frequency of the faulty bearing. In Figure 4-1, repeated here for convenience, the vibration signals for a bearing with inner race, outer race and ball fault are shown along with their corresponding envelope signals.

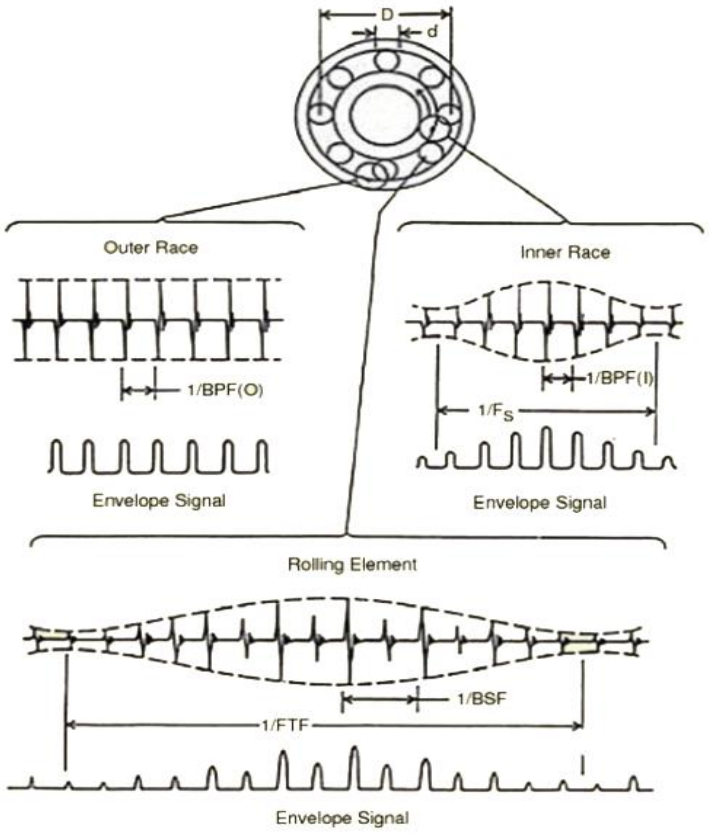

Figure 4-1: Time Vibration signals for bearings with outer race fault, inner race fault and ball fault. Source: [28].

In recent decades, much attention has focused on the development of new digital signal analysis methods for modeling bearing vibration signals so as to discriminate between normal operation and different faulty conditions.

Some conventional methods, after sampling the vibration signal $v(t)$ with sample frequency f_s, feature the vibration signal $v(n) = v\left(\frac{n}{f_s}\right)$ with statistical measures of first, second or higher order such as variance, skewness or kurtosis and with measures such as crest factor, impulse factor and root mean square which feature the impulsive nature of the bearing vibration signal [5].

Other methods model the vibration signals generated by faulty bearings as an amplitude modulated (AM) signal, defined as:

$$v(n) = A(n)\cos(2\pi f_b n) = A\cos(2\pi f_{bf} n)\cos(2\pi f_b n) \qquad \text{[Eq. 4-1]}$$

where f_b is the resonance frequency of the bearing and $A(n)$ the AM signal or signal envelope whose f_{bf} is the bearing fault characteristic frequency that have to be detected.

The AM signal can be extracted using the high frequency resonance analysis or envelope analysis [6] which implies band-pass-filtering the $v(n)$ bearing vibration signal. Then, Fourier transform is used to obtain f_{bf}. The main disadvantage of this technique is the difficulty in the correct selection of the central frequency and the bandwidth of the band-pass filter.

Recent methods in bearing fault diagnosis include more advanced signal processing methods such as spectral kurtosis [7], wavelet analysis and empirical mode decomposition (EMD) [8]. Spectral kurtosis offers a way of designing optimal band-pass filter for bearing fault diagnosis. Wavelet analysis and EMD are time-frequency techniques that decompose the raw vibration signal in different frequency bands. Then, several features such as entropy or statistics are extracted from the different frequency bands.

Recently, as an alternative to obtain the AM signal from the raw vibration signal, [6], [10] proposed the nonlinear Teager-Kaiser energy operator (TKEO) [11]. The AM signal and the frequency modulated (FM) signal from a mono-component AM-FM signal can be extracted using TKEO [12]. H. Li et al. [9] proposed TKEO to extract the AM signal (AM-TK signal) from bearing vibration signal, without using a band-pass filtering process, just with some simple operations over TKEO. Liang et al. [10] proposed the application of the TKEO over the raw bearing vibration signal without computing the AM signal. Then, the Fourier transform is applied and the f_{bf} is identified.

In this Thesis, we propose to use TKEO to obtain the vibration signal in the Teager–Kaiser domain (TK signal) and then to feature it with statistical and energy-based features. The objective is to show how the statistical and energy-based features extracted from the TK signal outperform the diagnosis results when extracting the same features from the raw time vibration signal (time signal), the AM signal obtained by pass-band filtering (AM signal) and the AM signal obtained by using the TKEO (TK-AM signal). A comparative analysis between statistical and energy-based features extracted from TK signal, TK-AM signal, AM signal and time signal (T signal) is accomplished.

Next, the conventional envelope analysis and the Teager-Kaiser energy operator are explained. From the conventional envelope analysis the AM signal is extracted. The TK signal is extracted directly from the Teager-Kaiser operator and the TK-AM signal is extracted from the Teager-Kaiser operator after doing some calcularions. The T signal is the raw vibration signal.

Conventional Envelope analysis: AM signal

The conventional analysis to obtain the amplitude demodulated signal ($A(n)$ in [Eq. 4-1]) is called envelope analysis or high frequency resonance analysis [6]. This procedure implies the following steps: (i) band-pass filtering the bearing vibration signal, (ii) application of the Hilbert transform to the band-pass filtered signal, and (iii) low-pass filtering the resulting signal. The step (i) requires a visual inspection of the

bearing vibration spectrum to estimate the central frequency and the bandwidth of the band-pass filter.

Teager-Kaiser energy operator: TK-AM signal and TK signal

The Teager-Kaiser energy operator was derived by Kaiser in 1990 [11] to measure the energy of the mechanical process that generated a single time-varying signal. TKEO can detect modulations in AM-FM signals by estimating the product of their time-varying amplitude and frequency. It is considered as a high-resolution energy estimator. The TKEO for continuous time signals v(t) is:

[Eq. 4-2]

$$\psi_c[v(t)] = [\dot{v}(t)]^2 - v(t)\ddot{v}(t)$$

where $\dot{v}(t) = dv/dt$

It can be shown [11] that the discrete version of the TKEO is:

$$\psi[v(n)] = v^2(n) - v(n-1)v(n+1) \qquad \text{[Eq. 4-3]}$$

Maragos et al. [12] developed a method to estimate the amplitude envelope (AM signal) and the instantaneous frequency (FM signal) of speech formant signals using the TKEO. The amplitude modulated signal can be extracted from TKEO (TK-AM signal) as follows [12]:

$$|A(n)| = \frac{2\psi[v(n)]}{\sqrt{\psi[v(n+1) - v(n-1)]}} \qquad \text{[Eq. 4-4]}$$

This technique has been applied in bearing fault diagnosis in [9] to extract the TK-AM signal without using a band-pass filter.

The direct application of TKEO over the raw vibration signal $v(n)$ ([Eq. 4-3]) [10] can perform more effective bearing fault detection. In the TK domain the faulty samples can be easily discriminated because the TK signal highlights the characteristic

impulse train which is due to the impact of the rollers with the defect. This effect can be seen in Figure 4-2 which shows an example of TK signals for normal and fault conditions. Therefore, it is expected that features obtained from the TK signal will discriminate effectively between normal and fault bearing conditions without estimating the AM envelope. The direct computation of TKEO over the vibration signal has the following advantages: (i) it does not require the use of a band-pass filter. Therefore, the appropriate estimation of the central frequency and bandwidth of the band-pass filter is avoided.; (ii) Three adjacent samples of the signal are used to compute the TKEO. This fact makes the TKEO implementation very simple and computationally efficient.

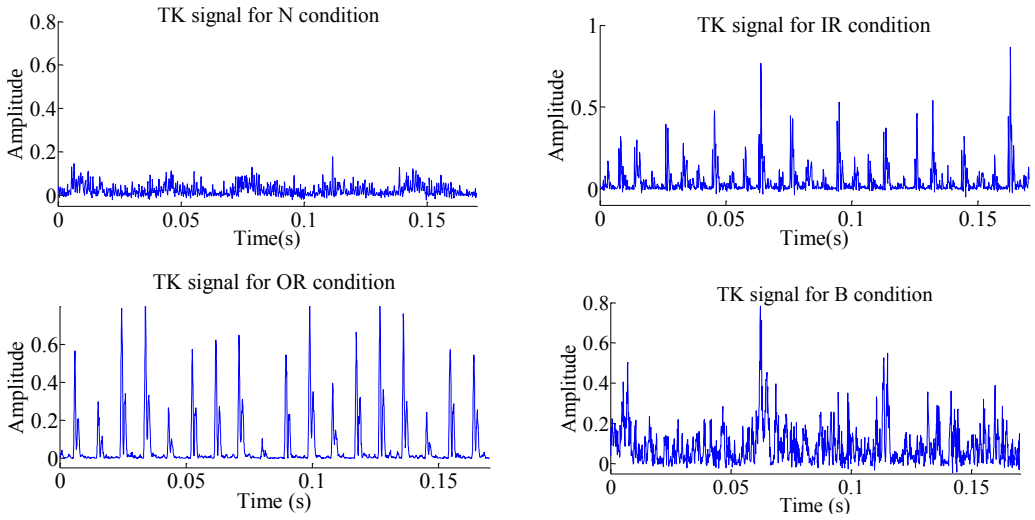

Figure 4-2: Teager-Kaiser transformed signals (TK signals) for different bearing conditions: normal condition (upper-left), inner race faul condition (upper-right), outer race fault condition (bottom-left) and ball condition (bottom-right).

From the AM signal, the TK-AM signal and from the TK signal a set of statistical, energy-based and entropy features are extracted and a performance comparison between the different methods are carried out. The extracted features from the AM signal, the TK-AM signal and the TK signal are: features that characterize the amplitude [1]: peak value and peak-to-peak value; statistical measures: standard deviation, skewness and kurtosis; third, features that quantify the energy in the signal [1]: root mean square (rms), squared mean root (smr); fourth, features that quantify the impulsive nature of the vibration signal [1]: crest factor (peak value/rms), L factor (peak value/smr), shape factor (rms/peak value), impulsive factor (peak value/mean) and finally the Shannon entropy that measures the disorder or complexity of a system [14]. Finally, we have the featured AM signal, the featured AM-TK signal and the featured

TK signal.

The proposed method is first applied to the Case Western Database to show how the proposed method outperforms the method that uses statistical features in fault diagnosis, i.e. discriminating between different bearing faults: inner race fault (IR), outer race fault (OR) and ball fault (B). The diagram of the experiment for fault diagnosis is shown in Figure 4-3. Then, the proposed method is applied to the UH-60 database. As this database is a run-to-failure database (fault degradation) the method is applied with some differences which are explained in the corresponding section. See Figure 4-4 for the diagram of the experiment for fault evolution along time. In the next subsection the singularities of the application in each database are explained and the results are shown.

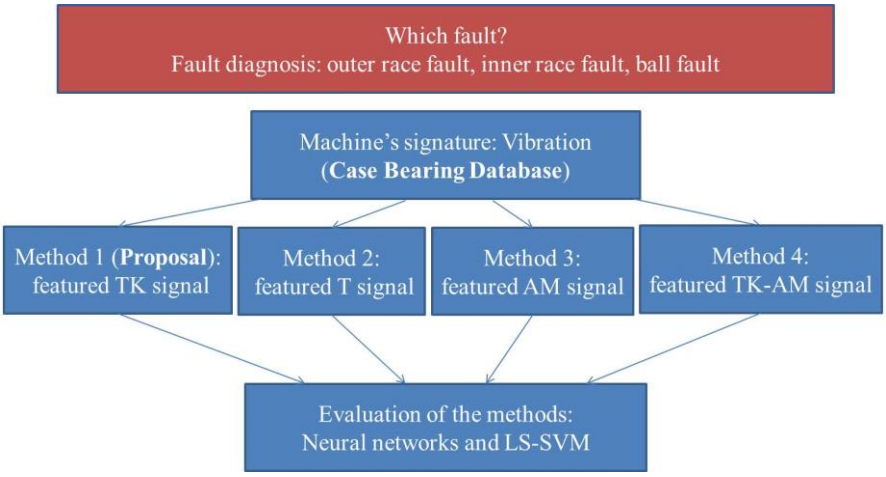

Figure 4-3: Diagram of the experimentation in bearing fault diagnosis. The proposal is compared with other methods in the state of the art and an evaluation with two classifiers is carried out.

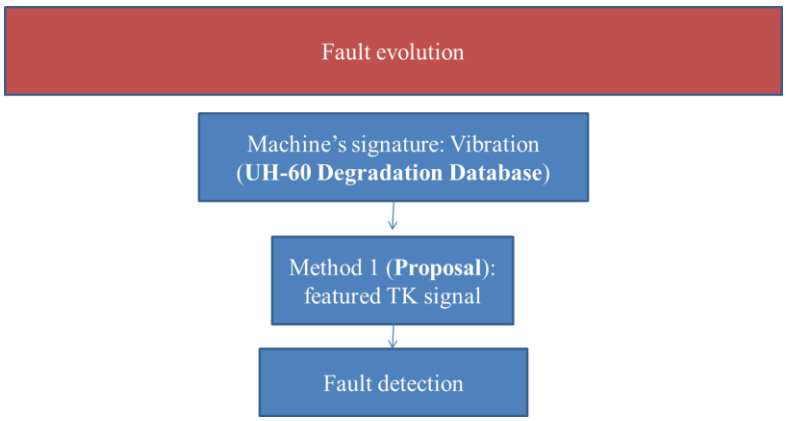

Figure 4-4: Diagram of the experimentation in bearing fault evolution. The proposal is applied to a run-to-failure bearing vibration database.

4.1.1 Evaluation and results of the proposal for bearing fault diagnosis

Following the diagram in Figure 4-3, the proposed methods 1 to 4 were evaluated in the Case Vibration Bearing database for fault diagnosis. To quantitative evaluate the proposed method, two classifiers are used to evaluate the discrimination ability of the features between normal condition, IR fault, OR fault and B fault: a neural network classifier and a Least Square-Support Vector Machine (LS-SVM) classifier. Moreover, the features extracted from the TK signal are sorted by relevance order with the floating forward feature selection procedure. Then, features from the different signals are evaluated (in order of relevance) with the two mentioned classifiers. A detailed explanation of the experimentation is carried out in the following paragrahps and the results are shown.

Frame segmentation and feature extraction

First, the mean is removed from the vibration signal of each file of the database and then the vibration signal is normalized between -1 and 1. Then, the vibration signal is divided into time frames of 0.17 seconds which are overlapped by 33%. Each frame comprises 5 revolutions of the shaft. Each frame is transformed to the TK domain using [Eq. 4-3]. Then, the mentioned features are extracted from the TK signal. We call the features extracted from the TK signal TK features. In order to compare the results, the same features are also extracted from the time vibration signal $v(n)$ (T features), from the AM signal by means of envelope analysis (AM features) and from the AM signal by means of the Teager-Kaiser method (TK-AM signal).

Relevance of the TK features

In order to select the subset of TK features with gives the best success rate, the TK features are sorted by relevance order using the sequential floating forward selection (SFFS) algorithm [22] and then are evaluated incrementally with the neural network classifier and the LS-SVM classifier. SFFS is an heuristic algorithm that search the subset of features of the original set which has the best success rate. The procedure to sort the features by relevance order using the SFFS is described next.

The database is split into a training subset and a testing subset by choosing randomly three files from normal condition and nine files from each fault condition (30 files in total) for the training set and leaving the remaining files for the testing set (10 files in total). The data in the training and testing setare z-score normalized using the mean and variance of the training set. The SFFS algorithm is applied 60 times with different training and testing subsets randomly chosen. As a result, a different subset of best features is obtained each time the SFFS algorithm is applied. The classifier used by the SFFS to obtain the success rate is a 1-nearest neighbor classifier. At the beginning of the experiment, a 60(times) x 12 (features) matrix is initialized at zero values. Each time the SFFS is applied a subset of best features is obtained. Their position in the matrix is marked with '1'. At the end of the 60 repetitions, each column is summed so as the number of times a feature is within the subset of best features is obtained. Finally, the features are sorted by relevance in descending order: the feature that most times appears in the subset of best features is the most relevant one and the feature that least times appears in the subset of best features is the least relevant one.

Classification

Once the TK features are sorted by relevance order, they are incrementally evaluated using two classifiers: a neural network classifier and a LS-SVM classifier. The incremental evaluation of the features consists in the following: first, the most relevant feature is evaluated, then the most relevant is evaluated along with the second most relevant and so on. As a result, the subset of TK features which gives the best success rate can be selected. The same procedure is done with the T, AM and TK-AM features.

Neural Network Classifier

The features are fed into a multilayer feed forward neural network (NN) with one hidden layer trained to discriminate between normal condition, IR fault condition, OR fault condition and B fault condition. The neural network is a standard classifier and can be used to reproduce the results easily. Supervised learning is carried out using the resilient back propagation train algorithm [23]. The number of neurons in the hidden layer is selected using cross-validation technique and the output layer has 4 neurons.

The NN input is the vector of features belonging to one frame: $\boldsymbol{p} = [p_1, \ldots p_R]^T$ (T is transposition of the vector $\boldsymbol{p}$) and R is the number of features in the vector. As the features are evaluated incrementally, when one feature is evaluated R = 1, when two features are evaluated R = 2 and when all the features are evaluated R = 12. The activation functions for the hidden layer are tansigmoid functions (hyperbolic tangents). The output layer of the NN has 4 nodes corresponding to the 4 bearing conditions: $\boldsymbol{a^2} = [a_1^2, a_2^2, a_3^2, a_4^2]^T$, where a_1^2 is the output for normal condition, a_2^2 is the output for IR fault condition, a_3^2 is the output for OR fault condition and a_4^2 is the output for B fault condition. The activation functions for the neurons of the output layer are linear activation functions.

In order to train and test the NN, the database is split into a training subset and a testing subset and the data are normalized in the same way of the feature selection procedure. The training subset is used to choose the size of the hidden layer (i.e. the number of neurons of the hidden layer S). The NN is trained with varying S from 1 to 20. For each S value, the training subset is subdivided using the 3-fold cross-validation technique, i.e. the training subset is divided in three different subsets: two of them are used to train the neural network and the remaining one (called validation subset) is used to compute the success rate. The value of S with the best success rate is chosen as the size of the hidden layer. Finally, the NN with the final configuration is trained and then evaluated with the testing subset.

In the testing phase, each frame is classified according to the maximum output value of the neural network. For example, if $a_1^2 = \max\{a_1^2, a_2^2, a_3^2, a_4^2\}$, the frame is classified as normal condition. Then each file is classified between normal, IR, OR or B fault conditions according to the more voted rule, i.e. if the majority of the frames are classified as normal condition, the file is classified as normal condition. All the process is repeated 60 times, randomly choosing different files for training and testing set and the results were averaged. As a result, the success rate is obtained.

The training process is stopped when any of these conditions occurs: the maximum number of iterations, set to 5000, is reached; the maximum amount of time, set to infinite, is exceeded; the performance of E (error function) is minimized to the

goal, set to 0.01; the performance gradient ($\frac{\partial E}{\partial w_{ij}}$) falls below the minimum gradient, set to 0.015; or the validation error has increased more than 5 times since the last time it decreased. In order to set the stopping criteria values, the training error and the validation error curves are taken into account. The training error curve has to reach a horizontal line. It means the NN has learned the data. In our experiment, the NN reach the horizontal line when the goal is 0.01 or the performance gradient falls below 0.015. In a training process, training error is going down and validation error first also goes down but then may begin to rise. At that moment, the overfitting problem can arise. To avoid the overfitting of the NN, the training process is stopped when the validation error increases more than 5 times since the last time it decreased, even though the rest of stopping criteria has not been reached.

Least-square Support Vector Machine (LS-SVM)

The least-square support vector machine (LS-SVM) classifier [24] is used to validate the results obtained by the neural network classifier. LS-SVM classifier [24] is a modified version of the SVM classifier. The standard SVM is solved using quadratic programming methods whereas LS-SVM is designed to be solved using a set of linear equations.

SVMs and LS-SVM classifiers are originally designed to solve bi-class classification problems. In our case, a four-class classification problem is addressed. For this reason, an one-vs-all scheme is used. In this scheme, four one-vs-all binary LS-SVM classifiers are implemented. Each binary classifier makes binary decisions between one class and all other classes.

Gaussian radial basis functions (RBF) were used as kernels functions in the binary LS-SVM classifiers. In order to make an LS-SVM model in the training phase, we need two tuning parameters: γ which is the regularization parameter, determining the trade-off between the training error minimization and smoothness and θ, which is the bandwidth of the Gaussian radial basis function. These parameters are tuning using a cross-validation process.

The database is randomly split into a training subset and a testing subset in the same way of the neural network classifier. The regularization parameter and the bandwidth parameter of the LS-SVM are adjusted using the training subset with the same technique used in the neural network classifier, i.e. 3-fold cross-validation. In the testing phase, each frame is classified according to the maximum output value of the four binary classifiers. For example, if the maximum corresponds to the binary classifier which discriminates between normal and the rest of conditions, the frame is diagnosed as normal. Finally, each file is diagnosed with the more voted rule. All the process is repeated 60 times, randomly choosing different files for training and testing set and the results were averaged. As a result, the success rate is obtained.

Results and Discussion

The results in the feature selection procedure and the success rates obtained with the TK, T, AM and AM-TK features are shown in Figure 4-5 and Figure 4-6. Figure 4-5 shows the evaluation with the neural network classifier of the TK features sorted by relevance order (marked with 'o'). The order of relevance of the TK features is explicitly written in the top of the figure. The X-axis is the number of features evaluated (i.e. 1 is the L factor, 2 is the L factor along with the Shape factor, and 12 are all the features), the Y-axis is the success rate obtained in the evaluation of the features. Figure 3 also shows the success rates for the T (marked with an inverted triangle), AM (marked with '.') and TK-AM features (marked with 'x'), sorted with the same relevance order obtained for the TK features and evaluated in the same manner. Figure 4-6 shows the same information of Figure 4-5 but using a LS-SVM classifier to obtain the success rates. Both figures show an increment of the success rates with the increment of the number of features evaluated. In general, the results of the LS-SVM classifier outperform the success rates obtained using the neural network classifier.

In the case of the neural network classifier, the best success rate of 89.17% is obtained using the first 9 most relevant TK features: L factor, shape factor, skewness, kurtosis, Shannon entropy, peak to peak value, peak value, impulse factor and crest factor. In the case of the LS-SVM classifier, the best success rate of 90% is obtained using only the first 3 most relevant TK features: L factor, shape factor and skewness. This shows the higher generalization capacity of the LS-SVM.

Table 4-1 shows the averaged results of the TK, T, AM and TK-AM features for the neural network classifier and for the LS-SVM classifier using the complete set of 12 features. The standard deviation (σ) of the results is also shown. In the case of the neural network classifier, the TK features outperform the T features by 3.5% and the TK-AM features by 12.83%. The TK features give similar results to the AM features. However, in the computing of the AM features, a visual inspection of the spectrum is conducted to determine the central frequency and the bandwidth of the band-pass filter. Table 4-1 also shows the success rate after TK feature selection (in parenthesis in the TK features column). In the case of the neural network classifier, there is an increment of 3.67% in the success rate of TK features after feature selection. In this case, the best results of the 9 selected TK features are more evident: the 9 selected TK features outperform the T features by 7.17%, the TK-AM features by 16.5% and the AM features by 3.67%. In fact, the success rate obtained with the 9 selected TK features outperforms the rest of the success rates. It can be observed in Figure 4-5, where the maximum value of the success rate is 89.17% which corresponds to the 9 selected TK features. In the case of the LS-SVM classifier, the results show that the TK features outperform the T features by 5%, the TK-AM features by 5.83% and the AM features by 4%. In Figure 4-5, it can be observed that the maximum success rate of 90% is achieved with only 3 TK features. The success rates of TK features outperform the rest of features in all the cases.

Finally, the results of the evaluation of the TK features before and after feature selection (in bold) are shown in the confusion matrix of Table 4-2 for neural network classifier. The same information is shown in Table 4-3 for the LS-SVM classifier. In this case, the results with the 3 first TK features are the same that the results obtained with the 12 TK features, so they are not shown in Table 4-3. In both tables, the results show that TK features discriminate with great accuracy the normal condition and the IR fault condition from the other conditions. However, the success rate of the OR and B fault conditions are misclassified with OR, B and normal conditions. The reason for this is that the peaks of the envelope in the B fault condition are not as evident as in the other conditions. In the neural network classifier, if the 9 selected TK features are used, the B fault success rate is increased 11.11%. As a result, the misclassification between B fault condition and the rest of conditions is lower.

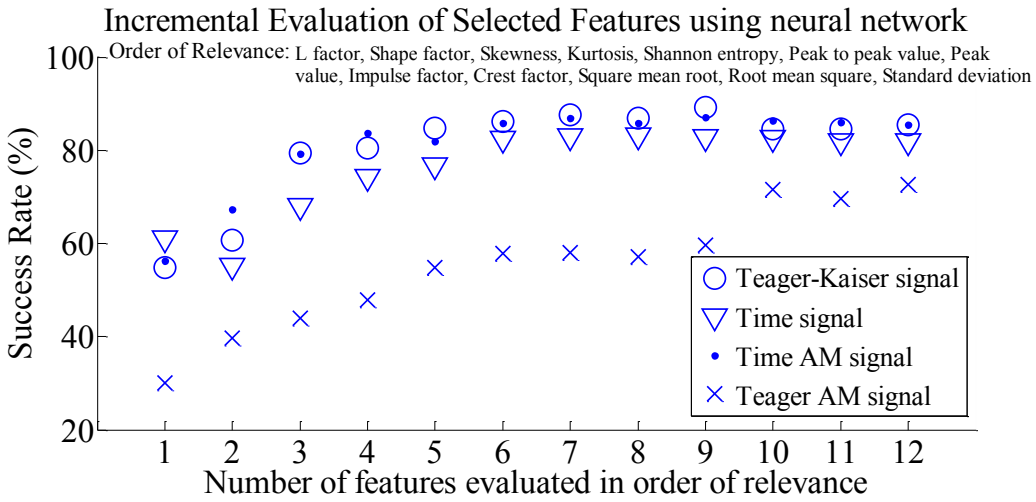

Figure 4-5: Success rates using TK, T, AM and TK-AM features in order of relevance with the neural network classifier.

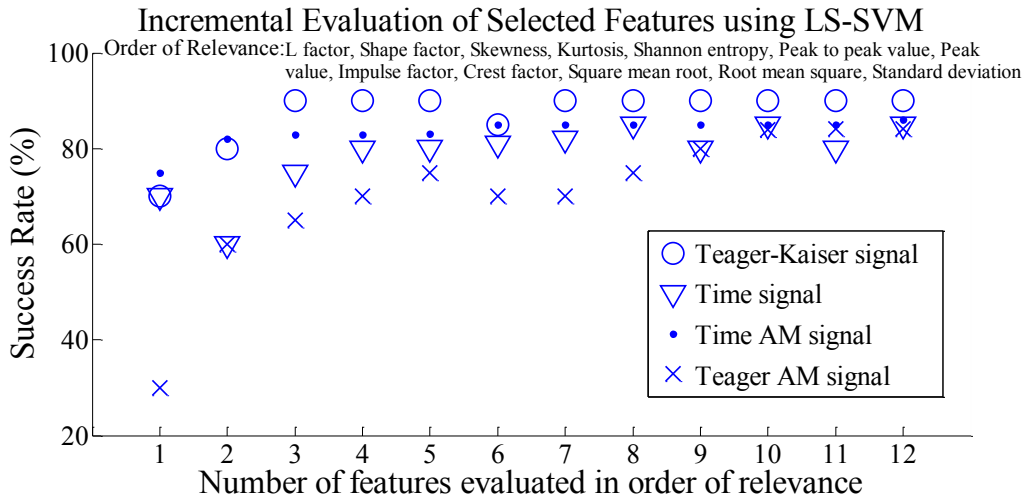

Figure 4-6: Success rates using TK, T, AM and TK-AM features in order of relevance with the LS-SVM classifier.

TABLE 4-1: SUCCESS RATES USING TK, T, TK-AM AND AM FEATURES

Classifier	TK features	T features	TK-AM features	AM features
Neural Network	85.5 (σ=5.66) 89.17(σ=4.97)*	82(σ=7.77)	72.67(σ=10.71)	85.5(σ=6.99)
LS-SVM	90(σ=4.97) 90(σ=3.66)*	85(σ=7.07)	84.17(σ=6.99)	86(σ=7.07)

TABLE 4-2: CONFUSION MATRIX OF NORMAL, IR, OR, B FAULT CONDITIONS USING ALL THE TK FEATURES AND THE 9 TK FEATURES SELECTED (SHOWN IN BOLD) FOR NEURAL NETWORK CLASSIFIER

Detector Decision (%)	Actual Diagnosis (%)			
	Normal	IR	OR	B
Normal	100 (σ=0) **100 (σ=0)**	0(σ=0) **0(σ=0)**	0(σ=0) **0(σ=0)**	0(σ=0) **0(σ=0)**
IR	0(σ=0) **0(σ=0)**	91.56(σ=0.36) **94.33(σ=0.54)**	8.44(σ=0.36) **5.67(σ=0.54)**	0(σ=0) **0(σ=0)**
OR	11.11(σ=2.51) **5.67(σ=1.57)**	0(σ=0) **0(σ=0)**	70(σ=1.02) **71(σ=1.31)**	18.89(σ=2.77) **23.33(σ=2.37)**
B	3.33(σ=1.02) **1.67(σ=0.36)**	5.56(σ=1.57) **3.33(σ=1.02)**	8.89(σ=2.21) **3.67(σ=0.36)**	80.22(σ=3.19) **91.33(σ=1.57)**

TABLE 4-3: CONFUSION MATRIX OF NORMAL, IR, OR, B FAULT CONDITIONS USING ALL THE TK FEATURES FOR LS-SVM CLASSIFIER

Detector Decision (%)	Actual Diagnosis (%)			
	Normal	IR	OR	B
Normal	100(σ=0)	0(σ=0)	0(σ=0)	0(σ=0)
IR	0(σ=0)	95.56(σ=3.57)	4.44(σ=3.57)	0(σ=0)
OR	0(σ=0)	2.11(σ=1.57)	81.22(σ=2.57)	16.67(σ=2.57)
B	0(σ=0)	0(σ=0)	17(σ=2.57)	83(σ=2.57)

4.1.2 Evaluation with the UH-60 Helicopter Database for bearing degradation assessment

The Teager-Kaiser transformed is also applied to the endurance test of an inboard input pinion bearing of a Black Hawk Helicopter, a run-to-failure bearing vibration database (see Chapter 3) where a rolling element of the bearing was damaged. The database consists of 62 datasets of 10 seconds each. The first evidence of degradation in the roller bearing SB-2205 occurred in the data set number 40. For each dataset the Teager-Kaiser transform is applied and the following features are extracted from the raw vibration signal (T signal) and from the Teager-Kaiser transformed signal (TK signal): root mean square, crest factor, skewness, kurtosis [3].

Some previous works have focused on degradation indexes for the UH-60 database. The very first work [26] applied an existing library of diagnostics, including band pass filtering in different bands but these procedures did not detect a degradation of the bearing health in the early stages. For this reason, following works tried to improve this result. McInerny et. al [27] analysed envelope analysis extracting some

features in different band pass ranges. The results show that the kurtosis of the Q band [2500-3800Hz] envelope provides an earlier indication of this bearing failure. A more recent work uses cyclic spectral analysis to analyse the vibration signal [25]. Based on this study, an index of cyclostationarity is reported to have a better sensitivity to the presence of a fault. The use of the Teager-Kaiser operator followed by the extraction of time features avoids the inspection of different frequency bands and it is simpler and faster.

Evolution of features

In Figure 4-7 and Figure 4-8 the evolution of the extracted features from the TK signal and from the T signal are shown. It can be observed that none of the features extracted from the T signal shows significant changes over the endurance test. The values of the features extracted from the TK signal show an increment from the dataset 40. This fact is more obvious in the case of the root mean square and kurtosis. The results show that root mean square and kurtosis features extracted from the signal transformed to the Teager-Kaiser domain are good indicators of the bearing degradation. For comparison, the features were computed using the envelope signal of the Q band [2500-3800Hz] [27] and the results are plotted in Figure 4-9. The results show an increment in the values of skewness, kurtosis and RMS between data set 40 and data set 50. Then, the values of these features decrease. Around data set 58 their values increase again. Therefore, they do not show a monotonic increment as the fault develops.

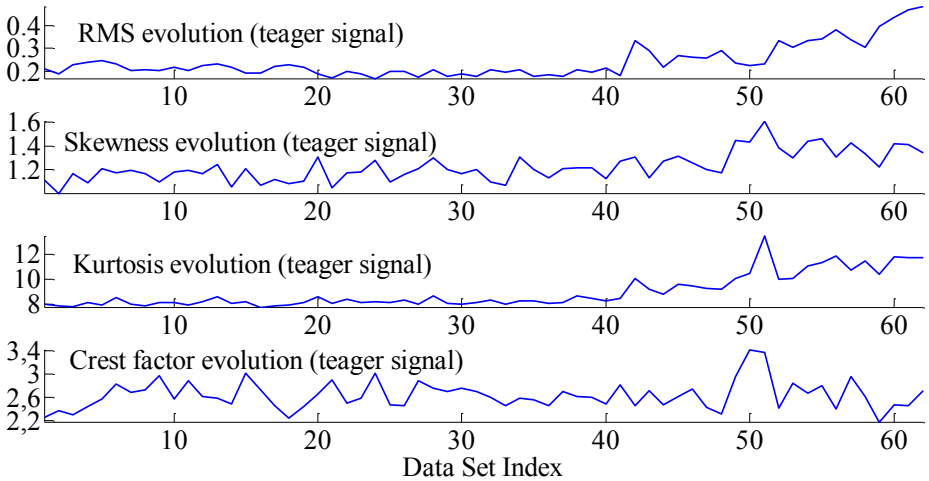

Figure 4-7: Evolution of the features extracted from the TK signal.

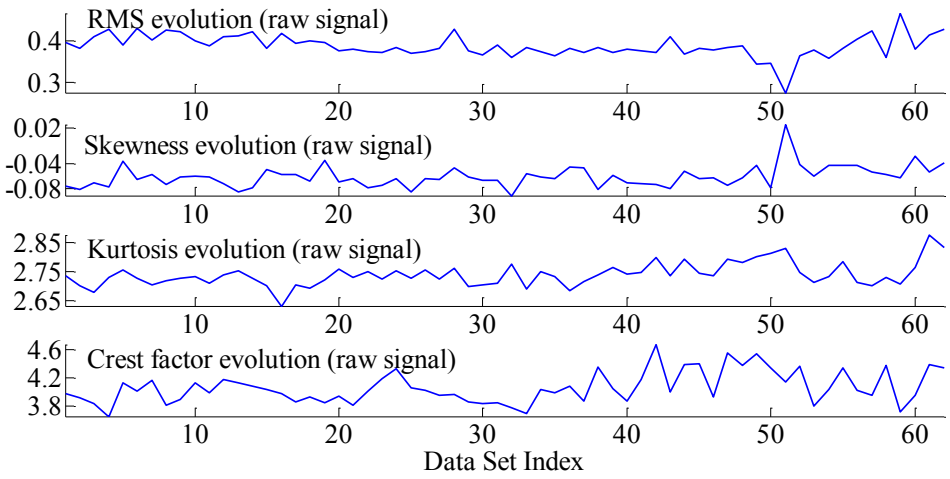

Figure 4-8: Evolution of the features extracted from the raw vibration signal (T signal).

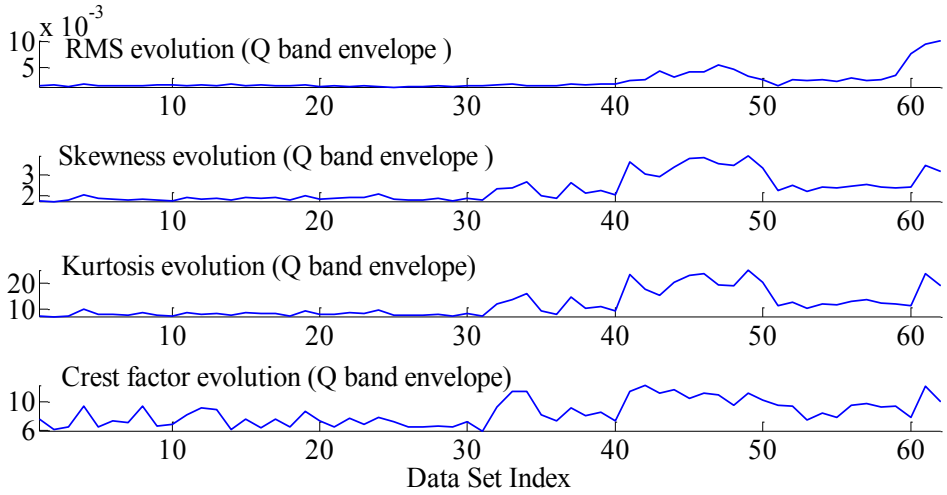

Figure 4-9: Evolution of the features extracted from the envelope signal of the Q band[2500-3800Hz].

4.1.3 Conclusions

In this Thesis we propose the use of statistics, energy-based and impulsive measures extracted from the Teager-Kaiser signal in bearing fault diagnosis. The vibration signal is transformed into the Teager-Kaiser domain using the Teager-Kaiser operator. A standard and easily reproducible neural network classifier is used to evaluate the discrimination ability of the extracted features between normal bearing, outer race fault, inner race fault and ball fault. Moreover, a LS-SVM classifier is also used to validate

the results obtained by the neural network. The results show that the use of statistical, based-energy and impulsive features extracted from the Teager-Kaiser signal in bearing fault diagnosis outperforms the results obtained by the same features extracted from the time vibration signal, from the time envelope signal (computed using TKEO) and from the time envelope computed using band-pass filter. In addition, the use of the Teager-Kaiser signal avoids visual inspection of the bearing spectrum to determine the center frequency and the bandwidth of the band-pass filter. The computation of the extracted features and of the TKEO itself is also simpler and faster than band-pass filtering.

The proposed method is also applied to a run-to-failure bearing vibration database obtained from an endurance test of a Black Hawk Helicopter. The results show that root mean square and kurtosis features extracted from the signal transformed to the Teager-Kaiser domain are good indicator of the bearing degradation.

4.2 Proposal of Lempel-Ziv complexity measure based on wavelet package transform for bearing degradation assessment

The aim of bearing fault diagnosis techniques is to detect the kind of fault presented in a bearing (i.e. outer-race fault, inner-race fault or ball fault in the case of discrete defects). Once the kind of bearing fault is diagnosed (i.e. inner race fault, outer race fault or ball fault), it is important to assess the severity of the fault (fault identification), i.e. how large the fault is. Another important task in condition monitoring is the early detection of a fault (to follow the degradation of a component from normal condition to fault condition).

In this Thesis, we have developed a new methodology to assess the severity of bearings with outer race fault and inner race fault with different degrees of severity (depicted in Figure 4-10). The proposed method combines the wavelet package transform technique and the Lempel-Ziv complexity to assess the fault severity of bearings with outer race and inner race fault. We evaluate the proposed method in the Case Western Vibration Bearing database, the UH-60 helicopter database and in the IMS bearing database. Wavelet packet transform is a time-frequency technique that basically decomposes the signal into detail (low frequency components) and

approximations signals (high frequency components) in different levels of decomposition or scales. Wavelet packet transform is used as a preprocessing tool to select the node with higher energy (i.e. the node where the fault lies). Then, the Lempel-Ziv complexity is used to measure the severity of the fault. As the Lempel-Ziv complexity values are bounded between 0 and 1, it is a good indicator of the severity of the bearing fault.

In this section, a description of the methods for fault severity assessment in bearings literature is carried out. Next, the preprocessing tool (the wavelet packet transform) and the Lempel-Ziv complexity are explained. Then, the proposed methodology is shown and finally a set of experiments in bearings is carried out to show the usefulness of our proposal and a comparison with some methods in literature is also accomplished.

State of the art

The severity assessment in bearings in literature is mainly addressed with time-domain features including kurtosis, root mean square, crest factor and amplitudes [20], [21]. Kurtosis increases in single-point faulty bearings from a value of 3 (in the case of free-fault bearing) to higher values when the bearing has a single-point defect. However, when the single-point defect is in advanced stages kurtosis values return to 3 [20]. Root mean square, crest factor, amplitudes are other techniques to follow the degradation of the fault. However, they have the same problems that kurtosis. Their values are not consistent with the evolution of the fault. There are other techniques in frequency domain such as energy features extracted from envelope analysis. The main disadvantage of these features are that thery are not bounded.

Lempel-Ziv complexity was firstly investigated in bearing severity assessment Lempel-Ziv complexity in [15]. The authors proposed LZ for outer-race bearing fault deterioration. They extracted the LZ values from the raw vibration signal. They showed that the LZ value increases as the size of the outer race bearing fault increases. H. Hong et al. [16] proposed a new version of the Lempel-Ziv complexity as a bearing fault severity measure based on the continuous wavelet transform (CWT). The applications to the bearing inner- and outer-race fault signals have demonstrated that the new version

of Lempel–Ziv complexity can effectively measure the severity of both inner- and outer-race faults. This technique uses the CWT to obtain the sub-band where the fault lies. Then, the signal is amplitude demodulated and the envelope signal and the carrier signal are obtained. Finally, the Lempel-Ziv complexity is computed for the envelope signal and for the carrier signal and a weighted summed is computed. They use different weights depending on the fault (IR fault or OR fault). In this Thesis, we propose a simpler way to assess the severity in bearing using wavelet package transform to obtain the sub-band where the fault lies and then applying Lempel-Ziv complexity to this sub-band.

Methods

Wavelet Packet Transform

Wavelet packet transform (WPT) is an extension of the discrete wavelet that allows a finer resolution of frequencies at both high frequencies and low frequencies. WPT can simultaneously break the signal up into detail (low frequency components) and approximations signals (high frequency components) in different levels of decomposition or scales. In bearing fault diagnosis the fault information lies in high frequency. For this reason, the wavelet packet transform is a common analysis tool for bearing fault diagnosis.

Mathematically, wavelet packets are a collection of functions $\{2^{-j/2}W_n(2^{-j}t-k), n \in N, j,k \in Z\}$ generated recursively from the following expressions:

$$W_{2n}(t) = \sqrt{2}\sum_m h(m)W_n(2t-m) \qquad \text{[Eq. 4-5]}$$

$$W_{2n+1}(t) = \sqrt{2}\sum_m g(m)W_n(2t-m) \qquad \text{[Eq. 4-6]}$$

where *h* and *g* are the quadrature mirror filters, $W_0(t)$ is the scaling function and $W_1(t)$ is the wavelet mother function, *k* is a time-localization parameter, *j* is a scale parameter (depth) and *n* is an oscillation parameter.

The wavelet packet coefficients for a discrete signal can be obtained using the following iterative expressions:

$$c_{j+1,2n}(k) = c_{j,n}(k) * h(-2k) = \sum_l h(l-2k)c_{j,n}(l), 0 < n < 2^j - 1 \qquad \text{[Eq. 4-7]}$$

$$c_{j+1,2n+1}(k) = c_{j,n}(k) * g(-2k) = \sum_l g(l-2k)c_{j,n}(l), 0 < n < 2^j - 1 \qquad \text{[Eq. 4-8]}$$

The original signal can be reconstructed using the following iterative expression:

$$c_{j,n}(l) = \sum_k h(l-2k)c^k_{j+1,2n,} + \sum_k g(l-2k)c^k_{j+1,2n+1}, 0 < n < 2^j - 1 \qquad \text{[Eq. 4-9]}$$

Wavelet packets are organized in trees, where the scale *j* defines the depth or level of the tree and *n* is the position or node in the tree. For each scale j, $n = 0,\ldots,2^j - 1$. From each node of the tree, two children nodes are obtained. One of the children node is obtained by low-pass filtering (using the impulse response *h*) followed by down-sampling and the other children node is obtained by high-pass filtering (using the impulse response *g*) followed by down-sampling. It is important to mention that the frequency order of the nodes for a level is not necessary the same as the node order because of aliasing introduced by down-sampling. For example, a signal with 1kHz bandwidth decomposed using a wavelet tree of decomposition level (scale) *j* = 3 have eight nodes at level 3 ($n = 0,\ldots,7$). The frequency content for each node (in natural order, i.e. $n = 0,\ldots,7$) is the following: *n* = 0, (0-125 Hz); *n* = 1, (125-250 Hz); *n* = 2, (375-500 Hz); *n* = 3, (250-375 Hz); *n* = 4, (875-1000 Hz); *n* = 5, (750-875 Hz); *n* = 6, (500-625 Hz); *n* = 7, (625-750 Hz). Therefore, the frequency order is not the same as node natural order (also called Paley order). To obtain the node in frequency order (from low frequency to high frequency), the nodes need to be reordered.

Lempel-Ziv complexity

Lempel and Ziv proposed a complexity measure that can characterize the degree of order or disorder and development of spatiotemporal patterns in a time series [18], [19]. The signal is transformed into binary sequences and Lempel-Ziv algorithm gives the number of distinct patterns contained in the given finite sequence. After normalization, the relative Lempel-Ziv complexity measure (LZC) reflects the rate of new pattern occurrences in the sequence. LZC values range from near 0 (deterministic sequence) to 1 (random sequence). To compute the LZC of a given sequence *s*, the sequence has to be coded using a finite symbol set *A*. Using the standard coding squeme, the sequence to be coded *s* is divided in α equiprobables bins, where α is the number of diferent symbols in *A*. An element of the symbol set *A* is assigned to each value of the signal according to the bin in which the value lies. Finally, a new sequence of symbols *S* is obtained. This sequence *S* is subsequently scanned looking for original subsequences of different lengths. The complexity value is related with the number of different subsequences found. Thus, if *A** denotes the set of all finite length sequences over the finite symbol set *A*, and $l(S)$ denotes the length of a sequence $S \in A^*$, then according to [19].

$$A^n = \{S \in A^* l(S) = n\}, n \geq 0 \qquad \text{[Eq. 4-10]}$$

and for every $S \in A^n$, the Lempel-Ziv complexity can be expressed as

$$c(n) < \frac{n}{(1-\varepsilon_n)\log_a(n)} \qquad \text{[Eq. 4-11]}$$

where $\varepsilon_n \to 0$ if $n \to \infty$ and α is the number of different symbols in the symbol set *A*. The upper bound for $c(n)$ is

$$\lim_{n\to\infty} c(n) = b(n) = \frac{n}{\log_a(n)} \qquad \text{[Eq. 4-12]}$$

Therefore, $c(n)$ can be normalized by using this upper limit

$$0 \le C(n) = \frac{c(n)}{b(n)} \le 1 \qquad \text{[Eq. 4-13]}$$

For $\alpha = 2$ two symbols are used to code the signal (0 and 1). For $\alpha = 3$ there exit 3 symbols (0, 1 and 2). The LZC value depends both on the number of symbols used in the coding squeme and on the length of the sequence *s*. According to [16] length of sequence higher than 3600 is enough.

Proposal

We propose a new method for fault severity assessment in bearings (depicted in Figure 4-10). The proposed method combines the wavelet packet transform and the Lempel-Ziv complexity to assess the fault severity of bearings with outer race and inner race. As explained before in this Chapter, the LZC over the raw vibration signal has been used in bearing literature to outer-race ault severity assessment [15]. However, this technique is affected by noise. We show that our proposal is less affected by noise.

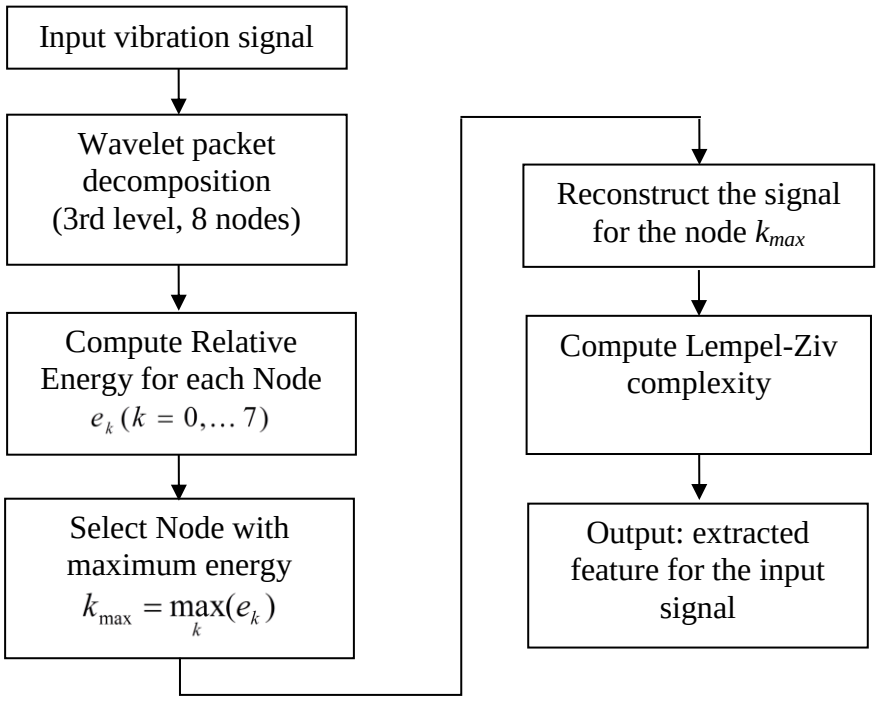

Figure 4-10: Proposed methodology for bearing severity fault assessment.

First, the raw vibration signal is decomposed using the wavelet packet transform with a level 3 of decomposition (8 nodes). Daubechies 6 (db6) (see Figure 4-11) was used as the mother wavelet because has an impulsive shape according to the impulsive fault bearing characteristics (see figure 4-12). The WPT is used to obtain the node where the fault lies and remove unwanted signals. Initially, mother wavelets db2 to db5 and db7 to db9 and symlet wavelet mother familiy from order 2 to 9 were used. The results obtained are very similar between wavelet mothers with orders higher than 3.

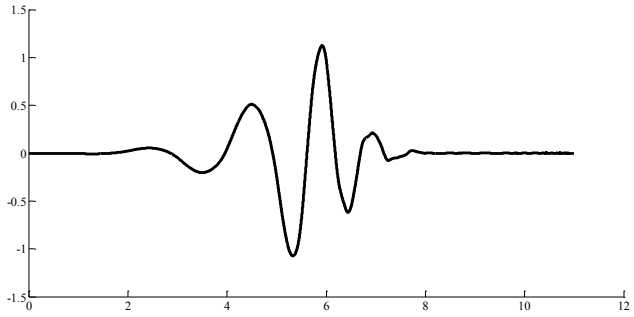

Figure 4-11: Waveform of the Daubechies 6 wavelet mother.

The vibration signals are broken up to 3 level ($j = 3$) of decomposition, obtaining 8 frequency bands (or 8 nodes) in this level of decomposition. Signals are reconstructed from the wavelet coefficients associated to each node. The reconstructed signal for each node is a new time series. If x denotes the original signal (the vibration signal), then $x_{j,n}$ is the reconstructed signals for *j*th level of decomposition and *n*th denotes the frequency-band of the signal. For $j = 3$, there are 8 frequency-band signals in level 3.

Then, the relative energy of the reconstructed signals of each node is computed, i.e. the energy of each node divided by the energy of the original raw signal. Then, the node with the maximum energy is selected. Relative energy features are computed from the reconstructed signals in level 3 of decomposition ($j = 3$). E denotes the energy of the original raw vibration signal $x(n)$:

$$E = \sqrt{\frac{\sum_{i=1}^{N}(x(i)-\bar{x})^2}{N-1}} \qquad \text{[Eq. 4-14]}$$

where $\bar{x}$ is the mean value of $x(n)$ and N is the number of samples of $x(n)$. Then, the relative energy of the reconstructed signals in level 3 is computed as:

$$e_n = \frac{\sqrt{\frac{\sum_{i=1}^{N}(x_{3,n}(i)-\bar{x}_{3,n})^2}{M-1}}}{E} \qquad \text{[Eq. 4-15]}$$

where $x_{3,n}$ (n = 0,...,7) are each of the reconstructed signals of level 3, M is the number of samples of $x_{3,n}$ and $\bar{x}_{3,n}$ is the mean value of each $x_{3,n}$.

The node with the maximum relative energy corresponds to the frequency band that contains the most fault features. A bearing with a localized fault will have the maximum relative energy located in high frequencies because the bearing is modelled as an amplitude modulated signal with the frequency of the carrier being the resonance frequency of the system. Therefore, features extracted from the selected node will have information about the fault.The node with the maximum relative energy is selected and the LZC is extracted from the reconstructed signal for this node.

The LZC gives information about the complexity of the reconstructed signal. This is the diagnostic feature vector extracted from the input frame. This procedure is applied for each frame and finally a feature vector is obtained.

The proposed methodology is applied to the Case Western Bearing Vibration Database, to the UH-60 helicopter database and to the IMS database. In order to compare with classical method in the literature, we extract kurtosis, Lempel-Ziv complexity from raw vibration data and kurtosis from wavelet package transform.

4.2.1 Evaluation with the Case Bearing Database

The proposed methodology is applied to the Case Bearing Database. Each sample of the database is divided in frames of 4096 samples each and for each frame the procedure shown in figure 4-11 is applied. As the sample frequency is $f_s = 12000$ Hz, the bandwitdth of the signal is $f_N = 6000$ Hz. Therefore, x has a frequency interval (0,6000]Hz, $x_{3,0}$ is the reconstructed signal in level 3 with a frequency range of (0, 750]Hz and $x_{3,7}$ is the reconstructed signal in level 3 with a frequency range of (5250, 6000]Hz. The nodes are reordered in frequency order.

In Figure 4-12-Figure 4-16 the relative energies for each node of the WPT (in level 3) for a frame is shown for the normal condition and for fault conditions IR, OR and B with different severities and different loads. In the figures a title is added to each subfigure: IRXXYY means inner race fault with XX mils of diameter and load YY. XX can be '07' for a severity of 7 mils in diameter, '14' for a severity of 14 mils in diameter or '21' for a severity of 21 mills in diameter. YY can be '00' for load 0, '01' for load 1, '02' for load 2 or '03' for load 3. The nodes of the wavelet packet were obtained in natural order (Paley order) and then were reordered in frequency order.

We can observe from the figures that the energy is concentrated in high frequency bands, where the fault characteristic lies. In the case of normal condition, the energy is concentrated in low frequency bands.

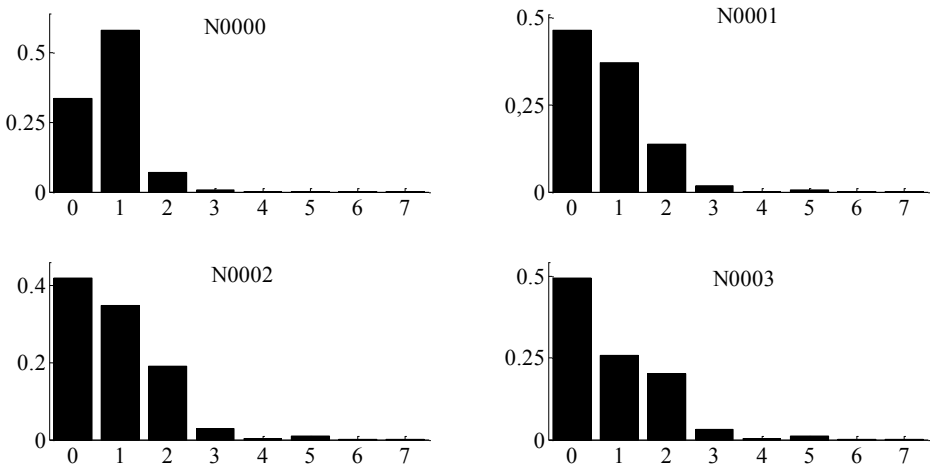

Figure 4-12: Relative energies for WPT nodes of level 3 of decomposition (ordered by frequency content) for a frame of 4096 samples extracted for normal vibration signals with different loads.

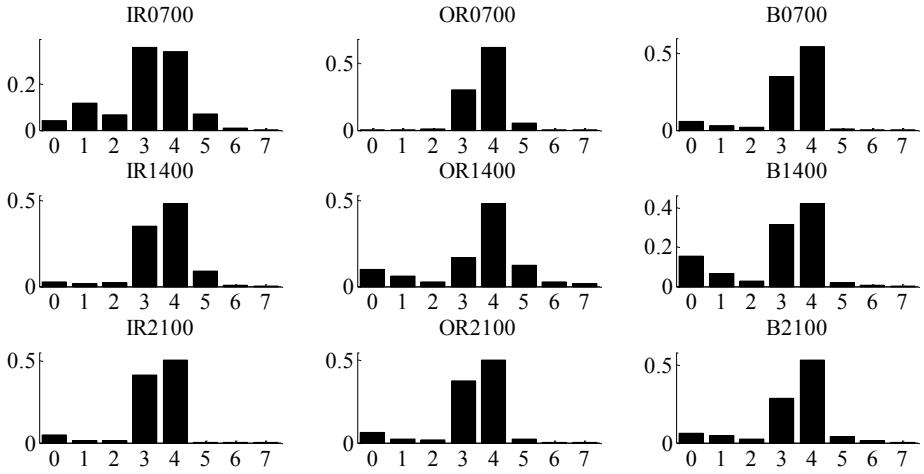

Figure 4-13: Relative energies for WPT nodes of level 3 of decomposition (ordered by frequency content) for a frame of 4096 samples extracted for vibration signals with inner race fault (left column), outer race fault (center column) and ball fault (right column) with different severities and for load 0.

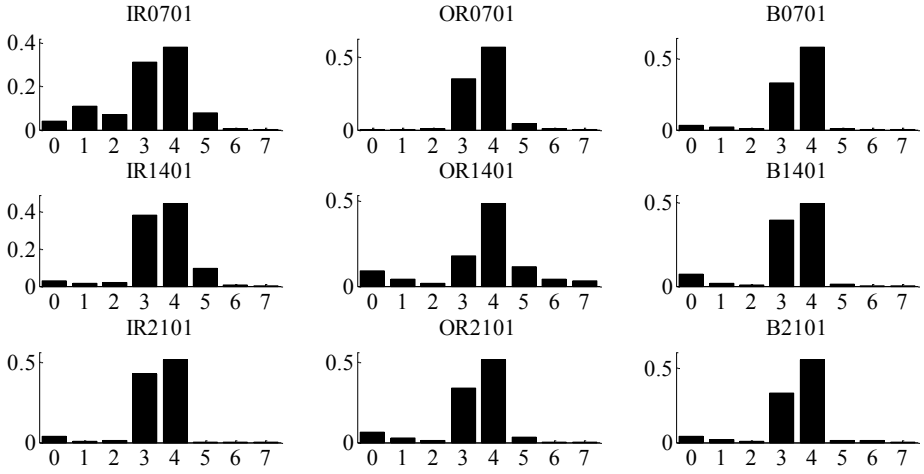

Figure 4-14: Relative energies for WPT nodes of level 3 of decomposition (ordered by frequency content) for a frame of 4096 samples extracted for vibration signals with inner race fault (left column), outer race fault (center column) and ball fault (right column) with different severities and for load 1.

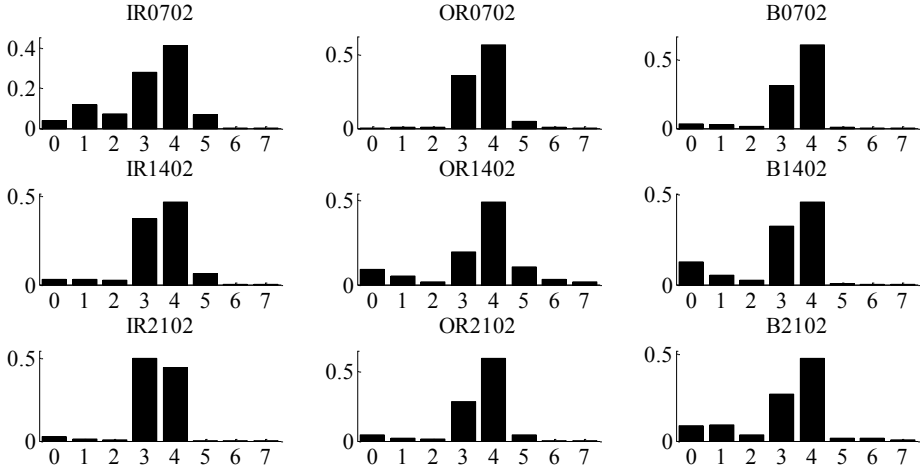

Figure 4-15: Relative energies for WPT nodes of level 3 of decomposition (ordered by frequency content) for a frame of 4096 samples extracted for vibration signals with inner race fault (left column), outer race fault (center column) and ball fault (right column) with different severities and for load 2.

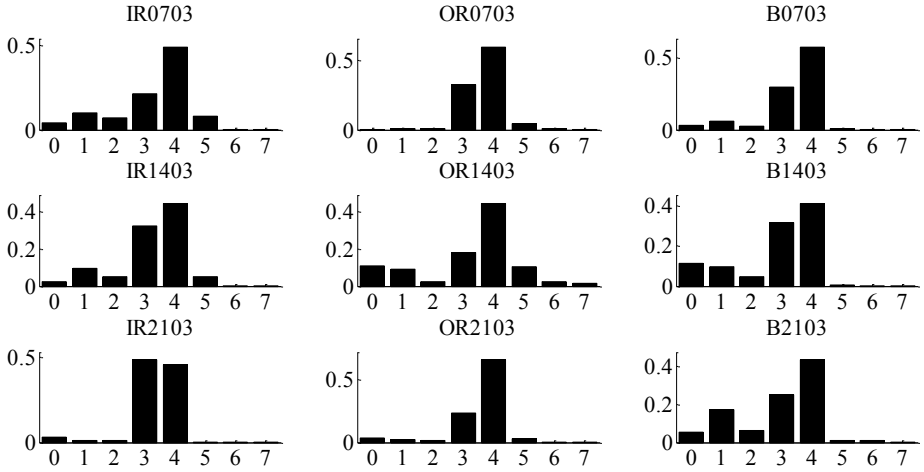

Figure 4-16: Relative energies for WPT nodes of level 3 of decomposition (ordered by frequency content) for a frame of 4096 samples extracted for vibration signals with inner race fault (left column), outer race fault (center column) and ball fault (right column) with different severities and for load 3.

After selecting the node of maximum energy, the LZC is computed. As mentioned in the LZC definition, LZC depends on the number of elements of the alphabet (α). A study of the variability of LZC with α is carried out for α = 2, 3, 4, 5. In Table 4-4 the mean and standard deviation values (between parentheses) of the LZC for each value of α for each kind of fault, each severity and each load are shown. The following conclusions can be extracted from Table 4-4: the values of the LZC for OR condition increase monotonically with the severity of the fault for $\alpha > 2$. The values of the LZC for IR condition decrease monotonically with the severity of tha fault for $\alpha > 2$. The best discrimination between severities is obtaine for $\alpha = 4$. The values of the LZC for B condition do not follow a clear tendency and depends of the load and the value of α. If the normal condition is included in the analysis, there is a monotonic increment of the LZC value from normal condition to OR condition with the maximum severity. These results are in concordance with literature results using the LZC from the raw vibration signal [15], [16]. According to these observations, the LZC is computed for α = 4 and this measure is discarded as a severity measure for B condition. However, it can be used to detect ball fault as the value of the LZC of the node of maximum energy is higher in ball fault with slight severity than in normal condition.

TABLE 4-4: MEAN VALUES AND STANDARD DEVIATION (BETWEEN PARENTHESES) OF THE LZCEMAXWPT FOR NORMAL CONDITION AND IR, OR AND B CONDITIONS FOR EACH LOAD (L) AND WITH DIFFERENT NUMBER OF SYMBOLS (ALFA).

L	α	N	IR07	IR14	IR21	OR07	OR14	OR21	B07	B14	B21
0	2	0,3637 (0,0142)	0,5286 (0,0089)	0,5257 (0,0121)	0,4388 (0,0223)	0,5079 (0,0099)	0,4756 (0,0116)	0,5276 (0,0133)	0,4492 (0,0105)	0,4308 (0,0113)	0,4424 (0,0126)
	3	0,4313 (0,0106)	0,5445 (0,0107)	0,5499 (0,0147)	0,4398 (0,0238)	0,4912 (0,0102)	0,5128 (0,0084)	0,5337 (0,0119)	0,4736 (0,0106)	0,4478 (0,0107)	0,4654 (0,0115)
	4	0,4468 (0,0072)	0,5494 (0,0085)	0,5465 (0,0102)	0,4475 (0,0220)	0,4907 (0,0074)	0,5146 (0,0098)	0,5286 (0,0106)	0,4748 (0,0092)	0,4422 (0,0101)	0,4660 (0,0085)
	5	0,4683 (0,0098)	0,5650 (0,0098)	0,5607 (0,0135)	0,4555 (0,0155)	0,5242 (0,0071)	0,5276 (0,0074)	0,5399 (0,0105)	0,4820 (0,0096)	0,4549 (0,0087)	0,4714 (0,0077)
1	2	0,2825 (0,0172)	0,5241 (0,0098)	0,5243 (0,0122)	0,4498 (0,0195)	0,4755 (0,0138)	0,4745 (0,0113)	0,5298 (0,0121)	0,4468 (0,0107)	0,4311 (0,0149)	0,4153 (0,0116)
	3	0,3038 (0,0112)	0,5481 (0,0095)	0,5466 (0,0113)	0,4594 (0,0216)	0,4571 (0,0129)	0,5154 (0,0088)	0,5357 (0,0107)	0,4782 (0,0096)	0,4373 (0,0162)	0,4552 (0,0104)
	4	0,3246 (0,0120)	0,5519 (0,0088)	0,5479 (0,0107)	0,4565 (0,0209)	0,4607 (0,0110)	0,5159 (0,0094)	0,5312 (0,0103)	0,4789 (0,0084)	0,4354 (0,0134)	0,4580 (0,0080)
	5	0,3384 (0,0099)	0,5656 (0,0087)	0,5599 (0,0078)	0,4707 (0,0181)	0,4993 (0,0097)	0,5272 (0,0099)	0,5409 (0,0101)	0,4889 (0,0119)	0,4537 (0,0115)	0,4659 (0,0091)
2	2	0,2947 (0,0151)	0,5311 (0,0088)	0,5144 (0,0119)	0,4800 (0,0153)	0,4835 (0,0089)	0,4887 (0,0129)	0,5231 (0,0099)	0,4264 (0,0108)	0,4356 (0,0214)	0,4192 (0,0119)
	3	0,3181 (0,0105)	0,5492 (0,0118)	0,5362 (0,0104)	0,4874 (0,0140)	0,4789 (0,0109)	0,5209 (0,0095)	0,5326 (0,0118)	0,4655 (0,0087)	0,4376 (0,0193)	0,4527 (0,0110)
	4	0,3388 (0,0104)	0,5455 (0,0070)	0,5349 (0,0103)	0,4812 (0,0109)	0,4741 (0,0084)	0,5210 (0,0091)	0,5276 (0,0104)	0,4718 (0,0094)	0,4418 (0,0153)	0,4566 (0,0100)
	5	0,3512 (0,0100)	0,5614 (0,0101)	0,5477 (0,0112)	0,4917 (0,0102)	0,5053 (0,0083)	0,5318 (0,0111)	0,5373 (0,0086)	0,4764 (0,0083)	0,4571 (0,0137)	0,4663 (0,0077)
3	2	0,3238 (0,0119)	0,5189 (0,0130)	0,5027 (0,0129)	0,4908 (0,0107)	0,5004 (0,0117)	0,5055 (0,0121)	0,5177 (0,0098)	0,4087 (0,0111)	0,4417 (0,0249)	0,4217 (0,0114)
	3	0,3409 (0,0093)	0,5457 (0,0088)	0,5262 (0,0125)	0,5018 (0,0163)	0,4956 (0,0107)	0,5304 (0,0115)	0,5236 (0,0128)	0,4524 (0,0092)	0,4480 (0,0245)	0,4550 (0,0088)
	4	0,3589 (0,0100)	0,5434 (0,0074)	0,5235 (0,0093)	0,4987 (0,0112)	0,4911 (0,0099)	0,5339 (0,0094)	0,5221 (0,0085)	0,4526 (0,0072)	0,4389 (0,0223)	0,4554 (0,0069)
	5	0,3699 (0,0076)	0,5614 (0,0093)	0,5359 (0,0081)	0,5114 (0,0094)	0,5149 (0,0113)	0,5476 (0,0089)	0,5308 (0,0087)	0,4585 (0,0090)	0,4588 (0,0178)	0,4634 (0,0094)

A comparison with other features used in literature is done [5], [15]. For simplicity we call our proposal 'LZC (EmaxWPT)'. The other features extracted for comparison are: the kurtosis extracted from the raw vibration signal ('Kurtosis (raw signal)'), the kurtosis of the node with maximum energy ('Kurtosis (EmaxWPT)'), the LZC extracted from the raw vibration signal ('LZC (raw signal)'). Figure 4-17 and Figure 4-18 show the results obtained for each method. The mean values of the extracted features for OR fault and for IR fault for each fault severity and for each load are represented. We can see that the mean of the LZC is monotonically increasing with the severity of fault in the OR fault and monotonically decreasing with the fault deterioration in the IR fault for the 'LZC (EmaxWPT)'. In the case of the 'Kurtosis (raw signal)' and the 'Kurtosis (EmaxWPT)' the values decrease for OR07 to OR14 and then increase for OR14 to OR21. In the case of the IR fault, the results are just the opposite. The values of the kurtosis increase for IR07 to IR14 and then decrease for IR14 to IR21. For the case of the LZC raw, the values increase form OR07 to OR14 and then decrease from OR14 to OR21. In the case of the IR fault the values decrease monotonically.

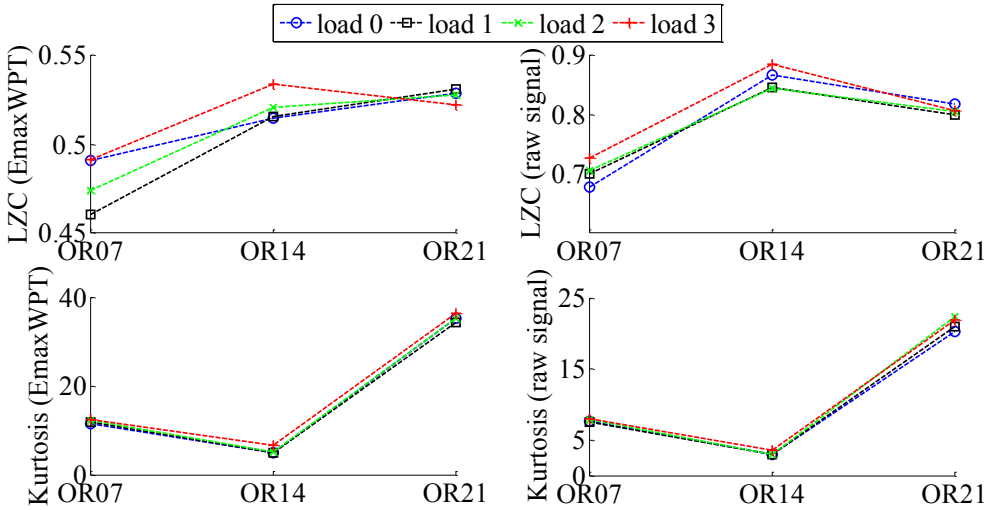

Figure 4-17: Evolution of the mean values obtained for each method: proposed method 'LZC (EmaxWPT)' (uppe-left), 'LZC (raw signal)' (upper-right), 'Kurtosis (EmaxWPT)' (bottom-left) and 'Kurtosis (raw signal)' (bottom-right) for outer race fault with different severities and different loads.

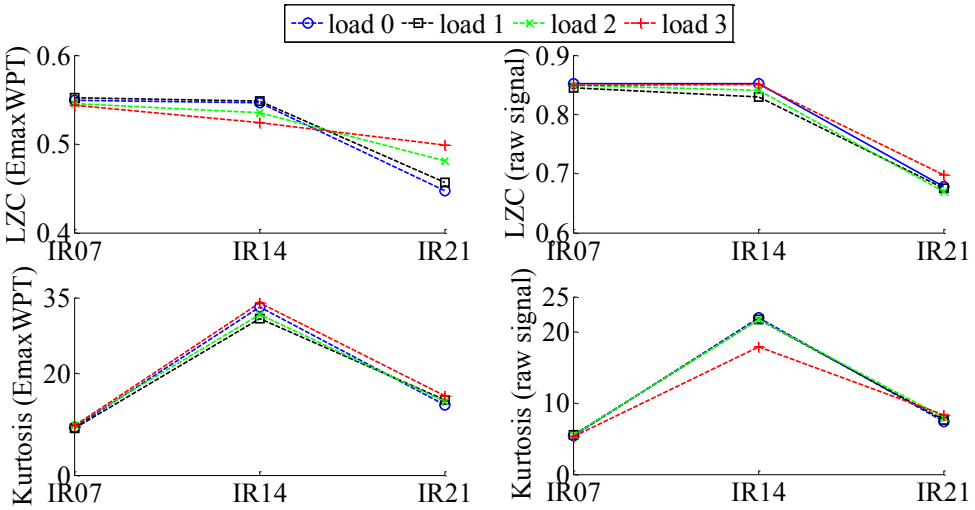

Figure 4-18: Evolution of the mean values obtained for each method: proposed method 'LZC (EmaxWPT)' (uppe-left), 'LZC (raw signal)' (upper-right), 'Kurtosis (EmaxWPT)' (bottom-left) and 'Kurtosis (raw signal)' (bottom-right) for inner race fault with different severities and different loads.

Figure 4-19 and Figure 4-20 show the same results as Figure 4-17 and Figure 4-18 with the normal condition added to the figures. In the case of OR fault, it can be observed from Figure 4-19 that the proposed method 'LZC (EmaxWPT)' follows monotonically the degradation from normal condition to OR fault condition, outperforming the rest of methods.

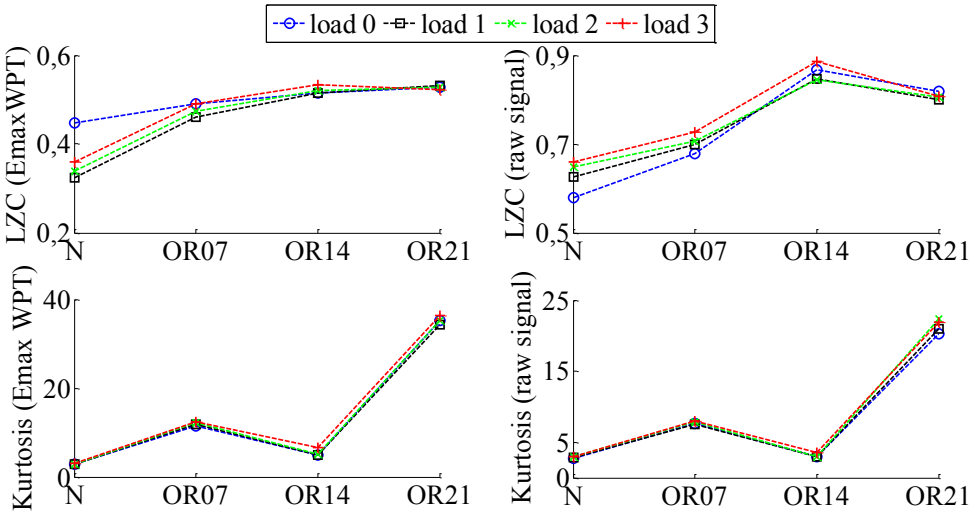

Figure 4-19: Evolution of the mean values obtained for each method: proposed method 'LZC (EmaxWPT)' (uppe-left), 'LZC (raw signal)' (upper-right), 'Kurtosis (EmaxWPT)' (bottom-left) and 'Kurtosis (raw signal)' (bottom-right) for outer race fault with different severities and different loads. The normal condition is also considered.

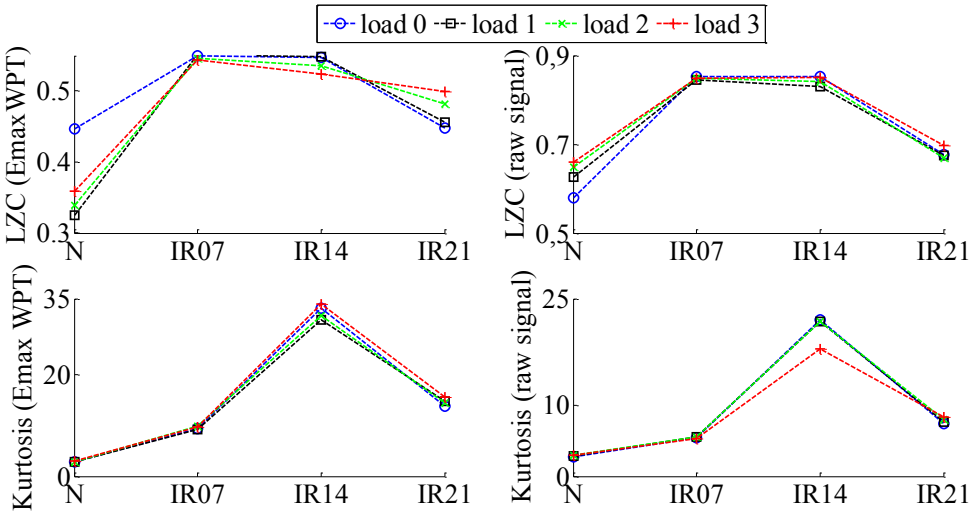

Figure 4-20: Evolution of the mean values obtained for each method: proposed method 'LZC (EmaxWPT)' (uppe-left), 'LZC (raw signal)' (upper-right), 'Kurtosis (EmaxWPT)' (bottom-left) and 'Kurtosis (raw signal)' (bottom-right) for inner race fault with different severities and different loads. The normal condition is also considered.

The robustness of the algorithm to Gaussian noise is also studied. Gaussian noise was added to the original vibration signal with different signal to noise ratios (SNR): 20dB, 15dB, 10dB, 5dB and 0dB. Then, the proposed method is applied (with $\alpha = 4$) for each SNR and for the original signal without noise added. Kurtosis of the raw signal, kurtosis of the maximum energy node and the LZC of the raw signal are also computed for each SNR and for the original signal. The motivation of this experiment is to show how the proposed method is more robuts to noise than computing the LZC from the raw vibration signal. The LZC measures the complexity in a signal. For random signals, the LZC is 1. Therefore, if the signals are contaminated with undesired Gaussian noise, the LZC will increase its value. If LZC is extracted from the raw vibration signal, it will be difficult to determine if the increasing or decreasing of the LZC is due to a fault or to noise. However, if the LZC is extracted from the node of the maximal energy associated to impulsive fault, the Gaussian noise will not affect in the same degree the signal. The following figures (Figure 4-21-Figure 4-28) show the results for each method and confirm our thoughts.

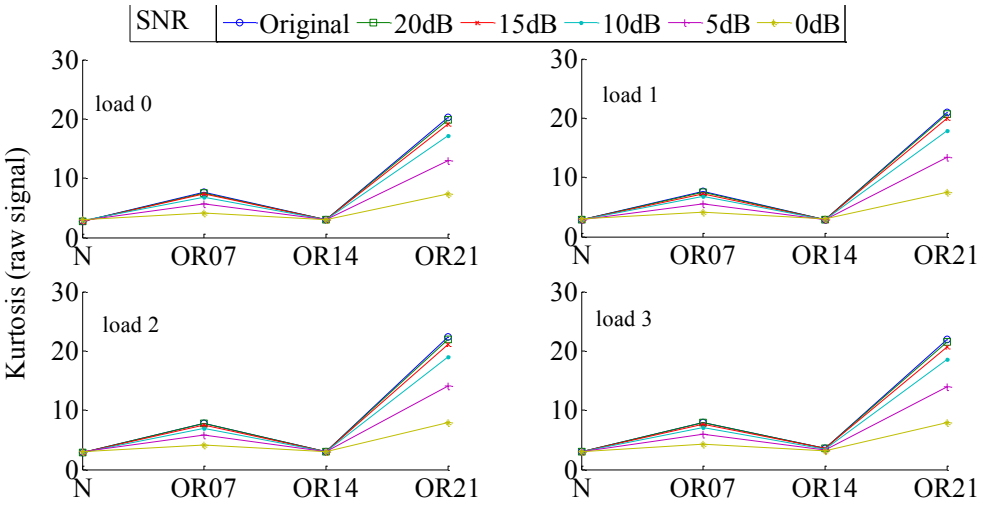

Figure 4-21: Evolution of the mean values obtained for 'Kurtosis (raw signal)' method applied for outer race fault condition and normal condition varying the amount of noise added to the original vibration signal. The results are shown for load: load 0 (upper-left), load 1(upper-right), load 2 (bottom-left), load 3 (bottom-right).

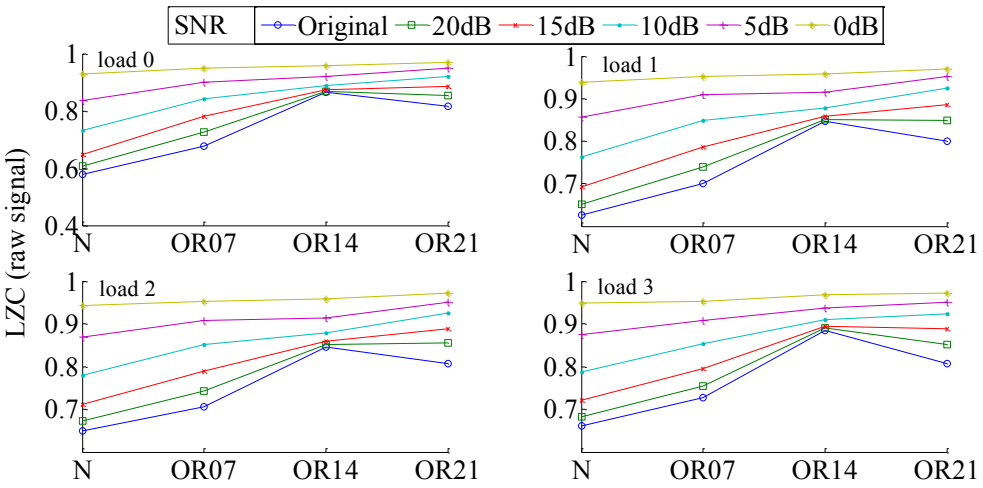

Figure 4-22: Evolution of the mean values obtained for 'LZC (raw signal)' method applied for outer race fault condition and normal condition varying the amount of noise added to the original vibration signal. The results are shown for load: load 0 (upper-left), load 1(upper-right), load 2 (bottom-left) and load 3 (bottom-right).

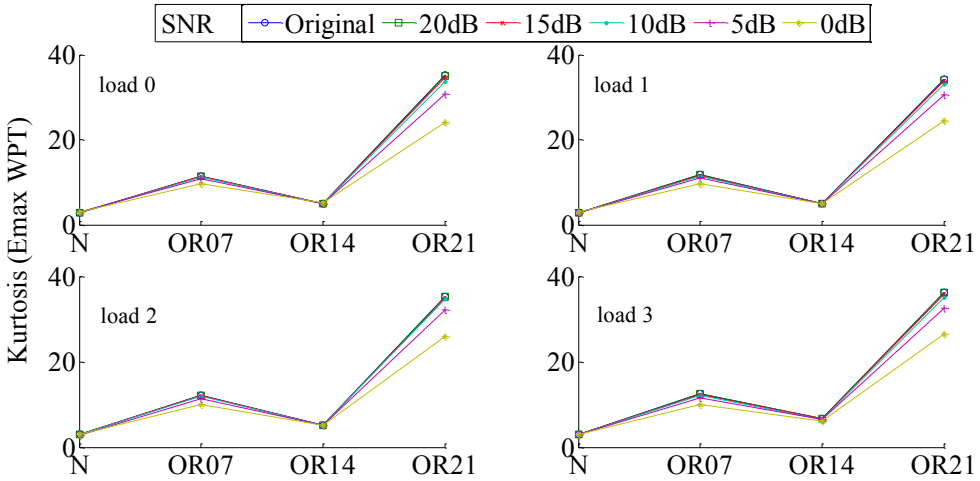

Figure 4-23: Evolution of the mean values obtained for 'Kurtosis (EmaxWPT)' method applied for outer race fault condition and normal condition varying the amount of noise added to the original vibration signal. The results are shown for load: load 0 (upper-left), load 1(upper-right), load 2 (bottom-left) and load 3 (bottom-right).

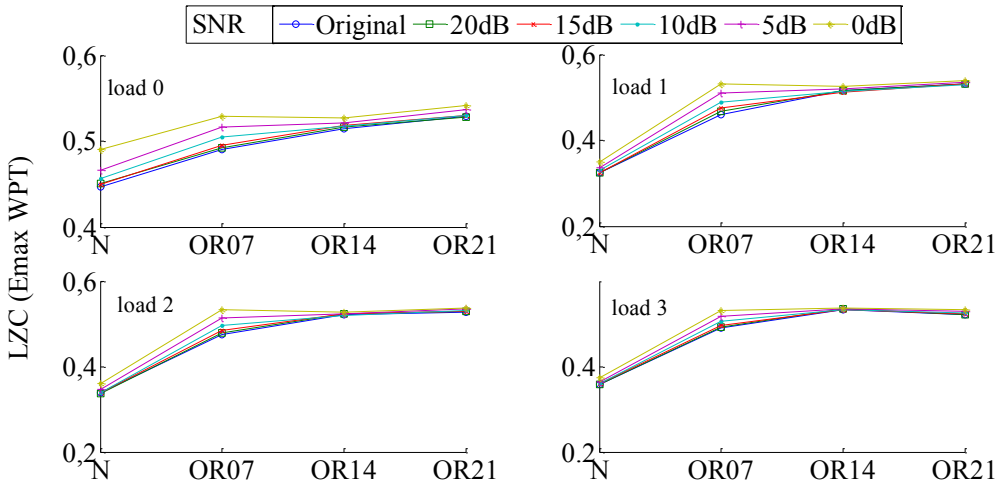

Figure 4-24: Evolution of the mean values obtained for the proposed method 'LZC (EmaxWPT)' applied for outer race fault condition and normal condition varying the amount of noise added to the original vibration signal. The results are shown for load: load 0 (upper-left), load 1(upper-right), load 2 (bottom-left) and load 3 (bottom-right).

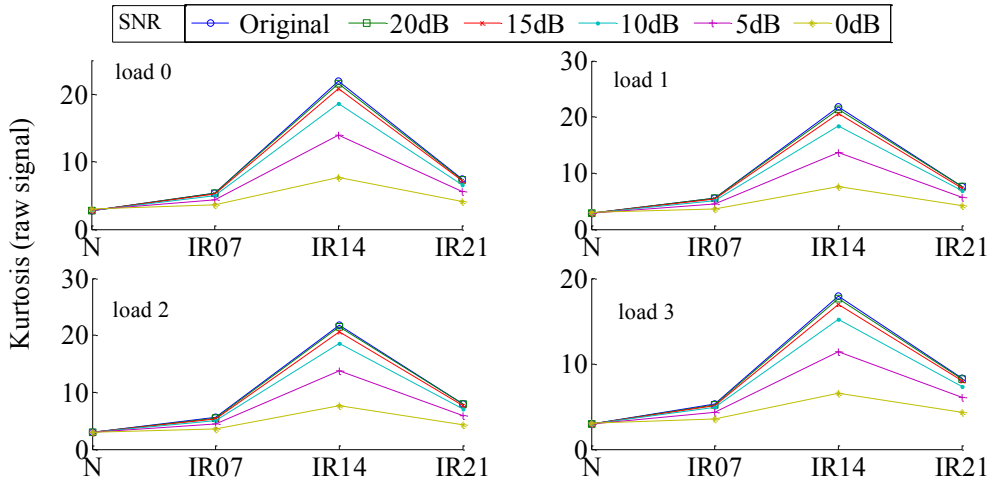

Figure 4-25: Evolution of the mean values obtained for 'Kurtosis (raw signal)' method applied for inner race fault condition and normal condition varying the amount of noise added to the original vibration signal. The results are shown for load: load 0 (upper-left), load 1(upper-right), load 2 (bottom-left) and load 3 (bottom-right).

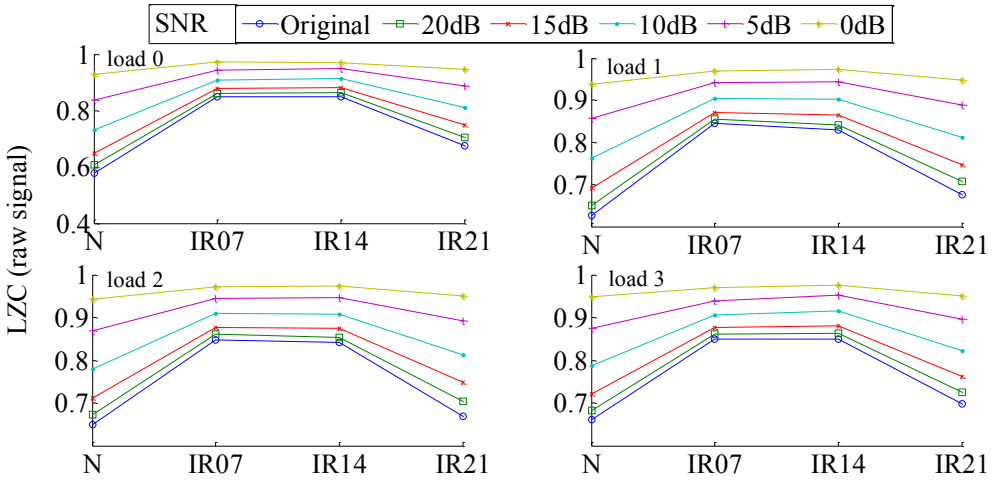

Figure 4-26: Evolution of the mean values obtained for 'LZC (raw signal)' method applied for inner race fault condition and normal condition varying the amount of noise added to the original vibration signal. The results are shown for load: load 0 (upper-left), load 1(upper-right), load 2 (bottom-left) and load 3 (bottom-right).

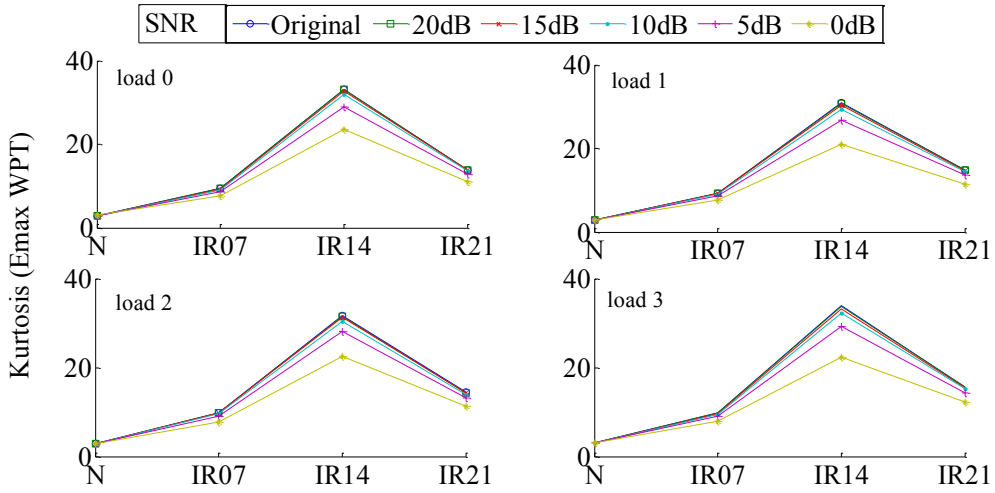

Figure 4-27: Evolution of the mean values obtained for 'Kurtosis (EmaxWPT)' method applied for inner race fault condition and normal condition varying the amount of noise added to the original vibration signal. The results are shown for load: load 0 (upper-left), load 1(upper-right), load 2 (bottom-left) and load 3 (bottom-right).

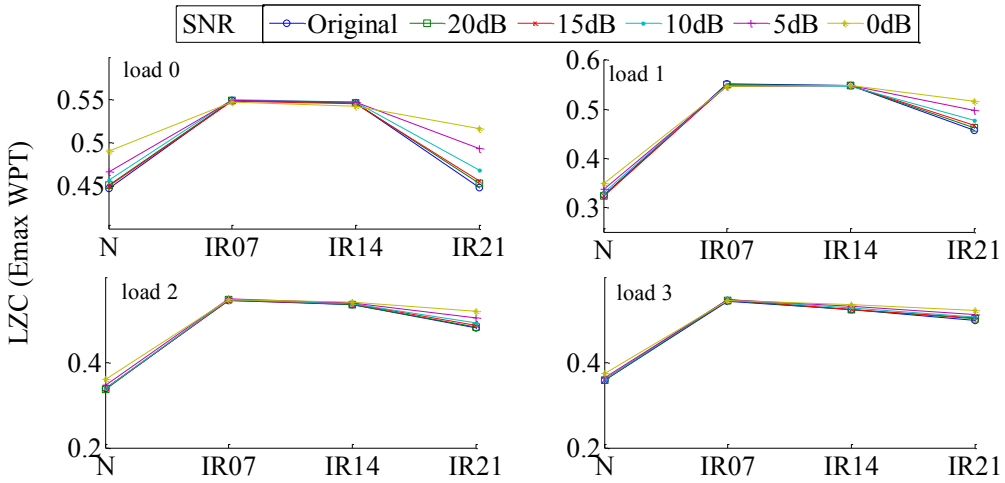

Figure 4-28: Evolution of the mean values obtained for the proposed method 'LZC (EmaxWPT)' applied for inner race fault condition and normal condition varying the amount of noise added to the original vibration signal. The results are shown for load: load 0 (upper-left), load 1(upper-right), load 2 (bottom-left) and load 3 (bottom-right).

4.2.2 Evaluation with the UH-60 Helicopter Database for bearing degradation assessment

The proposed method of the Lempel-Ziv complexity based on wavelet packet transform is also evaluated with UH-60 Black Hawk Helicopter database where a rolling element of the bearing was damaged during an endurance test. Although our proposal does not follow monotonically a fault in a rolling element, according to the results with the Case Western database it should detect a ball fault. For this reason, we apply the proposal to the UH-60 helicopter database.

As each dataset in the UH-60 database is 10 seconds (with a sample frequency of 100kHz) and the computation of the LZC is very slow with such amount of data, each dataset is divided in frames of 1 second each. The results are averaged per dataset.

The results are shown in Figure 4-29 for 'Kurtosis (raw signal)', 'LZC (raw signal)', 'Kurtosis (EmaxWPT)' and the proposed method 'LZC (EmaxWPT)'. As it is observed, none of the features can detect the fault. The 'LZC (raw signal)' and our proposal 'LZC (EmaxWPT)' shows an increase in their values in dataset 48, long after the fault.

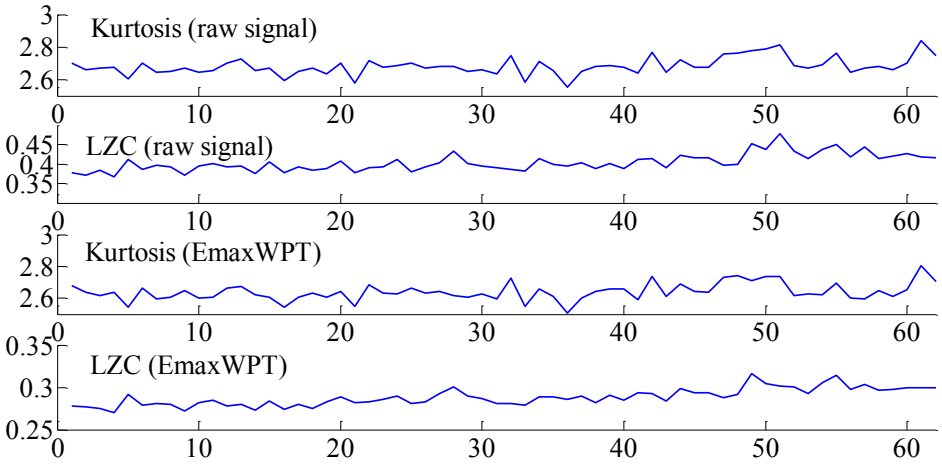

Figure 4-29: Evolution of the features using kurtosis and Lempel-Ziv complexity from the raw signal and kurtosis and Lempel-Ziv complexity from the node with maximal energy of the wavelet paket transform.

4.2.3 Evaluation with the IMS database

The IMS database is a run-to-failure experiment of 164 hours in where an outer race fault is developed in a bearing. Previous paper indicates that the start of the fault is 89 hours after the beginning of the experiment [29].

In this case, the proposed method is applied to each sample of the database (each sample has 20000 data points corresponding to 1 second of signal). As the sample frequency is $f_s = 20000\,\text{Hz}$, the bandwidth of the signal is $f_N = 10000\,\text{Hz}$. Therefore, x has a frequency interval (0,10000]Hz, $x_{3,0}$ is the reconstructed signal in level 3 with a frequency range of (0, 1250]Hz and $x_{3,7}$ is the reconstructed signal in level 3 with a frequency range of (8750, 10000]Hz. Kurtosis from the raw signal, kurtosis from the node of maximal energy of the WPT and the LZC from the raw signal are also extracted and the results compared.

Figure 4-30, Figure 4-31, Figure 4-32 and Figure 4-33 show the evolution of the features extracted by the 'Kurtosis (raw signal)' method, by the 'Kurtosis (EmaxWPT)' method, by the 'LZC (raw signal)' method and by the proposed method 'LZC (EmaxWPT)' respectively. The figures reveal that the kurtosis extracted from the raw vibration signal increase and then decrease again. Moreover, the first indication of fault is at 117 hours from the beginning of the run-to-failure experiment. The kurtosis extracted with the method KurtosisEmaxWPT shows a more consistent tendence that the kurtosis extracted from the raw vibration signal and the first indication of fault is at 89 hours from the beginning of the experiment. The LZCraw shows values near 1 in the normal condition. The reason can be the noise and signals of the rest of the gear that interfere with the bearing signal. 89 hours after the beginning of the experiment, the LZC values start decreasing. Then, the LZC values change with not clear tendency. When the LZCEmaxWPT method (proposed method) is applied, the LZC increase their values 89 hours after the beginning of the experiment (when the fault starts developing) and remains around the same values of complexity until the end of the experiment.

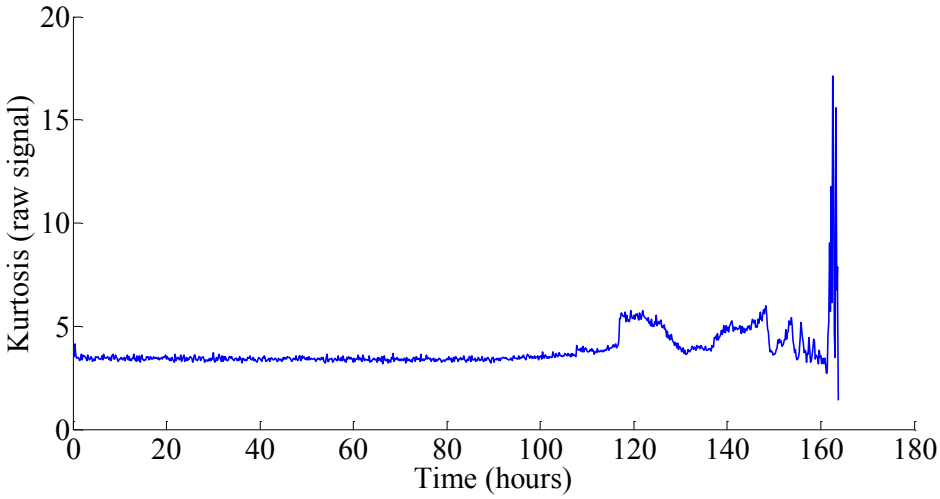

Figure 4-30: Evolution of the Kurtosis extracted from the raw vibration signal of a run-to-failure experiment of the bearing that eventually developed an outer-race fault.

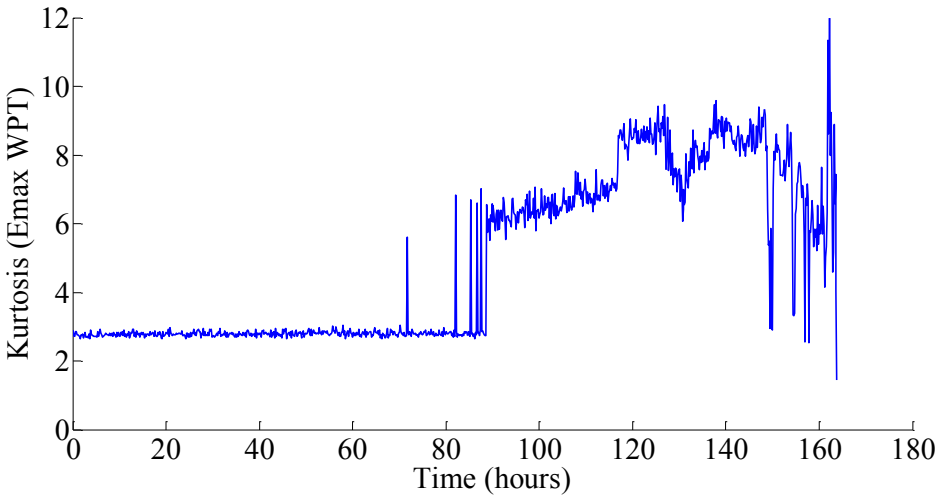

Figure 4-31: Evolution of the Kurtosis extracted from the node of maximal energy of the WPT of a run-to-failure experiment of the bearing that eventually developed an outer-race fault.

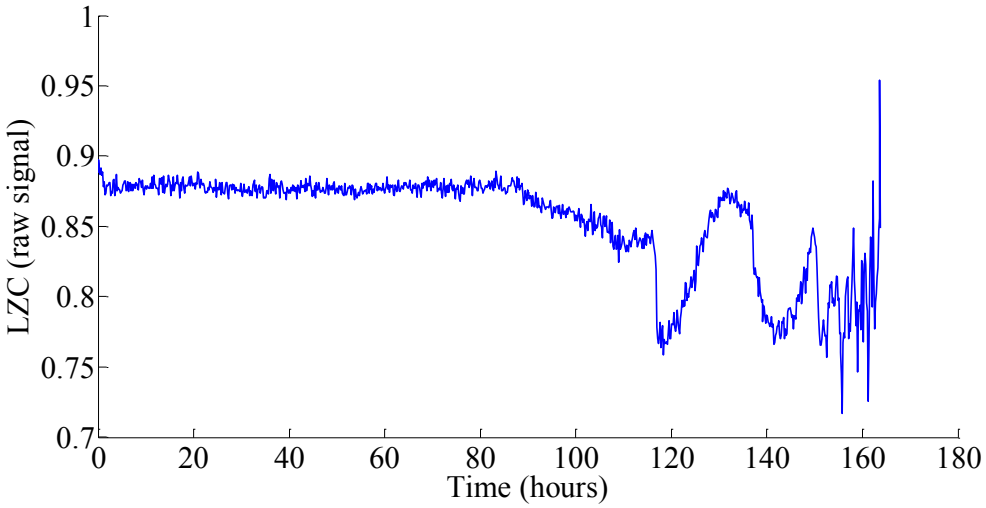

Figure 4-32: Evolution of the Lempel-Ziv complexity extracted from the raw vibration signal of a run-to-failure experiment of the bearing that eventually developed an outer-race fault.

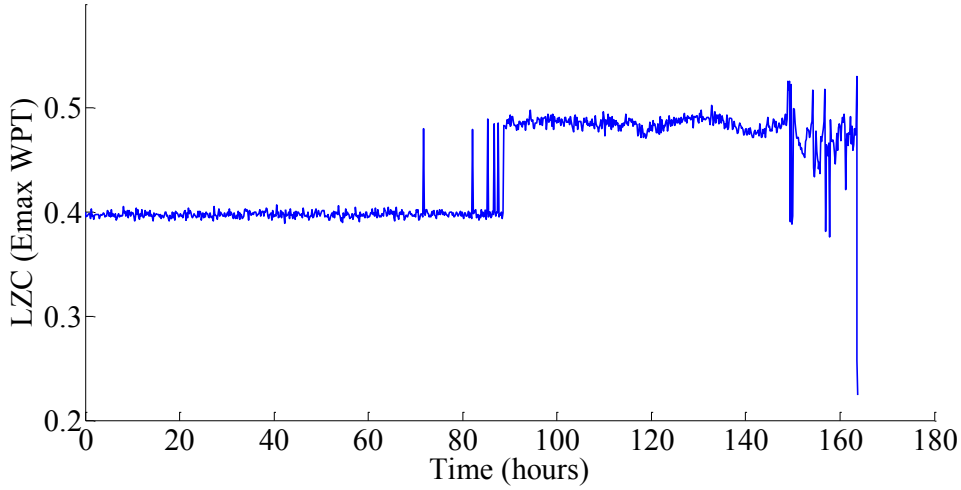

Figure 4-33: Evolution of the Lempel-Ziv complexity extracted from the node of maximal energy of the WPT of a run-to-failure experiment of the bearing that eventually developed an outer-race fault.

4.2.4 Conclusions

We have proposed a method to assess the fault severity, also called fault identification (how large the fault is), using the wavelet packet transform and the Lempel-Ziv complexity for inner race fault and for outer race fault. In the case of inner-race fault, the values of Lempel-Ziv complexity decrease when the fault evolves and in the case of the outer-race fault the values of Lempel-Ziv complexity increase when the fault evolves. The results obtained with the proposed method are in concordance with the

results in literature [15], [16]. In [15] the Lempel-Ziv complexity was applied to raw bearing vibration signals for normal and outer-race fault conditions. The Lempel-Ziv complexity increases from normal to outer-race fault with high level of severity. However, as we have shown in our experiments, when the raw bearing vibration signal is contaminated with Gaussian noise, the Lempel-Ziv complexity is affected, leading to incorrect interpretation of the Lempel-Ziv complexity values. In [16], the authors propose the use of the Lempel-Ziv complexity and the continuous wavelet transform in outer-race fault and inner-race fault severity assessment. A method to select the best scale in the continuous wavelet transform based on energy and kurtosis was proposed. Then, the coefficients in the best scale are recovered and amplitude demodulated. The final value of the Lempel-Ziv complexity is a weighted summed of the Lempel-Ziv complexity extracted over the coefficients at the best scale and the Lempel-Ziv complexity extracted over the amplitude demodulated coefficients at the best scale. Using this method, they also found that the Lempel-Ziv complexity increase with the outer-race fault severity and decrease with the inner-race fault severity. In our proposal, it is not necessary to compute the amplitude demodulated signal of the signal in the node with maximal energy and therefore we only compute Lempel-Ziv complexity one time.

One of the main advantages of using Lempel-Ziv complexity is that it is bounded between 0 and 1. With the use of the wavelet packet transform and the selection of the node with maximal energy (the node in which the fault lies), the effects of gaussian noise contamination is reduced.

In the case of outer-race fault, this method can follow the fault degradation from normal condition to fault condition monotonically. It is worth to mention that the results obtained with the ball fault are not monotonically increasing or decreasing with the fault severity. However, the ball faut can be detected with the proposed method.

The method was applied to two run-to-failure experiments: UH-60 helicopter database and IMS database. In the case of the UH-60 helicopter the proposed method does not detect the fault in early stages. A possible reason is that the wavelet packet is not detecting the correct node where the fault lies. More research is needed in this case.

In the case of the IMS database the proposed method detects the fault in the outer race and outperforms the other methods.

4.3 Contributions of this Chapter

The contributions of this Chapter are:

1. A new feature extraction methodology to detect bearing faults at inner race, outer race and ball race using the Teger-Kaiser nonlinear operator with statistics features. A comparison with conventional techniques is done and the proposed methodology outperforms the conventional one. The method is also applied to follow the degradation of a bearing with a ball fault. Several publications have been generated [1]-[3].

2. A new methodology to assess the severity of inner-race and outer-race faults is proposed. The methodology is based on wavelet package transform and Lempel-Ziv complexity measure. A publication has been generated [4].

Both contributions are based on nonlinear techniqes.

4.4 References

[1] Henríquez, P., Alonso, J. B., Ferrer, M. A., & Travieso, C. M. (2013). Application of the Teager–Kaiser energy operator in bearing fault diagnosis.*ISA transactions*, *52*(2), 278-284.

[2] Henríquez, P., Alonso, J. B., Ferrer, M. A., Travieso, C. M. (2011, May-June). Application of Higher Order Statistics of Teager-Kaiser Energy Transformed Vibration Signal for Bearing Fault Diagnosis. In *Proc. of the 24th Int. Congress on Condition Monitoring and Diagnostics Engineering Management* (pp. 265-274), Stavanger, Norway.

[3] Henríquez, P., White, P., Alonso, J. B., Ferrer. M. A. (2011, October). Application of Teager-Kaiser Energy Operator to the Analysis of Degradation of a Helicopter Input Pinion Bearing. In *Proc. of the International Conference Surveillance 6* (pp. 265-274), University of Technology of Compiègne, France.

[4] Henríquez, P., Alonso, J. B., Ferrer, M. A., Travieso, C. M. (2014, September). Degradation assessment in bearings with outer race fault. In *27th International Congress of Condition Monitoring and Diagnostic Engineering Management (COMADEM 2014)* (pp. 1-6), Brisbane, Australia.

[5] Samanta, B., Al-Balushi, K. R., & Al-Araimi, S. A. (2006). Artificial neural networks and genetic algorithm for bearing fault detection. *Soft Computing*, *10*(3), 264-271.

[6] McFadden, P. D., & Smith, J. D. (1984). Vibration monitoring of rolling element bearings by the high-frequency resonance technique—a review. *Tribology international*, *17*(1), 3-10.

[7] Zhang, Y., & Randall, R. B. (2009). Rolling element bearing fault diagnosis based on the combination of genetic algorithms and fast kurtogram.*Mechanical Systems and Signal Processing*, *23*(5), 1509-1517.

[8] Lu, X., & Wang, J. (2011, April). Bearing fault diagnosis based on redundant second generation wavelet denoising and EEMD. In *Consumer Electronics, Communications and Networks (CECNet), 2011 International Conference on*(pp. 1090-1093). IEEE.

[9] Li, H., Fu, L., & Zhang, Y. (2009, April). Bearing faults diagnosis based on teager energy operator demodulation technique. In *Measuring Technology and Mechatronics Automation, 2009. ICMTMA'09. International Conference on* (Vol. 1, pp. 594-597). IEEE.

[10] Liang, M., & Bozchalooi, I. S. (2010). An energy operator approach to joint application of amplitude and frequency-demodulations for bearing fault detection. *Mechanical systems and signal processing*, *24*(5), 1473-1494.

[11] Kaiser, JF., On a simple algorithm to calculate the energy of a signal. In: *international conference on acoustics, speech, and signal processing*; 1990. p. 381-384.

[12] Maragos, P., Kaiser, J. F., & Quatieri, T. F. (1993). Energy separation in signal modulations with application to speech analysis. *Signal Processing, IEEE Transactions on*, *41*(10), 3024-3051.

[13] Gavidia-Ceballos, L., Hansen, J. H., & Kaiser, J. F. (1996, October). Vocal fold pathology assessment using AM autocorrelation analysis of the Teager energy operator. In *Spoken Language, 1996. ICSLP 96. Proceedings., Fourth International Conference on* (Vol. 2, pp. 757-760). IEEE.

[14] Lei, Y., He, Z., Zi, Y., & Chen, X. (2008). New clustering algorithm-based fault diagnosis using compensation distance evaluation technique. *Mechanical Systems and Signal Processing*, *22*(2), 419-435.

[15] Yan, R., & Gao, R. X. (2004). Complexity as a measure for machine health evaluation. *Instrumentation and Measurement, IEEE Transactions on*, *53*(4), 1327-1334.

[16] Hong, H., & Liang, M. (2009). Fault severity assessment for rolling element bearings using the Lempel–Ziv complexity and continuous wavelet transform. *Journal of sound and vibration*, *320*(1), 452-468.

[17] Wu, J. D., & Liu, C. H. (2009). An expert system for fault diagnosis in internal combustion engines using wavelet packet transform and neural network. *Expert systems with applications*, *36*(3), 4278-4286.

[18] Lempel, A., & Ziv, J. (1976). On the complexity of finite sequences.*Information Theory, IEEE Transactions on*, *22*(1), 75-81.

[19] Kaspar, F., & Schuster, H. G. (1987). Easily calculable measure for the complexity of spatiotemporal patterns. *Physical Review A*, *36*(2), 842-848.

[20] Al-Ghamd, A. M., & Mba, D. (2006). A comparative experimental study on the use of acoustic emission and vibration analysis for bearing defect identification and estimation of defect size. *Mechanical systems and signal processing*, *20*(7), 1537-1571.

[21] Caesarendra, W., Widodo, A., & Yang, B. S. (2010). Application of relevance vector machine and logistic regression for machine degradation assessment.*Mechanical Systems and Signal Processing*, *24*(4), 1161-1171.

[22] Pudil, P., Novovičová, J., & Kittler, J. (1994). Floating search methods in feature selection. *Pattern Recognition Letters*, *15*(11), 1119-1125.

[23] Riedmiller, M., & Braun, H. (1993). A direct adaptive method for faster backpropagation learning: The RPROP algorithm. In *Neural Networks, 1993., IEEE International Conference on* (pp. 586-591). IEEE.

[24] Van Gestel, T., Suykens, J. A., Baesens, B., Viaene, S., Vanthienen, J., Dedene, G., & Vandewalle, J. (2004). Benchmarking least squares support vector machine classifiers. *Machine Learning*, *54*(1), 5-32.

[25] Estupiñan, E., White, P., & San Martin, C. (2007). A cyclostationary analysis applied to detection and diagnosis of faults in helicopter gearboxes. In *Progress in Pattern Recognition, Image Analysis and Applications* (pp. 61-70). Springer Berlin Heidelberg.

[26] Hardman, W., Hess, A., & Sheaffer, J. (1999). SH-60 helicopter integrated diagnostic system (HIDS) program-diagnostic and prognostic development experience. In *Aerospace Conference, 1999. Proceedings. 1999 IEEE* (Vol. 2, pp. 473-491). IEEE.

[27] McInerny, S.A., Hardman, B., & Sun, Q. (2004). Investigation of fault detection algorithms applied to a helicopter input pinion bearing. In *15th Int. Cong. on Condition Monitoring and Diagnostic Engineering Management* (vol. 41, pp. 319-329) Sep. 2-4, (2002), Birmingham, UK.

[28] Randall, R. B. (2004). State of the art in monitoring rotating machinery-part 1. *Sound and vibration*, *38*(3), 14-21.

[29] Fernández-Francos, D., Martínez-Rego, D., Fontenla-Romero, O., Alonso-Betanzos, A. (2013). Automatic bearing fault diagnosis based on one-class *v*-SVM. *Computers and Industrial Engineering*, *64*, 357-365.

CHAPTER 5
Contributions to audio and vibration pump monitoring

In Chapter 4, we have focused our research in vibration bearing fault diagnosis and fault degradation. As stated before, vibration-based condition monitoring is a well-stablished technique in research literature. In this Chapter, we focus our research to pump fault diagnosis, specifically in hydraulic faults produced in the impeller, in seal fault and in system faults (fluid contaminated with impurities and strange objects). As in bearing fault diagnosis, vibration signal is one of the main sources of information in pump fault diagnosis, apart from other signals commonly used in pump fault diagnosis such as pressure, current, voltage, etc. As stated in Chapter 1, audio-based fault diagnosis in the audible range 0-20kHz has received little attention in research mainly due to unwanted contamination of the audio signal. However, acoustic signals can be acquired remotely, without attaching the sensor to the machine housing, eliminating mounting problems in certain machines and in certain environments. In pump fault diagnosis literature, multiple features are extracted in different signal domains from vibration signals in order to discriminate between different pump conditions: normal condition, mechanical and hydraulic faulty conditions. However, the works on audio-based diagnosis are limited only to the study of cavitation fault which is outside of the scope of this Thesis.

This Chapter is devoted to exploring audio-based pump fault diagnosis focusing on impeller-related faults, seal fault and system faults and using conventional features extracted from vibration signals in the state of the art. Once the vibration features in the state of the art are identified, they are implemented and then applied to the vibration and audio signals simultaneously acquired from the centrifugal test rig. We also propose new features to the state of the art mainly based on cepstrum, frequency and nonlinear techniques to both vibration and audio signals. In order to make a comparison attending to the nature of the signal i.e. vibration and audio signals, a deterministic feature selection technique is applied for each sensor and the selected features are evaluated in relevance order with two classifiers, a neural network classifier and a least-square support vector (LS-SVM) classifier, so as the discrimination ability of the features is evaluated.

This Chapter is divided in three main sections. In the first section, the methodology of the experimentation is explained. In the second section, the set of features extracted from vibration and audio signals are explained: features can be extracted in different signal domains (i.e time domain, frequency domain, etc). For this reason, we decide to divide the features according to different signal domains. For each signal domain, vibration features and audio features used in the literature are shown. Then, the features which are contributions of this Thesis are explained. The main contributions regarding features in pump condition monitoring are: the application of vibration features to the audio signal and the proposal of new features both in vibration and audio signals. All features (state-of-the-art features and proposed features) are evaluated with neural network and LS-SVM classifiers for each sensor individually. Feature selection is also applied to obtain the best features for this application for each sensor. In the third, fourth and fifth sections of the Chapter, the results of feature selection and feature evaluation are shown for each sensor.

5.1 Methodology

To quantify the ability of the audio and vibration features in pump fault diagnosis the squeme of Figure 5-1 is followed for vibration and audio signals. Signal represents the signal to be featured: vibration or audio signal. As it was shown in Chapter 3, four

sensors were used to acquire vibration and audio signals from the pump set up: two accelerometers and two microphones. The squeme of Figure 5-1 is applied for each sensor in order to obtain results for each sensor.

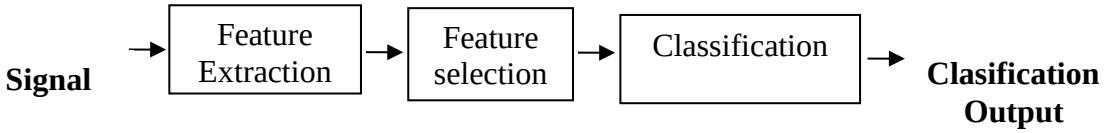

Figure 5-1: Squeme of the methodology used to quantify the ability of the features for vibration and audio based pump fault diagnosis.

First, a set of features is extracted for each sensor (feature extraction block). The features extracted are features from the state of the art of vibration and audio pump fault diagnosis and features proposed in this Thesis. The features extracted and the features proposed are explained in the second section of this Chapter. In order to extract the features, each file of the database (i.e. each observation) is divided in frames of 8192 samples (371.5 ms). For each frame, the set of features are extracted. Finally, the mean of each extracted feature is computed for each observation ($\mu_{F_j O_k}$):

$$\mu_{F_j O_k} = \sum_{i=1}^{N_{frames}} \frac{F_{j,i}}{N_{frames}} \qquad \text{[Eq. 5-1]}$$

where $\mu_{F_j O_k}$ is the final feature set: mean of each feature per each observation O_k (k = 1,…,370 because there are 370 files in the database), $F_{j,i}$ is the feature j (j = 1,…,98 because there are 98 features) in the frame i and N_{frames} is the number of frames used in each observation. 53 frames equally spaced are used per observation, so $N_{frames} = 53$. Before extracting the features and for each observation, the mean is removed and the signal is normalized between -1 and +1.

Once the features are extracted, the aim is to identify those most suitable features per sensor that best discriminate between different pump conditions. The process to select features from a feature set is called feature selection. The selection of well-suited features providing fault-related information and the discarding or weakening of irrelevant or redundant features improves system performance. In the feature

selection block, the features are selected with the sequential floating forward feature selection method (*SFFS*) and a relevance analysis (in a same way of Chapter 4) is carried out to obtain a reduced group of selected features. The reason for choosing the *SFFS* is that is a deterministic method so the same results are obtained with the same data and the compotutional cost is low. After applying *SFFS* and the relevance analysis a set of features will be obtained for each sensor.

The classifier block is related to assess the performance of the classification between different conditions of the pump. In the classification block, the classifier labels the observation using the extracted features into different classification units. The discrimination ability of the features in the classification of different kinds of faults is evaluated. Different configurations are implemented to discriminate between normal and fault conditions. The classification units or classes considered in this Thesis are the following:

- 8 classification units: normal condition (NOR), plate condition (PLA), leading edge damage condition (LED), trailing edge damage condition (TED), seal condition (SEA), sand condition (SAN) sand and paper condition (SAP) and pvc balls condition (PVC).

- 17 classification units. In this case the severities of the plate condition, the leading edge damage condition and the trailing edge damage condition are considered. The 17 classification units are: normal condition (NOR), plate condition with one portion of blade removed (PLA1), plate condition with two portions of blade removed (PLA2), plate condition with three portions of blade removed (PLA3), leading edge damage of sieze 5mm (LED1), leading edge damage of size 10mm (LED2), leading edge damage of size 15 mm(LED3), trailing edge damage of size 5 mm (TED1), trailing edge damage of size 10 mm (TED2), trailing edge damage of size 15 mm (TED3) seal condition (SEA), sand condtion (SAN), sand and paper condition (SAP) and pvc balls condition (PVC).

Two different classifiers are used to implement the classifier block: neural network classifier and LS-SVM classifier. In this Thesis, we have decided to use a standard feedforward neural network classifier with a resilient backpropagation

algorithm and a least-square support vector machine classifier to compare the results obtained with the neural network. The methodology used to evaluate the different databases for each sensor consists in dividing the data in a training set (70% of the samples of each class) and in a test set (30% of the samples of each class). The training set is divided into different folds to tune the classifiers parameters. The procedure is repeated 20 times.

5.2 Features for pump fault diagnosis

Centrifugal pump monitoring is mainly addressed using vibration signal or pressure signal as source of information with features extracted from time domain and from frequency domains. Time-frequency domain, especially the discrete wavelet transform is also investigated by some authors. In this subsection, a set of features from the state of the art of centrifugal pump fault diagnosis using vibration signal as source signal is implemented. In this Thesis, we contribute with the application of state-of-the-art vibration features to audio signal. We also propose new features not previously used in centrifugal pump fault diagnosis: features related to energy in the frequency, cepstrum and time-frequency domains and complexity measures and nonlinear measures.

Features are extracted from both vibration and audio signals acquired in the experimental test rig of this Thesis in different signal domains: time domain, frequency domain, cepstrum domain, time-frequency domain and nonlinear domain. In this Thesis we focus on the following faults: faults related to impellers, seal fault and system faults. For this reason we focus on features related to diagnose such kinds of faults in centrifugal pumps. For each signal domain, vibration and audio features in the state of the art are shown as well as the contributions carried out in this Thesis. In each feature, the kind of signal from which it is extracted is shown in parenthesis just beside the name of the feature.

5.2.1 Time Domain: Vibration and Audio Features in the state of the art

In pump fault diagnosis, the raw vibration signal (vibration signal in time domain) is featured with statistical and energy features from the pattern recognition field in order to

characterize different pumps conditions [3]-[8], [31] including impeller-related faults, system faults, seal faults and also mechanical faults. Kawabe et al. [3] proposed a set of statistical features applied to the time vibration signal of a centrifugal pump for discriminating between normal and fault conditions. Those features are based on the pattern recognition field. Wang et al. [31] use the same set of statistical features in vibration time signal and in reconstructed signals of discrete wavelet transform. In more recent research, Sakthivel et al. [4]-[6] and Farokhzad et al. [7] also applied a set of statistical features (mean, standard deviation, median, skewness, kurtosis, etc.) to the time vibration signal of a mono-block centrifugal pump with damage in the impeller plate, seal damage, outer-race damage in bearing, cavitation and normal condition. The statistical features proposed for the aforementioned authors are formulated next.

From now on $s[n]$ is a frame of vibration or audio time series from which the features are extracted.

Mean value (vibration)

Sakthivel et al. [4]-[6] and Farokhzad et al. [7] feature the time vibration signal with the mean value. The estimator of the mean value for a discrete frame $s[n]$ with N samples is:

$$\mu_{version\,1} = \sum_{i=1}^{N} \frac{s[i]}{N} \qquad \text{[Eq. 5-2]}$$

Other authors use the mean value of the absolute vibration signal $|s[n]|$ [3] (mean value absolute):

$$\mu_{version\,2} = \sum_{i=1}^{N} \frac{|s[i]|}{N} \qquad \text{[Eq. 5-3]}$$

The two versions of the mean value (mean value and mean value absolute) are implemented for $N = 8192$. For each observation, the mean value is obtained.

Standard deviation (vibration)

The standard deviation, a second order statistics, measures the power content of the vibration signal. The power contect differs from different pump conditions. There are two versions in the standard deviation computation: Sakthivel et al. [4]-[6] and Farokhzad et al. [7] use the standard deviation of the vibration signal and Kawabe et al. [3] uses the standard deviation of the absolute value of the signal (standard deviation absolute). These two versions are implemented.

$$\sigma_{version1} = \sqrt{\frac{\sum_{i=1}^{N} (s[i] - \mu_{version1})^2}{N-1}} \qquad \text{[Eq. 5-4]}$$

where $\mu_{version1}$ is the mean of the vibration signal

$$\sigma_{version2} = \sqrt{\frac{\sum_{i=1}^{N} (|s[i]| - \mu_{version2})^2}{N-1}} \qquad \text{[Eq. 5-5]}$$

where $\mu_{version2}$ is the mean of the absolute value of the vibration signal:

The two versions of the standard deviation (standard deviation and standard deviation absolute) are implemented for N = 8192. For each observation, the mean value is obtained.

Variance (vibration)

The variance of the time signal was also used by Sakthivel et al. [4]-[6] and Farokhzad et al. [7] to discriminate between different pump conditions. The variance value is also a measure of energy content in a signal, which varies between different pump conditions.

$$\sigma^2_{version1} = \frac{\sum_{i=1}^{N} (s[i] - \mu_{version1})^2}{N-1} \qquad \text{[Eq. 5-6]}$$

$$\sigma^2_{version2} = \frac{\sum_{i=1}^{N} (s[i] - \mu_{version2})^2}{N-1} \qquad \text{[Eq. 5-7]}$$

The two versions of the variance (variance and variance absolute) are implemented for N = 8192. For each observation, the mean value is obtained.

Skewness (vibration)

Skewness is a third order moment and a measure of symmetry, or the lack of symmetry around the mean of the probability distribution of a signal. It reflects positive or negative deviations from the mean. An estimator of the skewness was used by Sakthivel et al. [4]-[6], Wang et al. [31] and by Farokhzad et al. [7] using the time vibration signal and by Kawabe et al. [3] using the absolute value of the time vibration signal (skewness absolute).

$$SK_{version1} = \frac{\sum_{i=1}^{N} (s[i] - \mu_{version1})^3}{(N-1)\sigma^3_{version1}} \qquad \text{[Eq. 5-8]}$$

$$SK_{version2} = \frac{\sum_{i=1}^{N} (|s[i]| - \mu_{version2})^3}{(N-1)\sigma^3_{version1}} \qquad \text{[Eq. 5-9]}$$

The two versions of skewness (skewness and skewness absolute) are implemented and the mean value for each observation is obtained.

Skewness of peak values (vibration)

Wang et al. [31] used the skewness of the peak values of the vibration signal $s[n]$, $s_{peaks}[n]$.

$$SK_{peaks} = \frac{\sum_{i=1}^{P}(s_{peaks}[i] - \mu_{s_{peaks}})^3}{(P-1)\sigma_{s_{peaks}}^3} \qquad \text{[Eq. 5-10]}$$

where $\mu_{s_{peaks}} = \frac{\sum_{i=1}^{P} s_{peaks}[i]}{P}$ and $\sigma_{s_{peaks}} = \sqrt{\frac{\sum_{i=1}^{P}(s_{peaks}[i] - \mu_{s_{peaks}})^2}{P-1}}$ are the mean value and the standard deviation value of $s_{peaks}[n]$, P is the number of peaks (i.e. the number of samples in $s_{peaks}[n]$). The peaks values of the signal $s[n]$ where computed and then the skewness of these values calculated. Finally, the mean value per each observation is obtained.

The skewness of the peak values characterizes the asymmetry of the envelope signal in time domain respect to the mean value of the envelope. It is a measure of the shape of the time signal.

Skewness of valley values (vibration)

Wang et al. [31] also used the skewness of the valley values of the vibration signal $s[n]$, $s_{valleys}[n]$.

$$SK_{valleys} = \frac{\sum_{i=1}^{V}(s_{valleys}[i] - \mu_{s_{valleys}})^3}{(V-1)\sigma_{s_{valleys}}^3} \qquad \text{[Eq. 5-11]}$$

where $\mu_{s_{valleys}} = \frac{\sum_{i=1}^{V} s_{valleys}[i]}{V}$ and $\sigma_{s_{valleys}} = \sqrt{\frac{\sum_{i=1}^{V}(s_{valleys}[i] - \mu_{s_{valleys}})^2}{V-1}}$ are the mean value and standard deviation value of $s_{valleys}[n]$, V is the number of valleys (i.e. the number of samples in $s_{valleys}[n]$). The peaks values of the signal $s[n]$ where computed and then the skewness of these values calculated. Finally, the mean value per each observation is obtained.

The skewness of the valleys values as well as the skewness of the peaks characterizes the asymmetry of the envelope signal in time domain respect to the mean value of the envelope. It is a measure of the shape of the time signal.

Kurtosis (vibration)

Kurtosis is a fourth order moment and a measure of whether the data in a probability distribution are peaked or flat relative to a Gaussian distribution. Higher kurtosis means more of the variance is due to infrequent extreme deviations. An estimator of the kurtosis was used by Sakthivel et al. [4]-[6], Wang et al. [31] and by Farokhzad et al. [7] using the time vibration signal and by Kawabe et al. [3] using the absolute value of the time vibration signal.

$$K_{version1} = \frac{\sum_{i=1}^{N} (s[i] - \mu_{version1})^4}{(N-1)\sigma_{version1}^4} \qquad \text{[Eq. 5-12]}$$

$$K_{version2} = \frac{\sum_{i=1}^{N} (|s[i]| - \mu_{version1})^3}{(N-1)\sigma_{version1}^4} \qquad \text{[Eq. 5-13]}$$

The two version of kurtosis (kurtosis and kurtosis absolute) are implemented. Finally, the mean value per each observation is obtained.

Kurtosis of peak values (vibration)

Wang et al. [31] used the kurtosis of the peak values of the vibration signal $s[n]$, $s_{peaks}[n]$.

$$K_{peaks} = \frac{\sum_{i=1}^{P} (s_{peaks}[i] - \mu_{s_{peaks}})^4}{(P-1)\sigma_{s_{peaks}}^4} \qquad \text{[Eq. 5-14]}$$

where $\mu_{s_{peaks}}$ and $\sigma_{s_{peaks}}$ are the mean value and standard deviation value of $s_{peaks}[n]$, P is the number of samples in $s_{peaks}[n]$. The peaks values of the signal $s[n]$ where computed and then the kurtosis calculated. Finally, the mean value of *Kurtosis of Peak values* per each observation is obtained.

Kurtosis of valley values (vibration)

Wang et al. [31] used the kurtosis of the valley values of the vibration signal $s[n]$,- $s_{valleys}[n]$.

$$K_{valleys} = \frac{\sum_{i=1}^{V}(s_{valleys}[i] - \mu_{s_{valleys}})^4}{(V-1)\sigma_{s_{valleys}}^4} \qquad \text{[Eq. 5-15]}$$

where $\mu_{s_{valleys}}$ and $\sigma_{s_{valleys}}$ are the mean value and standard deviation value of $s_{valleys}[n]$, V is the number of samples in $s_{valleys}[n]$. The valleys values of the signal $s[n]$ where computed and then the kurtosis calculated. Finally, the mean value of *Kurtosis of Valley values* per each observation is obtained.

The kurtosis of the valleys values as well as the kurtosis of the peaks characterizes the shape of the envelope signal in time domain.

Median (vibration)

Sakthivel et al. [4]-[6] applied also the median for the vibration signal $s[n]$. The median of a signal $s[n]$ with N samples, $s[1]$, …, $s[N]$ can be computed reordering them so that $Y_1 < Y_2 < \ldots < Y_N$ where $Y_i\,(i = 1,\ldots,N)$ are the values of $s[n]$ in increasing order, being Y_1 the minimum value of $s[n]$ and Y_N the maximum value of $s[n]$. The median is:

$$MEDIAN \equiv \begin{cases} Y_{(N+1)/2} & if\ N\ is\ odd \\ \frac{1}{2}(Y_{N/2} + Y_{1+N/2}) & if\ N\ is\ even \end{cases} \quad \text{[Eq. 5-16]}$$

The median value is computed per each frame and finally the average value is obtained per observation.

Minimum value (vibration)

The minimum value refers to the minimum value of the signal and also was used by Sakthivel et al. [4]-[6] in pump condition monitoring. According to Sakthivel et al. when the pump parts get degraded the vibration level increases, so the minimum value of the vibration signals also increases.

$$MIN = \min(s[i]) \quad \text{[Eq. 5-17]}$$

The minimum value is computed per each frame and finally the average value is obtained per observation.

Maximum value (vibration)

The maximum value refers to the maximum value of the signal and also was used by Sakthivel et al. [4]-[6] in pump condition monitoring. When the pump parts degrade the vibration level increases, so the maximum value also increases.

$$MAX = \max(s[i]) \quad \text{[Eq. 5-18]}$$

The maximum value is computed per each frame and finally the average value is obtained per observation.

Range (vibration)

The range or peak-to-peak value measures the excursion of the signal (i.e. the difference between the minimum value and the maximum value of the signal) and it has also applied in pump condition monitoring [4]-[6].

$$RANGE = MAX - MIN \qquad \text{[Eq. 5-19]}$$

The range value is computed per each frame and finally the average value is obtained per observation.

Sum (vibration)

The sum of all data point values in a given signal is also a measure used in pump fault diagnosis [4]-[6] as a measure of the energy in a signal.

$$SUM = \sum_{i=1}^{N} s[i] \qquad \text{[Eq. 5-20]}$$

The sum value is computed per each frame and finally the average value is obtained per observation.

Variation rate (vibration)

The variation rate is used by Kawabe et al. [3] in pump fault diagnosis. The variation rate is the ratio between the standard deviation of the absolute value of the signal $s[n]$ and the mean value of the absolute value of the signal $s[n]$. The variation rate is a measure of dispersion independent of the units of the mean. The higher the variation rate, the greater the dispersion of the signal.

.

$$VR = \frac{\sigma_{version2}}{\mu_{version2}} \qquad \text{[Eq. 5-21]}$$

The variation rate is computed per each frame and then the average value is obtained per observation.

Variation rate of peak values (vibration)

The variation rate of the peak values is the ratio between the standard deviation and the mean of the peaks of $s[n]$ ($s_{peaks}[n]$):

$$VR_{peaks} = \frac{\sigma_{s_{peaks}}}{\mu_{s_{peaks}}} \qquad \text{[Eq. 5-22]}$$

where $\mu_{s_{peaks}}$ and $\sigma_{s_{peaks}}$ are the mean value and standard deviation value of $s_{peaks}[n]$.

The variation rate of peak values is a measure of dispersion of the envelope of the signal $s[n]$. The variation rate of peak values is compute per each frame and the average value is obtained per each observation.

Variation rate of valley values (vibration)

The variation rate of the valleys values is the ratio between the standard deviation and the mean of the valleys of $s[n]$ ($s_{valleys}[n]$):

$$VR_{valleys} = \frac{\sigma_{s_{valleys}}}{\mu_{s_{valleys}}} \qquad \text{[Eq. 5-23]}$$

where $\mu_{s_{valleys}}$ and $\sigma_{s_{valleys}}$ are the mean value and standard deviation value of $s_{valleys}[n]$.

The variation rate of valleys values is a measure of dispersion of the envelope of the signal $s[n]$. The variation rate of valleys values is compute per each frame and the average value is obtained per each observation.

Ratio of number of peaks and number of zero-crossing (vibration)

Another measure in time domain is the ratio between the number of peaks and the number of zero-crossing in the vibration signal [31]. It can be expressed as:

$$PeakZC = \frac{P}{ZC} \qquad \text{[Eq. 5-24]}$$

where P is the number of samples of $s_{peaks}[n]$ and ZC is the number of $s[n]$ passing zero. The ZC is also a feature itself. The zero-crossing feature and the ratio of number of peaks and number of zero-crossing are computed per each frame and the mean value is obtained per observation.

Ratio of number of valleys and number of zero-crossing (vibration)

The ratio between the number of valleys and the number of zero-crossing in the vibration signal [31] can be expressed as:

$$ValleyZC = \frac{V}{ZC} \qquad \text{[Eq. 5-25]}$$

where V is the number of samples of s_{valley} and ZC is the number of zero-crossing in $s[n]$. This feature is computed per each frame and the mean value is obtained per observation.

Ratio of averaged peaks and mean value absolute (vibration)

Kawabe et al. [3] proposed the ratio between the mean value of the peaks and the mean value of the absolute value of the signal.

$$AvPRatio = \frac{\mu_{s_{peaks}}}{\mu_{version2}} \qquad \text{[Eq. 5-26]}$$

where $\mu_{s_{peaks}}$ is the mean value of $s_{peaks}[n]$ (peak values of $s[n]$) and $\mu_{version2}$ is the mean value of $|s[n]|$. This feature is computed per each frame and the mean value is obtained per observation.

Ratio of averaged ten peaks and averaged peaks (vibration)

Kawabe et al. [3] proposed the ratio between the mean of the ten higher peaks in the signal and the mean value of the peaks.

$$Av10PRatio = \frac{\left|\mu_{10peaks}\right|}{\mu_{s_{peaks}}} \qquad \text{[Eq. 5-27]}$$

where $\mu_{s_{peaks}}$ is the mean value of $s_{peaks}[n]$ (peak values of $s[n]$) and $\mu_{10peaks}$ is the mean value of the 10 peak values (from top peak value to tenth value). This feature is computed per each frame and the mean value is obtained per observation.

Ratio of averaged peaks and standard deviation of peaks (vibration)

Kawabe et al. [3] proposed the ratio between the mean and standard deviation of the peaks values of $s[n]$.

$$Av\sigma Ratio = \frac{\mu_{s_{peaks}}}{\sigma_{s_{peaks}}} \qquad \text{[Eq. 5-28]}$$

where $\mu_{s_{peaks}}$ is the mean value of $s_{peaks}[n]$ (peak values of $s[n]$) and $\sigma_{s_{peaks}}$ the standard deviation of $s_{peaks}[n]$. This feature is computed per each frame and the mean value is obtained per observation.

Ratio of averaged valleys and standard deviation of valleys (vibration)

Kawabe et al. [3] proposed the ratio between the mean and standard deviation of the valley values of $s[n]$.

$$Av\sigma VRatio = \frac{\mu_{s_{valleys}}}{\sigma_{s_{valleys}}} \qquad \text{[Eq. 5-29]}$$

where $\mu_{s_{valleys}}$ and $\sigma_{s_{valleys}}$ are the mean value and standard deviation value of $s_{valleys}[n]$. This feature is computed per each frame and the mean value is obtained per observation.

Energies in time (vibration)

Three ways of quantifying the energy in time are used in [3], [31] for vibration pump fault diagnosis.

$$EnergyTime\_1 = \frac{\sum_{i=1}^{N}\sqrt{|s[i]|}}{N\sqrt{\sigma_{version2}}} \qquad \text{[Eq. 5-30]}$$

$$EnergyTime\_2 = \frac{\sum_{i=1}^{N}(s[i])^2}{N\sigma_{version2}^{\ 2}} \qquad \text{[Eq. 5-31]}$$

$$EnergyTime\_3 = \frac{\sum_{i=1}^{N}\log_{10}|s[i]|}{N\log_{10}\sigma_{version2}};\ s[i] \neq 0 \qquad \text{[Eq. 5-32]}$$

The energy in time 1, 2 and 3 are computed per frame and the average value is obtained per observation.

Root Mean Square (RMS) (vibration)

Farokhzad et al. [7] applies the root mean square of the vibration signal to pump fault diagnosis in a pump with impeller fault, seal fault and cavitation. The root mean square (S_{rms}) quantifies the energy in a signal.

$$s_{rms} = \sqrt{\frac{\sum_{i=1}^{N} (s[i])^2}{N}} \qquad \text{[Eq. 5-33]}$$

This feature is computed per each frame and the mean value is obtained per observation.

Crest factor (vibration)

Farokhzad et al. [7] applies the crest factor, which quantifies the impulsiveness in a signal. Crest factor of a time series $s[n]$ is the ratio between the maximum value of a signal and the root mean square of the signal.

$$s_{crestFactor} = \frac{MAX}{RMS} \qquad \text{[Eq. 5-34]}$$

The crest factor is computed per each frame and the average value is computed per each observation.

Fourth, fifth and sixth central moments (vibration)

Farokhzad et al. [7] features the vibration time signal with the fourth central moment, the fifth central moment and the sixth central moment which are defined in the following equations.

$$s_{4thmoment} = \frac{\sum_{i=1}^{N} (s[i] - \mu_{version1})^4}{N} \qquad \text{[Eq. 5-35]}$$

$$s_{5thmoment} = \frac{\sum_{i=1}^{N} (s[i] - \mu_{version1})^5}{N} \qquad \text{[Eq. 5-36]}$$

$$s_{6thmoment} = \frac{\sum_{i=1}^{N} (s[i] - \mu_{version1})^6}{N} \qquad \text{[Eq. 5-37]}$$

These features are computed per each frame and finally the mean value is computed per each observation.

5.2.2 Contributions in time domain features

In pump fault diagnosis the features extracted from time domain are aimed to statistically characterize the time vibration signal in order to discriminate between different pump conditions. All the previous features extracted from time domain are applied in vibration and pressure signals for diagnosis of impeller related faults, seal faults, system faults and bearing faults in centrifugal pumps. As far as the author of this Thesis knowledge, there is no research papers dealing with pump monitoring in the audible spectrum (0-20kHz) apart from papers related to cavitation faults in centrifugal pumps where root mean square, crest factor and variance features have been used [8].

In Figure 5-2, Figure 5-3, Figure 5-4 and Figure 5-5 examples of vibration and audio time signals acquired from sensors Radial Inlet Accel and Inlet Micro of the test-rig of this Thesis are shown for different pump conditions. Normal and plate conditions are shown in Figure 5-2. In Figure 5-3 leading edge damage and trailing edge damage conditions are shown. Figure 5-4 shows seal and sand conditions and finally Figure 5-5 shows sand and paper and PVC balls conditions. From the figures, it is obvious that the signals have different shapes in different conditions for vibration and audio signals. So the energy and statistical features in time domain might discriminate between different pump condition both in vibration and audio signals.

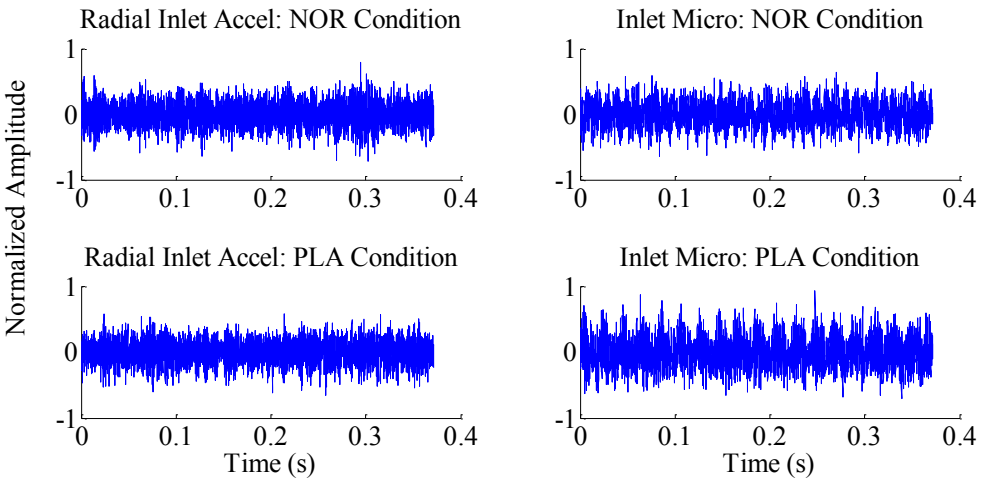

Figure 5-2: Time frames (8192 samples) from sensor Radial Inlet Accel (vibration) and Inlet Micro (audio) for normal (NOR) and plate (PLA) condition.

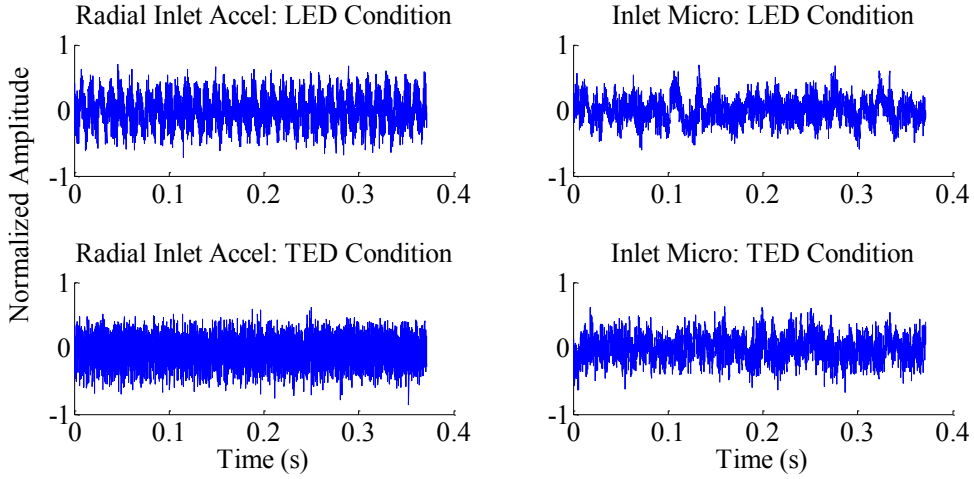

Figure 5-3: Time frames (8192 samples) from sensor Radial Inlet Accel (vibration) and Inlet Micro (audio) for leading edge damage (LED) and trailing edge damage (TED) condition.

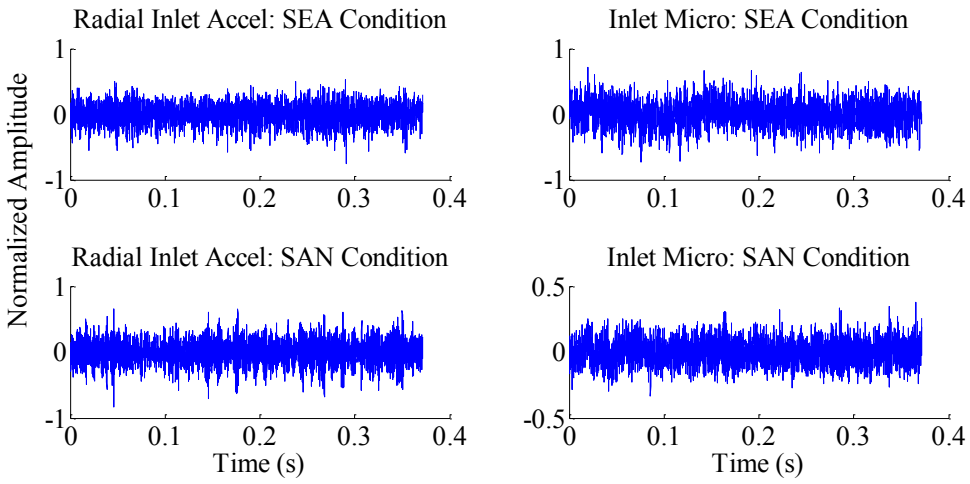

Figure 5-4: Time frames (8192 samples) from sensor Radial Inlet Accel (vibration) and Inlet Micro (audio) for seal (SEA) and sand (SAN) condition.

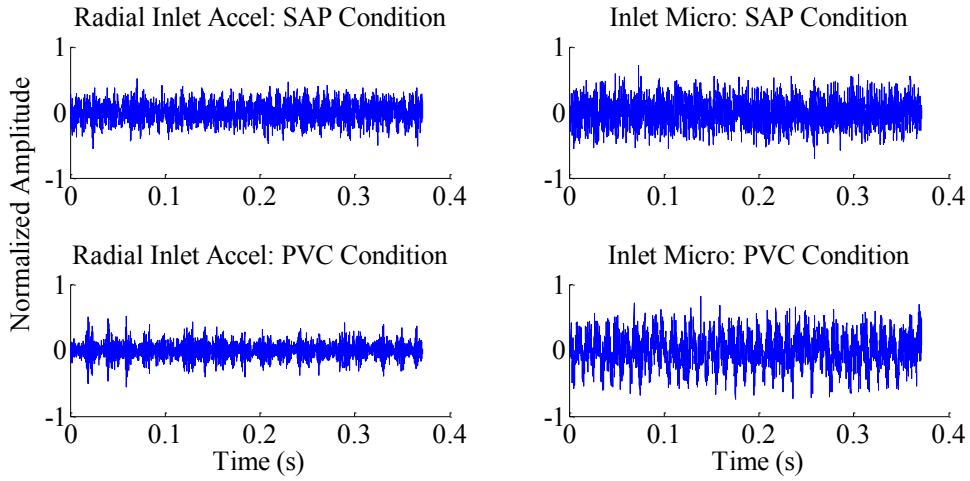

Figure 5-5: Time frames (8192 samples) from sensor Radial Inlet Accel (vibration) and Inlet Micro (audio) for sand and paper (SAP) and pvc balls (PVC) condition.

5.2.3 Frequency Domain: Vibration and Audio Features in the state of the art

Most research in pump monitoring is carried out using features extracted from frequency domain. Frequencies at pump frequency (or rotation frequency) RF, vane-passing frequency (also called blade-passing frequency) VPF and their harmonics are widely used to detect impeller damage [9]-[17], [31]. Usually the change of energy at the frequency of rotation of the pump rotor and vane-passing frequency may be an indicator of an impeller-related fault [9]-[17]. An obstacle in inlet, outlet or conduits provoke an energy loss at the location of the obstacle and can cause energy changes at

rotational frequency [10], [11]. Cavitation is usually detected using measures of broad-band noise in spectra [9]-[17]. Changes in amplitude (an energy measure) of the mentioned frequencies can characterize an impeller, seal or system faults [10], [11]. Other studies in centrifugal pump use statistical features on spectra [32]. The spectral amplitudes are also used as features [14].

To extract features in frequency domain, the spectrum of the signal has to be estimated. The spectrum estimator is the periodogram: it can be defined as the Fourier transform of a frame (of vibration or audio signal) $s[n]$:

$$\hat{S}(w) = \frac{1}{NFFT}|S(w)| \qquad \text{[Eq. 5-38]}$$

where $|S(w)|$ is the Fourier transform of the frame $s[n]$.

There are some authors that extract statistical features in frequency domain [32] to discriminate between different kinds of faults (impeller damage, cavitation, misalignment, etc.) in centrifugal pumps. Once the Fourier transform of the frame is obtained, the following statistical features in frequency domain are extracted in [32]:

Center frequency (vibration)

The center frequency is defined as [32]:

$$\overline{w} = \frac{\sum_{i=1}^{NFFT} w_i S(w_i)}{\sum_{i=1}^{NFFT} S(w_i)} \qquad \text{[Eq. 5-39]}$$

where $S(w_i)$ is the spectrum for w_i, $i = 1,2,\ldots,NFFT$, $NFFT$ is the number of spectrum lines and w_i is the frequency value of the ith spectrum line. The center frequency is computed per each frame with $NFFT$ = 8192 points and the mean value is obtained per observation.

Standard deviation frequency (vibration)

The standard deviation frequency is a measure of energy in spectrum [32]:

$$\sigma_{freq} = \sqrt{\frac{\sum_{i=1}^{NFFT}(w_i - \overline{w})^2 S(w_i)}{NFFT - 1}} \qquad \text{[Eq. 5-40]}$$

The standard deviation frequency is computed per each frame with *NFFT* = 8192 points and the mean value is obtained per observation.

Skewness frequency (vibration)

The skewness frequency is a measure of symmetry of the probability distribution of the spectra [32]:

$$SK_{freq} = \frac{\sum_{i=1}^{NFFT}(w_i - \overline{w})^3 S(w_i)}{\sigma_{freq}^3 NFFT} \qquad \text{[Eq. 5-41]}$$

The skewness frequency is computed per frame and the mean value is computed per observation.

Kurtosis frequency (vibration)

The kurtosis frequency is a measure of how peaked is the probability distribution of the spectra [32]:

$$K_{freq} = \frac{\sum_{i=1}^{NFFT}(w_i - \overline{w})^4 S(w_i)}{\sigma_{freq}^4 NFFT} \qquad \text{[Eq. 5-42]}$$

The kurtosis frequency is computed per frame and the mean value is obtained per observation.

Energies in frequency (vibration)

Other features that measure the energy distribution in the spectrum are the following [32].

$$EnergyFreq\_1 = \frac{\sum_{i=1}^{NFFT} \sqrt{\left| w_i - \overline{w} \right|} S(w_i)}{\sqrt{\sigma_{freq}} NFFT} \quad \text{[Eq. 5-43]}$$

$$EnergyFreq\_2 = \sqrt{\frac{\sum_{i=1}^{NFFT} w_i^2 S(w_i)}{\sum_{i=1}^{NFFT} S(w_i)}} \quad \text{[Eq. 5-44]}$$

$$EnergyFreq\_3 = \sqrt{\frac{\sum_{i=1}^{NFFT} w_i^4 S(w_i)}{\sum_{i=1}^{NFFT} w_i^2 S(w_i)}} \quad \text{[Eq. 5-45]}$$

$$EnergyFreq\_4 = \frac{\sum_{i=1}^{NFFT} w_i^2 S(w_i)}{\sqrt{\sum_{i=1}^{NFFT} S(w_i) \sum_{i=1}^{NFFT} w_i^4 S(w_i)}} \quad \text{[Eq. 5-46]}$$

Each energy feature is computed per frame and its mean value is obtained per observation.

Maximum amplitude in frequency (vibration)

The maximum amplitude in frequency is computed as follows [32]:

$$MAX = \max(S(w)) \qquad \text{[Eq. 5-47]}$$

This feature is computed per frame and then the mean value is obtained per observation.

Variation Rate frequency (vibration)

Variation rate frequency is defined in the same way of time domain: the ratio of the standard deviation and the center frequency [32].

$$VR_{freq} = \frac{\sigma_{freq}}{\overline{w}} \qquad \text{[Eq. 5-48]}$$

The variation rate frequency is computed per frame and its mean value is obtained per observation.

Different works on vibration, pressure and flow spectra in pump fault diagnosis focus their analysis at the discrete frequencies produced by the fluid-dynamic forces [10], [11], [19], [21] which are the rotor frequency (RF), the vane-passing frequency VPF (RF x number of blades of the impeller) and their harmonics. Zhao et al. [15], [16] extracted energy features from spectra of vibration signal from a slurry centrifugal pump. Impeller with no fault and impeller with damage in the trailing vane edge and in the leading vane edge were considered. The features extracted in works [15], [16] are the following:

Energy at rotor frequency and their harmonics (vibration)

The spectrum amplitudes at the pump characteristic frequencies, i.e. pump frequency (RF = 1X), the second harmonic (2X), the third harmonic (3X), the fourth harmonic (4X), the VPF and twice the VPF are used as features [15]. In this Thesis, the pump has seven blades and the RPM is 2925. In Table 5-1, the corresponding frequencies are shown:

TABLE 5-1: CHARACTERISTIC FREQUENCIES IN A CENTRIFUGAL PUMP

Rotor frequency	2^{nd} harmonic	3^{rd} harmonic	4^{th} harmonic	Vane-pass frequency	Twice vane-pass freq
RF = 1X	2X	3X	4X	VPF = 7X	2VPF
48.75 Hz	97.50 Hz	146.25 Hz	195 Hz	341.25 Hz	682.50 Hz

The features extracted are the amplitudes in the spectrum at the characteristic frequencies of the pump for each frame. In order to compute the amplitudes at the characteristic frequencies of the pump, a range of frequencies around the characteristic frequencies is considered. The mean value is obtained per observation.

Root mean squares in frequency range related to rotor frequency and their harmonics (vibration)

The root mean square in the spectra in the following six frequency ranges [15] are extracted for each frame: [0-1X], [0-2X], [0-3X], [0-4X], [0-VPF], [0-2VPF]. The mean value is obtained per observation.

Energy ratios at rotor frequency and their harmonics (vibration)

In [16], the valuable frequencies are the pump characteristic frequencies and the other frequencies in spectrum are treated as noise. The noise is computed as follows:

$$Noise = \sqrt{\frac{1}{NFFT}\sum_{j=1}^{NFFT} S^2(j)},\ j \neq 1X, 2X, 3X, 4X, VPF, 2VPF \qquad \text{[Eq. 5-49]}$$

where $S(j)$ are the amplitudes in spectrum of the frequencies different of the pump characteristic frequencies and *NFFT* is the number of spectrum lines. The total amplitude is then:

$$S_{total} = S(1X) + S(2X) + S(3X) + S(4X) + S(VPF) + S(2VPF) + Noise \qquad \text{[Eq. 5-50]}$$

where S(1X), S(2X), S(3X), S(4X), S(VPF), S(2VPF) are the amplitudes at 1X, 2X, 3X, 4X, VPF and 2VPF in spectrum. In order to implement the algorithm to compute the value of the spectrum at the characteristic pump frequencies, a range of frequencies around the characteristic pump frequencies is considered.

The features extracted per frame are the amplitude ratios at the pump characteristic frequencies, which are computed as follows:

$$S_{1X}\,ratio = \frac{S(1X)}{S_{total}} \quad \text{[Eq. 5-51]}$$

$$S_{2X}\,ratio = \frac{S(2X)}{S_{total}} \quad \text{[Eq. 5-52]}$$

$$S_{3X}\,ratio = \frac{S(3X)}{S_{total}} \quad \text{[Eq. 5-53]}$$

$$S_{4X}\,ratio = \frac{S(4X)}{S_{total}} \quad \text{[Eq. 5-54]}$$

$$S_{VPF}\,ratio = \frac{S(VPF)}{S_{total}} \quad \text{[Eq. 5-55]}$$

$$S_{2VPF}\,ratio = \frac{S(2VPF)}{S_{total}} \quad \text{[Eq. 5-56]}$$

$$Noiseratio = \frac{Noise}{S_{total}} \quad \text{[Eq. 5-57]}$$

The mean value of the amplitude ratios extracted per frame is computed per observation.

Normalised spectral entropy (audio and vibration)

The normalised spectral entropy [19] was proposed for detecting onset of cavitation in a centrifugal pump using vibration and airborne (audio) signals. This feature was previously used in bearing degradation assessment [20]. We propose to use this feature to impeller-related faults, system faults and seal fault. The normalised spectral entropy of the spectrum *S* is computed as follows [19]:

First, the spectrum *S* of a frame *s*[*n*] is normalised:

$$p_i = \frac{S(i)}{\sum_{j=1}^{NFFT} S(j)} \qquad \text{[Eq. 5-58]}$$

where $\sum_{i=1}^{NFFT} p_i = 1$ and *NFFT* is the length of spectrum sequence. The spectrum is considered like a probability distribution and then the spectral entropy (SE) can be computed as the entropy of the distribution:

$$SE = -\sum_{i=1}^{NFFT} p_i \log_2(p_i) \qquad \text{[Eq. 5-59]}$$

As *SE* may change with the length of the spectrum sequence, the spectral entropy is normalized by the length of the spectrum sequence, obtaining the normalized spectral entropy (*SEn*):

$$SEn = \frac{SE}{\log_2(NFFT)} \qquad \text{[Eq. 5-60]}$$

Normalised spectral entropy ranges between 0 and 1. For spectra with flat amplitude distribution, the value of normalised spectral entropy is larger. For spectra with the same amplitudes at each frequency, the value of normalised spectral entropy is 1. For spectra with amplitudes concentrated in few frequency components, the value of normalised entropy is near 0, especially when a unique frequency component has non-zero amplitude. As the spectrum of different fault pump conditions considered in this Thesis has different shapes, it is reasonable to use this feature to characterize the vibration and audio signals (see Figure 5-6 and Figure 5-7).

The normalized spectral entropy is computed per each frame and then the mean value is obtained per observation.

5.2.4 Contributions in frequency domain features

As in time domain, most features extracted from frequency domain in centrifugal pump monitoring are extracted from vibration and pressure signals. The espectral entropy [19] and statistical features in the frequency domain such as kurtosis are features also extracted from audio signal in centrifugal pump monitoring to detect cavitation [48].

Most state-of-the art frequency features are related to energy distribution in vibration spectrum. This seems reasonable because impeller-related faults and systems faults produce changes in flow that can affect vane-passing frequency, rotor frequency and their harmonics and can also generate broadband noise. In Figure 5-6 and Figure 5-7 spectra of different pump conditions (free-fault condition, plate condition, leading edge damage condition, trailing edge damage condition, seal condition, sand condition, sand and paper condition and pvc balls condition) are shown for vibration and audio signals simultaneously acquired. There are changes in the energy distribution between normal and fault conditions both in vibration and audio signals. So, it is reasonable to apply the state-of-the-art features to audio signals.

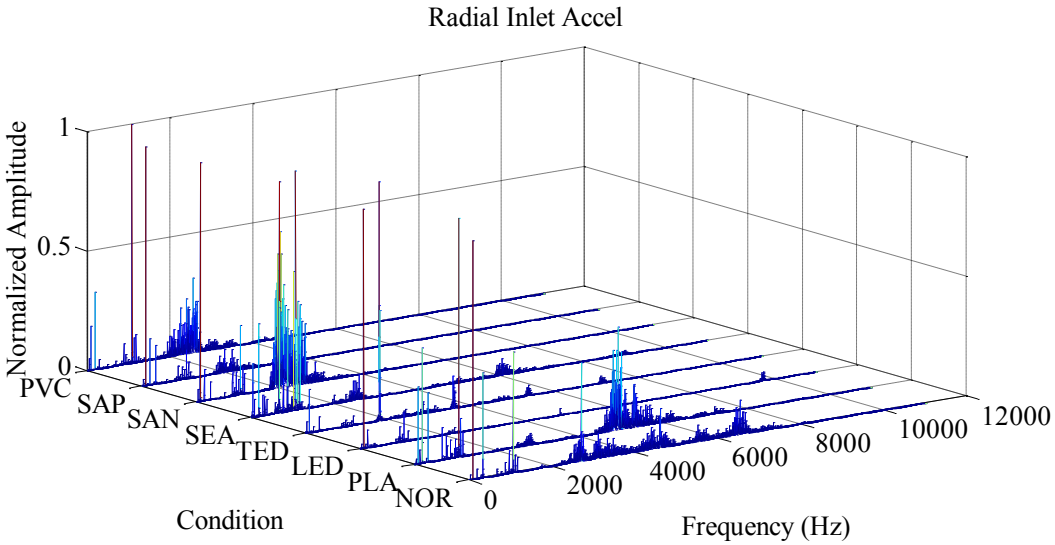

Figure 5-6: Spectra of vibration frames (8192 samples) from sensor Radial Inlet Accel for different pump conditions: normal (NOR), plate (PLA), leading edge damage (LED), trailing edge damage (TED), seal (SEA), sand (SAN), sand and paper (SAP) and pvc balls (PVC) conditions.

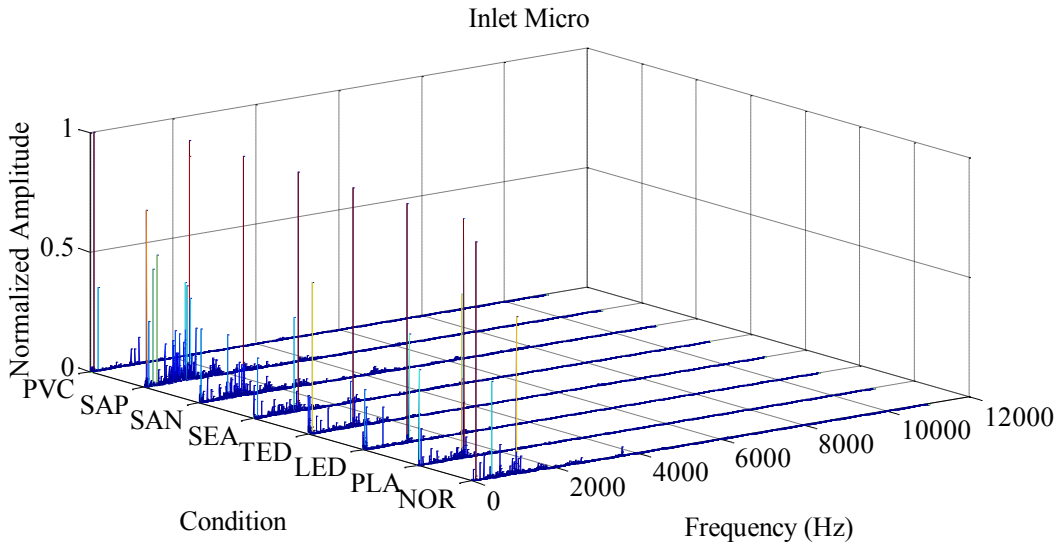

Figure 5-7: Spectra of audio frames (8192 samples) from sensor Inlet Micro for different pump conditions: normal (NOR), plate (PLA), leading edge damage (LED), trailing edge damage (TED), seal (SEA), sand (SAN), sand and paper (SAP) and pvc balls (PVC) conditions.

In order to obtain a better representation, Figure 5-8 and Figure 5-9 show the spectra in the range [2.6-1000]Hz of the Figure 5-6 and Figure 5-7 respectively. In audio signal, the normal condition spectrum has the characteristic pump frequencies (rotor frequency, vane-passing frequencies and their harmonics) as well as the fan motor frequency. As stated in Chapter 3 when an initial analysis of the baseline spectrum of audio signal was carried out, the discrete frequencies dominate in the spectrum and there is no noise. In PLA, LED and TED conditions, amplitude changes in the pump characteristic frequencies are observed. Moreover, broad-band noise is present in low frequency range (from 2.6Hz to 100Hz approximately). This might be due to possible recirculation of the flow. In the case of PLA condition this is not so evident. For SEA, SAN, SAP, PVC (seal condition and system fault conditions) more noise is present in the range 400-1000 Hz than in the case of normal condition. System fault conditions can lead to partial obstruction of the piping system, producing low flow rate and the generation of turbulence (broadband) noise. In Figure 5-7, it is also observed the peak at 1077Hz. As stated in Chapter 3, it is believed that this peak is due to structural resonances. Some noise is also present in fault conditions at higher frequencies than 1kHz in audio spectra.

In the case of the vibration signals, the change in the amplitude of the pump characteristic frequencies is also observed. The noise is less evident in the vibration

signals of fault conditions in frequency range [2.6-1000]Hz (Figure 5-8) than in audio spectra. However, there are differences between conditions in higher frequencies (from 1kHz-6kHz).

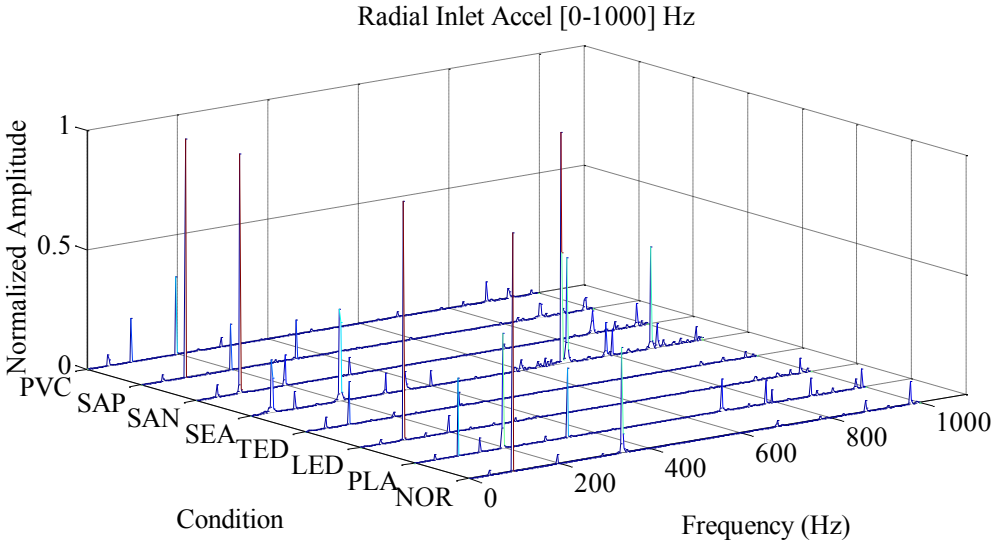

Figure 5-8: Spectra of vibration frames (8192 samples) from sensor Radial Inlet Accel in frequency range [0-1000]Hz for different pump conditions: normal (NOR), plate (PLA), leading edge damage (LED), trailing edge damage (TED), seal (SEA), sand (SAN), sand and paper (SAP) and pvc balls (PVC) conditions.

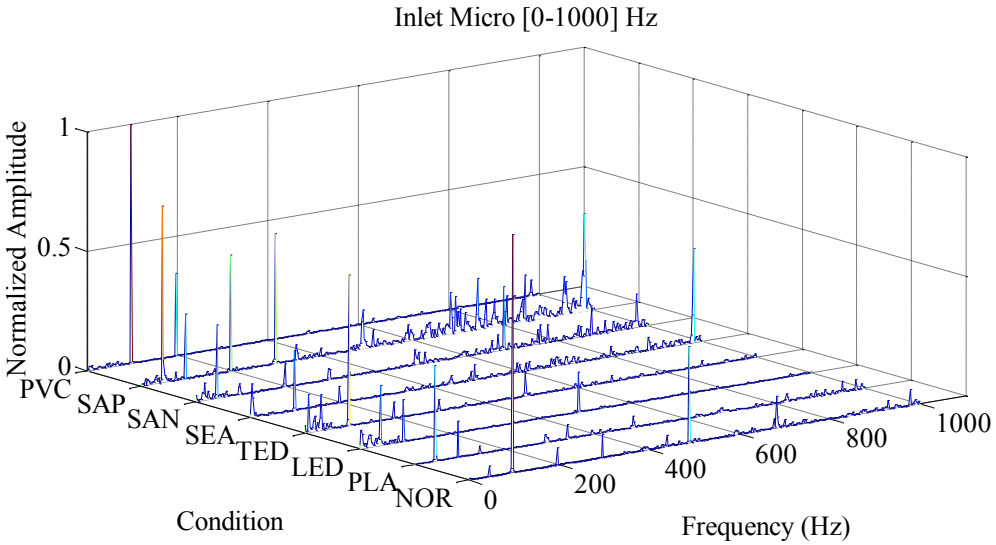

Figure 5-9: Spectra of audio frames (8192 samples) from sensor Inlet Micro in frequency range [0-1000]Hz for different pump conditions: normal (NOR), plate (PLA), leading edge damage (LED), trailing edge damage (TED), seal (SEA), sand (SAN), sand and paper (SAP) and pvc balls (PVC) conditions.

Based on the observations of audio and vibration spectra, we propose three features in both vibration and audio signals in frequency domain: harmonic to noise ratio, harmonic to noise ratio (iterative method) and normalised noise energy. These features can quantify the relationship between the harmonic components (multiples of the rotor frequency and vane-passing frequency) and noise components of the vibration and audio signals.

Harmonic to Noise ratio

The harmonic to noise ratio is the relationship between the pump characteristic frequencies (1X, 2X, 3X, 4X, VPF, 2VPF) and the rest of frequencies in the spectra which are treated as noise. The harmonic to noise ratio can be defined as:

$$HNR = 10\log_{10}\left(\frac{S(1X)+S(2X)+S(3X)+S(4X)+S(VPF)+S(2VPF)}{Noise}\right) \quad \text{[Eq. 5-61]}$$

The harmonic to noise ratio is computed per frame and then the mean value is obtained per observation.

Harmonic to Noise ratio (iterative method)

The harmonic to noise ratio (iterative method) is a measure from speech characterization field which measures the relationship between the harmonic and noise components of a voice signal [25]. It can be defined as:

$$HNR_{iterative} = 10\log_{10}\left(\frac{\frac{1}{N}\sum_{i=1}^{N}|H(w)|^2}{\frac{1}{N}\sum_{i=1}^{N}|N(w)|^2}\right) \quad \text{[Eq. 5-62]}$$

where $H(w)$ is the harmonic component and $N(w)$ is the noise component. To separate between the harmonic and noise components in a voice signal iterative methods are

used [27]. The following steps are used to obtain an estimation of the noise components in a frame of vibration and in a frame of audio signal:

1. The Fast Fourier transform (FFT) of *N* points is computed for each frame.
2. The harmonic components of the spectrum of the frame are removed and replaced by a null value. In this case, the harmonic components of the spectrum are the multiples of the pump frequency (1X), i.e. *n*X where $n = 1, \ldots, 452$.
3. The inverse Fast Fourier transform is computed and the samples with indexes higher than *N* are removed.
4. The FFT is computed again and the noise spectral components are replaced by the spectral components of the original frame.
5. Steps 3 and 4 are repeated five times.

Once the noise components of the spectrum are obtained, the harmonic component is computed as the difference of the FFT of the original frame and the noise components.

The Harmonic to Noise ratio is computed per each frame and the mean value is obtained per observation.

Normalised Noise Energy (iterative method)

The normalised noise ratio is another feature from the voice signal characterization field [26] that estimates the ratio between the noise components (noise energy) and the total energy of the signal. The normalized noise ratio can be expressed as:

$$NNR = 10\log_{10}\left(\frac{\frac{1}{N}\sum_{i=1}^{N}|N(w)|^2}{\frac{1}{N}\sum_{i=1}^{N}|S(w)|^2}\right) \qquad \text{[Eq. 5-63]}$$

where the numerator is the noise energy and the denominator is the energy of the signal. To obtain the noise component the iterative procedure explained in Harmonic to Noise ratio measure is used.

The normalized noise energy is computed per each frame and the mean value is obtained per observation.

5.2.5 Cepstrum Domain: Vibration and Audio Features in the state of the art

Cepstrum domain is used in fault diagnosis of different machines or part of machines such as gears and bearings [49]. However, as author knowledge, there are not features extracted from cepstrum domain in centrifugal pump fault diagnosis with faults related to impellers, seal or the system.

5.2.6 Contributions in cepstrum domain features

In cepstrum domain, we contribute with a set of features that characterize energy in the characteristic pump quefrencies (harmonic components) and relationships between harmonic components and noise components.

The power cepstra of a discrete signal $s[n]$ of length N are defined as:

$$p_s(n) \equiv F^{-1}\{\log(|S(w)|^2)\} \qquad \text{[Eq. 5-64]}$$

where $F^{-1}\{\ \}$ represents the inverse Fourier transform.

Using the power cepstrum the harmonic components of the vibration and audio signal from the centrifugal pump can be identified. The cepstrum are rectified to obtain a better representation. As an example, in Figure 5-10 and Figure 5-11 the representations of the rectified cepstrum of two audio signals in normal condition and in LED condition are shown. The cepstral energy at the rotor frequency (RF = 1X) and twice the rotor frequency are marked. In Figure 5-12 and Figure 5-13 the rectified cepstra of vibration

signals in normal and LED condition acquired simultaneously that the audio signals are shown.

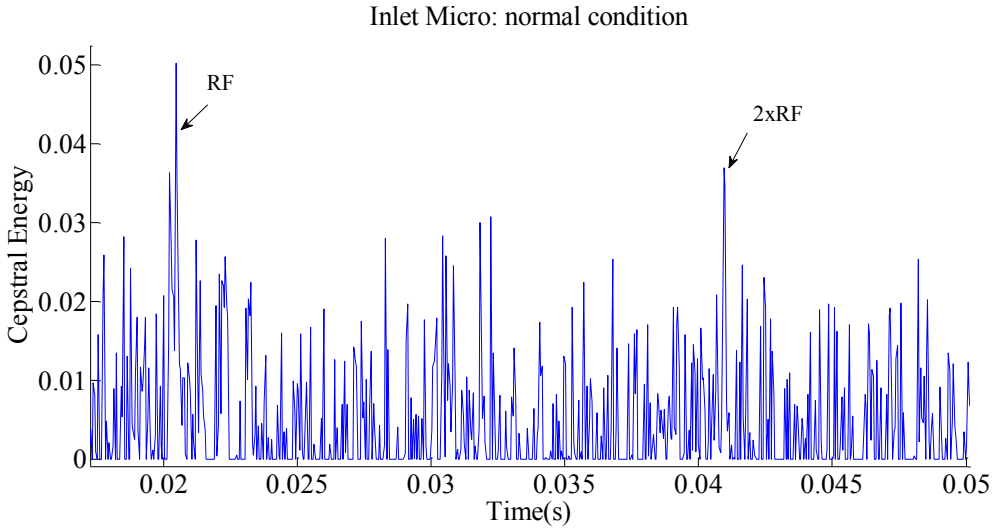

Figure 5-10: Rectified cepstrum of an audio frame from sensor Inlet Micro in normal condition.

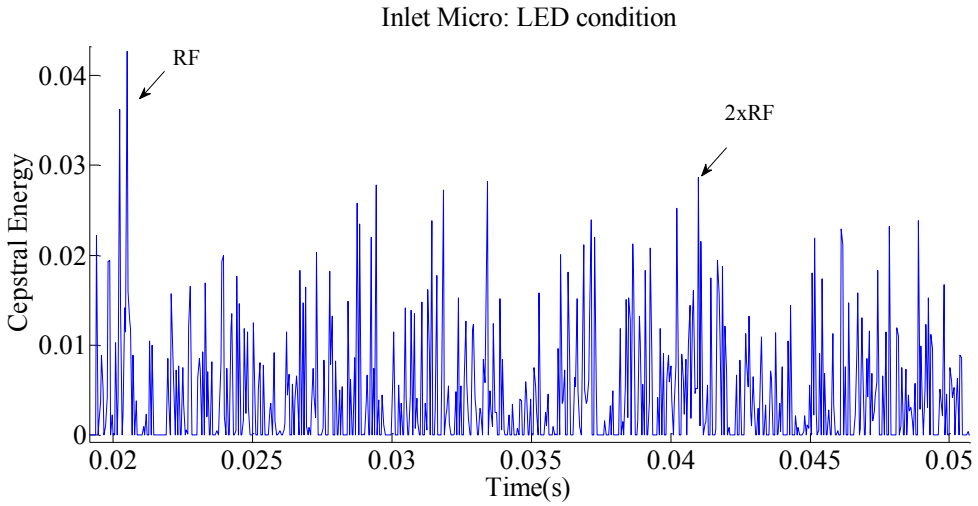

Figure 5-11: Rectified cepstrum of an audio frame from sensor Inlet Micro in LED condition.

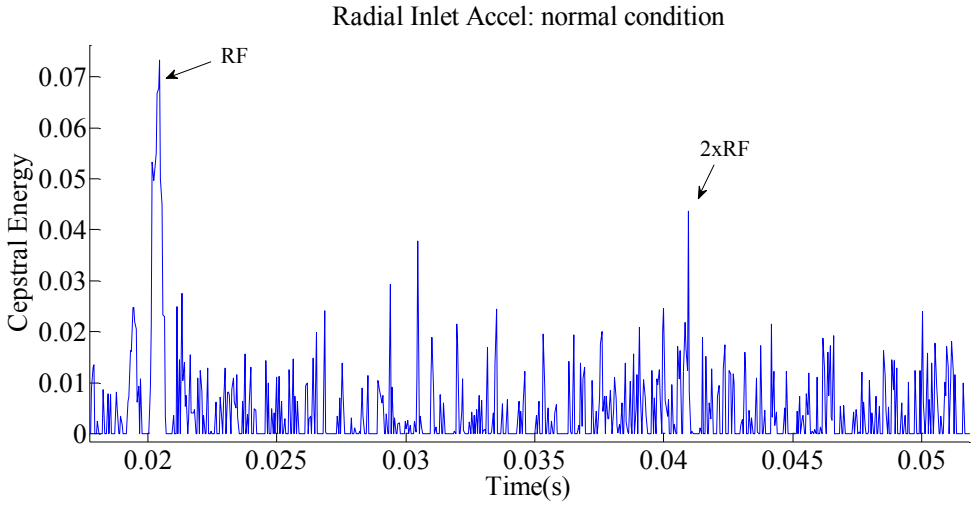

Figure 5-12: Rectified cepstrum of a vibration frame from sensor Radial Inlet Accel in normal condition.

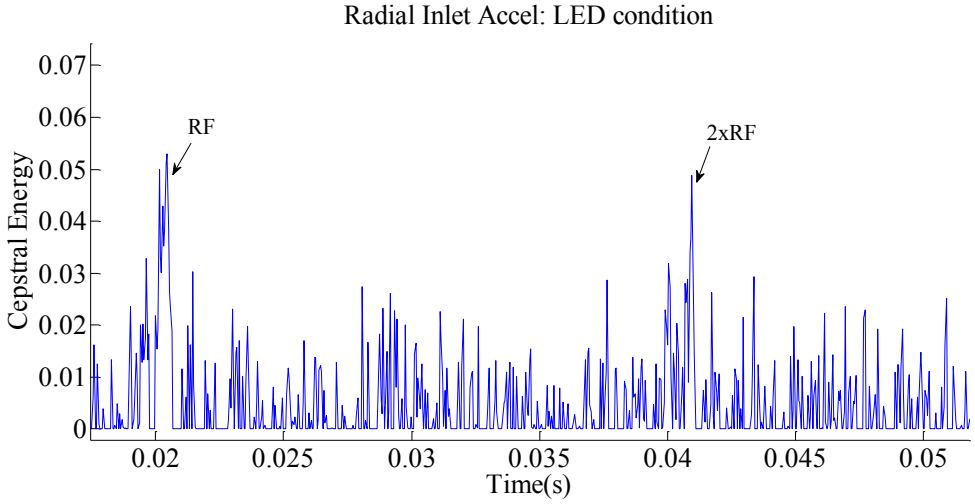

Figure 5-13: Rectified cepstrum of a vibration frame from sensor Radial Inlet Accel in LED condition.

Cepstral energies at pump characteristic quefrencies

Once the rectified power cepstrum is computed, the cepstral energies at pump characteristic quefrencies are estimated (1/1X, 1/2X, 1/3X, 1/4X, 1/VPF, 1/2VPF) as the sum of the cepstral components around those quefrencies. Six cepstral energies are obtained. Each of them is computed per frame and the mean value is obtained per observation.

Cepstral energy ratios at pump characteristic quefrencies

The cepstral energy ratios are the cepstral energy at the characteristic pump quefrencies divided by the total energy of the rectified cepstrum. Six cepstral energy ratios are obtained per frame and the mean value is computed per observation.

Cepstral Harmonic to Noise ratio

The cepstral harmonic to noise ratio quantifies the ratio between the harmonic component (the pump characteristic quefrencies) and the noise components in the cepstral domain. The harmonic energy in cepstrum domain is estimated as the sum of the energies at the pump characteristic quefrencies. The noise energy is estimated as the difference between the total energy of the rectified cepstrum and the energies at each pump characteristic quefrencies. The cepstral harmonic to noise ratio can be expressed as follows:

$$CHNR = 10\log\left(\frac{\frac{1}{L}\sum_{n=1}^{L}|C_H(n)|}{\frac{1}{L}\sum_{n=1}^{L}|C_N(n)|}\right) \qquad \text{[Eq. 5-65]}$$

where the numerator is the estimation of the energies at the pump characteristic quefrencies (harmonic component) and the denominator is the estimation of the noise energy in cepstrum domain. The cepstral harmonic to noise ratio is computed for each frame. The mean value is obtained per observation.

Cepstral Normalised Noise Energy

The cepstral normalised noise energy quantifies the relationship between the noise component and the total energy in the rectified power cepstrum domain. The noise component is estimated as in the *Cepstral Harmonic to Noise ratio*. The cepstral normalized noise energy can be expressed as:

$$CHNR = 10\log\left(\frac{\frac{1}{L}\sum_{n=1}^{L}|C_N(n)|}{\frac{1}{L}\sum_{n=1}^{L}|C_S(n)|}\right) \qquad \text{[Eq. 5-66]}$$

where the numerator is the estimated noise energy and the denominator the estimated total energy in the rectified cepstrum. The cepstral normalized noise energy is computed per frame and the mean value is obtained per observation.

5.2.7 Time-Frequency Domain Vibration and Audio Features in the state of the art

Most analysis in time-frequency domain in centrifugal pump diagnosis is carried out using the wavelet transform. Continuous and discrete wavelet transforms have been applied in fault diagnosis of different pump conditions: impeller damage, cavitation, bearings damage [28]-[33]. In general, the vibration signal is decomposed in different levels and statistical time features and statistical frequency features are extracted from the different levels of decomposition and are used as features in a classification system. In this Thesis, we have decided implement other kind of wavelet transform, the wavelet packet transform, already explained in Chapter 4 for bearing fault degradation, due to its versatility to decompose the signal in both high and low frequency levels. As the wavelet packet transform is a generalization of the discrete wavelet transform, we have decided not implement the continuous and discrete wavelet transform. We contribute with the use of the wavelet packet transform and the extraction of energy features from the nodes of the wavelet packet.

5.2.8 Contributions in time-frequency domain features

In this Thesis, we propose the use of the wavelet packet transform to centrifugal pump fault diagnosis. The selection of the wavelet mother was studied in a previous work (part of which is published in [1]). The selected wavelet mother is the 'Daubechies 2 ('db2'). We selected the level of decomposition according to the frequency range of each node so as each node encompass a frequency range up to VPF. The level of decomposition selected is 5. As the sample frequency is 22050Hz, in the fifth level of decomposition we have 32 nodes and each node has a frequency range of 344.5 Hz. We

have to take into account that the bandwith of the radial accelerometer is up to 2.6kHz. In order to obtain the same number of features for each sensor, we decided to use only the seven first nodes of the 5^{th} level of decomposition (from 0-2411.7Hz). The relative energy of the five-level nodes is computed as the energy of each node divide by the energy of the frame signal. So, we have 7 features in the time-frequency domain.

Relative energies in nodes 1-7 of the wavelet packet transform

The wavelet packet transform is applied at a frame $s[n]$ using the wavelet mother Daubecheis 2 ('db2') and five levels of decomposition. The relative energies (energy of the node divided by the energy of the original frame $s[n]$) of the first seven nodes of fifth level are computed.

Seven relative energies are computed per frame. The mean value of each feature is obtained per observation.

5.2.9 Nonlinear Domain Vibration and Audio Features in the state of the art

Centrifugal pumps operate with flowing fluids and have complicated interaction between the machine components and the flow itself [10], [11]. For this reason, it is reasonable to use measures to quantify complexity and predictability in a time series in order to discriminate between different pump conditions. However, there are few works investigating those kinds of features in pump fault diagnosis. Recently, Yunlong et al. [35] proposed the use of the empirical mode decomposition (a time-frequency technique) to decompose the original vibration signal into intrinsic mode functions (IMFs). Authors take the first eigth IMFs and extract the Lempel-Ziv complexity for each one. Then, the entropy of those eight values is computed. This procedure is applied to a centrifugal pump with mechanical faults such as unbalance, incorrect alignment and looseness. Dong et al. [34] applies the local mean decomposition (another technique in time-frequency domain) to decompose the pressure signal in product functions and then the entropy of the first two product functions is computed. This procedure is applied to mechanical faults (outer-race fault, inner-race fault, cylinder leakage, relief valve blockage and relief valve leakage) of an hydraulic pump system.

No previous works using complexity measures or measures based on nonlinear dynamics in pump fault diagnosis with fault related to impeller damage, seal damage or system faults were found by the author of this Thesis.

5.2.10 Contributions in nonlinear domain features

In this section, we propose a set of features to quantify the complexity of audio and vibration signals of a centrifugal pump. Some of the features are based on nonlinear dynamic system theory and other features are complexity and predectibility measures.

Nonlinear Dynamics Systems: Taken's embedding

Deterministic dynamical systems describe the time evolution of a system in some phase space $\Gamma \in \Re^m$ (m-dimensional vectorial space), where a state is specified by a vector. The evolution in time can be expressed by ordinary differential equations or by maps in discrete time. The dynamical system underlying the fluid dynamics and their interaction with the pump components is very complex and its equations are unknown. Nevertheless, Takens' embedding theorem [36] establishes that it is possible to reconstruct a phase space diffeomorphically equivalent to the original one from the time series of a system. The delays method is used to reconstruct the state-space vector formed by time-delayed samples of the observation (the vibration or the audio signal $s[n]$)

$$\bar{s}_n = [s[n], s[n-\tau], \ldots, s[n-(m-1)\tau]] \qquad \text{[Eq. 5-67]}$$

where $s[n]$ is the vibration/audio signal, m is the minimum embedding dimension of the phase space reconstructed and τ is the time delay. The vibration and audio signals are embedded in the reconstructed phase space and their long-term evolution in the reconstructed phase space is called attractor. τ can be determined by calculating the first minimum of mutual information [37] and the false neighbors method [38] can be used to estimate the minimum value of the embedding m.

Mutual information function

The mutual information function measures the mutual dependency between two variables. When these two variables are a discrete signal $s[n]$ and its delayed version $s[n+\tau]$, the mutual information function measures the quantity of information we already possess about the value of $s[n+\tau]$ if we know $s[n]$. The mutual information estimator reads as [37], [39]:

$$I(\tau) = \sum_{i,j} p_{i,j}(\tau) \ln\left[\frac{p_{ij}(\tau)}{p_i p_j(\tau)}\right] \qquad \text{[Eq. 5-68]}$$

where p_i is the probability of finding a value of $s[n]$ inside the *i*th bin of the data histogram and p_{ij} the joint probability that $s[n]$ is in bin *i* and $s[n+\tau]$ in bin *j*.

The first minimum of the mutual information function marks the delay where mutual information adds maximal information to the knowledge we have from $s[n]$. The value of the mutual information function in the first minimum (MI) quantifies the degree of irregular behavior of a time series in the time of maximum difference of a signal with its delayed version.

Correlation dimension

The correlation dimension gives an idea of the complexity of the dynamics. More complex systems have a higher correlation dimension. In random processes, correlation dimension is not bounded, while in deterministic systems there tends to be a finite value and it can be a non integer number (fractal dimension). CD is given as [39]:

$$D_2 = \frac{d \ln C(\varepsilon, N)}{d \ln \varepsilon} \cong \lim_{\Delta \ln \varepsilon \to 0} \frac{\Delta \ln C(\varepsilon, N)}{\Delta \ln \varepsilon} \qquad \text{[Eq. 5-69]}$$

with $C(\varepsilon,N)$ being the correlation sum of a set of points $\bar{s}_n$ (n = 1,...,N) of the vibration or audio signal attractor in the reconstructed embedding.

$$C(\varepsilon, N) = \frac{1}{N(N-1)} \sum_{i=1}^{N} \sum_{\substack{j=1 \\ j \neq i}}^{N} \theta(\varepsilon - \left\| \bar{s}_i - \bar{s}_j \right\|) \qquad \text{[Eq. 5-70]}$$

where $\theta(s) = 0$ if $s \leq 0$ and $\theta(s) = 1$ if $s > 0$ which counts the number of points inside the sphere with radius ε around $\bar{s}_i$. $C(\varepsilon, N)$ is the average fraction of points within a distance of ε from any other point. D_2 is estimated by calculating the local slope of the curve $\ln C(\varepsilon)$ against $\ln \varepsilon$ when the curve has a plateau for different values of the embedding dimension.

In this Thesis, the Takens-Theiler estimator [40] of D_2 is computed (CD). Takens-Theiler estimator is a maximum-likelihood estimator of D_2 and can be obtained as follows:

$$D_{TT}(\varepsilon) = \frac{C(\varepsilon)}{\int_0^{\varepsilon} \frac{c(\varepsilon')}{\varepsilon'} d\varepsilon'} \qquad \text{[Eq. 5-71]}$$

The procedure to compute CD is the following. First, the minimum embedding dimension is estimated using the false neighbors method. Then, the Takens-Theiler estimator of the correlation dimension (CD) is computed for different values of m. The value of m varies from the minimum embedding dimension to the minimum embedding dimension plus 3. For example, if the minimum embedding dimension estimated for the frame is 3, the Takens-Theiler estimator is computed for the following embedding dimensions: 3, 4, 5 and 6 and therefore four different curves are obtained. When a plateau is found in the curves (the scaling range where the value of the Takens-Theiler estimator is independent of m and ε), the value of the straight line that fits this plateau is the CD estimator.

Shannon entropy

Entropy describes the quantity of disorder or complexity of a system. Shannon entropy (SE) and correlation entropy (CE) were estimated as follows.

Shannon entropy of a system reads as:

$$H = -\sum_i p_i \ln p_i \qquad \text{[Eq. 5-72]}$$

If we consider a system in which its output falls into the unit interval and we divide it into bins, p_i is the probability that one of the outputs falls into *th* bin. The SE measures the degree of disorder of the probability distribution of a time series [39]. The SE is estimated as the maximum value of the mutual information function.

Correlation entropy

The correlation entropy estimator (CE) quantifies the loss of information in time in a dynamic system [39]. It is zero, positive, and infinite for regular, chaotic and random systems respectively. The correlation entropy is the Rényi entropy of order 2. In order to formulate the correlation entropy, let us consider observables where the partition elements are intervals I_j of size ε. Let us introduce joint probabilities $p_{i_1,i_2,\ldots,i_m}$ that an arbitrary time *n* the observable falls into the interval I_{i_1} and in time *n*+1 it falls into the interval I_{i_2} and so on. Then, the block entropies of block size *m* is given as [39]:

$$H_q(m,\varepsilon) = \frac{1}{1-q} \ln \sum_{i_1,i_2,\ldots,i_m} p^q_{i_1,i_2,\ldots,i_m} \qquad \text{[Eq. 5-73]}$$

The correlation entropy is defined as:

$$h_2 = \sup_I \lim_{m\to\infty} \frac{1}{m} H_2(m,\varepsilon) \qquad \text{[Eq. 5-74]}$$

The correlation entropy is estimated using the same procedure of the correlation dimension estimator.

Normalised Lempel-Ziv complexity

The normalized Lempel-Ziv complexity [41], [42] is a complexity measure that quantifies the degree of order or disorder and development of spatiotemporal patterns in a time series. Lempel-Ziv complexity was presented and studied in Chapter 4, so we do not repeat here the formulation. We compute the Lempel-Ziv complexity with 4 symbols for each frame. The average value is obtained per observation.

Hurst exponent

The rescaled-range (RS) method was introduced by Hurst [43] as a tool for evaluating the persistence or antipersistence of a time series. The method consists of dividing the series into intervals of a given size λ and calculating the average ratio R/S of the range (the difference between the maximum and minimum values of the series) to the standard deviation from each interval. The size λ is varied and a curve of the rescaled range R/S as a function of λ is obtained. The Hurst exponent can be estimated as the slope of the curve. A Hurst exponent (H) equal to 0.5 corresponds to a regular Brownian motion (random motion) and to the absence of memory effects, $H > 0.5$ ($H < 0.5$) corresponds to persistent (antipersistent) behaviour of the time series and to the presence of memory affecting the motion.

In an anti-persistent time series an increase will most likely be followed by a decrease or vice-versa (i.e., values will tend to revert to a mean). The closer the H value is to 0, the stronger is the tendency for the time series to revert to its long-term means value. This means that future values have a tendency to return to a long-term mean. In a persistent time series an increase in values will most likely be followed by an increase in the short term and a decrease in values will most likely be followed by another decrease in the short term. The closer the H value is to 1, the stronger the trend. Mathematically, the Hurst exponent is computed as follows:

Given an interval of size λ, whose left end is located a point i_0, the average of the time series x of the interval is computed as:

$$\langle x \rangle_\lambda = \frac{1}{\lambda} \sum_{t=i_0}^{i_0+\lambda-1} x_t \qquad \text{[Eq. 5-75]}$$

An accumulated deviation from the mean is defined as

$$X(t,\lambda) = \sum_{u=1}^{t} x_u - \langle x \rangle_\lambda \qquad \text{[Eq. 5-76]}$$

A range is extracted from the above operations

$$R(\lambda) = \max(X(t,\lambda)) - \min(X(t,\lambda)) \qquad \text{[Eq. 5-77]}$$

And the corresponding standard deviation

$$S = \sqrt{\sum_{t=1}^{\lambda} \{x(t) - \langle x \rangle_\lambda\}^2} \qquad \text{[Eq. 5-78]}$$

Finally, the rescaled range $R(\tau)/S(\tau)$ is obtained and its average is determined over all intervals. The rescaled range should satisfy the scaling form:

$$RS(\lambda) = \frac{R(\lambda)}{S(\lambda)} \approx \lambda^H \qquad \text{[Eq. 5-79]}$$

where H is the Hurst exponent.

The Hurst exponent is extracted per each frame and the average value is obtained per observation.

Higuchi fractal dimension

The Higuchi's algotihm is a technique for computing the fractal dimension of a time series directly without the embedding process. The fractal dimension quantifies the complexity of the time series. In order to obtain the fractal dimension *D*, Higuchi [44] considered the times series $s[1], s[2], \ldots, s[N]$ as a set of observations taken at regular interval. From this series, a new one, s_k^m is constructed, which is defined as follows:

$$s_k^m; s[m], s[m+k], s[m+2k], \ldots, s[m+\left(\frac{N-m}{k}\right)k] \qquad \text{[Eq. 5-80]}$$

with $m = 1,2,\ldots,k$, where (.) that is the bigger integer, and both *k* and *m* are integers, indicating *m* and *k* the initial time and the interval time, respectively.

Higuchi defines the length of the curve associated to each time series, s_k^m as follows:

$$L_m(k) = \frac{1}{k}\left(\sum_{i=1}^{\left[\frac{N-m}{k}\right]} s(m+ik) - s(m+(i-1)k)\right)\left(\frac{N-1}{\left[\frac{N-m}{k}\right]k}\right) \qquad \text{[Eq. 5-81]}$$

where the term $\frac{N-1}{\left[\frac{N-m}{k}\right]k}$, represents a normalization factor. Higuchi takes the average value $\langle L(k)\rangle$ of the lengths associated to the time series given by Eq 5-80. If the average value follows a power law:

$\langle L(k)\rangle \propto k^{-D}$

then the curve is fractal with dimension *D*.

5.3 Feature identification

Once the features are extracted from each sensor, the feature selection procedure is applied. In the following table the 98 features extracted from the vibration and audio signals of each sensor are enumerated and an identifier is added to each feature (Id.).

TABLE 5-2: FEATURES EXTRACTED FROM VIBRATION AND AUDIO SIGNALS

Feature Id	Feature Name	Signal domain
1	Mean of mean value	Time
2	Mean of mean value absolute	Time
3	Mean of standard deviation	Time
4	Mean of standard deviation absolute	Time
5	Mean of variance	Time
6	Mean of variance absolute	Time
7	Mean of skewness	Time
8	Mean of skewness absolute	Time
9	Mean of skewness of peak values	Time
10	Mean of skewness of valley values	Time
11	Mean of kurtosis	Time
12	Mean of kurtosis absolute	Time
13	Mean of kurtosis of peak values	Time
14	Mean of kurtosis of valley values	Time
15	Mean of median	Time
16	Mean of minimum values	Time
17	Mean of maximum values	Time
18	Mean of range values	Time
19	Mean of sum values	Time
20	Mean of variation rate	Time
21	Mean of variation rate of peak values	Time
22	Mean of variation rate of valley values	Time
23	Mean of the number of peaks and number of zero-crossing ratio	Time

Feature Id	Feature Name	Signal domain
24	Mean of the number of valleys and number of zero-crossing ratio	Time
25	Mean of the ratio of averaged peaks and mean value absolute	Time
26	Mean of ratio of averaged ten peaks and averaged peaks	Time
27	Mean of ratio of averaged peaks and standard deviation of peaks	Time
28	Mean of ratio of averaged valleys and standard deviation of valleys	Time
29	Mean of energy in time 1	Time
30	Mean of energy in time 2	Time
31	Mean of energy in time 3	Time
32	Mean of root mean square	Time
33	Mean of crest factor	Time
34	Mean of 4th central moment	Time
35	Mean of 5th central moment	Time
36	Mean of 6th central moment	Time
37	Mean of Zero crossing rate	Time
38	Mean of amplitude at rotor (1X) frequency	Frequency
39	Mean of amplitude at 2X frequency	Frequency
40	Mean of amplitude at 3X frequency	Frequency
41	Mean of amplitude at 4X frequency	Frequency
42	Mean of amplitude at vane-passing frequency	Frequency
43	Mean of amplitude at twice vane-passing frequency	Frequency
44	Mean of amplitude at 1X ratio	Frequency
45	Mean of amplitude at 2X ratio	Frequency
46	Mean of amplitude at 3X ratio	Frequency
47	Mean of amplitude at 4X ratio	Frequency
48	Mean of amplitude at vane-pass frequency ratio	Frequency
49	Mean of amplitude at twice vane-pass frequency ratio	Frequency
50	Mean of noise ratio	Frequency
51	Mean of root mean square in [0-1X]	Frequency
52	Mean of root mean square in [0-2X]	Frequency
53	Mean of root mean square in [0-3X]	Frequency

Feature Id	Feature Name	Signal domain
54	Mean of root mean square in [0-4X]	Frequency
55	Mean of root mean square in [0-VPF]	Frequency
56	Mean of root mean square in [0-2VPF]	Frequency
57	Mean of harmonic to noise ratio (dB)	Frequency
58	Mean of normalized noise energy (iterative method) (dB)	Frequency
59	Mean of harmonic to noise ratio (iterative method) (dB)	Frequency
60	Mean of central frequency	Frequency
61	Mean of standard deviation frequency	Frequency
62	Mean of skewness frequency	Frequency
63	Mean of kurtosis frequency	Frequency
64	Mean of frequency rate	Frequency
65	Mean of energy in frequency (energy freq 1)	Frequency
66	Mean of maximum amplitude in spectrum	Frequency
67	Mean of energy in frequency (energy freq 2)	Frequency
68	Mean of energy in frequency (energy freq 3)	Frequency
69	Mean of energy in frequency (energy freq 4)	Frequency
70	Mean of normalized spectral entropy	Frequency
71	Mean of cepstral energy at 1/1X	Cepstrum
72	Mean of cepstral energy ratio at 1/1X	Cepstrum
73	Mean of cepstral energy at 1/2X	Cepstrum
74	Mean of cepstral energy ratio at 1/2X	Cepstrum
75	Mean of cepstral energy at 3X	Cepstrum
76	Mean of cepstral energy ratio at 1/3X	Cepstrum
77	Mean of cepstral energy at 1/4X	Cepstrum
78	Mean of cepstral energy ratio at 1/4X	Cepstrum
79	Mean of cepstral energy at vane pass quefrency	Cepstrum
80	Mean of cepstral energy ratio at vane pass quefrency	Cepstrum
81	Mean of cepstral energy at twice vane pass quefrency	Cepstrum
82	Mean of cepstral energy ratio at twice vane pass quefrency	Cepstrum
83	Mean of cepstral normalized Noise Energy	Cepstrum
84	Mean of cepstral Harmonic to Noise ratio	Cepstrum

Feature Id	Feature Name	Signal domain
85	Mean of relative energy in node 1 wavelet packet	Wavelet
86	Mean of relative energy in node 2 wavelet packet	Wavelet
87	Mean of relative energy in node 3 wavelet packet	Wavelet
88	Mean of relative energy in node 4 wavelet packet	Wavelet
89	Mean of relative energy in node 5 wavelet packet	Wavelet
90	Mean of relative energy in node 6 wavelet packet	Wavelet
91	Mean of relative energy in node 7 wavelet packet	Wavelet
92	Mean of Lempel Ziv complexity value (n = 4)	Nonlinear
93	Mean of Hurst exponent value	Nonlinear
94	Mean of 1^{st} minimum of mutual information function	Nonlinear
95	Mean of Shannon entropy	Nonlinear
96	Mean of correlation dimension	Nonlinear
97	Mean of correlation entropy	Nonlinear
98	Mean of Higuchi fractal dimension	Nonlinear

5.4 Relevance study of the selected features

In this section, the results of the relevance study of the selected features (methodology explained in Chapter 4) are shown for each sensor. Two different cases are considered: 8 classification units (i.e. 8 pump conditions) and 17 classification units (i.e. 17 pump conditions).

5.4.1 Case study: 8 classification units

The results of the selected features sorted by relevance order are shown for each sensor for the case of 8 classification units in Table 5-3. Freq is the frequency of appearance of a feature.

TABLE 5-3: RELEVANCE ORDER FOR 8 CLASSIFICATION UNITS

8 classification units (NOR, PLA, LED, TED, SEA, SAN, SAP, PVC)								
Relevance Order	RadialInletAccel		RadialAccel		InletMicro		OutletMicro	
	Feature	Freq	Feature	Freq	Feature	Freq	Feature	Freq
1	68	53.3%	92	55%	47	71.6%	68	65%
2	7	36.6%	71	35%	90	50%	15	35%
3	22	31.6%	91	31.6%	24	26.6%	47	35%
4	77	30%	68	30%	86	26.6%	23	30%
5	9	21.6%	21	26.6%	92	25%	44	28.3%
6	25	20%	8	21.6%	38	21.6%	87	28.3%
7	8	15%	9	18.3%	25	20%	46	26.6%
8	10	15%	24	18.3%	60	18.3%	42	25%
9	24	15%	72	16.6%	87	16.6%	7	23.3%
10	37	15%	14	13.3%	21	15%	8	23.3%
11	44	15%	49	13.3%	10	11.6%	14	21.6%
12	70	15%	7	11.6%	41	11.6%	86	21.6%
13	83	15%	28	10%	45	11.6%	50	20%
14	23	13.3%	75	10%	9	8.3%	85	20%
15	78	13.3%	90	10%	28	8.3%	90	20%
16	71	11.6%	2	6.6%	44	8.3%	12	16.6%
17	21	10%	26	6.6%	23	6.6%	35	16.6%
18	67	10%	83	5%	48	6.6%	43	16.6%
19	69	10%	23	5%	7	5%	45	16.6%
20	38	8.3%	37	5%	27	5%	48	16.6%
21	72	8.3%	45	5%	37	5%	57	16.6%
22	86	8.3%	47	5%	39	5%	24	15%
23	14	6.6%	62	5%	93	5%	25	15%
24	41	6.6%	69	5%	8	3.3%	93	15%
25	62	6.6%	86	3.3%	14	3.3%	10	11.6%
26	84	6.6%	10	3.3%	22	3.3%	9	10%
27	12	5%	11	3.3%	26	3.3%	11	10%

8 classification units (NOR, PLA, LED, TED, SEA, SAN, SAP, PVC)								
Relevance Order	RadialInletAccel		RadialAccel		InletMicro		OutletMicro	
	Feature	Freq	Feature	Freq	Feature	Freq	Feature	Freq
28	17	5%	12	3.3%	42	3.3%	71	10%
29	27	5%	20	3.3%	51	3.3%	91	10%
30	28	5%	41	3.3%	68	3.3%	94	10%
31	33	5%	50	1.6%	85	3.3%	22	8.3%
32	43	5%	13	1.6%	12	1.6%	56	8.3%
33	47	5%	15	1.6%	15	1.6%	60	8.3%
34	49	5%	25	1.6%	40	1.6%	13	6.6%
35	60	5%	38	1.6%	43	1.6%	20	6.6%
36	79	5%	48	1.6%	46	1.6%	37	6.6%
37	85	5%	58	1.6%	49	1.6%	38	6.6%
38	2	3.3%	59	1.6%	59	1.6%	53	6.6%
39	26	3.3%	60	1.6%	67	1.6%	62	6.6%
40	40	3.3%	76	1.6%	69	1.6%	69	6.6%
41	73	3.3%	77	1.6%	91	1.6%	1	5%
42	87	3.3%	84	1.6%	98	1.6%	26	5%
43	88	3.3%	85	1.6%	1	0%	27	5%
44	94	3.3%	87	1.6%	2		30	5%
45	3	1.6%	93	1.6%	3		31	5%
46	4	1.6%	1	0%	4		51	5%
47	5	1.6%	3		5		54	5%
48	11	1.6%	4		6		70	5%
49	34	1.6%	5		11		84	5%
50	45	1.6%	6		13		28	3.3%
51	58	1.6%	16		16		39	3.3%
52	64	1.6%	17		17		40	3.3%
53	80	1.6%	18		18		41	3.3%
54	90	1.6%	19		19		49	3.3%
55	91	1.6%	22		20		52	3.3%

8 classification units (NOR, PLA, LED, TED, SEA, SAN, SAP, PVC)								
Relevance Order	RadialInletAccel		RadialAccel		InletMicro		OutletMicro	
	Feature	Freq	Feature	Freq	Feature	Freq	Feature	Freq
56	92	0%	27	0%	29	0%	67	3.3%
57	1		29		30		73	3.3%
58	6		30		31		83	3.3%
59	13		31		32		88	3.3%
60	15		32		33		2	1.6%
61	16		33		34		3	1.6%
62	18		34		35		4	1.6%
63	19		35		36		5	1.6%
64	20		36		50		19	1.6%
65	29		39		52		21	1.6%
66	30		40		53		29	1.6%
67	31		42		54		33	1.6%
68	32		43		55		55	1.6%
69	35		44		56		58	1.6%
70	36		46		57		64	1.6%
71	39		51		58		65	1.6%
72	42		52		61		66	1.6%
73	46		53		62		89	1.6%
74	48		54		63		97	1.6%
75	50		55		64		6	0%
76	51		56		65		16	
77	52		57		66		17	
78	53		61		70		18	
79	54		63		71		32	
80	55		64		72		34	
81	56		65		73		36	
82	57		66		74		59	
83	59		67		75		61	

8 classification units (NOR, PLA, LED, TED, SEA, SAN, SAP, PVC)								
Relevance Order	RadialInletAccel		RadialAccel		InletMicro		OutletMicro	
	Feature	Freq	Feature	Freq	Feature	Freq	Feature	Freq
84	61	0%	70	0%	76	0%	63	0%
85	63		73		77		72	
86	65		74		78		74	
87	66		78		79		75	
88	74		79		80		76	
89	75		80		81		77	
90	76		81		82		78	
91	81		82		83		79	
92	82		88		84		80	
93	89		89		88		81	
94	93		94		89		82	
95	95		95		94		92	
96	96		96		95		95	
97	97		97		96		96	
98	98		98		97		98	

5.4.2 Case study: 17 classification units

The results of the selected features sorted by relevance order are shown for each sensor for the case of 17 classification units in Table 5-4. In this case, the severity of the faults is considered.

TABLE 5-4: RELEVANCE ORDER FOR 17 CLASSIFICATION UNITS

17 classification units (NOR, PLA1, PLA2, PLA3, LED1, LED2, LED3, TED1, TED2, TED3, SEA, SAN, SAP, PVC)								
Relevance Order	RadialInletAccel		RadialAccel		InMicro		OutMicro	
	Feature	Freq	Feature	Freq	Feature	Freq	Feature	Freq
1	68	83.3%	86	48.3%	90	73.3%	90	68.8%
2	87	36.6%	24	43.3%	14	53.3%	48	55%
3	14	31.6%	68	40%	42	51.6%	42	50%
4	22	31.6%	90	38.3%	47	50%	43	45%
5	66	31.6%	23	36.6%	92	50%	87	45%
6	70	31.6%	91	33.3%	87	48.3%	47	41.6%
7	21	30%	46	30%	59	46.6%	98	41.6%
8	91	30%	89	30%	27	45%	24	40%
9	27	28.3%	25	28.3%	28	43.3%	68	40%
10	28	26.6%	28	26.6%	8	41.6%	46	38.3%
11	41	26.6%	7	25%	41	41.6%	69	36.6%
12	72	26.6%	76	25%	44	41.6%	23	33.3%
13	10	23.3%	88	25%	67	41.6%	86	31.6%
14	24	23.3%	69	23.3%	25	40%	93	31.6%
15	43	23.3%	10	21.6%	26	40%	94	30%
16	46	23.3%	27	21.6%	12	38.3%	9	28.3%
17	67	23.3%	83	21.6%	21	36.6%	14	28.3%
18	83	23.3%	8	20%	33	36.6%	71	26.6%
19	90	23.3%	15	20%	38	36.6%	22	25%
20	25	18.3%	37	20%	69	36.6%	37	25%
21	37	18.3%	72	20%	13	35%	49	25%
22	49	18.3%	74	20%	19	35%	51	25%
23	84	18.3%	77	20%	37	35%	25	23.3%
24	85	18.3%	87	20%	60	35%	50	21.6%
25	35	16.6%	20	18.3%	9	33.3%	8	20%
26	44	16.6%	21	18.3%	23	33.3%	10	20%

17 classification units (NOR, PLA1, PLA2, PLA3, LED1, LED2, LED3, TED1, TED2, TED3, SEA, SAN, SAP, PVC)								
Relevance Order	RadialInletAccel		RadialAccel		InMicro		OutMicro	
	Feature	Freq	Feature	Freq	Feature	Freq	Feature	Freq
27	88	16.6%	30	18.3%	53	33.3%	13	20%
28	89	16.6%	73	18.3%	86	33.3%	54	20%
29	51	15%	75	18.3%	11	31.6%	89	20%
30	60	15%	84	18.3%	22	31.6%	91	20%
31	61	15%	92	18.3%	54	31.6%	11	18.3%
32	17	13.3%	9	16.6%	85	31.6%	57	18.3%
33	34	13.3%	29	16.6%	52	30%	60	18.3%
34	36	13.3%	39	16.6%	68	30%	64	18.3%
35	57	13.3%	45	16.6%	89	30%	67	18.3%
36	69	13.3%	67	16.6%	91	30%	72	18.3%
37	73	13.3%	60	15%	20	28.3%	12	16.6%
38	93	13.3%	71	15%	39	28.3%	27	16.6%
39	98	13.3%	96	15%	56	28.3%	53	16.6%
40	7	11.6%	98	15%	88	28.3%	84	16.6%
41	8	11.6%	12	13.3%	93	28.3%	85	16.6%
42	9	11.6%	13	13.3%	55	26.6%	26	15%
43	15	11.6%	26	13.3%	62	26.6%	29	15%
44	40	11.6%	31	13.3%	24	25%	33	15%
45	47	11.6%	48	13.3%	45	25%	39	15%
46	52	11.6%	78	13.3%	48	25%	56	15%
47	55	11.6%	94	13.3%	97	25%	20	13.3%
48	58	11.6%	47	11.6%	10	23.3%	31	13.3%
49	59	11.6%	85	11.6%	29	23.3%	52	13.3%
50	71	11.6%	1	10%	40	23.3%	55	13.3%
51	74	11.6%	14	10%	71	23.3%	83	13.3%
52	94	11.6%	19	10%	98	23.3%	88	13.3%
53	95	11.6%	33	10%	51	21.6%	21	11.6%

17 classification units (NOR, PLA1, PLA2, PLA3, LED1, LED2, LED3, TED1, TED2, TED3, SEA, SAN, SAP, PVC)								
Relevance Order	RadialInletAccel		RadialAccel		InMicro		OutMicro	
	Feature	Freq	Feature	Freq	Feature	Freq	Feature	Freq
54	18	10%	56	10%	58	21.6%	38	11.6%
55	19	10%	79	10%	50	20%	73	11.6%
56	23	10%	11	8.3%	7	18.3%	30	10%
57	26	10%	53	8.3%	15	18.3%	59	10%
58	29	10%	57	8.3%	30	18.3%	95	10%
59	39	10%	70	8.3%	95	18.3%	7	8.3%
60	50	10%	93	8.3%	49	16.6%	15	8.3%
61	77	10%	97	8.3%	61	16.6%	44	8.3%
62	86	10%	22	6.6%	46	15%	45	8.3%
63	16	8.3%	44	6.6%	63	15%	1	6.6%
64	42	8.3%	52	6.6%	70	15%	28	6.6%
65	64	8.3%	54	6.6%	72	15%	41	6.6%
66	92	8.3%	58	6.6%	31	11.6%	74	6.6%
67	5	6.6%	64	6.6%	35	11.6%	97	6.6%
68	11	6.6%	2	5%	43	11.6%	17	5%
69	20	6.6%	34	5%	83	11.6%	19	5%
70	30	6.6%	40	5%	96	11.6%	62	5%
71	32	6.6%	42	5%	74	10%	63	5%
72	33	6.6%	49	5%	81	10%	65	5%
73	53	6.6%	51	5%	84	10%	61	3.3%
74	54	6.6%	63	5%	94	10%	81	3.3%
75	56	6.6%	66	5%	73	8.3%	92	3.3%
76	96	6.6%	81	5%	3	6.6%	96	3.3%
77	2	5%	5	3.3%	5	6.6%	2	1.6%
78	3	5%	16	3.3%	36	6.6%	16	1.6%
79	6	5%	35	3.3%	82	6.6%	18	1.6%
80	31	5%	38	3.3%	58	5%	35	1.6%

17 classification units (NOR, PLA1, PLA2, PLA3, LED1, LED2, LED3, TED1, TED2, TED3, SEA, SAN, SAP, PVC)								
Relevance Order	RadialInletAccel		RadialAccel		InMicro		OutMicro	
	Feature	Freq	Feature	Freq	Feature	Freq	Feature	Freq
81	38	5%	41	3.3%	64	5%	36	1.6%
82	62	5%	55	3.3%	66	5%	40	1.6%
83	65	5%	62	3.3%	76	5%	70	1.6%
84	76	5%	65	3.3%	2	3.3%	75	1.6%
85	82	5%	80	3.3%	17	3.3%	78	1.6%
86	97	5%	95	3.3%	18	3.3%	3	0%
87	1	3.3%	3	1.6%	65	3.3%	4	
88	4	3.3%	4	1.6%	75	3.3%	5	
89	12	3.3%	6	1.6%	79	3.3%	6	
90	13	3.3%	17	1.6%	80	3.3%	32	
91	45	3.3%	36	1.6%	1	1.6%	34	
92	48	3.3%	50	1.6%	4	1.6%	58	
93	75	3.3%	59	1.6%	6	1.6%	66	
94	78	3.3%	61	1.6%	16	1.6%	76	
95	79	3.3%	82	1.6%	32	0%	77	
96	63	1.6%	18	0%	34		79	
97	81	1.6%	32		77		80	
98	80	0%	43		78		82	

5.5 Evaluation of the features for pump fault diagnosis

In this section, the features are incrementally evaluated from the feature with higher relevance (higher probability of appearance in the group of selected features) to the feature with less relevance in two different classifiers: a neural network classifier and a LSSVM classifier. This procedure is done for each sensor.

The success rate is obtained for each classifier and each sensor. The experiment is repeated 20 times and the results are averaged.

5.5.1 Case study: 8 classification units

In Figure 5-14 the incremental evaluation of the features for a neural network classifier and for each sensor is shown. In Figure 5-15, the evaluation using a LSSVM classifier is shown. From the figures it is obvious that the LSSVM classifier gives higher success rates with less number of features evaluated.

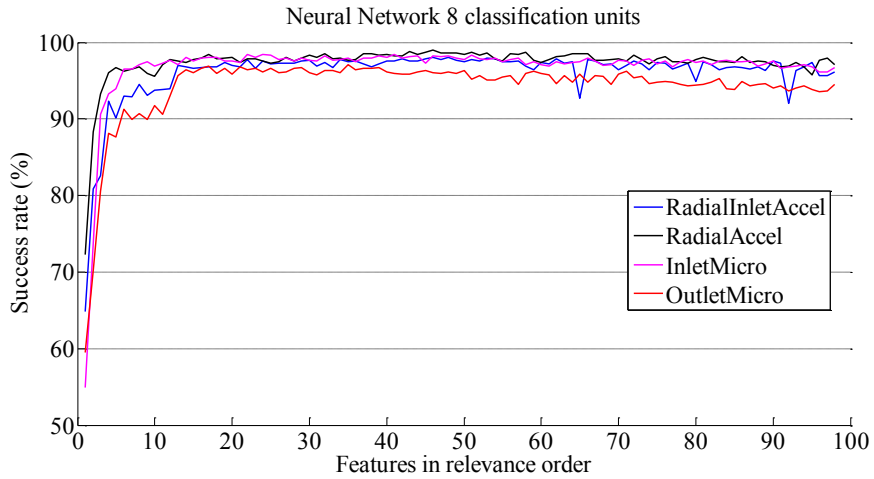

Figure 5-14: Sequential evaluation of the features for each sensor in pump fault diagnosis using a neural network classifier to discriminate between 8 pump conditions.

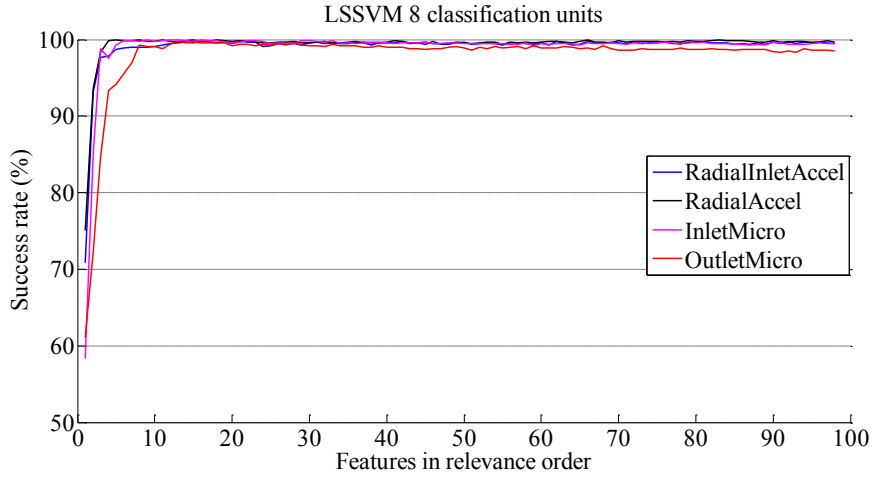

Figure 5-15: Sequential evaluation of the features for each sensor in pump fault diagnosis using a LSSVM classifier to discriminate between 8 pump conditions.

5.5.2 Case study: 17 classification units

In Figure 5-16 the incremental evaluation of the features for a neural network classifier and for each sensor is shown. In In Figure 5-17, the evaluation using a LSSVM classifier is shown. The LSSVM classifier has better success rates than the neural network classifier.

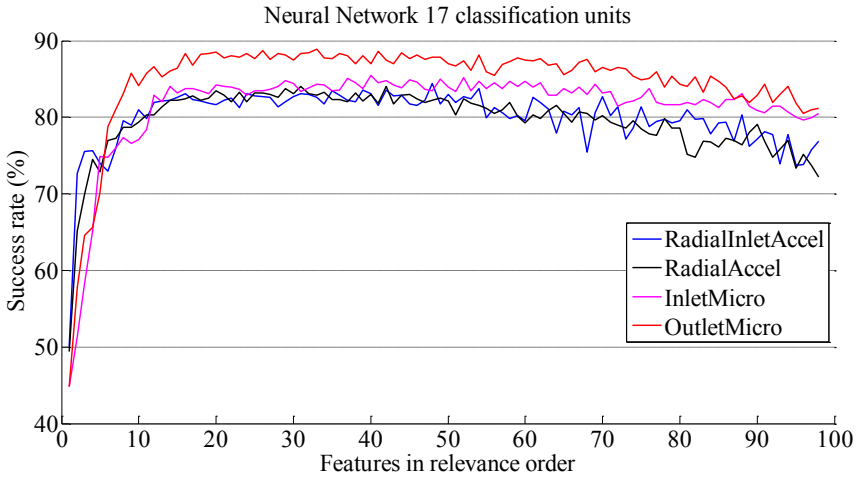

Figure 5-16: Sequential evaluation of the features for each sensor in pump fault diagnosis using a neural network classifier to discriminate between 17 pump conditions.

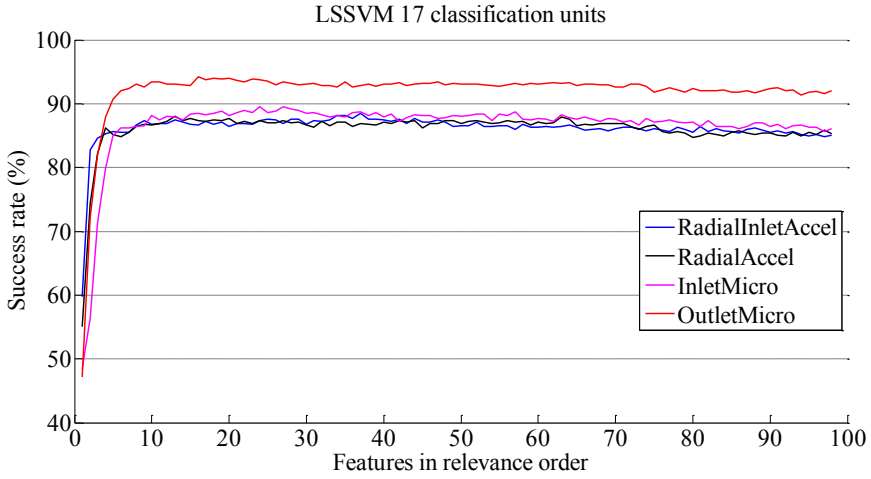

Figure 5-17: Sequential evaluation of the features for each sensor in pump fault diagnosis using a LSSVM classifier to discriminate between 8 pump conditions.

5.5.3 Selected features per sensor

As the number of features is incremented in the incremental evaluation curves, the success rate is stabilized. In some cases with 17 classification untis, the success rate slightly decreases when increasing the number of features. Moreover, the number of features to obtain a stabilized success rate differs for each sensor. Therefore, in order to select a final number of features for each sensor, we propose the following method:

1) For each sensor the maximum success rate in the classification between pump conditions is found: SR_{max}
2) 2% of SR_{max} is calculated and the number of features that first encounters with the 2% of SR_{max} is obtained.

Using this procedure a reduced number of features with high classification rates are obtained. This procedure is applied in the case of the neural network classifier because it is the worst case. Following this procedure, the number of the final selected features per sensor for 8 classification units and for 17 classification units is shown in Table 5-5 and Table 5-6 respectively. The success rate of the selected features is shown both for neural network and LS-SVM ckassifiers. For example, for Radial Inlet Accel and for 8 classification units, the first 13 features in the relevance order table (Table 5-3) are selected which give a 96.98% of success rate with the neural network classifier and a 99.59% of success rate with the LS-SVM classifier.

TABLE 5-5: SELECTED FEATURES AND CLASSIFICATION RATES PER SENSOR FOR 8 CLASSIFICATION UNITS.

Sensor	Selected Features from Table 5-3	Neural Network Success Rates	LS-SVM Success Rates
Radial Inlet Accel	13 first features	96.98%,	99.59%
Radial Accel	11 first features	97.07%	99.91%
Inlet Micro	7 first features	96.53%	99.82%
Outlet Micro	13 first features	96.98%	99.59%

TABLE 5-6: SELECTED FEATURES AND CLASSIFICATION RATES PER SENSOR FOR 17 CLASSIFICATION UNITS.

Sensor	Selected Features from Table 5-4	Neural Network Success Rates	LS-SVM Success Rates
Radial Inlet Accel	16 first features	83.11%	86.71%
Radial Accel	16 first features	82.39%	87.30%
Inlet Micro	14 first features	84.01%	87.48%
Outlet Micro	16 first features	88.29%	94.23%

5.6 Discussion and Conclusions

According to the incremental evaluation of the features, the success rate reaches values near 100% in discriminating between 8 pump conditions and between 85% and 90% in discriminating between 17 pump conditions with the exception of the Outlet Micro sensor with a classification rate near 95% in discriminating between 17 pump conditions. This shows that Outlet Micro sensor is more robust when the number of classification units increases.

From the incremental evaluation curves it is obvious that LSSVM classifier has better success rates than the neural network classifier. In the case of 8 classification units LSSVM increase the classification rates between 0.5% and 2% respect to the neural networkd classifier. In the case of 17 classification units the increment is between 4% and 6% in the success rates. This shows the superiority of the LSSVM classifier.

Provided that the number of features to obtain a stabilized success rate differs for each sensor, we proposed a method to select a final number of features for each sensor (see Table 5-5 and Table 5-6). The success rates of the selected features are high for all the sensors considered, both vibration and audio signals. Therefore, the audio signal has proven to be a good option in pump fault diagnosis for impeller-related fault, seal fault and system faults. A study of the fusion of audio and vibration signals with the selected features per sensor is carried out in Chapter 6.

Regarding the selected features per sensor the following observations can be made. In general, the selected features for all sensors are energies at pump characteristic

frequencies (in frequency and cepstral domains), the distribution of energy in spectrum and in the wavelet packet tree, statistical features in time domain (especially skewness and kurtosis) and periodicity in time domain (zero-crossing ratios). Some features related to harmonic to noise ratio and related to noise energy are also selected. Complexity features such as Lempel-Ziv complexity and Hurst exponent are also selected.

It is obvious that as more classification units we have, more information is needed. For this reason, in discriminating between 17 pump conditions, the number of final selected features increases. In general, in discriminating between 17 pump conditions, more features related to energies at pump charactacteristic frequencies are selected.

As a conclusion, most of the selected features are related to energy changes in spectrum. This seems reasonable since the hydraulic faults considered in this Thesis change the flow inside the pump therefore changing the energy at pump characteristic frequencies as well as the energy distribution in spectrum and generating turbulence noise.

5.7 Contributions

The contributions of this Chapter are:

1. The application of state-of-the-art features extracted from vibration signals in pump fault diagnosis to audio signals. Part of this contribution is in two conference papers [1], [2].

2. The proposal of 31 new features in pump fault diagnosis extracted from both vibration and audio signals. The new features are extracted in frequency domain, cepstrum domain, time-frequency domain and nonlinear domain. Part of this contribution is in two conference papers [1], [2].

3. The study of feature selection for audio and vibration signals.

5.1 References

[1] Henríquez, P.; Alonso, J. B.; Ferrer, M. A.; Travieso, C. M.; Gómez, G. (2012). Fault diagnosis using audio and vibration signals in a circulating pump. *Journal of Physics: Conference Series 25th Int.Congress on Condition Monitoring and Diagnostic Engineering*, 2012, 364, 012135.

[2] Henríquez, P.; Alonso, J. B.; Ferrer, M. A.; Travieso, C. M. (2014). Application of complexity measures to pump fault diagnosis. *27th Int. Congress on Condition Monitoring and Diagnostic Engineering*.

[3] Kawabe, Y. Maegawa, K., Toyota, T., Chen, P. (1997 October 28-31). Diagnosis method of centrifugal pumps by rough sets and partially-linearized neural networks. In *IEEE International Conference on Intelligent Processing Systems* (pp. 1490-1494), Beijing, China.

[4] Sakthivel, N. R., Sugumaran, V., & Nair, B. B. (2010). Comparison of decision tree-fuzzy and rough set-fuzzy methods for fault categorization of mono-block centrifugal pump. *Mechanical Syst. and Signal Process.*, *24*, 1887-1906.

[5] Sakthivel, N. R., Sugumaranb, V., & Babudevasenapatia, S. (2010). Vibration based fault diagnosis of monoblock centrifugal pump using decision tree. *Expert Systems with Applications, 37*, 4040–49.

[6] Sakthivel, N. R., Nairc, B. B., Sugumaran, V. (2012). Soft computing approach to fault diagnosis of centrifugal pump. *Applied Soft Computing*, *12*,1574-1581.

[7] Farokhzad, S, Ahmadi, H., Jaefari, A., AsadiAsad Abad, M. R., & Ranjbar Kohan, M. (2013). Vibration based fault detection of centrifugal pump by fast Fourier transform and adaptive neuro-fuzzy inference system. *Journal of Mechanical Engineering and Technology*. DOI: 10.18005/JMET0103001.

[8] Al-Hashmi, S.A. (2013, October). Statistical analysis of acoustic signal for cavitation detection. *International Journal of Emerging Technology and Advanced Engineering*, *3*(4).

[9] D. Casada, "Detection of pump degradation," 22nd Water Reactor Safety Information Meeting, Bethesda, Maryland, October 24-26, 1994.

[10] Parrondo, J., Velarde, S., C. Santolaria. (1998). Development of a predictive maintenance system for a centrifugal pump. *Journal of Quality in Maintenance Engineering*, *4*(3), 198-211.

[11] Parrondo, J. L., Velarde, S., Pistono, J., & Ballesteros, R. (1999). Diagnosis based on condition monitoring of fluid-dynamic abnormal performance of centrifugal pumps. In *Proceedings of the International Seminar on Modal Analysis* (Vol. 3, pp. 1365-1372). Katholieke Universitetit Leuven.

[12] Higham, E., Perovic, S. (2001). Predictive maintenance of pumps based on signal analysis of pressure and differential pressure (flow) measurements. *Trans. of the Institute of Measurement and Control*, *23*(4), 226-248.

[13] Wang, K., Lei, B. (2001). Using B-spline neural network to extract fuzzy rules for a centrifugal pump monitoring. *Journal of Intelligent Manufacturing*, *12*, 5-11.

[14] Yuan, S., Chu, F. (2006). Support vector machines-based fault diagnosis for turbo-pump rotor. *Mechanical Systems and Signal Processing*, *20*, 939–952.

[15] Zhao, X. M., Hu, Q. H., Lei, Y. G., Zuo, M. J. (2010). Vibration-based fault diagnosis of slurry pump impellers using neighbourhood rough set models. In *Proc. of the Institution of Mechanical Engineers, Part C: Journal of Mechanical Engineering Science*, *224*, 995-1006.

[16] Zhao, X., Zuo, M. J., & Patel, T. H. (2012). Generating an indicator for pump impeller damage using half and full spectra, fuzzy preference-based rough sets and PCA. *Meas. Sci. Technol. 23*(4), 045607.

[17] Farokhzad, S. (2013). Vibration based fault detection of centrifugal pump by fast fourier transform and adaptive neuro-fuzzy inference system. *Journal of Mechanical Engineering and Technology 1*(3), 82-87.

[18] Devi, S., Siva, L., Shanker N. R., & Prabakaran, K. (2010). A Comparative Study between Vibration and Acoustic Signals in HTC Cooling Pump and Chilling Pump. *Int. J. of Eng. and Technol., 2*.

[19] Al Thobiani, A., Gu, F., & Ball, A. (2010 June 22-24). The monitoring of cavitation in centrifugal pumps based on the analysis of vibro-acoustic measurements. In *CM 2010 and MFPT 2010*, UK.

[20] Pan, Y. N., Chen, J., Li, X. L. (2009). Spectral entropy: a complementary index for rolling element bearing performance degradation assessment. In *Proc. of the Institution of Mechanical Engineers, Part C: Journal of Mechanical Engineering Science*, 223, 1223-1231.

[21] Al-Hashmi, S.A. (2012, September 23-26). Spectrum Analysis of Acoustic Signals for Cavitation Detection. In 2*012 IEEE Symposium on Industrial Electronics and Applications (ISIEA2012)*, Bandung, Indonesia.

[22] Saeid Farokhzad, H.A., (2013). Acoustic Based Cavitation Detection of Centrifugal Pump by Neural Network. *Journal of Mechanical Engineering and Technology*, *1*(1), 1-5.

[23] Mollazade, K., Ahmadi, H., Omid, M., & Alimardani, R. (2009). Vibration-based fault diagnosis of hydraulic pump of tractor steering system by using energy Technique. *Modern Applied Science*, 3, 59–66.

[24] Cudina, M. (2003). Detection of cavitation phenomenon in a centrifugal pump using audible sound. *Mechanical Systems and Signal Processing 17*(6), 1335–1347.

[25] Boyanov, B; Hadjitodorov, S. (1997). Acoustic analysis of pathological voices. A voice analysis system for the screening of laryngeal diseases. *IEEE Engineering in Medicine and Biology Magazine*, *16*(4), 74-82.

[26] Feijoo, S., et al. (1989). Acoustic evaluation of glottal cancer based on short-term stability measures. *Proceedings of the Annual International Conference of the IEEE Engineering in Medicine and Biology Society 2*, 675-676.

[27] Yegnanarayana, B., d'Alessandro, C., Darsinos, V. (1988). An Iterative Algorithm for Decomposition of Speech Signals into Periodic and Aperiodic Components. *IEEE transaction on Speech and Audio Processing*, *6*(1), 1-10.

[28] Muralidharan, V., Sugumaran, V. (2013). Feature extraction using wavelets and classification through decision tree algorithm for fault diagnosis of mono-block centrifugal pump. *Measurement*, *46*, 353–359.

[29] Muralidharan, V., Sugumaran, V. (2013). Selection of discrete wavelets for fault diagnosis of monoblock centrifugal pumps using the J48 algorihtm. *Applied Artificial Intelligence: An International Journal*, *27*(1), 1-19.

[30] Gao, Y., Zhang, Q. (2006). A wavelet packet and residual analysis based method for hydraulic pump health diagnosis. In *Proc. of IMechE, Part D: Journal of Automobile Engineering*, *220*(6) 735-745.

[31] Wang, H., Chen, P. (2009). Intelligent diagnosis method for a centrifugal pump using features of vibration signals. *Neural Computing and Applications 18,* 397–405.

[32] Wang, H., Chen, P. (2007). Fault diagnosis of centrifugal pump using symptom parameters in frequency domain. *Agricultural Engineering International: The CIGR*

Ejournal. *9*, Manuscript IT 07 005.

[33] Koo, I. S., Kim, W.W. (2000). The development of reactor coolant pump vibration monitoring and a diagnostic system in the nuclear power plant. *ISA Transactions, 39*, 309-316.

[34] Dong, Z., Xueqin, T., Zeng, J. (2013). Mechanical Fault Diagnosis Based on LMD Approximate Entropy and LSSVM. *TELKOMNIKA*, *11*(2), 803-808.

[35] Yunlong, Z., Peng, Z. (2012). Vibration Fault Diagnosis Method of Centrifugal Pump Based on EMD Complexity Feature and Least Square Support Vector Machine. *Energy Procedia 17*, 939 – 945.

[36] Takens, F. "Detecting strange attractors in turbulence," *Lecture notes in math*, vol. 898, pp. 366–81, 1981.

[37] Fraser, A.M., Swinney, H.L. (1986). Independent coordinates for strange attractors from mutual information. *Phys. Rev. A 33* 1134–1140.

[38] Kennel, M. B., Brown, R., Abarbanel, H.D.I. (1992). Determining embedding dimension for phase-space reconstruction using a geometrical construction. *Phys. Rev. A 45*, 3403–3411.

[39] Kantz, H., Schreiber, T. "Nonlinear Time Series Analysis," fourth ed., Cambridge University Press, Cambridge , 1997.

[40] Theiler, J. (1988). Lacunarity in a best estimator of fractal dimension. *Phys. Lett. A 133*, 195-200.

[41] Kaspar, F., Shuster, H.G. (1987). Easily calculable measure for complexity of spatiotemporal patterns. *Phys. Rev. A 36*, 842-848.

[42] Lempel, A., Ziv, J. (1976). On the complexity of finite sequences. *IEEE Trans. Inf. Theory 22*, 75–81.

[43] Hurst, H. E., Black, R.P., Simaika, Y.M. Long-Term Storage: an experimental study. London, 1965.

[44] Higuchi, T. (1988). Approach to an irregular time series on basis of the fractal theory. *Physica D 31*, 277-283.

[45] Pudil, P., Novovicová, J., & Kittler, J. (1994). Floating search methods in feature selection. *Pattern Recognit Lett., 15*, 1119–1125.

[46] Dyson, G. (2005). Impeller rerate to reduce hydraulically generated vibration. In *Proceedings of the 22nd International Pump Users Symposium* (pp. 10-15).

[47] Albraik, A., Althobiani, F., Gu, F., & Ball, A. (2012). Diagnosis of Centrifugal Pump Faults Using Vibration Methods. In *25th International Congress on Condition Monitoring and Diagnostic Engineering, Journal of Physics: Conference Series* 364.

[48] Al Thobiani, Faisal (2011) The Non-intrusive Detection of Incipient Cavitation in Centrifugal Pumps. Doctoral thesis, University of Huddersfield.

[49] Choi, Y. C., & Kim, Y. H. (2007). Fault detection in a ball bearing system using minimum variance cepstrum. *Measurement Science and Technology*, *18*(5), 1433

CHAPTER 6
Results of Audio and Vibration fusion in pump monitoring

This Chapter is devoted to fusion of audio and vibration signals acquired from the centrifugal pump to diagnose different kinds of faults. Our aim is to analise how the fusion of audio and vibration signals affects the results in classification. In the first part of this Chapter, the methodology carried out is explained. Then the results of the fusion are shown.

6.1 Methodology for audio and vibration fusion in pump fault diagnosis

In literature, there are several methods for data fusion. In this Thesis, we apply some conventional methods in order to fusion audio and vibration information at different levels: feature level, score level and abstract level (also called decision level) [1]. Combinations of 2, 3 and 4 sensors are evaluated for the fusion at each level using neural network and LS-SVM classifiers.

The fusion at feature level comprises the concatenation of features extracted from different sensors. The selected features obtained for each sensor (see Table 5-5 and Table 5-6 of Chapter 5) are concatenated and evaluated with two different classifiers: neural network classifier and LSSVM classifier. As in the case of individual sensor evaluation, the evaluation is repeated 20 times with different training and test sets and the results are averaged. In subsection 6.2, the results of the feature fusion for each case study (8 classification units and 17 classification units) are shown in Table 6-1, Table 6-3, Table 6-2 and Table 6-4.

The fusion at score level is carried out using simplifications of the Bayes rule [1]. The scores of the classifiers are fused using the sum rule, the product rule, the minimum rule and the maximum rule. The scores of a classifier are the outputs of a classifier before a class label is assigned, i.e. before a decision is made. The sum rule consists in averaging the scores of two or more classifiers. In the product rule, the scores are multiplied. The minimum and the maximum scores are selected in the minimum and maximum rules respectively.

In the fusion at score level, the selected features for each sensor are evaluated individually with a neural network classifier. Then the scores of each evaluation are fusioned with the forementioned rules using different sensor combinations. This procedure is repeated for each case study (8 classification units and 17 classification units). The whole process is also carried out using the LS-SVM classifier. In Table 6-5, Table 6-6, Table 6-7, Table 6-8, the results for each case study (8 classification units and 17 classification untis) and for each classifier (neural network classifier and LSSVM classifier) are shown.

In the fusion at decision level, the majority vote rule is applied. The majority vote rule is a function of the votes received for each class from each single classifier. The class with the largest number of votes is the winner class. In the fusion at decision level, the features selected for each sensor are evaluated with a classifier. Therefore, a class is assigned for each sensor by the classifier. Then the class with the largest number of votes is selected. This process is carried out for each case study (8 classification units and 17 classification units) and for each classifier. When there is a tie in the votes, the class with the highest score at score level is selected. In Table 6-9, Table 6-10, Table

6-11 and Table 6-12, the results of the fusion at decition level for each case study and for each classifier are shown.

The tables with the results of the fusion at each level are shown in subsections 6.2, 6.3, and 6.4 for feature fusion, score fusion and decision fusion respectively. For each sensor combination, the average and standard deviation of the classification success rates are shown. In all tables the results for each individual sensor are shown for making comparison easier.

For simplicity, the sensors are renamed as follows: Radial Inlet Accel is RI, Radial Accel is RA, Inlet Micro is IN, Outlet Micro is OU. For example, the combination of Radial Inlet Accel and Inlet Micro is shown as RIIN.

6.2 Results of fusion at feature level

TABLE 6-1: FEATURE FUSION USING NEURAL NETWORK CLASSIFIER AND 8 CLASSIFICATION UNITS

Combination of 2 sensors													
RI	RA	IN	OU	RIRI	RARA	ININ	OUOU	RIRA	RIIN	RIOU	RAIN	RAOU	INOU
96.98 (1.78)	97.07 (2.32)	96.53 (1.50)	95.68 (2.16)	96.76 (3.09)	95.45 (3.35)	97.16 (1.41)	96.08 (2.01)	97.88 (1.06)	97.75 (1.48)	98.11 (0.87)	97.93 (0.97)	98.20 (1.55)	98.38 (1.19)

Combination of 3 sensors											
RI	RA	IN	OU	RIRIRI	RARARA	INININ	OUOUOU	RIRAIN	RIRAOU	INOURI	INOURA
96.98 (1.78)	97.07 (2.32)	96.53 (1.50)	95.68 (2.16)	97.12 (1.04)	96.22 (2.08)	96.26 (2.07)	96.35 (1.5)	98.69 (0.80)	98.47 (2.23)	98.20 (1.60)	98.38 (1.48)

Combination of 4 sensors								
RI	RA	IN	OU	RIRIRIRI	RARARARA	ININININ	OUOUOUOU	RIRAINOU
96.98 (1.78)	97.07 (2.32)	96.53 (1.50)	95.68 (2.16)	97.03 (1.85)	95.90 (1.69)	96.26 (2.07)	95.86 (2.38)	98.15 (1.11)

TABLE 6-2: FEATURE FUSION USING NEURAL NETWORK CLASSIFIER AND 17 CLASSIFICATION UNITS

Combination of 2 sensors													
RI	RA	IN	OU	RIRI	RARA	ININ	OUOU	RIRA	RIIN	RIOU	RAIN	RAOU	INOU
83.11 (2.88)	82.39 (3.71)	84.01 (3.24)	88.29 (4.61)	95.72 (3.21)	95.14 (2.03)	96.67 (2.01)	95.72 (1.49)	95.99 (2.52)	96.89 (2.04)	96.58 (2.28)	97.34 (1.53)	96.17 (1.7)	96.94 (2.31)

Combination of 3 sensors											
RI	RA	IN	OU	RIRIRI	RARARA	INININ	OUOUOU	RIRAIN	RIRAOU	INOURI	INOURA
83.11 (2.88)	82.39 (3.71)	84.01 (3.24)	88.29 (4.61)	96.08 (2.34)	94.14 (2.8)	97.34 (1.45)	96.40 (1.83)	97.16 (1.69))	96.04 (3.41)	97.12 (1.51)	94.14 (1.81)

Combination of 4 sensors								
RI	RA	IN	OU	RIRIRIRI	RARARARA	ININININ	OUOUOUOU	RIRAINOU
83.11 (2.88)	82.39 (3.71)	84.01 (3.24)	88.29 (4.61)	94.86 (3.14)	93.60 (3.87)	96.98 (1.69)	94.19 (3.13)	97.48 (2.10)

TABLE 6-3: FEATURE FUSION USING LSSVM CLASSIFIER AND 8 CLASSIFICATION UNITS

Combination of 2 sensors													
RI	RA	IN	OU	RIRI	RARA	ININ	OUOU	RIRA	RIIN	RIOU	RAIN	RAOU	INOU
99.59 (0.74)	99.91 (0.28)	99.82 (0.37)	99.73 (0.51)	99.59 (0.9)	98.96 (1.1)	99.73 (0.51)	99.50 (0.68)	99.59 (0.68)	99.59 (0.62)	99.82 (0.47)	99.41 (0.73)	99.68 (0.6)	99.77 (0.4)

Combination of 3 sensors											
RI	RA	IN	OU	RIRIRI	RARARA	ININ IN	OUOUOU	RIRAIN	RIRAOU	INOURI	INOURA
99.59 (0.74)	99.91 (0.28)	99.82 (0.37)	99.73 (0.51)	99.55 (0.69)	98.87 (1.09)	99.86 (0.33)	99.10 (0.65)	99.73 (0.51)	99.82 (0.37)	99.86 (0.44)	99.59 (0.62)

Combination of 4 sensors								
RI	RA	IN	OU	RIRIRIRI	RARARARA	ININININ	OUOUOUOU	RIRAINOU
99.59 (0.74)	99.91 (0.28)	99.82 (0.37)	99.73 (0.51)	99.73 (0.59)	99.14 (0.74)	99.77 (0.5)	99.41 (0.67)	99.59 (0.8)

TABLE 6-4: FEATURE FUSION USING LSSVM CLASSIFIER AND 17 CLASSIFICATION UNITS

Combination of 2 sensors													
RI	RA	IN	OU	RIRI	RARA	ININ	OUOU	RIRA	RIIN	RIOU	RAIN	RAOU	INOU
86.71 (1.57)	87.30 (1.62)	87.48 (2.09)	94.23 (1.32)	99.19 (0.92)	99.10 (1.01)	99.28 (0.86)	99.28 (0.55)	99.37 (1.17)	99.23 (0.89)	99.32 (0.77)	98.87 (0.82)	99.55 (0.75)	99.55 (0.55)

Combination of 3 sensors											
RI	RA	IN	OU	RIRIRI	RARARA	ININ IN	OUOUOU	RIRAIN	RIRAOU	INOURI	INOURA
86.71 (1.57)	87.30 (1.62)	87.48 (2.09)	94.23 (1.32)	99.41 (0.89)	98.83 (1.28)	99.41 (0.79)	99.32 (0.77)	99.46 (0.74)	99.23 (0.79)	99.64 (0.68)	99.73 (0.51)

Combination of 4 sensors								
RI	RA	IN	OU	RIRIRIRI	RARARARA	ININININ	OUOUOUOU	RIRAINOU
86.71 (1.57)	87.30 (1.62)	87.48 (2.09)	94.23 (1.32)	99.59 (0.85)	99.19 (1.24)	99.46 (0.90)	99.19 (0.77)	99.77 (0.58)

6.3 Results of Fusion at score level

TABLE 6-5: RESULTS OF SCORE FUSION IN NEURAL NETWORK CLASSIFIER USING 8 CLASSIFICATION UNITS

Combination of 2 sensors														
RI	RA	IN	OU		RIRI	RARA	ININ	OUOU	RIRA	RIIN	RIOU	RAIN	RAOU	INOU
96.98 (1.78)	97.07 (2.32)	96.53 (1.50)	95.68 (2.16)	Sum	96.98 (1.78)	97.07 (2.32)	96.53 (1.50)	95.68 (2.16)	98.51 (1.71)	98.69 (1.15)	98.78 (1.06)	99.01 (0.77)	98.83 (1.06)	98.11 (0.92)
				Product	96.98 (1.76)	96.89 (2.27)	96.40 (1.7)	95.50 (2.43)	98.51 (1.76)	98.74 (0.97)	98.60 (0.99)	98.92 (0.95)	98.96 (0.73)	98.11 (1.24)
				Min	96.98 (1.78)	97.07 (2.32)	96.53 (1.5)	95.68 (2.16)	98.38 (1.69)	98.33 (1.02)	98.24 (1.26)	98.47 (1.37)	98.42 (0.82)	97.84 (1.18)
				Max	96.98 (1.78)	97.07 (2.32)	96.53 (1.5)	95.68 (2.16)	98.06 (1.83)	97.88 (1.06)	98.02 (1.29)	98.24 (1.07)	98.06 (1.32)	97.79 (1.29)

Combination of 3 sensors												
RI	RA	IN	OU		RIRIRI	RARARA	INININ	OUOUOU	RIRAIN	RIRAOU	INOURI	INOURA
96.98 (1.78)	97.07 (2.32)	96.53 (1.50)	95.68 (2.16)	Sum	96.98 (1.78)	97.07 (2.32)	96.53 (1.50)	95.68 (2.16)	99.28 (0.69)	99.23 (0.79)	99.01 (0.58)	99.19 (0.87)
				Product	96.98 (1.78)	97.07 (2.32)	96.53 (1.50)	95.68 (2.16)	99.01 (1.17)	99.05 (0.95)	98.69 (0.90)	99.01 (0.71)
				Min	96.98 (1.78)	97.07 (2.32)	96.53 (1.50)	95.68 (2.16)	98.96 (1.14)	98.87 (0.96)	98.51 (1.18)	98.87 (0.77)
				Max	96.98 (1.78)	97.07 (2.32)	96.53 (1.50)	95.68 (2.16)	98.20 (1.17)	98.38 (1.29)	98.06 (0.98)	98.15 (1.07)

Combination of 4 sensors									
RI	RA	IN	OU		RIRIRIRI	RARARARA	ININININ	OUOUOUOU	RIRAINOU
96.98 (1.78)	97.07 (2.32)	96.53 (1.50)	95.68 (2.16)	Sum	96.98 (1.78)	97.07 (2.32)	96.53 (1.5)	95.68 (2.16)	99.37 (0.78)
				Product	96.98 (1.76)	96.89 (2.27)	96.40 (1.7)	95.50 (2.43)	98.92 (1.04)
				Min	96.98 (1.78)	97.07 (2.32)	96.53 (1.5)	95.68 (2.16)	99.05 (0.90)
				Max	96.98 (1.78)	97.07 (2.32)	96.53 (1.5)	95.68 (2.16)	98.24 (1.15)

TABLE 6-6: RESULTS OF SCORE FUSION IN NEURAL NETWORK CLASSIFIER USING 17 CLASSIFICATION UNITS

Combination of 2 sensors														
RI	RA	IN	OU		RIRI	RARA	ININ	OUOU	RIRA	RIIN	RIOU	RAIN	RAOU	INOU
83.11 (2.88)	82.39 (3.71)	84.01 (3.24)	88.29 (4.61)	Sum	83.11 (2.88)	82.39 (3.71)	84.01 (3.24)	88.29 (4.61)	85.95 (2.08)	86.40 (2.22)	90.59 (2.56)	86.67 (2.86)	91.17 (2.57)	91.53 (2.84)
				Product	82.30 (2.98)	81.58 (3.64)	83.51 (3.19)	87.84 (4.59)	85.95 (2.14)	86.89 (2.20)	90.99 (2.34)	87.07 (2.96)	91.04 (1.86)	91.58 (2.27)
				Min	83.11 (2.88)	82.39 (3.71)	84.01 (3.24)	88.29 (4.61)	84.95 (3.22)	86.44 (2.27)	91.08 (2.41)	86.31 (2.33)	89.91 (2.12)	90.86 (2.45)
				Max	83.11 (2.88)	82.39 (3.71)	84.01 (3.24)	88.29 (4.61)	83.83 (3.46)	84.68 (2.83)	87.70 (4.11)	85.23 (3.90)	88.33 (3.81)	88.78 (4.30)

Combination of 3 sensors												
RI	RA	IN	OU		RIRIRI	RARARA	INININ	OUOUOU	RIRAIN	RIRAOU	INOURI	INOURA
83.11 (2.88)	82.39 (3.71)	84.01 (3.24)	88.29 (4.61)	Sum	83.11 (2.88)	82.39 (3.71)	84.01 (3.24)	88.29 (4.61)	87.21 (1.79)	92.39 (2.12)	92.39 (2.57)	91.89 (2.28)
				Product	83.11 (2.88)	82.39 (3.71)	84.01 (3.24)	88.29 (4.61)	86.71 (2.26)	92.07 (2.33)	92.21 (1.97)	91.40 (1.72)
				Min	83.11 (2.88)	82.39 (3.71)	84.01 (3.24)	88.29 (4.61)	87.03 (2.35)	91.58 (1.92)	91.40 (1.93)	91.04 (2.12)
				Max	83.11 (2.88)	82.39 (3.71)	84.01 (3.24)	88.29 (4.61)	84.32 (3.96)	86.94 (3.88)	87.84 (4.60)	88.20 (4.20)

Combination of 4 sensors									
RI	RA	IN	OU		RIRIRIRI	RARARARA	ININININ	OUOUOUOU	RIRAINOU
83.11 (2.88)	82.39 (3.71)	84.01 (3.24)	88.29 (4.61)	Sum	83.11 (2.88)	82.39 (3.71)	84.01 (3.24)	88.29 (4.61)	92.16 (2.03)
				Product	82.30 (2.98)	81.58 (3.64)	83.51 (3.19)	87.84 (4.59)	91.71 (1.97)
				Min	83.11 (2.88)	82.39 (3.71)	84.01 (3.24)	88.29 (4.61)	91.17 (2.24)
				Max	83.11 (2.88)	82.39 (3.71)	84.01 (3.24)	88.29 (4.61)	86.94 (4.61)

TABLE 6-7: RESULTS OF SCORE FUSION IN LSSVM CLASSIFIER USING 8 CLASSIFICATION UNITS

Combination of 2 sensors														
RI	RA	IN	OU		RIRI	RARA	ININ	OUOU	RIRA	RIIN	RIOU	RAIN	RAOU	INOU
99.59 (0.74)	99.91 (0.28)	99.82 (0.37)	99.73 (0.51)	Sum	99.59 (0.74)	99.91 (0.28)	99.82 (0.37)	99.73 (0.51)	**100 (0)**	**100 (0)**	**100 (0)**	**100 (0)**	**100 (0)**	99.95 (0.20)
				Product	14.50 (4.84)	15.05 (3.89)	10.45 (4.29)	14.68 (4.69)	8.69 (3.35)	7.21 (3.38)	7.21 (3.01)	9.19 (3.82)	10.50 (2.67)	7.07 (3.11)
				Min	99.59 (0.74)	99.91 (0.28)	99.82 (0.37)	99.73 (0.51)	99.95 (0.2)	99.95 (0.2)	99.91 (0.28)	100 (0)	99.91 (0.28)	99.91 (0.28)
				Max	99.59 (0.74)	99.91 (0.28)	99.82 (0.37)	99.73 (0.51)	99.95 (0.2)	99.95 (0.2)	99.95 (0.20)	**100 (0)**	**100 (0)**	99.95 (0.20)

Combination of 3 sensors												
RI	RA	IN	OU		RIRIRI	RARARA	INININ	OUOUOU	RIRAIN	RIRAOU	INOURI	INOURA
99.59 (0.74)	99.91 (0.28)	99.82 (0.37)	99.73 (0.51)	Sum	99.59 (0.74)	99.91 (0.28)	99.82 (0.37)	99.73 (0.51)	**100 (0)**	**100 (0)**	**100 (0)**	**100 (0)**
				Product	99.59 (0.74)	99.91 (0.28)	99.82 (0.37)	99.73 (0.51)	99.28 (1.00)	99.23 (0.79)	99.23 (0.67)	99.55 (0.55)
				Min	99.59 (0.74)	99.91 (0.28)	99.82 (0.37)	99.73 (0.51)	99.95 (0.20)	99.95 (0.20)	99.91 (0.28)	**100 (0)**
				Max	99.59 (0.74)	99.91 (0.28)	99.82 (0.37)	99.73 (0.51)	99.95 (0.20)	99.95 (0.20)	99.95 (0.20)	**100 (0)**

Combination of 4 sensors								
RI	RA	IN	OU		RIRIRIRI	RARARARA	ININININ	OUOUOUOU	RIRAINOU
99.59 (0.74)	99.91 (0.28)	99.82 (0.37)	99.73 (0.51)	Sum	99.59 (0.74)	99.91 (0.28)	99.82 (0.37)	99.73 (0.51)	**100 (0)**
				Product	14.50 (4.84)	15.05 (3.89)	10.45 (4.29)	14.68 (4.69)	4.32 (1.91)
				Min	99.59 (0.74)	99.91 (0.28)	99.82 (0.37)	99.73 (0.51)	99.95 (0.20)
				Max	99.59 (0.74)	99.91 (0.28)	99.82 (0.37)	99.73 (0.51)	99.95 (0.20)

TABLE 6-8: RESULTS OF SCORE FUSION IN LSSVM CLASSIFIER USING 17 CLASSIFICATION UNITS

Combination of 2 sensors														
RI	RA	IN	OU		RIRI	RARA	ININ	OUOU	RIRA	RIIN	RIOU	RAIN	RAOU	INOU
86.71 (1.57)	87.30 (1.62)	87.48 (2.09)	94.23 (1.32)	Sum	86.71 (1.57)	87.30 (1.62)	87.48 (2.09)	94.23 (1.32)	87.39 (1.60)	87.88 (2.01)	93.65 (1.81)	88.29 (2.19)	93.92 (1.34)	94.32 (1.52)
				Product	7.97 (3.30)	8.42 (3.47)	6.98 (3.34)	10.90 (3.88)	3.74 (2.75)	3.02 (1.85)	3.51 (1.87)	3.56 (2.59)	4.95 (2.45)	4.19 (2.62)
				Min	86.71 (1.57)	87.30 (1.62)	87.48 (2.09)	94.23 (1.32)	87.34 (1.42)	88.02 (1.46)	93.29 (1.77)	88.29 (2.19)	93.11 (1.44)	93.69 (2.11)
				Max	86.71 (1.57)	87.30 (1.62)	87.48 (2.09)	94.23 (1.32)	87.52 (1.78)	87.84 (1.95)	93.02 (2.20)	88.24 (2.18)	93.74 (1.88)	93.56 (1.76)

Combination of 3 sensors												
RI	RA	IN	OU		RIRIRI	RARARA	INININ	OUOUOU	RIRAIN	RIRAOU	INOURI	INOURA
86.71 (1.57)	87.30 (1.62)	87.48 (2.09)	94.23 (1.32)	Sum	86.71 (1.57)	87.30 (1.62)	87.48 (2.09)	94.23 (1.32)	88.20 (2.04)	92.39 (2.20)	92.84 (2.16)	92.57 (2.34)
				Product	86.71 (1.57)	87.30 (1.62)	87.48 (2.09)	94.23 (1.32)	88.42 (2.29)	90.59 (2.64)	90.18 (2.10)	90.23 (2.78)
				Min	86.71 (1.57)	87.30 (1.62)	87.48 (2.09)	94.23 (1.32)	88.15 (2.19)	92.57 (1.70)	92.97 (2.08)	92.75 (1.86)
				Max	86.71 (1.57)	87.30 (1.62)	87.48 (2.09)	94.23 (1.32)	88.20 (1.80)	92.43 (1.99)	92.25 (1.71)	92.97 (2.35)

Combination of 4 sensors									
RI	RA	IN	OU		RIRIRIRI	RARARARA	ININININ	OUOUOUOU	RIRAINOU
86.71 (1.57)	87.30 (1.62)	87.48 (2.09)	94.23 (1.32)	Sum	86.71 (1.57)	87.30 (1.62)	87.48 (2.09)	94.23 (1.32)	91.89 (2.56)
				Product	7.97 (3.30)	8.42 (3.47)	6.98 (3.34)	10.90 (3.88)	1.08 (1.33)
				Min	86.71 (1.57)	87.30 (1.62)	87.48 (2.09)	94.23 (1.32)	92.39 (2.04)
				Max	86.71 (1.57)	87.30 (1.62)	87.48 (2.09)	94.23 (1.32)	91.98 (1.80)

6.4 Results of Fusion at abstract level

TABLE 6-9: ABSTRACT FUSION USING NEURAL NETWORK CLASSIFIER WITH 8 CLASSIFICATION UNITS

RI	RA	IN	OU	RIRA	RIIN	RIOU	RAIN	RAOU	INOU	RIRAIN	RIRAOU	INOURI	INOURA	RIRAINOU
96.98	97.07	96.53	95.68	97.21	96.49	96.22	96.35	96.67	95.45	98.83	98.83	98.47	98.69	98.92
(1.78)	(2.32)	(1.50)	(2.16)	(1.65)	(1.37)	(1.86)	(1.59)	(2.28)	(1.64)	(0.78)	(0.78)	(0.93)	(1.19)	(0.75)

TABLE 6-10: ABSTRACT FUSION USING NEURAL NETWORK CLASSIFIER WITH 17 CLASSIFICATION UNITS

RI	RA	IN	OU	RIRA	RIIN	RIOU	RAIN	RAOU	INOU	RIRAIN	RIRAOU	INOURI	INOURA	RIRAINOU
83.11	82.39	84.01	88.29	82.79	83.33	86.44	83.42	85.72	85.63	86.71	88.47	89.10	89.10	89.41
(2.88)	(3.71)	(3.24)	(4.61)	(3.02)	(3.60)	(4.23)	(3.19)	(3.46)	(3.68)	(3.52)	(2.69)	(2.69)	(2.94)	(2.83)

TABLE 6-11: ABSTRACT FUSION USING LSSVM CLASSIFIER WITH 8 CLASSIFICATION UNITS

RI	RA	IN	OU	RIRA	RIIN	RIOU	RAIN	RAOU	INOU	RIRAIN	RIRAOU	INOURI	INOURA	RIRAINOU
99.59	99.91	99.82	99.73	99.64	99.73	99.68	99.77	99.82	99.73	**100**	**100**	**100**	**100**	**100**
(0.74)	(0.28)	(0.37)	(0.51)	(0.74)	(0.51)	(0.53)	(0.40)	(0.37)	(0.42)	**(0)**	**(0)**	**(0)**	**(0)**	**(0)**

TABLE 6-12: ABSTRACT FUSION USING LSSVM CLASSIFIER WITH 17 CLASSIFICATION UNITS

RI	RA	IN	OU	RIRA	RIIN	RIOU	RAIN	RAOU	INOU	RIRAIN	RIRAOU	INOURI	INOURA	RIRAINOU
86.71	87.30	87.48	94.23	87.21	86.98	90.54	87.52	91.13	90.45	87.21	89.91	90.18	90.95	90
(1.57)	(1.62)	(2.09)	(1.32)	(1.93)	(2.54)	(1.50)	(2.45)	(2.01)	(1.90)	(1.84)	(1.72)	(1.87)	(2.33)	(1.85)

6.5 Discussion and Conclusions

As shown in Chapter 5 and repeated in this chapter, the classification success rates for each individual sensor, both vibration and audio sensors, are quite high in discriminating between 8 pump conditions using both neural network and LS-SVM as classifiers. The classification rates are higher than 95.5% in all individual sensors and the sensor with the highest success rate is Radial Accel vibration sensor with 99.91% using LS-SVM classifier.

The classification success rates for each individual sensor are also quite good in discriminating between 17 pump conditions. All sensors have individual classification rates higher than 82% and the sensor with the highest classification rate is Outlet Micro audio sensor with 94.23% using LS-SVM classifier.

As the individual sensors have high classification success rates in discriminating between 8 pump conditions, the sensor fusion increase slightly the classification accuracy. Sensor fusion sometimes even decrease the classification accuracy respect the individual sensor with higher classification accuracy in the fusion. The highest increment in the classification accuracy accurs at score level where there is an increment around 2% with respect to the classification accuracy of an individual sensor using neural network classifiers. In the case of using LS-SVM classifiers, success rates of 100% are reached at score level in the combination of two sensors, three sensors and all sensors. Abstract level fusion has an increment around 1% in the classification success rates with respect to individual sensors using neural network classifier and increments lower than 1% or no increment when using LS-SVM. The abstract fusion of 3 and 4 sensors reaches 100% of success rates using LS-SVM classifier. In general, fusion at feature level does not increase the success rates.

In the case of discriminating between 17 pump conditions, the fusion at feature level greatly increase the classification success rates with respect to the individual success rates. There is an increment between 9% and 13% in the success rate using neural network classifiers and an increment between 5% and 13% using LS-SVM

classifiers. This seems reasonable because the classifier obtains more information from the new features. Moreover, the fusion rule which gives better results is the sum rule. The combination at feature level of only one vibration sensor and one audio sensor gives success rates near 100% using a LS-SVM classifier. However, fusion at score and abstract levels gives slight increments in the success rates.

As a conclusion, the fusion of audio and vibration sensors increase significantly the success rates with respect to individual sensors at feature level in the case of discriminating between 17 pump conditions. In the case of discriminating between 8 pump conditions, the increment in the success rates with the fusion is not so significative. The reason is that the success rates of individual sensors are quite high. According to the results, a pump monitoring system which a success rate near 100% in discriminating between 17 pump conditions could be implemented with only two sensors: a vibration sensor and an audio sensor.

6.6 Contributions

In this Chapter we contribute with a study of vibration and audio fusion at feature level, score level and abstract level in fault pump diagnosis.

6.7 References

[1] Kuncheva, L. I. (2004). Combining pattern classifiers: methods and algorithms. John Wiley & Sons.

CHAPTER 7
Conclusions and future work

This Chapter is devoted to the conclusions and future lines of the research work carried out in this Thesis.

7.1 Conclusions

The objective of this Thesis is to improve the performance in condition monitoring system in fault diagnosis and fault identification using vibration and audio signals in two applications (bearings and pumps) with special emphasis in the feature extraction stage and in the use of audio signals as source of information. Based on the research carried out in the two application areas of this Thesis (bearings and pumps) and the results obtained we can conclude that both the use of audio signals as source of information and the use of nonlinear techniques can improve the performance in condition monitoring systems.

In bearing application, bearing vibration databases with free-fault bearings and bearings with faults are collected from repositories in Internet. Two methods based on nonlinear techniques are proposed for bearing fault diagnosis and bearing fault degradation. These methods show to have good classification success rates discriminating between different bearing faults and also showed to be good indicators of

bearing degradation. Based on the results we can conclude then that the application of nonlinear methods in bearing fault diagnosis and in bearing fault degradation can improve condition monitoring performance.

Provided that most fault diagnosis is carried out using vibration signals and less attention has been paid to audio signal as source of information in fault diagnosis, an exploratory study of the use of audio signals in fault diagnosis is carried out in this Thesis. For such a study, a database of audio and vibration signals (two vibration sensors and two audio sensors) acquired simultaneously from a centrifugal pump test rig is recorded in our laboratory. A set of state-of-the-art features is extracted from vibration signals and applied to audio signals. Moreover, a set of 31 new features extracted from frequency, cepstrum, time-frequency domains as well as complexity features and features related to nonlinear dynamics time series is proposed in vibration and audio pump fault diagnosis. After feature selection, the state-of-the-art features and the proposed features are evaluated using two classifiers for both vibration and audio signals. The results of the evaluation show that audio signals have similar success rates than vibration signals. In discriminating between 8 pump conditions, the success rates 99.82% and 99.59% for audio sensors and 99.91% and 99.59% for vibration sensors are obtained. In discriminating between 17 pump conditions, the success rates are 87.48% and 94.23% for audio sensors and 86.71% and 87.30% for vibration sensors. Based on these results, we can conclude that audio signals might be used as information source in pump fault diagnosis.

In order to analyse whether audio and vibration fusion improve the results in classification, combination of audio and vibration signals are carried out at feature level, score level and decision level. The results show a significant increment in the success rates when combining one audio sensor and one vibration sensor in discriminating between 17 pump conditions: a success rate of 99.55% is achieved. In discriminating between 8 pump conditions, the diagnosis success rate reaches 100% when combining one audio sensor and one vibration sensor. Based on the results in the fusion study, we can conclude that vibration and audio fusion improves the classification success rate.

In summary, the main results and contributions obtained from this Thesis are:

The methods based on nonlinear techniques for bearing fault diagnosis and fault identification.

The centrifugal pump audio and vibration database acquired, which will be released for research purposes in the near future.

The experimental evaluation of features extracted from audio signals in pump fault diagnosis which shows the feasibility of using audio signals as source of information in pump monitoring.

The set of features proposed for centrifugal pump fault diagnosis.

7.2 Future Work

A number of future research lines arise from the work carried out in this Thesis. We consider of special interest the following ones:

Searching for an indicator to follow the severity in bearings with ball faults. In Chapter 4 we propose a method for fault severity assessment in bearings that can assess the severity of inner-race and outer-race faults in bearings. However, the ball fault severity can not be followed monotonically by the proposed method. More research is needed in this case.

Extending the evaluation of audio signals to other kinds of pumps and machinery. The research carried out in this Thesis about using audio signals in pump fault diagnosis can be applied to other kinds of pumps in order to generalize the results. Moreover, it can be extended to other kinds of machines to study the feasibility of audio-based monitoring.

Searching for an indicator of damage in pump monitoring. In this Thesis, we have study the feasibility of using audio signals for pump fault diagnosis for impeller-related faults, seal fault and system faults. It is also important in pump monitoring to

find indicators that follow the evolution of a fault from normal condition to a fault condition with different severities. This research line will be explored in the future.

The study of audio-based monitoring in real industrial scenarios. Audio signals can be affected by unwanted sources of noise in industrial scenarios. Research efforts need to be made in order to include audio-based monitoring in industrial scenarios.

APPENDIX
Extension to Voice

Nonlinear and complexity measures used in this Thesis can also be applied in other kinds of signals different from vibration and audio signals of machines. An example of such signals is the voice signal. There are evidences of a nonlinear voice production system. For this reason, and for the fact that the background of the author of this Thesis in research is related to voice pathology detection using nonlinear features, a set of nonlinear features based on chaos theory as well as complexity measures have been extracted from voice signals for voice pathology detection (i.e.discrimination between normal and pathological voice using recorded voice signals) and emotional voice detection (i.e. discrimination between normal and different emotional states through the recorded voice signal). This Appendix of the Thesis is devoted to the motivation, description and results of the work carried out on such signals using nonlinear and complexity features. The first part of this Appendix is devoted to the work carried out in voice pathology detection and the second part is devoted to the work carried out in emotional detection through voice signal. The structure of the first part of the Appendix is based on a publication by the author of this Thesis [1] and the second part is based on the following publications by the author of this Thesis [38]-[40].

8.1 Voice pathology detection

The author of this Thesis proposed nonlinear measures based on the nonlinear dynamics theory to quantify the quality of the recorded voice [1]. The aim was to study the usefulness of six nonlinear chaotic measures in the automatic discrimination of two levels of voice quality (healthy and pathological speakers) measured from voice recordings. In order to assess the usefulness of the measures an automatic classification system based on neural networks was used. This research work was the first in voice pathology detection literature using the proposed feature together in order to discriminate between healthy and pathological speakers for screening purposes. The results obtained in the experimentation show that these characteristics provide high classification rates in the discrimination between healthy and pathological voice signals.

8.1.1 Motivation

The main methods used by the medical community to evaluate the speech production system and diagnose pathologies are either direct ones which require direct inspection of vocal folds (using laryngoscopical techniques such as fiberscope) and cause discomfort to the patient, or subjective ones in which voice quality is evaluated by a doctor's direct audition (GRBAS and RBH methods [2], [3]). These techniques require trained expert doctors. The use of voice quality measures obtained from recorded voice allows us to quantify the voice quality and to document the patient evolution using objective measures. They are noninvasive, quick and automatic techniques and can be a help to traditional techniques used in medicine.

The use of these techniques combined with classification methods provides the development of expert aided systems for the detection of speech system pathologies. In the last decades, some studies have provided objective measures of voice quality. Measures are obtained of the voice signal in time, spectral and cepstral domains. The most important measures used in existing literature are: fundamental frequency [4], [5] whose determination is important because several measures depend on its correct estimation, pitch perturbation (jitter) [6], [7], amplitude perturbation (shimmer) [6], [7] harmonic to noise ratio [8], low to high energy ratio [9], normalized noise energy [10],

glottal to noise excitation ratio (GNE) [11], dynamic time warping and Itakura–Saito distorsion measure [12]. Using a combination of these sets of measures, laryngeal pathologies detection systems using recorded voice signal have been developed obtaining different success rates in the classification between healthy and pathological voices: 93.5% [13], 85.8% [14], 76.67% [15], 96.1% [16].

Nevertheless, most measures considered in these works do not take into account nonlinearity in the speech system despite the fact that some studies show the underlying process of speech generation exhibiting nonlinear components [17]-[21]. As a result, some works consider this new approach in order to reveal discriminative measures between healthy and pathological voices. Examples are measures based on high order statistics (HOS) [22], [23] and AM–FM modelling of voice signal [24]-[27].

Chaos theory, an area of nonlinear dynamics systems theory, applied to nonlinear time series has recently been adopted as a new nonlinear approach to speech signal processing. The application of nonlinear chaotic techniques in speech signal processing so far are based on chaotic modelling or extraction of chaotic characteristics (Lyapunov exponents, correlation dimension, etc.). The main chaotic characteristics studied are the Lyapunov exponents [28]-[30] and dimensions of attractor, especially the correlation dimension. The correlation dimension has been shown to be capable of distinguishing healthy voices from pathological ones [28], [31]-[33] and even distinguishing between different types of pathologies such as ataxic dysarthia and hyperkinetic extrapyramidal dysarthia [33]. A high-quality vowel synthesizer based on chaotic techniques has also been developed [34]. The entropy has been applied to detect complex dynamics in disordered speech [35] in a preliminary study.

In this work, we propose the use of six nonlinear features based on chaos theory to discriminate between healthy and pathological voices. The characteristics studied are: the Takens–Theiler estimator of correlation dimension (CD), first- and second-order Rényi entropies (RE1, RE2) correlation entropy (CE), the Shannon entropy (SE) and the value of the FMMI function. **The motivation of this study is to assess the usefulness of complexity measures to discriminate between healthy and pathological voices. Pathological voice shows a more irregular behavior than healthy voice. For that**

reason, it is feasible to use complexity measures. Two databases were used in order to validate and compare results: a multiquality database [22] and the MEEI database [36].

8.1.2 Experimentation

The proposed features are a set of six nonlinear features including: first and second-order Rényi entropies, the correlation entropy, the correlation dimension, the value of the first minimum of mutual information function and Shannon entropy.

The process used in the experiment is divided in three stages: signal preprocessing, extraction of the measurements and classification. In the signal preprocessing stage, the samples of the database are normalized between -1 and 1 and the mean is removed. Then, a selection of the stable part of the phonation for each vowel is carried out (this part is skipped in the case of the MEEI database). The central second of each vowel is used for the experiment.

Each vowel is segmented into 10 equally spaced asynchronous frames (nonoverlapped) using rectangular windows. The length of each frame is 30 ms. Measurements are extracted from these frames. In the case of the Shannon entropy, the entire voice is used. Finally, the values of the measurements per frame are averaged. This way, it is obtained a value per vowel and measurement.

The delay was chosen as a tradeoff between the FMMI function and the FZA function. FMMI and FZA were computed for each sample of the database. Then, the average values of FMMI and FZA were obtained. Finally, the mean value of these values was computed. The value of the delay is 8 samples (0.36 ms because the sample frequency used was 22050 Hz). The embedding dimension was varied between 1 and 10.

In the classification stage, each set of measurements per vowel is the input of a classifier, so five classifiers are used, one for each vowel. Each classifier is based on a standard neural network. They evaluate the measurements in a quantitative way and discriminate between healthy and pathological vowels. A sample of the database is

diagnosed as pathological if the number of pathological vowels detected is equal to or more than three.

For each classifier, multilayer feedforward neural networks with one hidden layer are used. Supervised learning is carried out using backpropagation train algorithm. The input layer is made up of either as many inputs as characteristics (when all characteristics are evaluated combined) or is made up of one input (when only one characteristic is evaluated). The output layer has one node. The activation functions on the hidden nodes are tansigmoids (hyperbolic tangents) and the activation function of the output node is linear. The connection weights and biases are initialized according to the Nguyen–Widrow initialization algorithm [37]. The training process is stopped when a relative error of 0.005 is reached.

The database is split into a training subset and a testing subset with 70% and 30% of each type of voice, respectively. The data in the training set are z-score normalized. The test set is normalized by subtracting the training set mean and dividing by the training set standard deviation for each characteristic. The test set is normalized according to the normalization values used for the training set. The characteristics are evaluated individually and combined. The experiments were repeated 20 times, each time using different training and test sets randomly chosen.

The equal error rate (EER), the point for which the false positives rate (healthy files classified as pathological files) equals the false negative rate (pathological files classified as healthy files), is obtained varying the threshold in the output of each classifier and computing the false positive rate and false negative rate (each characteristic individually and combined).

8.1.3 Results

An analysis of the data distribution for each measure and for each kind of voice (healthy and pathological voice) is carried out. Then, a neural network classifier is applied to obtain a quantitative value of the discrimination between healthy and pathological voices.

Study of the discrimination of the features

In Figure 8-1 the data distributions for each measurement extracted from the /a/ vowel of the multiquality database are shown. Figure 8-2 shows the same distributions for the MEEI database.

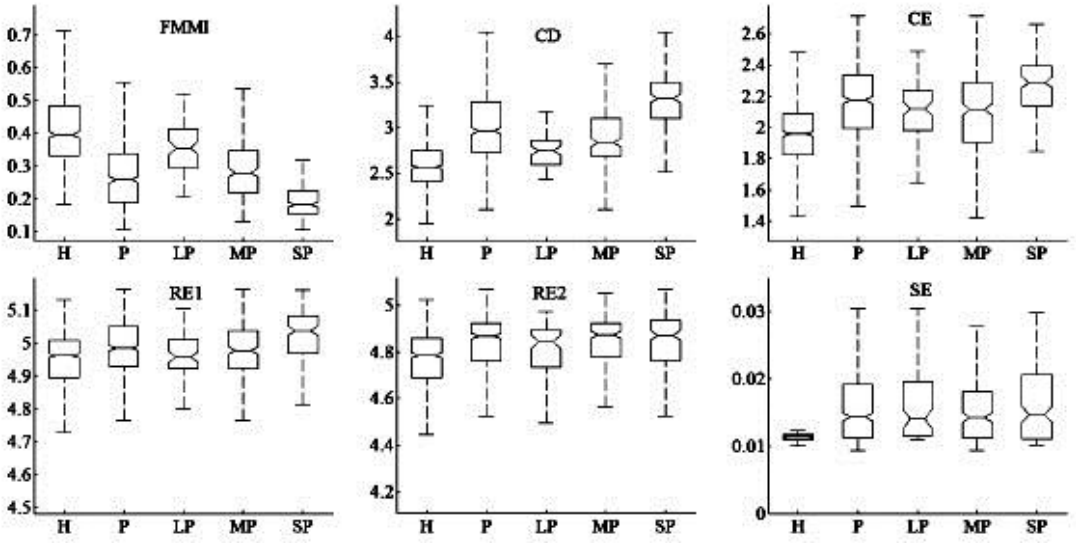

Figure 8-1: Data distribution of each kind of voice (H: healthy voice, P: pathological voice, LP: light pathological voice, MP: moderate pathological voice, SP: severe pathological voice) for each measurement extracted from the /a/ vowel of the multiquality database (FMMI: first minimum of the mutual information function. CD: correlation dimension. CE: correlation entropy. RE1: first-order Rényi block entropy. RE2: second-order Rényi block entropy. SE: Shannon entropy). Source: [1].

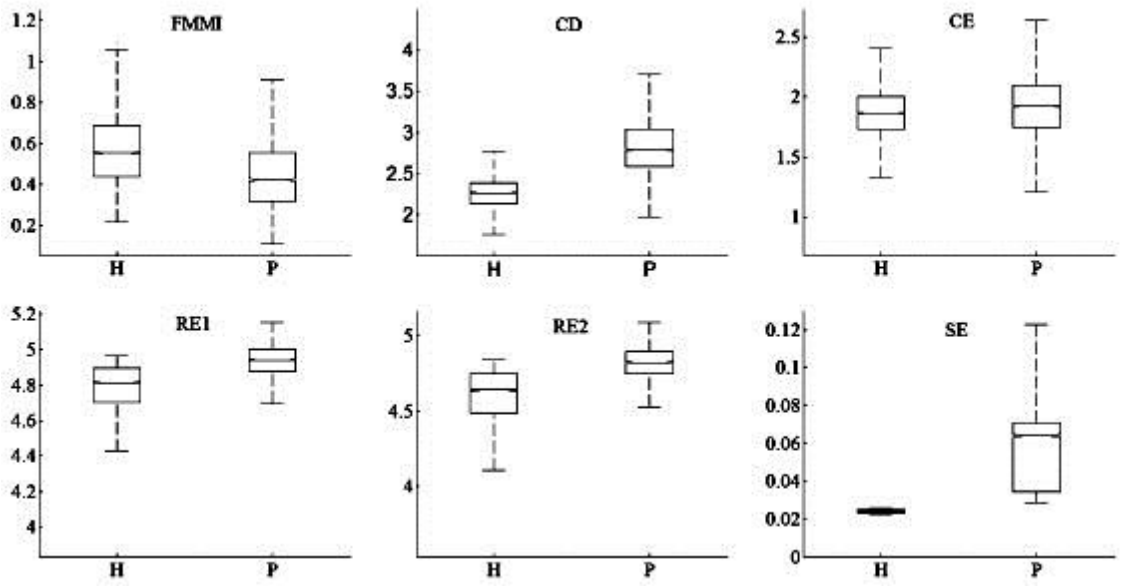

Figure 8-2: Data distribution of each kind of voice (H: healthy voice, P: pathological voice) for each measurement extracted from the MEEI database (FMMI: first minimum of the mutual information function. CD: correlation dimension. CE: correlation entropy. RE1: first-order Rényi block entropy. RE2: second-order Rényi block entropy. SE: Shannon entropy). Source: [1].

1.First minimum of the mutual information (FMMI)

The minimum value of the mutual information between a signal and its delayed version is higher in healthy voices. This means that in the time of maximum difference (i.e., when the FMMI occurs) of a signal with its delayed version, this difference is lower in healthy voices than in pathological voices.

2.Correlation dimension

More complex system has a higher CD, up to infinite value for stochastic signals. In the case of frames of healthy voices the CD has a lower value than in the case of frames of pathological voices. This is an indicator of a more complex geometrical structure in a pathological voice. According to Figure 8-1, the differences between the medians of H, P, LP, MP, and SP are evident. As a conclusion, CD is discriminative between H and P voices and between different kinds of pathological voices.

3.Shannon entropy and Rényi entropies

The RE1, RE2, and SE also show higher values in P voices than in H voices. This is an indicator of a more complex geometrical structure in pathological voices. These measurements are discriminative between H and P voices. However, they are less discriminative between the different kinds of pathological voices and even between LP and H voices (in the case of the RE1 measurement).

4.Entropy Correlation

The medians are higher in frames of pathological voices, as in the case of correlation dimension. This is an indicator that a P voice presents more loss of information in time than a H voice. Besides, the value of the CE is higher in SP than in MP and LP voices. The median of the MP is slightly higher than the median of LP voices. The CE is also discriminative between the different kinds of quality voices.

The data distribution for healthy (H) and pathological (P) voices of the MEEI database shows similar results to the multiquality database in the discrimination between H and P voices.

The main conclusion after observing the data distribution of the nonlinear measures is that the medians of H and P voices differ at the 5% significance level in all the cases.

Classification results

It has been shown that the studied measurements have different values for different kinds of voices. Once this fact is evident, we use a classification system in order to evaluate the discriminative usefulness of the characteristics against two voice qualities (healthy and pathological voices).

The results for the multiquality database [22] are shown in Table 8-1. The EER is shown for each vowel and each characteristic individually and combined. These results were obtained after evaluating the characteristics with different numbers of neurons in the hidden layer of the neural network. Finally, the best results were obtained

with 60 neurons in the hidden layer. According to Table 8-1, combination of all characteristics yields the lowest EER for each vowel. Once a threshold for each vowel has been chosen, the performance of the system is computed. Then a voice is diagnosed as pathological if the number of pathological vowels is equal to or more than three. Table 8-2 shows the confusion matrix of the system with the mean and standard deviation values obtained averaging the results for each individual experiment. The averaged global success of the system is 82.47% with a standard deviation of 3.1.

In the case of the MEEI database the same procedure was followed. In this case, the best results were obtained using ten neurons in the hidden layer. Table 8-3 shows the EER for each characteristic individually and combined. Shannon entropy and correlation dimension are the characteristics that show the better EER. Consequently, they show the better success rate. According to Table 8-4, in which the confusion matrix for MEEI database is shown for the EER point, the success rate for all characteristics combined is 99.69% with a standard deviation of 0.2.

TABLE 8-1: EQUAL ERROR RATES FOR MULTIQUALITY DATABASE: MEASURES INDIVIDUALLY AND COMBINED

Equal Error Rate (%)							
Vowel	FMMI*	CD*	CE*	RE1*	RE2*	SE*	Combined
A /a/	29.23	29.17	39.84	42.69	40.00	43.69	20
E /e/	43.86	45	35.28	37.78	42.5	40.38	29.44
I /i/	49.04	50.28	50.56	48.61	44.17	39.78	33.62
O /o/	35.28	28.85	37.22	41.11	41.54	34.72	31.9
U /u/	38.18	47.5	41.54	46.11	48.69	36.75	28.08

* FMMI: First minimum of the mutual information function. CD: Correlation dimension. CE: Correlation entropy. RE1: first-order Rényi block entropy. RE2: second-order Rényi block entropy. SE: Shannon entropy.

TABLE 8-2: SUCCESS RATE IN A CONFUSION MATRIX FOR MULTIQUALITY DATABASE

Detector's decision (%)	Actual diagnosis	
	Pathological	Healthy
Pathological	81.67 (σ = 7.68)	16.73 (σ = 5.19)
Healthy	18.33 (σ = 7.68)	82.27 (σ = 5.19)

TABLE 8-3: EQUAL ERROR RATES FOR MEEI DATABASE: MEASURES INDIVIDUALLY AND COMBINED

Equal Error Rate (%)							
Vowel	FMMI*	CD*	CE*	RE1*	RE2*	SE*	Combined
A /a/	38.81	8.66	41.96	44.42	41.25	3.12	0.31

* FMMI: First minimum of the mutual information function. CD: Correlation dimension. CE: Correlation entropy. RE1: first-order Rényi block entropy. RE2: second-order Rényi block entropy. SE: Shannon entropy.

TABLE 8-4: SUCCESS RATE IN A CONFUSION MATRIX FOR MEEI DATABASE

Detector's decision (%)	Actual diagnosis	
	Pathological	Healthy
Pathological	99.69 ($\sigma = 0.12$)	0.31 ($\sigma = 0.12$)
Healthy	0.31 ($\sigma = 0.12$)	99.69 ($\sigma = 0.12$)

8.1.4 Conclusions

The usefulness of six nonlinear chaotic characteristics: first and second-order Rényi entropies, the correlation entropy, the correlation dimension, the value of the first minimum of mutual information function and Shannon entropy, has been evaluated in order to distinguish between two voice qualities (healthy and pathological voices).

Two databases were used to evaluate the characteristics, a multiquality database [22] and a commercial one (MEEI Voice Disorders [36]) in order to obtain comparative results between them. The multiquality database comprises samples labeled with different kinds of voice quality according to the hoarseness (G) of the GRBAS scale. The MEEI database only has samples labeled as healthy and pathological voices.

A previous statistical study was carried to check the discrimination of the characteristics for both databases. In the multiquality database, the statistical study showed remarkable differences between healthy and pathological voices and even between the three different levels of pathologies for each of the characteristics studied. Generally, the quantitative evaluation of the measurements was correlated with the medical assessment.

The correlation dimension and the value of the first minimum of mutual information function were the characteristics that better discriminated among the different voice qualities of the multiquality database. The MEEI database also showed significative differences between the medians of the two classes of voice (healthy and pathological voices). As a conclusion, the medians of the healthy and pathological voices differ at the 5% significance level in both databases and in all the characteristics.
The characteristics were evaluated with neural networks to discriminate between healthy and pathological voices. Successful results were obtained for both databases. The global success rate obtained with the multiquality database [22] was 82.47% and with the MEEI database [36] 99.69%. This demonstrates that the six proposed characteristics are useful to discriminate between healthy and pathological speakers.
The difference between the two classification rates of both databases is due to the nonexistence of LP speakers in the MEEI database. LP speakers are more likely to be classified as normal speakers because the difference between healthy and LP or MP speakers is lower than between a healthy and an MP or an SP speaker. In the results, if the LP and MP speakers are removed, the success rate of the multiquality database is similar to the MEEI database (see SP speaker in Table 8-2 and compare with the MEEI results in Table 8-4).

The measurements studied in this research can be used to document the patient evolution. They can also be used in help systems for pathology diagnosis in the speech production system. As a new step, we propose the combination of the nonlinear characteristics evaluated here and classical characteristics used previously in order to evaluate if the combination results in better classification rates.

8.2 Emotional voice detection

During the period of the Thesis, we also worked on emotional speech characterizarion using complexity measures including mutual information, dimension correlation, entropy correlation, Shannon entropy, Lempel-Ziv complexity and Hurst exponent aiming at automatic emotion recognition. It was also the first study ever in emotional speech characterization. The complexity measures were extracted in a first work from the samples of a german emotional speech database [38], [39]. In a later work [40], two

more databases were added to the study: the Polish emotional speech database and the English LCD emotional database. Then, statistics such as mean, standard deviation, skewness and kurtosis are applied on the extracted measures. A three–class problem (neutral, fear and anger emotional states) was considered. A procedure to select a group of global optimal features is also proposed in this work. The selection is based on an affinity analysis of the previously selected features using the standard feature selection algorithm called Sequential Floating Forward Selection procedure. This method will not be explained in this Chapter. The feature selection procedure is accomplished over the Polish emotional speech database to select a reduced number of features. Then, the selected features are evaluated in the Berlin emotional speech database and in the LDC emotional database using a neural network classifier in order to assess the usefulness of the selected features. The results obtained in the experimentation show that complexity measures provide high classification rates in the discrimination between neutral, fear and anger emotional states in recorded voice signals.Global success rates of 72.28%, 75.4% and 80.75%, were obtained for the Polish emotional speech database, the Berlin emotional speech database and the LDC emotional speech database respectively.

8.2.1 Motivation

Speech is one of the main modes of communication between human beings and an effective way to express emotions. Automatic recognition of human emotions in speech aims at automatically detecting the speaker emotional state based on speech and has attracted the research community in the last few years due to its applications in industry. Emotion recognition systems open new horizons in artificial intelligence with the improvement of voice synthesizer. The addition of emotional speech in voice synthesizer produces more natural speech facilitating human-computer interaction or computer aided communications [41]. Another application is the automatic recognition of negative emotions (e.g. anger or rage) in call centers based on interactive-voice-response systems. It is useful to detect problems in the customer-system interaction to help the customer by offering a human operator, for example [42]-[44]. In surveillance applications, speech emotion recognition can take an important role in detecting security threats using word-spotting techniques with the combination of emotional recognition.

One of the key steps in automatic recognition of emotional speech is the extraction of features that effectively distinguish between the emotions to be classified. In emotion recognition literature, features can be divided in linguistic and acoustic features. Linguistic features focus on explicit linguistic message (dialog related features) and acoustic features focus on implicit message. Acoustic features include prosodic features (which are mostly related to pitch, energy and speaking rate) [45], spectral and cepstral features such as Mel Frequency Cepstral Coefficients [45], [46] and voice quality features such as harmonics-to-noise ratio, jitter or shimmer [47]. Features are usually extracted in a short-term basis, obtaining different number of features for each sample in the emotional database. Statistics variations of these features (functionals), such as their average, skewness, minimum, maximum and standard deviation are also frequently used. The use of functionals is probably justified by the supra-segmental nature of the phenomena found in emotional speech [47].

The success rates achieved in different works on automatic recognition of emotional speech are very difficult to compare due to the lack of a freely available corpus of reference and the lack of a standard methodology. Another issue is the different ways of considering emotions: as categorical discrete emotions or as continuous emotions in a multidimensional space (i.e. activation, valence, etc.). In the next few lines, we show examples of recent results obtained in the literature: using the Berlin emotional speech database [48] and classifying between 7 discrete emotions with both modulation spectral features and prosodic features a 91.6% of success rate is achieved [45]. A success rate of 88.6% is obtained using spectro-temporal features and prosodic features [45] using the same database [48] and classifying between 7 discrete emotions as well. In another work, a maximum of 79% of accuracy is obtained with a set of linguistic and acoustic features in the classification between anger and no-anger speech using three different databases of real emotions [44], [45].

Nonlinear dynamics systems theory has been adopted as a nonlinear approach to speech signal processing in the last two decades. Complexity features studied in the speech processing literature include dimension correlation, Rényi entropies [1], Lyapunov exponents [28], Hurst exponent [50] and Lempel-Ziv complexity [51]. These features have proved to be useful in distinguishing between different voice quality and in voice pathology detection.

We propose the study of a set of nonlinear measures or complexity measures in emotional speech to assess its discrimination ability between neutral state, fear emotional state and anger emotional state produced by actors in three different emotional speech database: the Polish emotional speech database [52], the Berlin emotional speech database [48] and the Emotional Prosody Speech and Transcripts of the Linguistic Data Consortium (LCD) [53]. The study of the discrimination ability between neutral and negative emotional states such as fear or anger is very useful in surveillance applications to detect security threats. The complexity measures extracted are: the value of the first minimum of the mutual information function (MI), the Shannon entropy (SE), the Taken's estimator of the correlation dimension (CD), the correlation entropy (CE), the Lempel-Ziv complexity (LZC) and the Hurst exponent (H). Mean (μ), standard deviation (σ), skewness (sk) and kurtosis (k) are applied to the extracted measures, obtaining 24 features.

8.2.2 Experimentation

This section describes the different steps of the experimental procedure: preprocessing and feature extraction, feature selection procedure and evaluation with the selected features using a neural network classifier. The feature selection procedure is accomplished in the Polish emotional speech database. In the evaluation step, the selected features are evaluated in the three databases in order to validate their usefulness in discriminating between neutral, fear and anger states.

Preprocessing & Feature Extraction

The data is preprocessed using a voice activity detector in order to remove the silences from the speech samples of the database. From each speech signal the mean is removed. After that, the signal is normalized between -1 and 1. Then, a short-term processing is applied in order to extract the features: each audio signal is divided into 50% overlapping windows (frames) of 55ms. According to Ruelle [25], the number of samples needed to carry out the embedding of the signal has to be chosen in the following way: if the calculated dimension of the system is below $2\log_{10}N$, where N is the total number of points in the original time series, then we are using a sufficient number of data points. In this paper, $N = 880$, so $2\log_{10}N = 5.889$ and the median values

of the correlation dimension of each emotion are below this quantity (see Figure 8-3) where the data distributions of the correlation dimension estimated for each database are shown).

The delay (τ) and the minimum embedding dimension (m) are estimated for each frame using the first minimum of the mutual information function technique and the false neighbours technique respectively. Then, six complexity measures are extracted for each frame: value of the first minimum of mutual information function (MI), Taken-Theiler estimator of the correlation dimension (CD), Shannon entropy (SE), correlation entropy (CE), Lempel-Ziv complexity (LZC) and Hurst exponent (H). Finally, for each measure, four statistical are computed: mean (μ), standard deviation (σ), skewness (sk) and kurtosis (k). Therefore, 24 features are extracted for each frame (mean of MI: μMI, mean of CD: μCD and so on).

Feature selection and evaluation of the selected features

A set of features are selected using a feature selection technique proposed by the author of this Thesis. In this Chapter, the proposed feature selection procedure will not be explained (see [39]). Once the selected features are identified, their discrimination ability between the different emotions is evaluated using a neural network. The database is split into a training subset and a test subset with 70% and 30% of each kind of emotional speech recordings, respectively. The experiments are repeated 25 times, each time using different training and test sets randomly chosen and the global success rate is computed as an average of the success rates in each iteration.

8.2.3 Results

The results obtained in the experiments are shown and discussed. First, we show a data distribution analysis of the complexity measures (MI, SE, CD, CE, LZC and H). Then, we show the results of the feature selection procedure. The feature selection procedure is performed in the Polish emotional speech database. Finally, we show the success rates for the three emotional databases: the Polish emotional speech database, the Berlin emotional speech database and the LDC emotional speech database using the GOFS previously identified.

Analysis of complexity measures

The complexity measures extracted from the three databases are analyzed. Figure 8-3, Figure 8-4 and Figure 8-5 show the distribution of the six complexity measures (MI, SE, CD, CE, LZC and H) for the Polish emotional speech database, for the Berlin emotional speech database and for the LDC emotional speech database respectively using boxplots. The boxes have lines at the lower quartile, median (center line) und upper quartile values. The whiskers are lines extending from each end of the boxes to show the extent of the rest of the data. Boxes whose notches do not overlap indicate that the medians of the two groups differ at the 5% significance level. In Figure 8-3, Figure 8-4 and Figure 8-5 the upper left illustration corresponds to the MI, the upper right illustration corresponds to the SE, the middle left illustration corresponds to the CD, the middle right illustration corresponds to the CE, the bottom left illustration corresponds to the LZC and finally the bottom right illustration corresponds to the H.

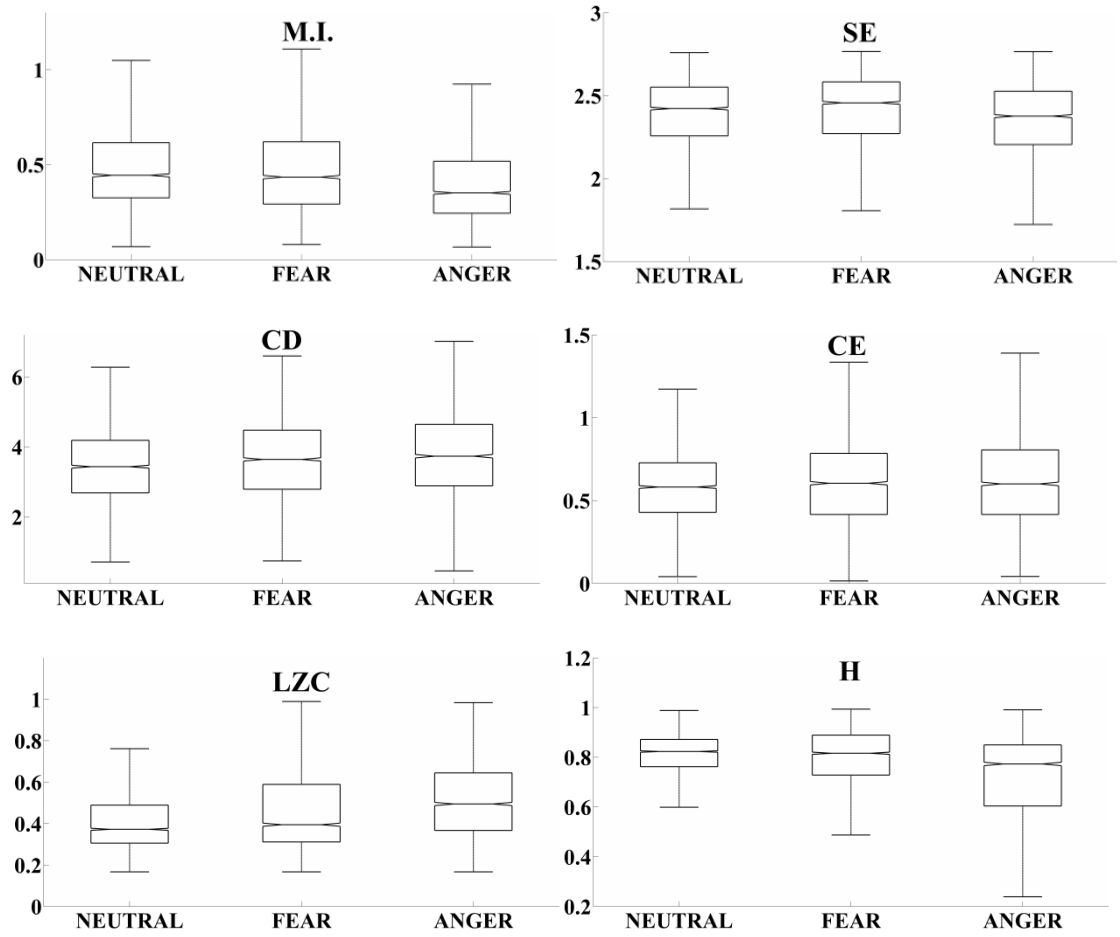

Figure 8-3: Data distribution of neutral, fear and anger emotional speech for each complexity measure extracted from the Polish emotional database. MI: value of the first minimum of the mutual information function (upper left), SE: Shannon entropy (upper right), CD: Taken's estimator of the correlation dimension (middle left), CE: correlation entropy (middle right), LZC: Lempel–Ziv complexity (bottom left), H: Hurst exponent (bottom right) [40].

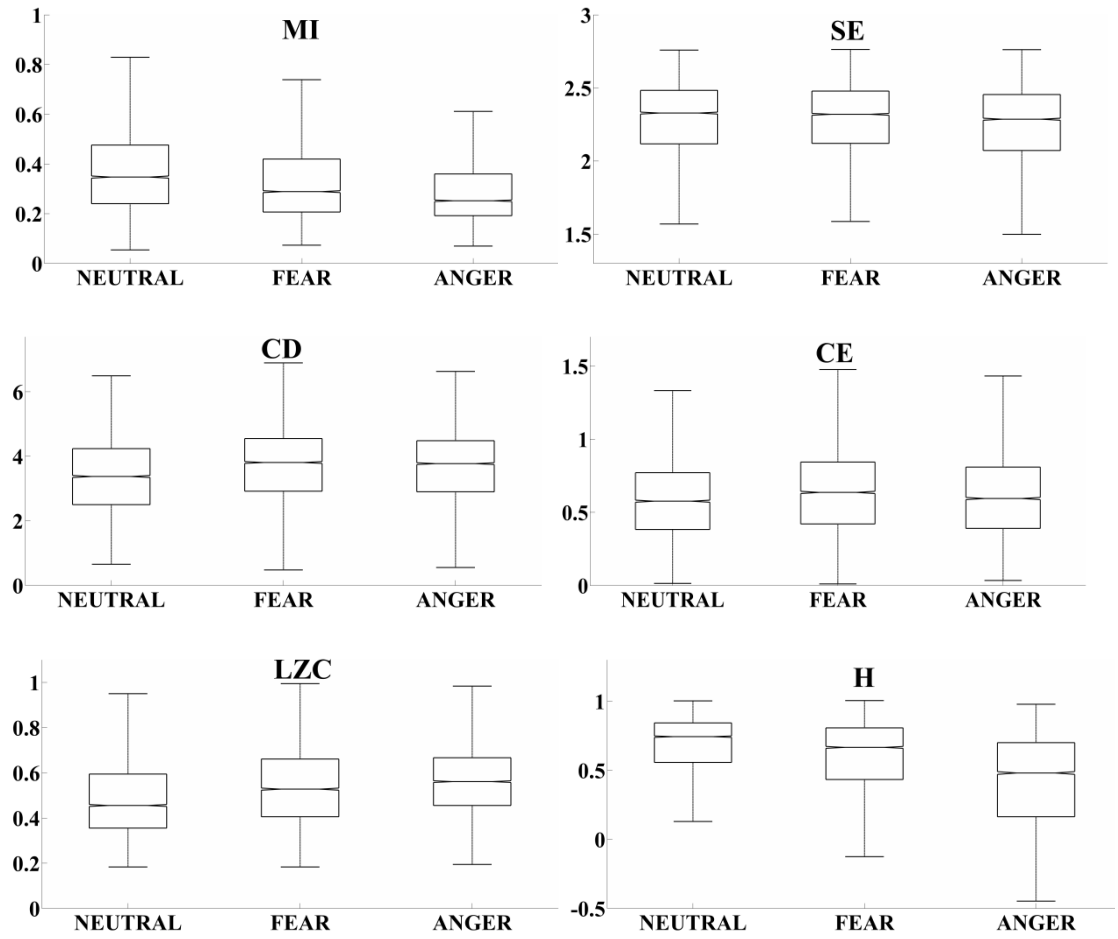

Figure 8-4: Data distribution of neutral, fear and anger emotional speech for each complexity measure extracted from the Berlin emotional database. MI: value of the first minimum of the mutual information function (upper left), SE: Shannon entropy (upper right), CD: Taken's estimator of the correlation dimension (middle left), CE: correlation entropy (middle right), LZC: Lempel–Ziv complexity (bottom left), H: Hurst exponent (bottom right) [40].

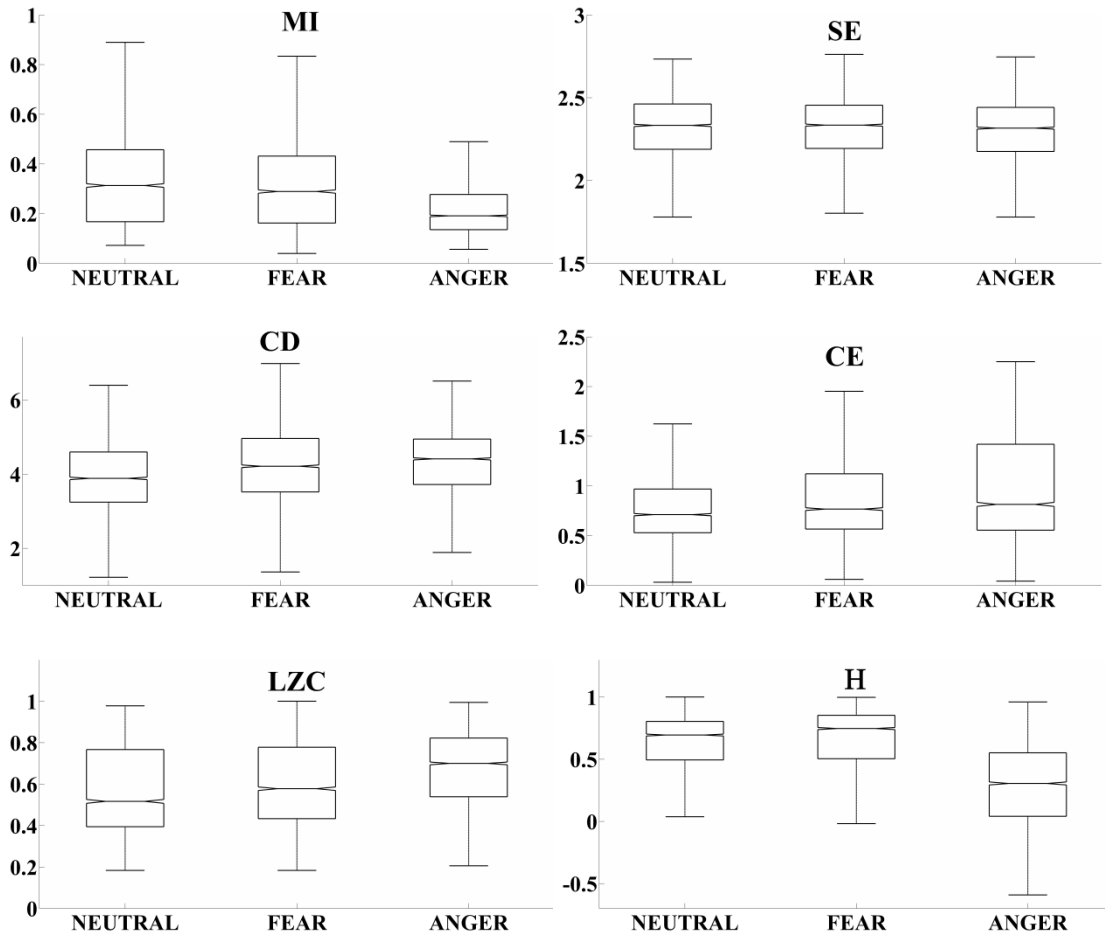

Figure 8-5: Data distribution of neutral, fear and anger emotional speech for each complexity measure extracted from the LDC emotional database. MI: value of the first minimum of the mutual information function (upper left), SE: Shannon entropy (upper right), CD: Taken's estimator of the correlation dimension (middle left), CE: correlation entropy (middle right), LZC: Lempel–Ziv complexity (bottom left), H: Hurst exponent (bottom right) [40].

According to the Figure 8-3 the median of the values of the first minimum of the mutual information function (MI) between a signal and its delayed version is higher in neutral speech than in fear emotional speech and in anger emotional speech. This means that in the time of maximum difference (i.e. when the first minimum of the mutual information occurs) of a signal with its delayed version, this difference is lower in neutral speech than in fear or anger emotional speech. This tendency is the same in the three databases. In the case of the Shannon entropy distributions, there are not clear differences between neutral, fear and anger emotional speech. The median of the distributions are overlapped in the case of the LDC database. However, they are more clearly separated in the case of the Berlin emotional speech database and in the case of the Polish emotional speech database.

The distribution of the Taken's estimator of the correlation dimension (CD) also shows a similar behavior in the three databases. The median values of the CD are higher in fear emotional speech and in anger emotional speech than in neutral speech. This is an indicator of a more complex geometrical structure in anger and fear emotional speech. However, there are not clear differences in the values of the CD between anger and fear emotional states in the Berlin database. The median of the correlation entropy (CE) distribution for neutral speech shows lower values than the median for anger and fear emotional speech. This is an indicator of a more complex structure in anger and fear speech than in neutral speech. The CE measure shows to be discriminative between neutral and fear and anger emotional speech. However, CE is less discriminative between fear and anger emotional speech.

The Lempel-Ziv complexity (LZC) distribution shows values more near to 1 for fear and anger emotional speech than in the case of neutral speech. This means that anger and fear emotional speech records show more complexity than neutral speech records. Finally, the Hurst exponent (H) shows that the median value of neutral speech is higher than median of fear and anger emotional speech. Values of H for fear and anger emotional speech are closer to 0.5, showing that this signals has more randomness components.

According to the data distributions, the six complexity measures are discriminative between neutral speech and negative emotional speech (anger emotional speech and fear emotional speech). However, in the case of the CE and CD the discrimination between fear emotional speech and anger emotional speech are less clear. Moreover, the data distributions are very similar in the three databases. This means that the discriminative ability of the complexity measures is independent from the language.

Results of feature selection

The following features were selected in the feature selection procedure: μMI, μH, sSE, sLZC.

Results of the databases evaluation with the selected features

The selected features (μMI, μH, sSE and sLZC) were evaluated with a neural network classifier (with 5 neurons in the hidden layer) for the three emotional speech databases (Polish, Berlin and LDC databases). The global success rates for the different emotional databases are shown in Table 8-5 with the standard deviation (σ). According to the results, the selected features show a good discrimination ability between three emotional speech states (neutral state, fear emotional state and anger emotional state) in the three databases.

TABLE 8-5: GLOBAL SUCCESS RATES OF THE SELECTED FEATURES IN THREE EMOTIONAL DATABASES

	Polish database	Berlin database	LDC database
Success rates (%)	72.78 (σ = 5.13)	75.40 (σ = 3.86)	80.75 (σ = 3.75)

Table 8-6, Table 8-7 and Table 8-8 show the confusion matrix of the selected features in the three emotional speech databases with the mean and standard deviation (σ) values obtained averaging the results for each individual experiment. According to the results, the selected features show good discrimination ability in the three databases between neutral, fear emotional state and anger emotional state. The discrimination ability between neutral and negative emotional states are higher than between fear and anger emotional speech in the case of the Polish emotional speech database and the Berlin emotional speech database. However, the LDC database shows good discrimination ability in anger emotional state against fear and neutral states. The similar results in the three databases show that the selected features are independent of the language.

TABLE 8-6: CONFUSION MATRIX OF THE SELECTED FEATURES IN POLISH EMOTIONAL SPEECH DATABASE

Classifier decision (%)	Actual emotional state		
	Neutral	Fear	Anger
Neutral	88.00 (σ = 11.04)	8.00 (σ = 10.34)	4.00 (σ = 4.88)
Fear	17.00 (σ = 10.06)	64.00 (σ = 14.77)	19.00 (σ = 14.54)
Anger	7.33 (σ = 8.44)	26.33 (σ = 13.32)	66.33 (σ = 15.86)

TABLE 8-7: CONFUSION MATRIX OF THE SELECTED FEATURES IN BERLIN EMOTIONAL SPEECH DATABASE

Classifier decision (%)	Actual emotional state		
	Neutral	Fear	Anger
Neutral	78.80 (σ = 7.81)	15.00 (σ = 6.45)	6.20 (σ = 3.89)
Fear	16.00 (σ = 10.10)	63.20 (σ = 11.35)	20.80 (σ = 10.07)
Anger	4.20 (σ = 5.34)	11.60 (σ = 8.38)	84.20 (σ = 8.74)

TABLE 8-8: FUSION MATRIX OF THE SELECTED FEATURES IN LDC EMOTIONAL SPEECH DATABASE

Classifier decision (%)	Actual emotional state		
	Neutral	Fear	Anger
Neutral	77.57 (σ = 8.76)	16.70 (σ = 7.50)	5.74 (σ = 4.65)
Fear	19.30 (σ = 9.57)	72.17 (σ = 8.33)	8.52 (σ = 4.78)
Anger	3.30 (σ = 3.82)	4.17 (σ = 3.19)	92.52 (σ = 4.44)

8.2.4 Conclusions

The usefulness of complexity features in discriminating between neutral state, fear emotional state and anger emotional state is evaluated. Six complexity measures including the value of first minimum of mutual information function, the Shannon entropy, the Takens estimator of the correlation dimension, the correlation entropy, the Lempel-Ziv complexity and the Hurst exponent are extracted from three emotional databases (the Polish emotional speech database, the Berlin emotional speech database and the LCD database). Then, the mean, standard deviation, skewness and kurtosis are applied to the six complexity measures and 24 features are obtained. Feature selection is accomplished to select a reduced number of features over the Polish emotional database. Finally, the selected features are evaluated in the Berlin emotional speech database and in the LDC emotional database using a neural network classifier.

A qualitative analysis of the six complexity measures extracted from the three emotional databases is accomplished with the observation of the data distribution of the complexity measures. From this analysis, the following conclusions are extracted. According to the data distributions analysis, the six complexity measures are discriminative between neutral speech, fear emotional speech and anger emotional speech. In general, fear and anger emotional speech records show more complexity than neutral speech records. The reason can be that in fear and anger speech records, people

tend to use more fricative sounds than in neutral state. Fricative sounds are noisier than voiced sounds. Moreover, the behavior of the data distributions of the six complexity measures is the same in the three databases. The databases consist of emotional speech records in Polish, German and English languages. We can conclude, therefore, that the complexity measures are independent from the language.

The four selected features (mean of the value of the first minimum of the mutual information function, the mean of the Hurst exponent, the standard deviation of the Shannon entropy and the standard deviation of the Lempel-Ziv complexity) were evaluated with a neural network classifier in the three databases. Global success rates of 72.28%, 75.4% and 80.75%, were obtained for the Polish emotional speech database, the Berlin emotional speech database and the LDC emotional speech database respectively in the discrimination between neutral, fear and anger emotional states. Possibly applications of an automatic recognition system that discriminate between neutral emotion and negative emotions such as fear and anger can be applied in call centers in order to detect problems in costumer-system interaction and in security applications in order to detect security threats.

8.3 Contributions

The contributions of this Chapter are the studies of nonlinear and complexity measures in pathological voice detection and in emotional voice detection.

8.4 References

[1] Henríquez, P., Alonso, J. B., Ferrer, M., Travieso, C. M., Godino-Llorente, J., & Díaz-de-María, F. (2009). Characterization of healthy and pathological voice through measures based on nonlinear dynamics. *Audio, Speech, and Language Processing, IEEE Transactions on*, *17*(6), 1186-1195.

[2] Hirano, M. Clinical Examination of Voice. New York: Springer, Verlag, 1981.

[3] Nawka, T., Anders, L. C., & Wendler, J. (1994). Die auditive Beurteilung heiserer Stimmen nach dem RBH System. *Sprache Stimme Gehör, 18*, 130-133.

[4] Boyanov, B., Hadjotodorov, S., Teston, B., & Doskov, D. (1997). Robust hybrid pitch detector for pathological voice analysis. In *Larynx 97* (pp. 55–58).

[5] Boyanov, B., Ivanov, T., & Chollet, G. (1993). Robust hybrid pitch detector. *Electron. Lett*., *29*(22), 1924–1926.

[6] H. Kasuya, Y. Endo, and S. Saliu, "Novel acoustic measurements of jitter and shimmer characteristics from pathologic voice," in Proc. Eurospeech' 93, Berlin, Germany, 1993, pp. 1973–1976.

[7] C. Ludlow, C. Bassich, N. Connor, D. Coulter, and Y. Lee, "The validity of using phonatory jitter and shimmer to detect laryngeal pathology," in Laryngeal Function in Phonation and Respiration. Boston, MA: Brown, 1987, pp. 492–508.

[8] Yumoto, E., Gould, W. J., & Baer, T. (1982). Harmonics to noise ratio as an index of the degree of hoarseness. The journal of the Acoustical Society of America, 71(6), 1544-1550.

[9] M. Yunik and B. Boyanov, "Method for evaluation of the noise-to-harmonic-component ratios in pathological and normal voices," Acustica, vol. 70, pp. 89–91, 1990.

[10] Kasuya, H., Ogawa, S., Mashima, K., & Ebihara, S. (1986). Normalized noise energy as an acoustic measure to evaluate pathologic voice. The Journal of the Acoustical Society of America, 80(5), 1329-1334.

[11] M. Frohlich, D. Michaelis, and H. W. Srube, "Acoustic ‘Breathiness Measures' in the description of pathologic voices," in Proc. Acoust., Speech, Signal Process. ICASSP'98, Seattle, WA, 1998, vol. 2, pp. 937–940.

[12] L. Gu, J. G. Harris, R. Shrivastav, and C. Sapienza, "Disordered speech assessment using automatic methods based on quantitative measures," EURASIP J. Appl. Signal Process., vol. 9, pp. 1400–1409, 2005.

[13] Boyanov, B., & Hadjitodorov, S. (1997). Acoustic analysis of pathological voices. A voice analysis system for the screening of laryngeal diseases.Engineering in Medicine and Biology Magazine, IEEE, 16(4), 74-82.

[14] Wallen, E. J., & Hansen, J. H. (1996, October). A screening test for speech pathology assessment using objective quality measures. In *Spoken Language, 1996. ICSLP 96. Proceedings., Fourth International Conference on* (Vol. 2, pp. 776-779). IEEE.

[15] De Oliveira Rosa, M., Pereira, J. C., & Carvalho, A. C. (1998, December). Evaluation of neural classifiers using statistic methods for identification of Laryngeal pathologies. In *Proc. 5th Brazilian Symp. Neural Netw.* (vol. 1, pp. 220–225).

[16] Hadjitodorov, S., & Mitev, P. (2002). A computer system for acoustic analysis of pathological voices and laryngeal diseases screening. *Medical engineering & physics*, *24*(6), 419-429.

[17] Ayache, S., Ouaknine, M., Dejonkere, P., Prindere, P., & Giovanni, A. (2004). Experimental study of the effects of surface mucus viscosity on the glottic cycle. *Journal of Voice*, *18*(1), 107-115.

[18] Teager, H. M., & Teager, S. M. (1990). Evidence for nonlinear sound production mechanisms in the vocal tract. In *Speech production and speech modelling* (pp. 241-261). Springer Netherlands.

[19] Berry, D. A., Herzel, H., Titze, I. R., & Krischer, K. (1994). Interpretation of biomechanical simulations of normal and chaotic vocal fold oscillations with empirical eigenfunctions. *The Journal of the Acoustical Society of America*, *95*(6), 3595-3604.

[20] Jiang, J. J., Zhang, Y., & Stern, J. (2001). Modeling of chaotic vibrations in symmetric vocal folds. *The Journal of the Acoustical Society of America*, *110*(4), 2120-2128.

[21] Steinecke I., & Herzel, H. (1995). Bifurcations in an asymmetric vocal-fold model. *J. Acoust. Soc. Amer.*, *97*(3), 1874-1884..

[22] Alonso, J. B., De León, J., Alonso, I. , & Ferrer, M. A. (2001). Automatic detection of pathologies in the voice by hos based parameters. *EURASIP J. Appl. Signal Process.*, *4*, 275–284.

[23] Boyanov, B., Hedjitodorov, S., & Ivanov, T. (1991). Analysis of voiced speech by means of Bispectrum. *Electron. Lett.*, *27*(24), 2267–2268.

[24] Gavidia-Ceballos, L., Hansen, J. H., & Kaiser, J. F. (1996, October). Vocal fold pathology assessment using AM autocorrelation analysis of the Teager energy operator. In *Spoken Language, 1996. ICSLP 96. Proceedings., Fourth International Conference on* (Vol. 2, pp. 757-760). IEEE.

[25] Hansen, J. H., Gavidia-Ceballos, L., & Kaiser, J. F. (1998). A nonlinear operator-based speech feature analysis method with application to vocal fold pathology assessment. *IEEE Trans. Biomed. Eng.*, *45*(3), 300–313.

[26] Cairns, D., Hansen, J. H., & Riski, J. E. (1996). A noninvasive technique for detecting hypernasal speech using a nonlinear operator. *IEEE Trans. Signal Process.*, *43*(1), 35–44.

[27] Cairns, D., Hansen, J. H., & Kaiser, J. F. (1996, October). Recent advances in hypernasal speech detection using the nonlinear Teager energy operator. In *Spoken Language, 1996. ICSLP 96. Proceedings., Fourth International Conference on* (Vol. 2, pp. 780-783). IEEE.

[28] Alonso, J. B., Díaz-de-María, F., Travieso, C. M., & Ferrer, M. A. (2005, April). Using nonlinear features for voice disorder detection. In *Proc. 3rd Int. Conf. Nonlinear Speech Process.* (pp. 94–106), Barcelona, Spain.

[29] Maragos, P., Dimakis, A. G., & Kokkinos, I. (2002). Some advances in nonlinear speech modeling using modulations, fractals, and chaos. In *Digital Signal Processing, 2002. DSP 2002. 2002 14th International Conference on*(Vol. 1, pp. 325-332). IEEE.

[30] Yu, P., Ouaknine, M., Revis, J., & Giovanni, A. (2001). Objective voice analysis for dysphonic patients: A multiparametric protocol including acoustic and aerodynamic measurements. *Journal of Voice*, *15*(4), 529–542.

[31] Hang, J. J., & Jiang, J. J. (2003). Nonlinear dynamic analysis in signal typing of pathological human voices. *Electron. Lett.*, *39*(13), 1021–1023.

[32] Jiang, J. J., & Zhang, Y. (2002). Nonlinear dynamic analysis of speech from pathological subjects. *Electron. Lett.*, *38*(6), 294–295.

[33] Aaccardo, A., Fabbro, F., & Mumolo, E. (1992, October). Analysis of normal and pathological voices via short-time fractal dimension. In *1992 14th Annual Int. Conf. of the IEEE Eng. Med. Biol. Soc.* (vol. 14, pp. 1270–1271).

[34] Banbrook M., & McLaughlin, S. (1996, October). Dynamical modelling of vowel sounds as a synthesis tool. In *Proc. 4th Int. Conf. Spoken Lang. Process.* (vol. 3, pp. 1981–1984).

[35] Little, M. A., McSharry, P. E., Moroz, I. M., & Roberts, S. J. (2006). Stroboscopic method for detecting complex dynamics in disordered speech. *IEEE Trans. Biomed. Eng.*, *1*, 1–6.

[36] Massachusetts Eye and Ear Infirmary, Voice Disorders Database, Version 1.03. Kay Elemetrics Corp., Lincoln Park, NJ, 1994, CD-ROM.

[37] Nguyen, D., & Widrow, B. (1990). Improving the learning speed of 2-layer neural networks by choosing initial values of the adaptive weights. In *Proc. Int. Joint Conf. Neural Netw.* (Vol. 3, pp. 21–26).

[38] Henríquez, P., Alonso, J. B., Ferrer, M. A., Travieso, C. M., & Orozco-Arroyave, J. R. (2011). Application of Nonlinear Dynamics Characterization to Emotional Speech. In *Advances in Nonlinear Speech Processing* (pp. 127-136). Springer Berlin Heidelberg.

[39] Henríquez, P., Alonso, J. B., Ferrer, M. A., Travieso, C. M., & Orozco-Arroyave, J. R. (2013). Global Selection of Features for Nonlinear Dynamics Characterization of Emotional Speech. *Cognitive Computation*, *5*(4), 517-525.

[40] Henríquez, P., Alonso, J. B., Ferrer, M. A., Travieso, C. M., Orozo-Arroyave, J. R. (2014). Nonlinear Dynamics Characterization of Emotional Speech. *Neurocomputing*, *132*, 126-135.

[41] Yildirim, S., Narayanan, S., Potamianos, A. (2011). Detecting emotional state of a child in a conversational computer game. *Comput. Speech Lang.*, *25*(1), 29–44.

[42] Burkhardt, F., Polzehl, T., Stegmann, J., Metze, F., & Huber, R. (2009, April). Detecting real life anger. In *Acoustics, Speech and Signal Processing, 2009. ICASSP 2009. IEEE International Conference on* (pp. 4761-4764). IEEE.

[43] Lefter, I., Rothkrantz, L.J., Van Leeuwen, D.A., & Wiggers, P. (2011). Automatic stress detection in emergency (telephone) calls. *Int. J. Intell. Def. Support Syst.*, *4*(2), 148–168.

[44] Polzehl, T., Schmitt, A., Metze, F., & Wagner, M. (2011). Anger recognition in speech using acoustic and linguistic cues. *Speech Commun. 53* (9), 1198–1209.

[45] Wu, S., Falk, T. H., Wai-Yip, C. (2009, July). Automatic recognition of speech emotion using long-term spectro-temporal features. In *Digital Signal Processing, 2009 16th International Conference on* (pp. 1-6). IEEE.

[46] Giannakopoulos, T., Pikrakis, A., & Theodoridis, S.A. (2009, April). A dimensional approach to emotion recognition of speech from movies. In *Acoustics, Speech and Signal Processing, 2009. ICASSP 2009. IEEE International Conference on* (pp. 65-68). IEEE.

[47] Schuller, B., Batliner, A., Steidl, S., & Seppi, D. (2011). Recognising realistic emotions and affect in speech: state of the art and lessons learnt from the first challenge. *Speech Commun. 53*(9), 1062–1087.

[48] A Database of German Emocional Speech, http://pascal.kgw.tu-berlin.de/emodb/.

[49] Wu, S., Falk, T. H., & Chan, W. Y. (2011). Automatic speech emotion recognition using modulation spectral features. *Speech communication*, *53*(5), 768-785.

[50] Vaziri, G., Almasganj, F., & Jenabi, M. S. (2008, May). On the fractal self-similarity of laryngeal pathologies detection: the estimation of hurst parameter. In *Information Technology and Applications in Biomedicine, 2008. ITAB 2008. International Conference on* (pp. 383-386). IEEE.

[51] Vaziri, G., Almasganj, F., Behroozmand, R. (2010). Pathological assessment of patients' speech signals using nonlinear dynamical analysis. *Comput. Biol. Med.*, *40* (1), 54–63.

[52] Staroniewicz, P., Majewski, W. (2009). Polish emotional speech database–recording and preliminary validation. In *Cross-Modal Analysis of Speech, Gestures, Gaze and Facial Expressions* (pp. 42-49). Springer Berlin Heidelberg.

[53] Liberman, M., Davis, K., Grossman, M., Martey, N. & Bell, J. (2002). Emotional Prosody Speech and Transcripts. *Linguistic Data Consortium, Philadelphia,* http://www.ldc.upenn.edu/.

In order to meet the requirements established by the University of Las Palmas de Gran Canaria to obtain the doctoral degree, the next chapter of this document comprises a summary in Spanish of the above contents.

UNIVERSIDAD DE LAS PALMAS DE GRAN CANARIA

INSTITUTO UNIVERSITARIO DE SISTEMAS INTELIGENTES Y APLICACIONES NUMÉRICAS EN INGENIERÍA

PROGRAMA DE DOCTORADO

SISTEMAS INTELIGENTES Y APLICACIONES NUMÉRICAS EN INGENIERÍA

Resumen de la Tesis Doctoral

Avances en Monitorización Preventiva de Maquinaria a tráves de Señales de Audio y Vibración[1]

Autora: Patricia Henríquez Rodríguez

Directores: Dr. D. Miguel Ángel Ferrer Ballester
Dr. D. Jesús Bernardino Alonso Hernández

Las Palmas de Gran Canaria, 22 de Octubre de 2015

[1]El presente documento ha sido realizado a partir de la financiación del Programa de Formación del Personal Investigador de la Agencia Canaria de Investigación, Innovación y Sociedad de la Información del Gobierno de Canarias con una tasa de confinanciación del 85% del Fondo Social Europeo y de los proyectos TEC2009-14123-C04 y TEC2012-38630-C04-02 del Ministerio de Economía y Competitividad del Gobierno de España.

Resumen de la Tesis

1 Introducción

La maquinaria en general y los equipos industriales en particular se deterioran a lo largo del tiempo por el estrés que sufren durante su vida operativa. El fallo inesperado en una máquina trabajando en un entorno industrial puede tener consecuencias graves tanto desde el punto de vida humano, por el posible accidente que pueda causar, como desde el punto de vista de costes de productividad. Es por ello que el mantenimiento de equipos industriales se ha convertido en un aspecto estratégico en muchas empresas. La palabra mantenimiento se emplea para designar las técnicas usadas para asegurar el uso correcto y continuo de maquinaria, equipos e instalaciones. Monitorizar de forma continua el estado de funcionamiento (o condición) de un activo físico (una máquina, parte de una máquina o un sistema compuesto de varias máquinas) es de vital importancia para la detección temprana de fallos y tiene una gran influencia en la continuidad operacional de muchos procesos industriales. Ayuda a reducir costes de

mantenimiento e incrementa la seguridad y confiabilidad de los equipos industriales. En la siguiente tabla se muestran en porcentajes las ventajas del uso de un sistema de monitorización de la maquinaria [1].

TABLA 1: VENTAJAS DE UN SISTEMA DE MONITORIZACIÓN [1]

Costes de mantenimiento	Reducción del 50% al 80%
Daños en los equipos	Reducción del 50% al 60%
Gastos en horas extras	Reducción del 20% al 50%
Esperanza de vida de la máquina	Incremento del 50% al 60%
Productividad total	Incremento del 20% al 30%

Los costes de mantenimiento se reducen debido al hecho de que se detectan fallos incipientes, evitando que dichos fallos crezcan y se conviertan en un problema grave y caro. Se reduce la probabilidad de aparición de fallos destructivos que dañen a los equipos y afecten a la seguridad de las personan. Se reducen las actividades de reparación y por lo tanto las horas extras dedicadas a ello. La esperanza de vida de la máquina se incrementa así como la productividad total puesto que se evitan paradas innecesarias de la maquinaria.

El interés creciente en las técnicas de monitorización del estado de la maquinaria para la detección, diagnóstico y degradación de fallos tanto en el campo de la investigación como en el de la industria es evidente por la gran cantidad de artículos publicados en el campo, por los esfuerzos de las organizaciones de estandarización (ISO, SAE, etc) y por la organización de diferentes conferencias en el campo del diagnóstico de fallos, como por ejemplo la conferencia COMADEM (*Condition Monitoring and Diagnostic Engineering Management*).

Técnicas de mantenimiento

Desde tiempos antiguos, la humanidad ha usado diferentes técnicas de mantenimiento. Los hombres primitivos afilaban sus enseres y armas y cosían sus pieles. Durante la revolución industrial, se empezaron a usar relés de protección de sobre-corriente y protección de fallo de tierra mientras que los últimos desarrollos incluyen técnicas de procesado de la señal y reconocimiento de patrones.

Generalmente, las técnicas de mantenimiento se dividen en dos: mantenimiento correctivo y mantenimiento preventivo. Este último se introdujo en los años 1950 y se divide a su vez en mantenimiento preventivo predeterminado y en mantenimiento basado en la condición, conocido como CBM en sus siglas en inglés (*condition-based maintenance*). El mantenimiento basado en la condición también se denomina mantenimiento predictivo.

En el ***mantenimiento correctivo*** se toman acciones después de que el fallo haya ocurrido. Estas acciones van dirigidas a arreglar el fallo o a postponer su reparación de acuerdo al criterio de personal cualificado.

En el ***mantenimiento preventivo predeterminado***, se realizan actividades de mantenimiento planificadas a intervalos periódicos para evitar que los componentes se degraden hasta el punto de que la máquina deje de funcionar. La máquina o parte de la máquina se repara o se cambia antes de que ocurra un fallo.

Las técnicas correctivas y de mantenimiento preventivo predeterminado han demostrado ser bastante costosas puesto que muchas veces se realizan cambios de pieza innecesarios, al parar la máquina para realizar el cambio de pieza se para la producción con lo cual se aumentan los costes de producción. Además las actividades planificadas de mantenimiento sueles ser costosas. Por estas razones, algunas industrias empezaron a realizar mantenimiento basado en la condición en los años 1980.

El ***mantenimiento preventivo basado en la condición (CBM) o mantenimiento predictivo*** se refiere a la monitorización del estado de la máquina en la cual se obtiene de forma continua información de parámetros que indican el estado de la máquina. La desviación de los parámetros de la condición normal indica el desarrollo de un fallo. La CBM lleva a cabo acciones de mantenimiento sólo cuando hay evidencia de comportamiento anormal. La CBM reduce el número de actividades planificadas reduciendo por tanto costes [1].

Etapas de un sistema de monitorización basado en la condición

En la figura 1 se muestran las etapas típicas de un sistema de monitorización que implementa mantenimiento basado en la condición. Estas etapas incluyen la adquisición de datos, el procesado de los datos y un sistema de ayuda a la decisión. La salida del sistema de monitorización será el diagnóstico del fallo (detectar el fallo y saber dónde se ha producido) y posiblemente también la identificación del fallo (qué grado de severidad presenta el fallo) para así determinar qué tiempo de vida útil le queda al elemento que está siendo supervisado.

A continuación se detallan cada una de las etapas de un sistema de monitorización de la condición. Puesto que la presente Tesis se centra en diversos aspectos de las distintas etapas de un sistema de monitorización de la condición, se explicará en cada etapa en qué se centra la presente Tesis.

Adquisición de datos: esta etapa consiste en la obtención de información relevante sobre el estado de la máquina. Los datos adquiridos pueden variar según la clase de máquina o la naturaleza del fallo. La información adquirida puede ser de muchos tipos [2]: datos de tipo valor como presión, temperatura, datos de análisis de aceite; datos de forma de onda (es decir, señales) como señales de vibración, de audio, señales de emisión acústica; y datos multidimensionales como imágenes. El conjunto de datos adquiridos se denomina firma de la máquina. La presente Tesis se centra en señales de vibración y en señales de audio como fuente de información.

Procesado de datos: los datos obtenidos en la etapa anterior se analizan para obtener información que permita detectar un posible fallo o diagnosticarlo. En esta Tesis se usan técnicas de procesado de la señal para analizar los datos y extraer información valiosa para la monitorización de la condición. Este proceso se denomina extracción de características.

Sistema de ayuda a la decisión o la clasificación de los datos previamente analizados en diferentes estados de la condición. En esta Tesis, se usan técnicas de reconocimiento de patrones, en concreto dos clasificadores que permiten, una vez entrenados, diagnosticar de forma automática el estado de la máquina.

Diagnóstico de fallos/Predicción de fallo. El objetivo de un sistema de monitorización de la condición es el diagnóstico e identificación de fallos. El diagnóstico de fallo consiste en la detección del fallo, que responde a la pregunta "¿hay un fallo?" y al aislamiento del fallo, que responde a la pregunta "¿dónde está el fallo?" usando las etapas mencionadas. La identificación del fallo se refiere a la determinación de la severidad o el tamaño del fallo y a veces también a la determinación del tiempo de comienzo del fallo (o predicción del fallo). En esta Tesis, se realiza diagnóstico de fallo e identificación de fallo.

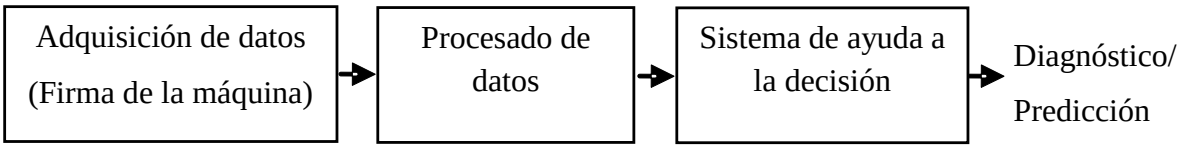

Figura 1: Etapas de un sistema de monitorización basado en la condición

Diagnóstico de fallos basado en vibración y audio: cojinetes y bombas centrífugas

Tal y como se ha explicado en el apartado anterior en las etapas de un sistema de monitorización basado en la condición, a la hora de adquirir datos de la máquina se pueden usar multitud de datos diferentes. En esta Tesis nos centramos en señales de vibración y de audio (en el espectro audible 0-20kHz). Es por eso que en este sub-apartado se introduce el diagnóstico de fallos basados en estas dos señales.

Asimismo, la investigación de la Tesis se centra en dos aplicaciones: cojinetes y bombas centrífugas. Los cojinetes son elementos esenciales en las máquinas rotativas puesto que soportan la estructura de la máquina permitiendo y facilitando su rotación.

Un fallo no detectado en un cojinete puede causar una avería catastrófica (contactos indeseados entre partes fijas y móviles de la máquina, bloqueo del motor, etc.). Las máquinas rotativas están muy extendidas en la industria. Ejemplos de máquinas rotativas son los motores y los generadores. Debido a la gran utilización de este tipo de máquinas, la aplicación de técnicas encaminadas a la vigilancia y control del estado de los cojinetes adquiere suma importancia. Aunque el coste de los cojinetes en comparación con la máquina en sí es muy bajo, el hecho de que haya que desmontar la máquina casi en su totalidad para cambiar un cojinete hace que las técnicas de monitorización basadas en la condición sean muy útiles para permitir que estos elementos funcionen hasta el máximo de su vida útil.

Por otra parte, las bombas centrífugas son máquinas que forman parte importante de muchos sistemas, puesto que permiten el movimiento de fluidos entre dos puntos del sistema. Se usan en la industria eléctrica, en la química, en la industria de extracción de petróleo, en sistemas de refrigeración, en spas y piscinas, etc. Por lo tanto, la monitorización de esta clase de máquinas es muy importante para el correcto funcionamiento de muchos sistemas industriales.

Tanto en los cojinetes como en las bombas centrífugas, así como en muchas otras clases de máquinas su monitorización se hace atendiendo normalmente a señales de vibración. Por supuesto también se usan otro tipo de datos como la corriente, voltaje o temperatura en el caso de los cojinetes y la presión en el caso de las bombas centrífugas. El diagnóstico de fallos basado en vibración (*vibration-based fault diagnosis*) se refiere al diagnóstico de fallos usando la señal de vibración como fuente de información. El diagnóstico de fallos basado en vibración es un área de estudio muy

desarrollada que incluye un amplio rango de técnicas que han evolucionado de forma rápida durante las últimas décadas. En la monitorización de la condición, las técnicas de diagnóstico de fallos basadas en vibración han sido ampliamente usadas debido a la facilidad de adquirir la señal de vibración de la máquina. Por esta razón, la mayoría de los artículos de investigación en la literatura del diagnóstico de fallos están enfocados al diagnóstico de fallos basado en vibración [2],[3],[46].

El diagnóstico de fallos basado en audio se refiere al diagnóstico de fallos usando la señal de audio como fuente de información (*audio-based fault diagnosis* o también llamado *airborne fault diagnosis*). El diagnóstico de fallos basado en audio usando micrófonos en el rango audible (0-20kHz) es un campo emergente con un gran potencial en el campo del diagnóstico de fallos puesto que los micrófonos son sensores no invasivos (no van montados encima de la máquina) y tienen mayores posibilidades de localización que los acelerómetros. Además, el uso de señales de audio podría mejorar la inspección de ciertos entornos industriales en los cuales un sistema de monitorización fijo es caro o el montaje de los sensores de vibración es complicado como por ejemplo en la industria de extracción de petróleo. Por estas razones, pensamos que el diagnóstico basado en audio necesita más esfuerzos de investigación. De hecho, la monitorización de la condición con señales de audio presenta menos estudios científicos que la vibración [2],[3],[46].

Por lo tanto, esta Tesis se enfoca en dos aplicaciones: cojinetes y bombas centrífugas. En el caso de los cojinetes se usan diferentes bases de datos de vibración públicas y nos centramos tanto en el diagnóstico de fallo como en la identificación del fallo (severidad del fallo). La investigación se ha enfocado en la etapa de procesado de

datos, proponiendo nuevos métodos basados en técnicas no lineales para extraer características que permitan diagnosticar e identificar fallos en cojinetes. Para evaluar la habilidad a la hora de discriminar entre fallos se usan dos clasificadores: redes neuronales y máquinas de soporte vectorial de mínimos cuadrados (*LS-SVM*).

En el caso de bomba centrífuga, nos centramos tanto en señales de vibración como en señales de audio. Al no haber bases de datos públicas, se ha creado una base de datos propia en la que se han adquirido señales de vibración y audio de forma simultánea de una bomba centrífuga de circulación. La intención es explorar el uso de las señales de audio en el diagnóstico de diversos fallos en la bomba centrífuga y comparar los resultados con los obtenidos con las señales de vibración, así como evaluar la combinación de ambos tipos de señales. Nos enfocamos igualmente en la etapa de procesado de datos, extrayendo características del estado del arte y proponiendo 31 nuevas características. Para evaluar la habilidad a la hora de discriminar entre fallos se usan los dos clasificadores comentados.

Estructura de la memoria de la Tesis

La memoria de la Tesis se estructura de acuerdo al tipo de estructura tradicional compleja [4] con una revisión de la técnica (o estado del arte) y dos aplicaciones diferentes (cojinetes y bombas centrífugas) donde se proponen métodos que se aplican en estudios experimentales. A continuación se realiza un breve resumen de cada capítulo de la memoria:

El capítulo 1 de la memoria introduce el tema de la monitorización del estado de maquinaria. Se expone la motivación de la presente Tesis, así como los objetivos, la metodología y las aportaciones realizadas. También se expone la estructura de la memoria.

En el capítulo 2 se realiza una revisión del estado de la técnica centrándose en las diferentes etapas de un sistema de monitorización basado en la condición (adquisición de datos, procesado de datos y sistema de ayuda a la decisión). En concreto, el capítulo se centra en trabajos que utilizan señales de vibración y audio como fuente de información, en técnicas de procesado de la señal para extraer características de las señales de audio y vibración y en técnicas de reconocimiento de patrones para ayudar a diagnosticar e identificar el fallo. La mayoría de máquinas o partes de máquinas analizados en el estado del arte de la presente Tesis son cojinetes, engranajes, motores y bombas. La motivación de la Tesis se basa en el análisis del estado del arte. Además, el estado del arte realizado es una aportación de esta Tesis. De hecho, la redacción del capítulo 2 está basada en un artículo de revista con índice de impacto publicado por la doctoranda [46].

El capítulo 3 se centra en las dos áreas de aplicación de la Tesis, cojinetes y bombas centrífugas y en las bases de datos utilizadas y generadas de ambos elementos. En el caso de los cojinetes se dan nociones básicas de los cojinetes y de cómo es la señal de vibración producida por ellos en estado de normalidad y en caso de fallo puntual. También se explican las bases de datos de vibración de cojinetes que han sido recopiladas de Internet para formar un corpus. Esta es otra aportación de la presente Tesis. En cuanto a la aplicación de la bomba de agua, se describe el funcionamiento de

las bombas centrífugas así como los tipos de fallos más comunes en ellas. También se explica de forma detallada el proceso de adquisición de la base de datos de vibración y audio de la bomba centrífuga, así como la generación de los diversos fallos y la estructura final de la base de datos. La base de datos generada es otra aportación de la presente Tesis.

El capítulo 4 se centra en las aportaciones realizadas en cojinetes. En concreto en el diagnóstico e identificación de fallos en cojinetes usando señales de vibración como fuente de información. Se explican los dos métodos propuestos que están basados en técnicas no lineales. La redacción del capítulo 4 de la presente Tesis está basada en tres publicaciones, una de ellas en revista con índice de impacto [47]-[49].

El capítulo 5 se centra en las aportaciones realizadas en la aplicación de la bomba centrífuga en el diagnóstico de fallos usando señales de audio y de vibración. El capítulo expone la metodología a aplicar en este estudio, se describen las características que se usan en la literatura del diagnóstico de fallos de bombas centrífugas usando señales de vibración y de audio así como también las características propuestas en esta Tesis. Finalmente se muestran los resultados de la evaluación de las características a la hora de discriminar entre los diferentes fallos y normalidad. Parte de la redacción del capítulo 5 está basada en dos publicaciones [51], [52].

El capítulo 6 se centra también en la aplicación de la bomba centrífuga. En este caso se realiza un estudio de la combinación de la información aportada por las señales de vibración y de audio y se presentan los resultados obtenidos.

Los capítulos 4, 5 y 6 tienen una parte introductoria donde se explica la metodología usada, una segunda parte donde se aplica la metodología a las bases de datos y una parte de resultados y conclusiones.

Con el capítulo 7 se concluye la tesis con un resumen de las aportaciones realizadas, los resultados obtenidos y las conclusiones generales y particulares obtenidas. Asimismo se describen las líneas futuras.

El anexo de la Tesis es un capítulo extra donde se muestra un resumen de la aplicación de algunas de las técnicas no lineales descritas durante la Tesis a la señal de voz en dos aplicaciones: detección de patologías laríngeas y detección de emociones. Es necesario resaltar que la doctoranda inicia su investigación en el campo de la señal de voz y que ha continuado con esa línea de investigación en paralelo con el desarrollo de la presente Tesis.

En la figura 2 se muestra la dependencia entre los capítulos de la memoria de Tesis. Para leer el capítulo 2 en necesario haber leído el capítulo 1. El capítulo 3 puede ser leído sin leer el capítulo 2 aunque se recomienda su lectura. Los capítulos 4, 5 y 6 deben ser leídos después del capítulo 3 y el capítulo 6 después del capítulo 5.

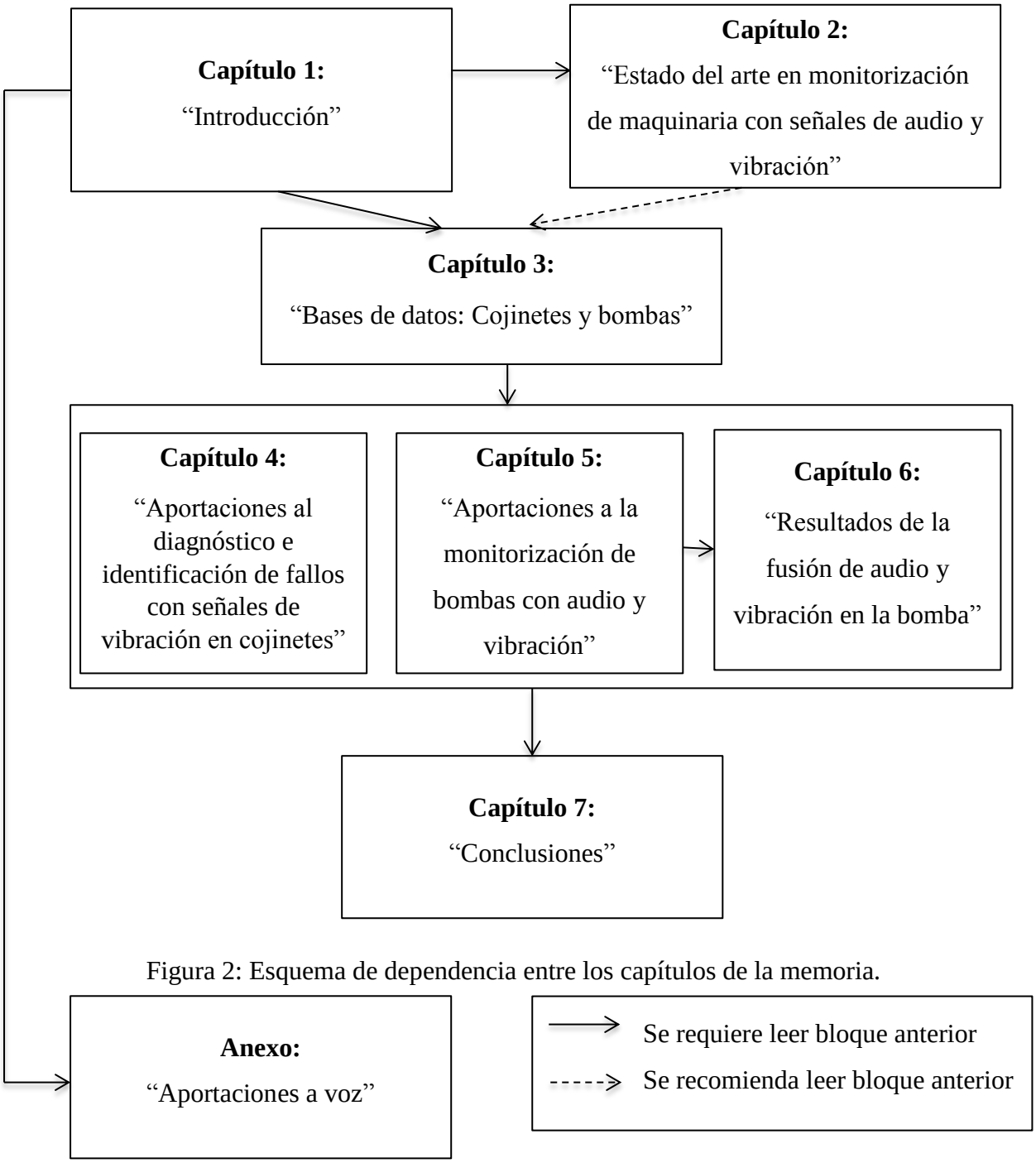

Figura 2: Esquema de dependencia entre los capítulos de la memoria.

Figura 2: Esquema de dependencia entre los capítulos de la memoria.

2 Planteamiento

En este apartado se expone la motivación y planteamiento de la Tesis que están basados en al análisis del estado del arte de monitorización de la condición en señales de audio y vibración [2], [3], [46].

En la figura 3 se muestra la distribución de los artículos de investigación analizados para llevar a cabo la redacción del estado del arte de la presente Tesis [46]. Se observa la distribución de los artículos por tipo de señal utilizada para realizar la monitorización (parte superior izquierda), también se muestra la distribución por años de los artículos revisados (parte superior derecha), la distribución de fallos en diferentes elementos de la maquinaria cuando se usan señales de vibración (parte inferior izquierda) y cuando se usan señales de audio (parte inferior derecha).

Como se observa en la figura 3 y como se corrobora en anteriores estados del arte [2], [3], la monitorización del estado de la máquina basada en señales de vibración es ampliamente usada. Esto es razonable por los siguientes dos aspectos: la facilidad de adquirir la firma de la máquina usando sensores de vibración y el hecho de que el camino de transmisión entre la máquina (o parte de la máquina) que es monitorizada y el sensor es menos sensible a interferencias indeseadas, cosa que no sucede en igual medida con las señales de audio. Por esto, en las aplicaciones que usan el audio como fuente de información se suele colocar el sensor entre 2cm y 20cm alejado del elemento que se quiere monitorizar [12].

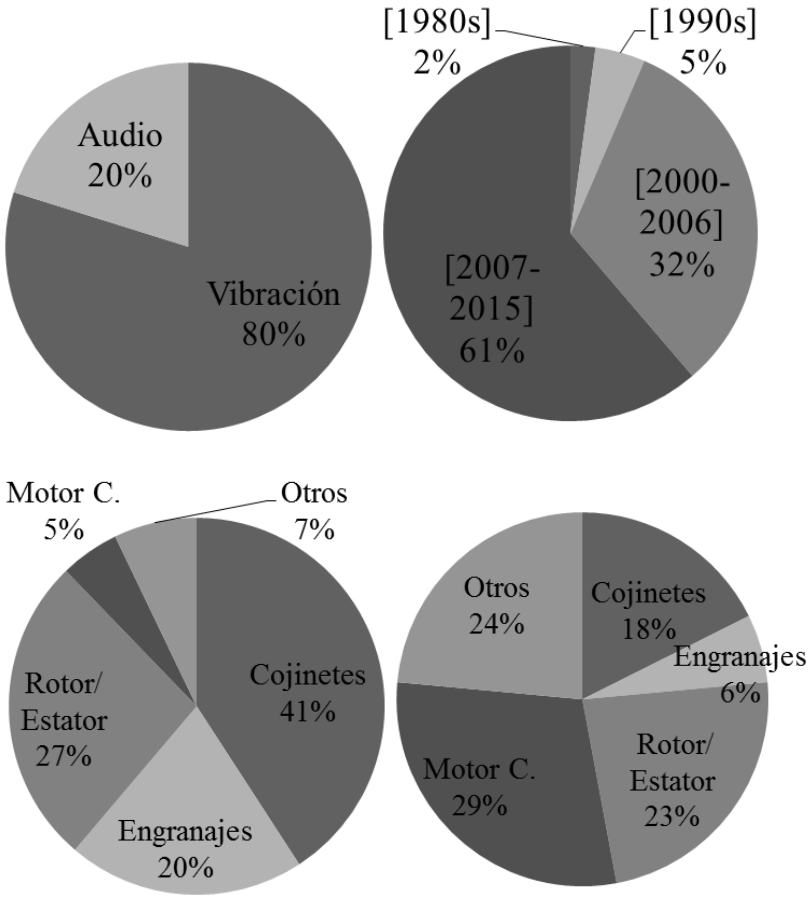

Figura 3: Distribución de los artículos usados para la redacción del estado del arte: distribución de artículos basados en señales de vibración y basados en señales de audio (superior izquierda); años de publicación de los artículos (superior derecha); distribución de elementos donde se producen los fallos analizados con señales de vibración (inferior izquierda) como con señales de audio (inferior derecha).

De la figura 3 se puede observar también que una gran cantidad de fallos se produce en los cojinetes. De hecho, de acuerdo con una encuesta sobre confiabilidad de motores [6] el 42% de los fallos de motores de más de 200 caballos de potencia se deben a fallos en los cojinetes. Motores de menor caballaje presentan aún más porcentaje de fallos en los cojinetes, llegando a ser del 90% [7]. Como ya se ha comentado en la introducción, las técnicas de monitorización de la condición son muy útiles para detectar si un cojinete presenta algún tipo de fallo. También en la figura 3 se puede observar que la mayor parte de la monitorización de cojinetes se realiza usando

señales de vibración. Por otra parte, a lo largo de la elaboración del estado del arte se realizó una búsqueda exhaustiva de bases de datos públicas, de libre acceso y gratuitas. Fruto de esa búsqueda se obtuvieron tres bases de datos de señales de vibración de cojinetes [30]-[32]. Basándonos en estas observaciones derivadas del estado del arte, la primera parte de esta Tesis se centra en el estudio de señales de vibración de cojinetes para el diagnóstico e identificación de fallos.

En la literatura de diagnóstico de fallos de cojinetes se encuentra una amplia variedad de técnicas de procesado de la señal usadas para extraer características de la señal de vibración en diferentes dominios de representación: dominio del tiempo [37], de la frecuencia [9], cepstral [10], tiempo-frecuencia [11]-[15], así como técnicas no lineales basadas en medidas de dinámica no lineal y medidas de complejidad y predictibilidad [28], [43]. Las técnicas no lineales permiten extraer características de la firma de la máquina que pueden revelar un entendimiento más preciso de la señal. De hecho, se han encontrado indicios de no linealidad en el funcionamiento de cojinetes [28]. Por este motivo, en la fase de procesado de la señal (en donde se extraen las características), nos hemos centrado en el estudio de técnicas no lineales dentro de la aplicación de los cojinetes tanto para diagnóstico como para identificación de fallos.

Si bien la monitorización usando señales de vibración es mucho más usada en comparación con el audio, en los últimos años se ha incrementado la investigación en torno a la monitorización basada en señales de audio [5],[19]-[27]. Además, si bien la localización de los micrófonos debe de ser lo más cercana posible a la máquina para evitar en la medida de lo posible interferencias con otros elementos, estos tienen más posibilidades de localización que los sensores de vibración [5]. Además, no tienen que

ser montados en la máquina, por lo que son elementos no invasivos en absoluto. Basándonos en estas observaciones, la segunda parte de la presente Tesis se centra en explorar la monitorización del estado de la máquina usando señales de audio.

Puesto que hay una carencia de bases de datos públicas de señales de audio en diagnóstico de fallos en maquinaria, en la presente Tesis se opta por grabar una base de datos propia. Dicha base de datos consta de señales de audio y de señales de vibración adquiridas simultáneamente de una bomba centrífuga de agua. Se adquieren también señales de vibración para comparar resultados.

Como ya hemos explicado, las señales de audio son menos usadas que las de vibración en el campo de diagnóstico de fallos, y el caso de las bombas centrífugas no es una excepción. Es por esto que la mayoría de características usadas en diagnóstico de fallos en bombas de agua son extraídas de señales de vibración. Por este motivo, en esta Tesis se realiza un estudio de las medidas usadas en señales de vibración para diagnóstico de fallos en bombas centrífugas y estas medidas se extraen también de las señales de audio. De igual forma se pretende, en base al estudio de las señales de audio y vibración de la bomba centrífuga proponer otras medidas que sean capaces de discriminar entre diferentes estados de normalidad y fallo de la bomba centrífuga.

Otra conclusión que se puede extraer al analizar el estado del arte es que hay escasos estudios en los que se trabaje conjuntamente con señales de audio y vibración [5], [22], [23]. Es por este motivo que en la presente Tesis se realiza un estudio de la combinación de señales de audio y vibración.

3 Objetivos

El objetivo de la presente Tesis es la mejora de los sistemas de monitorización del estado de la maquinaria en diagnóstico e identificación de fallo usando señales de vibración y de audio en dos aplicaciones (cojinetes y bombas de agua) con especial énfasis en la etapa de extracción de características y en la utilización del audio como fuente de información audio.

El objetivo de la presente Tesis puede ser dividido en objetivos parciales que deben ser alcanzados para lograr el objetivo general. Seguidamente se exponen los objetivos parciales:

1. Realizar una revisión general de las técnicas de procesado de señal usadas para la extracción de diferentes características así como de las técnicas reconocimiento de patrones usadas en el diagnóstico de fallos de maquinaria usando señales de vibración y de audio.

2. Realizar una búsqueda de bases de datos de vibración de cojinetes sin fallo y con diferentes tipos de fallos para generar así un repositorio de bases de datos con las que trabajar.

3. Desarrollar métodos no lineales que ayuden al diagnóstico y a la identificación de fallos en cojinetes.

4. Generar una base de datos de audio y vibración de una bomba centrífuga en diferentes estados de funcionamiento (sin fallo y con diferentes tipos de fallos) para poder realizar una evaluación de la capacidad de las señales de audio en el diagnóstico de fallos y compararlas con las señales de vibración.

5. Aplicar características del estado del arte usadas comúnmente en señales de vibración de bombas centrífugas a las señales de audio captadas de una bomba centrífuga y cuantificar la capacidad de las medidas en la discriminación entre varios estados de funcionamiento de la bomba centrífuga (estado normal y estados de fallo).

6. Buscar nuevas medidas para diagnóstico de fallos en bombas centrífugas y cuantificar su capacidad de discriminación entre varios estados de funcionamiento de la bomba centrífuga.

7. Comparar los resultados obtenidos con señales de vibración y de audio.

8. Realizar un estudio de utilización conjunta de señales de audio y vibración en la monitorización de una bomba centrífuga

4 Metodología

En el presente apartado se expone la metodología seguida en la presente Tesis para cumplir los objetivos propuestos.

Estado del arte

En primer lugar se realiza un estudio exhaustivo del estado de la técnica o estado del arte en el ámbito de la monitorización de maquinaria con señales de audio y vibración. Nos centramos en el estudio de técnicas de procesado de la señal para extraer características y en técnicas de reconocimiento de patrones usadas para discriminar entre diferentes estados de funcionamiento de la máquina. En el capítulo 2 de la Tesis se encuentra el estado del arte junto con un análisis crítico del mismo.

Obtención y generación de bases de datos

Se realiza una búsqueda de bases de datos que comprendan muestras de cojinetes en estado de funcionamiento normal (sin fallo) y funcionando con diversos fallos. Las bases de datos obtenidas son de vibración y están disponibles en internet [30]-[32]. Una de las bases de datos [30] comprende señales de vibración de cojinetes sin fallos y de cojinetes con fallos puntuales en el anillo externo (*outer-race fault*), en el anillo interno (*inner-race fault*) y con fallo en los elementos de rodamiento (*ball fault*). A modo de ilustración, en la figura 4 se muestran los diferentes elementos que componen un cojinete. Las otras dos bases de datos [31], [32] son *test-to-failure*. Es decir, se graba la señal de vibración hasta que el cojinete o cojinetes tienen un fallo.

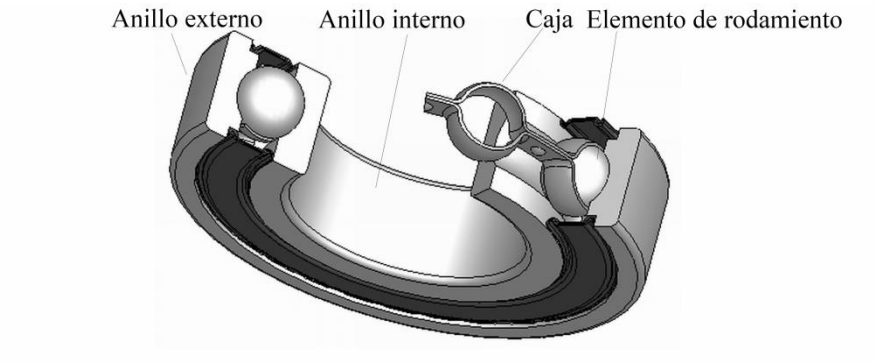

Figura 4: Componentes de un cojinete cuyo elemento de rodamiento son bolas.

Por otra parte, dado que no hay bases de datos públicas con señales de audio proveniente de maquinaria, se decide grabar una base de datos propia de señales de audio y vibración adquiridas de forma simultánea de una bomba de agua centrífuga de circulación (modelo ALP800) en un circuito cerrado formado por la bomba en sí y un tanque con 50 litros de agua. Antes de proseguir con la base de datos generada se explicará brevemente los principales elementos de una bomba centrífuga.

Una bomba centrífuga consta de dos elementos fundamentales, el rodete y la voluta. El rodete es el elemento rotatorio y la voluta el elemento estacionario. El rodete convierte la energía suministrada por el motor en energía cinética. La rotación del rodete fuerza al líquido a circular a través de la bomba desde la dirección axial hasta la dirección radial mientras se transfiere energía al líquido bombeado. La voluta convierte la energía cinética en energía de presión. En resumen, el rodete produce velocidad en el líquido y la voluta convierte dicha velocidad en presión. A modo de ilustración en la figura 5 se muestran las diferentes partes de una bomba de agua. Se indica también la dirección de fluido o líquido bombeado.

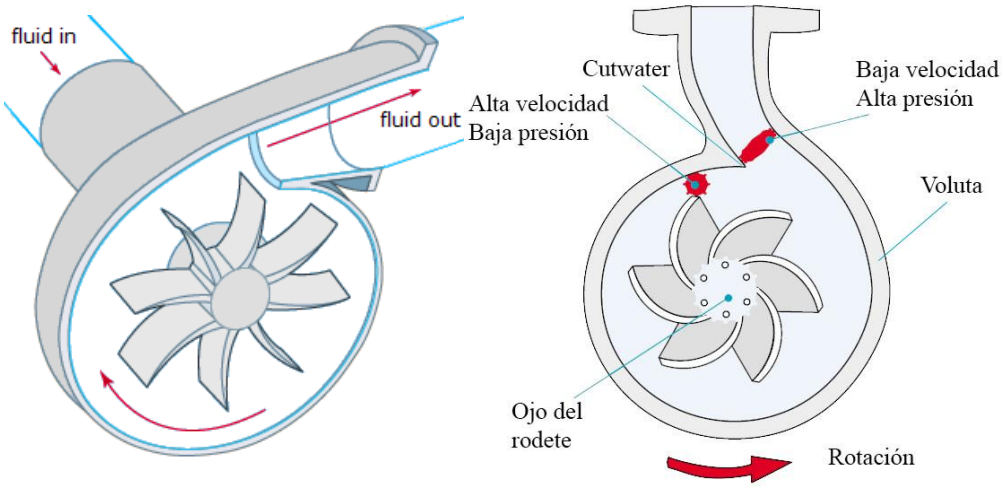

Figura 5: Partes principales de una bomba centrífuga. Dirección del fluido en la bomba (figura izquierda). Fuente: [32]. *Fluid in*: entrada del fluido. *Fluid out*: salida del fluido. Velocidad y presión del fluido en una bomba. Figura modificada de la fuente: [34].

En la figura 6 se muestra un rodete y se indican las diferentes partes que lo conforman. El rodete de una bomba centrífuga presente una serie de vanos delimitados por palas curvadas. Dichas palas también se denominan álabes. Los álabes son los que imparten fuerza centrífuga al fluido. Un rodete cerrado como el que se muestra en la figura 6 tiene platos en ambos lados que encierran completamente el rodete desde el ojo de succión (u ojo de rodete) a sus bordes. El ojo de rodete es la parte central del rodete. La región del álabe más cercana al ojo del rodete se denomina *leading edge* y la región en el borde del álabe se denomina *trailing edge*.

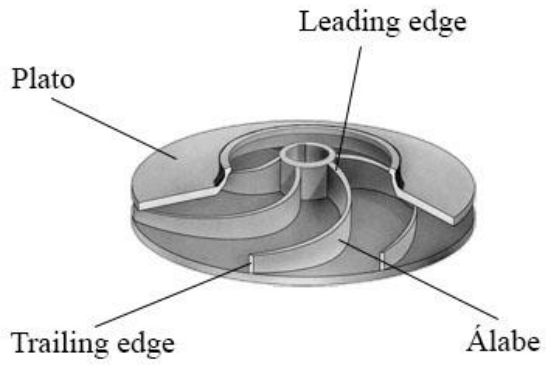

Figura 6: Partes de un rodete. Figura modificada de la fuente: [32].

En la figura 7 se muestra un plano de la sala donde se graba la base de datos de la bomba centrífuga. En el plano se observa un esquema del montaje realizado con la bomba (en verde), el tanque con 50 litros de agua (en celeste) y las tuberías que forman un circuito cerrado (en naranja). También se indica en la figura 7 la dirección de flujo del agua. La sala donde se graba la base de datos presenta 29dB de aislamiento acústico respecto a ruido aéreo.

En el montaje se usan 4 metros de tuberías de 3.81 cm de diámetro. La bomba usada es una bomba centrífuga circuladora de agua modelo ALP800 de 0.5 caballos de potencia y con 2925 RPM (revoluciones por minuto), equivalente a 48.75 Hz. El rodete de la bomba presenta 7 álabes.

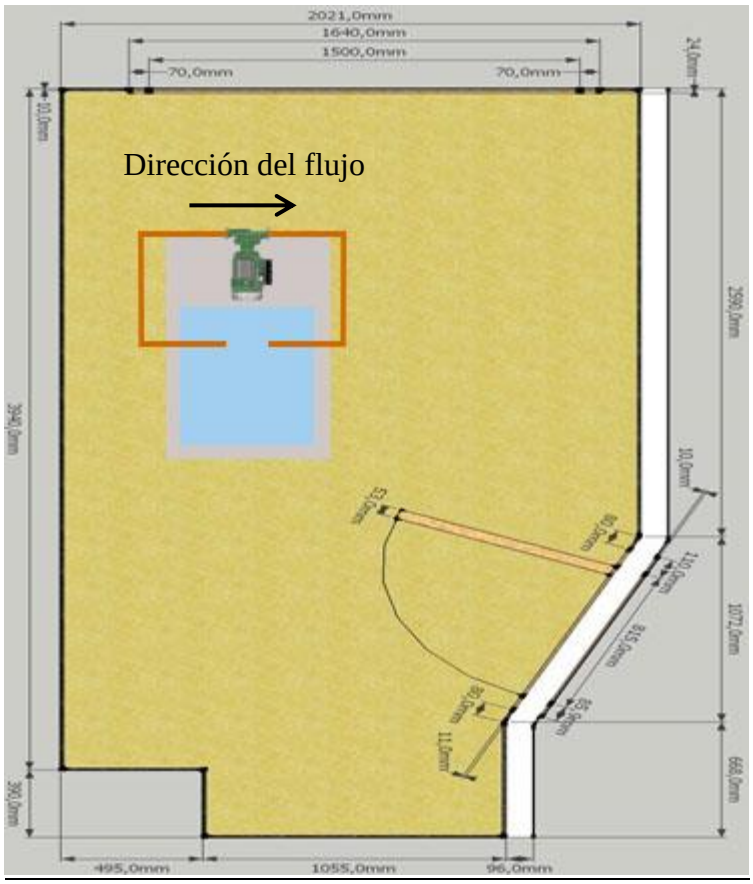

Figura 7: Esquemático de la sala donde se realiza la grabación de la base de datos junto con la posición y esquema del montaje.

En las figuras 8 y 9 se observan fotos de la bomba centrífuga modelo ALP800 utilizada para generar la base de datos de la presente Tesis. En la figura 7 se muestra la bomba de agua sin desmontar y en la figura 8 se muestra el rodete (foto de la izquierda) y la voluta.

Figura 8: Fotos de la bomba de agua modelo ALP 800.

Figura 9: Fotos de la bomba de agua modelo ALP 800. Rodete montado en el rotor (izquierda). Voluta, entrada y salida de la bomba (derecha).

Se graban diferentes estados de funcionamiento de la bomba: funcionando en estado normal (sin fallos) y con 8 tipos de fallos originados de forma artificial, excepto uno que se originó de forma espontánea. Los fallos generados responden a fallos típicos de bombas centrífugas: fallos en el rodete (también llamado impulsor), fallo en la goma de sellado y fallos del sistema.

Los fallos en el rodete generados incluyen fallos en el plato (o base) del rodete del rodete (ver figura 6), en el borde de los álabes cercano al ojo del rodete (*trailing edge*), en el borde superior de los álabes (*leading edge*) [35], [36]. Los fallos en el sistema incluyen la adición de diferentes elementos extraños al agua. Puesto que la bomba adquirida está diseñada para circular agua y en sus especificaciones se expone que debe ser usada con agua sin impurezas se añade al agua del tanque los siguientes elementos: arena, arena con papel y bolas de PVC de 6 mm de diámetro y 12 gramos de peso (una vez eliminada la arena y el papel). Cada vez que se daña un rodete, se cambia por uno nuevo para generar el siguiente fallo. En total se usan 4 rodetes. Además en los fallos del plato, del *leading edge* y del *trailing edge* se crearon 3 grados diferentes de severidad en cada caso.

En la figura 10 se muestran las diferentes severidades generadas en el plato del rodete consistentes en ir eliminando partes del plato.

Figura 10: Fotos del fallo en el plato del rodete. Rodete sin fallo (superior izquierda), rodete con una parte del plato eliminada (superior derecha), rodete con dos partes de plato eliminadas (inferior izquierda) y rodete con tres partes de plato aliminadas (inferior derecha).

En la figura 11 y 12 se muestran ejemplos de los fallos LED y TED respectivamente. En estos fallos se ha creado tres grados de severidad consistentes en el recorte de la longitud de los bordes de todos los álabes del rodete: recorte del 10% de la longitud total (5mm) , recorte del 20% de la longitud total (10mm) y recorte del 30% de la longitud total (15mm).

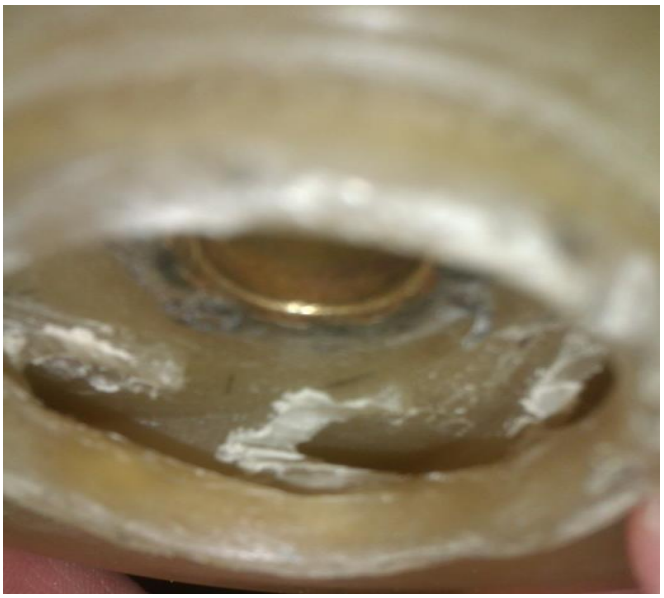

Figura 11: Foto del rodete con fallo en el *leading edge*. En la imagen se observa un recorte del borde *leading edge* de 5mm (fallo leve).

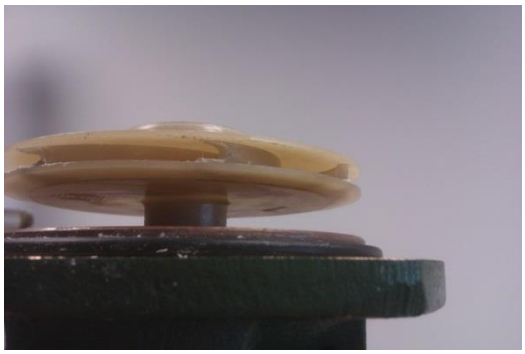

Figura 12: Foto del rodete con fallo en el *trailing edge*. En la imagen se observa un recorte del borde *trailing edge* de 5mm (fallo leve).

Para adquirir las señales se usan dos micrófonos y dos acelerómetros (sensores de vibración). En la figura 13 se observa la disposición de los micrófonos y de los acelerómetros usados. Ambos micrófonos tienen un ancho de banda de [3.15Hz-20kHz] y sensibilidad de 50mV/Pa. Están colocados apuntando a la entrada de agua de la bomba (micrófono etiquetado como *InletMicro*) y a la salida de agua de la bomba (micrófono etiquetado como *OutletMicro*) a unos 5 centímetros de la bomba.

En el montaje se usan dos acelerómetros, uno situado a la entrada de la bomba de agua y que tiene un ancho de banda [0.7Hz-10kHz] y sensibilidad 100mV/g (etiquetado como *RadialIneltAccel*) y otro situado encima de la voluta con ancho de banda [0.35Hz-2.6kHz] y sensibilidad 1000mV/g (etiquetado como *RadialAccel*).

Figura 13: Posición de los micrófonos y de los acelerómetros.

En resumen, la base de datos adquirida consta de 370 muestras por cada sensor de 59 segundos de duración cada una. En la siguiente tabla (tabla 2) se muestra la distribución de las muestras en diferentes clases (o estados de la bomba) así como el rodete usado en cada caso:

TABLA 2. CONDICIONES GRABADAS DE LA BOMBA CENTRÍFUGA.

Rodete #	Condición	Número de muestras por condición
1	Normal	20
1	Plato (severidad leve)	20
1	Plato (severidad media)	20
1	Plato (severidad alta)	18
2	Normal	20
2	Sellado	9
2	Arena	23
2	Arena y papel	62
2	Bolas de PVC	18
3	Normal	20
3	LED 5 mm (severidad leve)	20
3	LED 10 mm (severidad media)	20
3	LED 15 mm (severidad alta)	20
4	Normal	20
4	TED 5 mm (severidad leve)	20
4	TED 10 mm (severidad media)	20
4	TED 15 mm (severidad alta)	20

En el capítulo 3 se encuentran explicadas las diferentes bases de datos de cojinetes obtenidas y la generación de la base de datos de la bomba centrífuga.

Desarrollo de métodos no lineales para el diagnóstico e identificación de fallos en cojinetes con señales de vibración

Para desarrollar métodos para el diagnóstico e identificación de fallos en cojinetes usando señales de vibración, se realiza un estudio de las diferentes técnicas de procesado de la señal usadas para diagnóstico e identificación de fallos en cojinetes. Basándonos en ese estudio, se desarrollan dos métodos basados en técnicas no lineales, uno para el diagnóstico de fallos y otro para la detección e identificación del fallo (severidad del fallo). El método para el diagnóstico de fallos se basa en el operador no lineal Teager-Kaiser seguido de la extracción de características estadísticas y de energía. El método para la identificación de fallos se basa en la aplicación de la transformada

wavelet packet seguida de la complejidad de Lempel-Ziv. Los métodos propuestos se comparan con métodos presenten en la literatura del diagnóstico de fallos en cojinetes. La habilidad de las características propuestas para el diagnóstico de fallos en cojinetes se cuantifica utilizando dos clasificadores: un clasificador basado en redes neuronales y un clasificador de máquinas de soporte vectorial de mínimos cuadrados (LSSVM). En el caso de la identificación de fallo en cojinetes se propone un índice que determna la severidad del fallo en pista externa y pista interna y que además sigue la degradación de cojinetes con fallos en la pista externa.

Seguidamente se hace un breve resumen de la metodología aplicada a la hora de desarrollar los métodos propuestos.

Metodología para diagnóstico de fallos en cojinetes

Se realiza un estudio de diferentes técnicas de procesado de la señal con la finalidad de diagnosticar fallos en el anillo externo, en el anillo interno y en los elementos de rodamiento. Basándonos en este estudio se propone aplicar el operador no lineal Teager-Kaiser [40] a la señal de vibración de cojinete seguido de la extracción de características estadísticas y de energía con la finalidad de diagnosticar fallos en los diferentes elementos de un cojinete. Mediante la aplicación del operador Teager-Kaiser a la señal de vibración se obtiene otra señal que llamamos señal TK.

El objetivo es demostrar cómo las características estadísticas y de energía extraídas de la señal TK mejoran el diagnóstico de fallos en cojinetes con respecto a cuando se extraen las mismas características de la señal de vibración usando otros

métodos del estado del arte. En la figura 14 se observan el método propuesto (método 1) y los demás métodos del estado del arte que se evalúan: en el método 2 se extraen de la señal de vibración en el dominio del tiempo (señal T) las características estadísticas y de energía [8], en el método 3 se extraen de la señal de vibración demodulada en amplitud (señal AM) usando la técnica de análisis de envolvente comúnmente utilizada en cojinetes [39] y en el método 4 se extraen de la señal demodulada en amplitud obtenida a partir del operador Teager-Kaiser (señal TK-AM) [41].

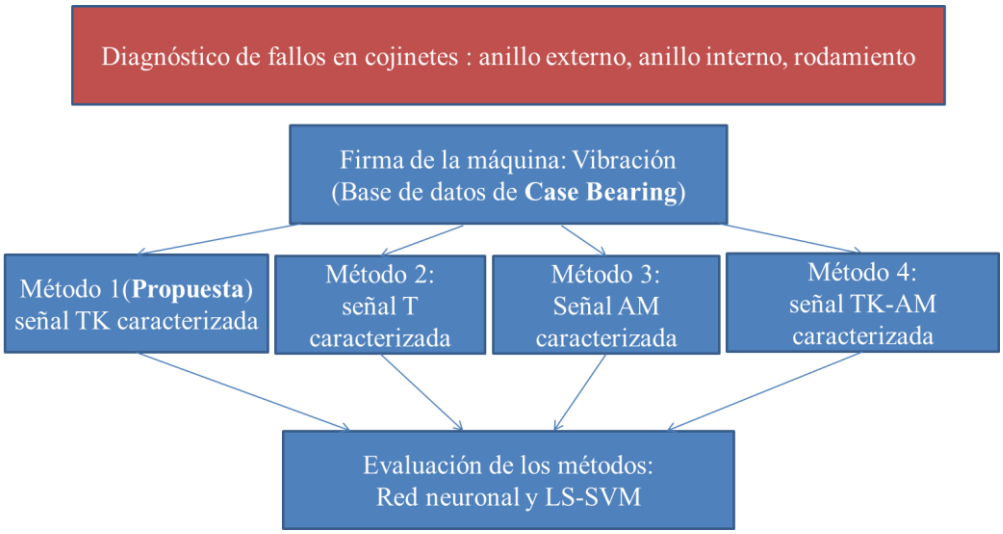

Figura 14: Esquema de la experimentación en diagnóstico de fallos de cojinetes.

Una vez obtenidas las características en cada uno de los métodos, se evalúa la habilidad de dichas características para discriminar entre normalidad y diferentes tipos de fallos de cojinetes. Para ello se realiza un estudio de relevancia de las características usando un método de selección de características denominado *sequential floating forward selection* (*SFFS*) [44]. El método de selección de características usado selecciona un subgrupo de características que mejores resultados dan a la hora de discriminar entre las diferentes clases del problema (en este caso entre normal, fallo en

cojinete externo, fallo en cojinete interno y fallo en rodamiento). La selección de características se aplica varias veces para obtener finalmente las características en orden de relevancia. Finalmente se usan dos clasificadores, uno de redes neuronales y otro de máquinas de soporte vectorial de mínimos cuadrados (*LS-SVM*) para evaluar las medidas ordenas por relevancia. Los resultados obtenidos con el método propuesto mejoran los obtenidos con los demás métodos comparados [47].

Es importante recalcar que a la hora de evaluar las características con los clasificadores se divide la base de datos en un conjunto de entrenamiento formado por el 70% de las muestras de cada clase y en un conjunto de test formado por el 30% de las muestras restantes. Con el conjunto de entrenamiento se ajustan los parámetros de los clasificadores usando la técnica de validación cruzada *k-fold* con $k = 3$. En el caso de las redes neuronales, donde el clasificador usado tiene la capa de entrada, la capa de salida y una capa oculta, se ajusta el número de neuronas de la capa oculta. En el caso del clasificador *LS-SVM* que ha sido programado para que utilice como *kernel* funciones de base radial Gaussiana, se ajusta el parámetro de regularización y el ancho de banda de la función de base radial Gaussiana.

Una vez aplicada la técnica propuesta a la base de datos de cojinetes que presenta fallos en diferentes partes de los mismos (base de datos *Case Western*) [30] se aplica la misma técnica a la base de datos de degradación del helicóptero [31] en la que un cojinete situado en una parte bastante inaccesible de uno de los trenes principales de transmisión de un helicóptero Black-Hawk tiene un fallo en uno de sus elementos rodantes al final de un test de resistencia. En la figura 15 se muestra el esquema de la propuesta aplicado a la degradación del cojinete. Los resultados usando el método

propuesto mejoran resultados obtenidos con esa misma base de datos a la hora de detectar el comienzo del fallo [49].

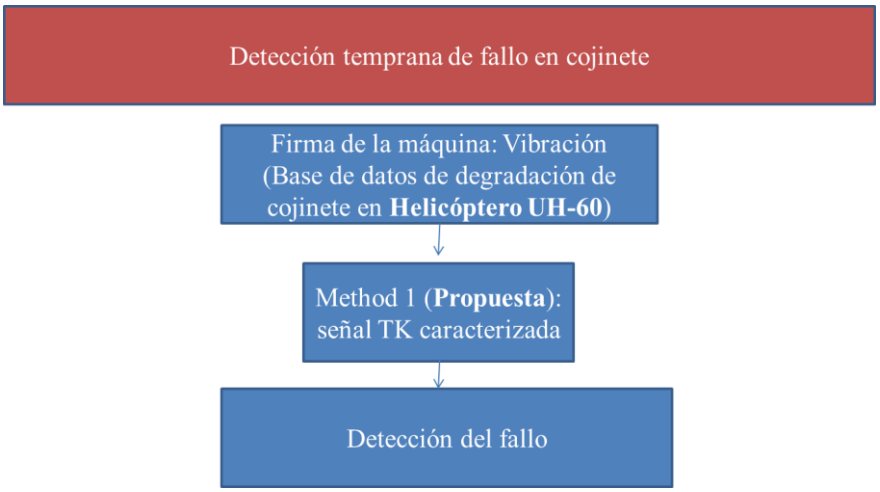

Figura 15: Diagrama de la aplicación del método propuesto a la degradación de un cojinete.

En la primera parte del capítulo 4 se encuentra el desarrollo del método propuesto y de la experimentación realizada junto con los resultados obtenidos.

Metodología para detección e identificación de fallo en cojinetes

Para desarrollar un índice que sirva para identificar la severidad del fallo en cojinete se realiza primeramente un estudio del estado de la técnica en técnicas de identificación de fallos (es decir, técnicas que son capaces de determinar la severidad del fallo en cuestión). Basándonos en ese estudio se propone la aplicación de la transformada *wavelet packet* a la señal de vibración seguida de la complejidad de Lempel-Ziv para la identificación de fallos en la cara externa y en la cara interna de cojinetes. El método es capaz de detectar fallo en los elementos de rodamiento, pero no de determinar la severidad del mismo. Además, el método propuesto es capaz de seguir de forma

monótona la evolución de fallos en cara externa. Se compara el método propuesto con otros tres métodos usados en la literatura: kurtosis, complejidad Lempel-Ziv aplicada a la señal de vibración sin preprocesar, kurtosis aplicado al nodo de máxima energía de la *wavelet packet* [37], [43]. También se realiza un estudio de la robustez del método propuesto frente a ruido blanco Gaussiano.

La figura 16 muestra un diagrama del método propuesto para la identificación de fallos en la cara externa e interna de cojinetes.

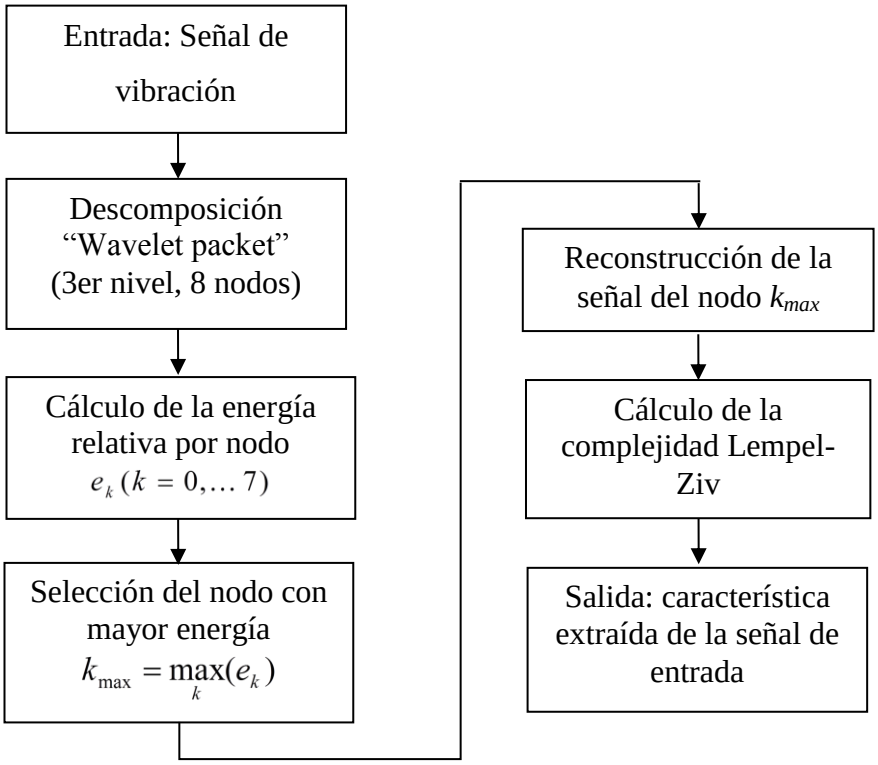

Figura 16: Método propuesto para la identificación de fallos en cojinetes.

Primero la señal de vibración se descompone usando la transformada *wavelet packet* con nivel de descomposición 3 (donde hay 8 nodos). La wavelet madre usada para la descomposición es la Daubechies 6 (db6) (ver figura 17) porque tiene una forma

de onda impulsiva, igual que la forma de onda de las señales de vibración de cojinetes con fallos puntuales. Una vez descompuesta la señal de vibración se reconstruye cada una de las señales de los nodos. Se calcula luego la energía de esas 8 señales con respecto a la energía de la señal de vibración original. Finalmente se selecciona el nodo con mayor energía relativa. Puesto que se ha usado una *wavelet* madre con forma impulsiva, el nodo con mayor energía será aquel donde se encuentre el fallo si lo hubiese. Así la transformada *wavelet* elimina partes de la señal indeseada y se centra en el fallo. Una vez obtenido el nodo con mayor energía se calcula la complejidad de Lempel-Ziv sobre la señal reconstruida del nodo de mayor energía. Con la complejidad de Lempel-Ziv se evalúa, como su propio nombre indica, la complejidad de la señal obtenida.

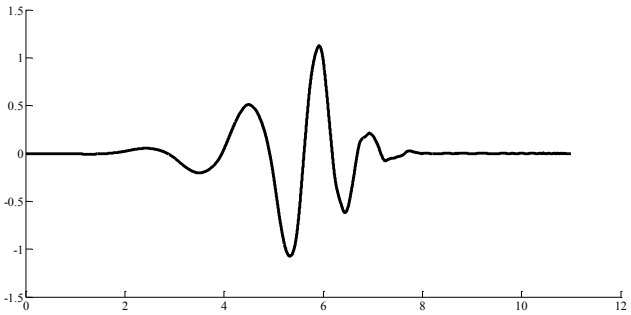

Figura 17: Forma de onda de la wavelet madre Daubechies 6.

El método propuesto se aplica a la base de datos *Case Western* [30] puesto que esta base de datos presenta señales de vibración de cojinete con fallos de diferente severidad (severidad leve, media y alta) en cara externa, cara interna y rodamiento. Asimismo también se aplican los otros tres métodos de la literatura mencionados anterioremente [42]. Los resultados obtenidos demuestran que el método propuesto da mejores resultados [52] sobre todo cuando se añade ruido blanco Gaussiano a las señales para comprobar lo robusto del algoritmo propuesto frente al ruido.

El método propuesto también se aplica a las otras dos bases de datos de cojinetes, las base de datos de degradación de cojinetes del *IMS* [32] y del helicóptero UH-60 (Black Hawk) [31]. En la base de datos del *IMS* el cojinete presenta un fallo de cara externa a lo largo del test *run-to-failure*. El método propuesto obtiene mejores resultados que los otros tres métodos con los que se ha comparado. En el caso de la base de datos del helicóptero, donde el fallo se produce en el elemento rodante del cojinete, los resultados no son tan satisfactorios y el método propuesto se comporta de forma similar el método de extraer la complejidad de Lempel-Ziv de la señal de vibración sin pre-procesar.

En la segunda parte del capítulo 4 se encuentra el desarrollo del método propuesto para la identificación de fallos en la cara interna y la cara externa de cojinetes así como la experimentación realizada junto con los resultados obtenidos.

Metodología usada para el diagnóstico de fallos en bomba de agua usando señales de audio y vibración

Una vez generada la base de datos de audio y vibración de la bomba centrífuga, nos centramos en el diagnóstico de los fallos generados en la bomba. El objetivo principal en este caso es determinar si con el audio como fuente de información se es capaz de distinguir entre los diferentes fallos de la bomba centrífuga. De igual forma se pretende comparar los resultados con los obtenidos usando señales de vibración.

La metodología usada para el diagnóstico de fallos en bomba de agua usando señales de audio y vibración se explica con la ayuda de la siguiente figura (figura 18).

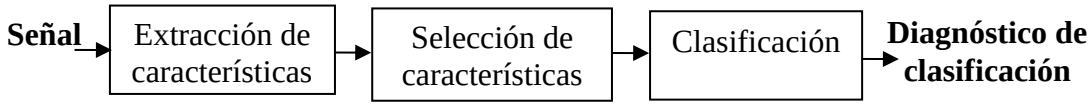

Figura 18: Esquema de la metodología llevada a cabo para cuantificar la habilidad de las características extraídas de la señal de audio y vibración en diagnóstico de fallos en bombas centrífugas.

Extracción de características

En el bloque de *Extracción de características* se extrae un conjunto de características tanto de la señal de vibración como de la señal de audio. En realidad, esto se hacer por sensor. Puesto que hay 4 sensores (2 de audio y 2 de vibración) se extraen características de las señales provenientes de los 4 sensores.

Las características que se extraen son características usadas en la literatura del diagnóstico de fallos en bombas centrífugas usando señales de vibración y de audio. Para identificar las características primero se debe realizar un estudio de las técnicas de procesado de la señal usadas en bombas centrífugas para el diagnóstico de fallos. Es necesario mencionar que puesto que la mayoría del diagnóstico de fallo en bombas centrífugas se realiza con señales de vibración así como con señales de presión, se encuentran escasas características que se hayan extraído usando el audio. Por ello las mismas características que se extraen de la señal de vibración se extraen también de la señal de audio.

Basándose en la inspección visual de las señales obtenidas en la base de datos generada, se proponen una serie de nuevas medidas no utilizadas anteriormente en el diagnóstico de fallos de bombas centrífugas.

Una vez identificadas las características del estado del arte y propuestas nuevas medidas, éstas se deben implementar.

Para extraer las características cada observación (o muestra) de la base de datos generada se divide en segmentos, también llamados tramas, de 8192 muestras cada uno, equivalentes a 371.5 ms. Las tramas se toman una cada tres por lo que si cada observación dura 59 segundos, tenemos 53 tramas por observación. Por cada una de las tramas se extrae el conjunto de características implementado. Antes de extraer las características a cada una de las observaciones se le quita la media y se normaliza entre -1 y 1.

Una vez extraídas las características por observación, se calcula el promedio de cada una de las características por observación.

Selección de características

Una vez que se extraen las características por observación de la base de datos, el objetivo es identificar aquellas más apropiadas por sensor que mejor discriminen entre los diferentes estados de la bomba centrífuga. El proceso de seleccionar características de un conjunto de características se denomina selección de características. Este proceso es importante puesto que la selección de características que aporten información relacionada con el fallo y el descarte de características que no aporten información mejora la tasa de éxito en el diagnóstico. Así pues, en el segundo bloque de la figura 18 se realiza la selección de características y un análisis de relevancia, el cual se explicó anteriormente cuando se explicó la metodología para el diagnóstico de fallos en cojinetes. Simplemente recordar que la técnica utilizada para la selección de

características se denomina *sequential floating forward selection* (*SFFS*) [44]. La razón por la que se ha elegido esta técnica de selección de características es porque es un método determinista y por lo tanto se obtendrán los mismos resultados cuando se repita. De igual forma el coste computacional de la técnica es bajo.

Después de aplicar la selección de características y de realizar el análisis de relevancia se obtendrá un conjunto de características por sensor.

Evaluación de las características: Clasificación

El bloque de clasificación de la figura 18 se utiliza para evaluar la capacidad de las características a la hora de discriminar entre los diferentes estados de la bomba centrífuga. Así que el clasificador nos dará una tasa de éxito en la clasificación de los diferentes estados de funcionamiento de la máquina.

El clasificador clasifica las observaciones en diferentes unidades de clasificación también llamadas clases con la información que obtiene las características. Las unidades de clasificación corresponden con los diferentes estados o condiciones de la máquina que se quieran clasificar. En la presente Tesis, se ha decidido implementar dos configuraciones diferentes, así que las unidades de clasificación consideradas son las siguientes (entre paréntesis está el acrónimo de la clase):

- 8 unidades de clasificación: estado normal (NOR), fallo en el plato del rodete (PLA), fallo en el *leading edge* (LED), fallo en el *trailing edge* (TED), fallo en

la goma del sellado (SEA), arena añadida al agua (SAN), arena y papel añadidos conjuntamente al agua (SAP) y bolas de PVC añadidas al agua (PVC).

- 17 unidades de clasificación. En este caso se tienen en cuenta las severidades en los casos de rotura del plato, del fallo *leading edge* y del fallo *trailing edge*. Las 17 unidades de clasificación son: estado normal (NOR), fallo en el plato del rodete con una porción de plato eliminada (PLA1), con dos porciones de plato eliminadas (PLA2) y con tres porciones de plato eliminadas (PLA3), fallo en el *leading edge* (LED1) de 5 mm de tamaño, de 10 mm de tamaño (LED2) y de 15 mm de tamaño (LED3), fallo en el *trailing edge* de 5 mm de tamaño (TED1), de 10 mm de tamaño (TED2) y de 15 mm de tamaño (TED3), fallo en la goma del sellado (SEA), arena añadida al agua (SAN), arena y papel añadidos conjuntamente al agua (SAP) y bolas de PVC añadidas al agua (PVC).

Al igual que en el caso del diagnóstico de fallos en cojinete se usan dos clasificadores: un clasificador de red neuronal y otro de máquinas de soporte vectorial de mínimos cuadrados (*LS-SVM*). El clasificador de red neuronal tiene estructura *feedforward* y un algoritmo de *resilient backpropagation*. El clasificador *LS-SVM* usa funciones Gaussianas de base radial. Al igual que en el caso de diagnóstico de fallos en cojinetes, la metodología para evaluar los diferentes casos (8 unidades de clasificación y 17 unidades de clasificación) consiste en dividir la base de datos en un conjunto de entrenamiento formado por el 70% de las observaciones de cada una de las clases de la base de datos y en un conjunto de test formado por el 30%. El conjunto de entrenamiento a su vez se usa para ajustar los parámetros de los clasificadores. El procedimiento se repite 20 veces y se promedian los resultados.

Finalmente se obtiene una tasa de éxito tanto en la clasificación de 8 unidades de clasificación como en la clasificación de 17 unidades de clasificación. También se realiza un análisis de los resultados obtenidos con las características seleccionadas.

En el capítulo 5 de la memoria de Tesis se expone la metodología seguida para el diagnóstico de fallos en bomba de agua, se explica cada una de las medidas extraídas, y se exponen y analizan los resultados obtenidos por sensor individual.

Metodología usada para la fusión de señales de audio y vibración en el diagnóstico de fallos en bomba de agua

Una vez obtenidos los resultados individuales en la clasificación entre los diferentes estados de la bomba centrífuga se procede a realizar un estudio de la combinación de las señales de audio y vibración para determinar si su unión aumenta la tasa de acierto obtenida por sensor.

La información obtenida de las señales de vibración y de audio se fusiona a diferentes niveles [45]: a nivel de características (*feature level*), a nivel de puntuación (*score level*) y a nivel abstracto o de decisión (*abstract level*).

La fusión a nivel de características consiste en la concatenación de las características extraídas por sensor. Es necesario recalcar que la fusión de la información se realiza sólo con las características seleccionadas por sensor que se obtuvieron en la etapa anterior (ver capítulo 5 de la Tesis). Las características concatenadas se evalúan usando dos clasificadores: uno basado en redes neuronales y

otro una máquina de soporte vectorial de mínimos cuadrados (*LS-SVM*). Puesto que hay dos sensores de vibración y dos sensores de audio, se realizan todas las combinaciones posibles combinando 2 sensores, 3 sensores y 4 sensores.

La fusión a nivel de puntuación o de *score* se realiza con las puntuaciones obtenidas a la salida de los clasificadores antes de tomar la decisión de asignar la salida a una clase en concreto. Las puntuaciones de los clasificadores se fusionan usando las siguientes reglas que son ampliamente usadas a la hora de realizar fusión a nivel de *score* y que además son una simplificación de la ley de Bayes [45]: regla del promedio (también llamada regla de la suma), regla del producto, regla del mínimo y regla del máximo [45]. La fusión a nivel de puntuación se realiza usando los dos clasificadores anteriormente mencionados y se realiza combinaciones de 2, 3 y 4 sensores.

Finalmente la fusión a nivel de decisión se realiza aplicando la regla del más votado (*majority vote rule*). Ilustremos esta regla con un ejemplo: tenemos las características de una muestra de la base de datos de 3 sensores (uno de vibración y dos de audio, por ejemplo). Las características del sensor 1 se evalúan en el clasificador de red neuronal 1 y da como resultado que la muestra pertenece a fallo LED. Las características del sensor 2 se evalúan en el clasificador de red neuronal 2 y da como resultado que la muestra pertenece al fallo LED. Igualmente las características del sensor 3 se evalúan en el clasificador de red neuronal 3 y da como resultado que la muestra es normal. Tenemos dos votos para el fallo LED y un voto para normalidad, así que gana el fallo LED puesto que es el más votado. En el caso de que todos los sensores den resultados diferentes entre sí, se escoge aquel que tenga el *score* más cercano a la clase.

En cada una de las técnicas de fusión, la evaluación con los clasificadores se repite 20 veces usando cada vez diferente conjuntos de entrenamiento y test aleatoriamente escogidos. Finalmente se obtiene el promedio de las 20 repeticiones. Se obtienen resultados por cada uno de los casos de estudio: 8 unidades de clasificación (normalidad y 7 tipos de fallo considerados) y 17 unidades de clasificación (normalidad y 10 tipos de fallo considerados puesto que se incluye la severidad de todos los fallos).

Una vez aplicadas las técnicas de fusión comentadas, se realiza un análisis de los resultados obtenidos.

En el capítulo 6 de la Tesis se describe la metodología usada para la fusión de las señales de audio y vibración y se muestran los resultados obtenidos así como el análisis de los resultados realizado.

5 Aportaciones originales

El objetivo de la presente Tesis es la mejora de los sistemas de monitorización del estado de la maquinaria en diagnóstico de fallo e identificación de fallo usando señales de vibración y de audio en dos aplicaciones (cojinetes y bombas de agua) con especial énfasis en la etapa de extracción de características y en el utilización de la señal de audio como fuente de información. En la consecusión del objetivo se han realizado diversas aportaciones originales. En este apartado se exponen las aportaciones originales de la presente Tesis.

Aportación original 1: Estado del arte

Uno de los objetivos de la Tesis es realizar una revisión de las técnicas de procesado de la señal y de las técnicas de reconocimiento de patrones en el contexto de monitorización de maquinaria. Basándonos en esta revisión se decidió trabajar en cojinetes y en bombas de agua y centrarse en algunos de los huecos encontrados en el estado del arte. Fruto de esta revisión se ha generado un artículo sobre el estado del arte, que es una contribución original de esta Tesis. Parte de la redacción del capítulo 2 de la Tesis está basado en el artículo generado [46].

Aportación original 2: Generación de base de datos de audio y vibración de bomba centrífuga

Puesto que la Tesis se centra en dos áreas de aplicación, cojinetes y bombas de agua, se necesitan obtener señales provenientes de estos dos elementos. Para el caso de los cojinetes se han usado bases de datos de vibración disponibles en internet. Estas bases de datos forman un corpus que puede ser utilizado en la división de investigación en

futuros estudios. Por otra parte, puesto que no hay disponibles de forma pública bases de datos de audio provenientes de maquinaria en esta Tesis se ha realizado la adquisición simultánea de señales de audio y vibración de una bomba centrífuga de agua de circulación. Este es otro aporte original de la presente Tesis. En el capítulo 3 se detalla el proceso de adquisición de la base de datos.

Aportación original 3: método para el diagnóstico de fallos en cojinetes

Centrándonos en la aplicación de las señales de vibración de cojinetes hemos contribuido en esta Tesis con dos métodos para el diagnóstico e identificación de fallos en cojinetes. Ambos métodos están basados en técnicas no lineales. El primero de ellos se basa en el operador no lineal Teager-Kaiser junto con la extracción de características estadísticas. Se realiza un estudio del método propuesto y se compara con otras técnicas en el dominio temporal. En este dominio, este método presenta mejores resultados que los del estado del arte. La metodología utilizada y los experimentos realizados con el método propuesto se describen en la primera parte del Capítulo 4 de la presente Tesis. Esta aportación de la Tesis ha sido publicada en un artículo de revista [47] y en varias conferencias [48], [49].

Aportación original 4: método para la identificación de fallos en cojinetes

El segundo método propuesto consiste en la aplicación de la transformada *wavelet packet* y la complejidad Lempel-Ziv para establecer el grado de severidad de cojinetes con fallo en la cara externa (*outer-race fault*) y con fallo en la cara interna (*inner-race fault*). En el caso de fallo en la cara externa el índice encontrado permite seguir de forma monótona la degradación de normal a fallo. Se ha realizado una comparación del

método propuesto con diversos métodos de la literatura. También se ha estudiado la robustez del método propuesto frente a ruido gaussiano. La metodología utilizada y los experimentos realizados con el método propuesto se describen en la segunda parte del Capítulo 4 de la presente Tesis. Esta contribución ha sido parcialmente publicada en una conferencia [50].

Aportación original 5: aplicación de características usadas en vibración en señales de audio para el diagnóstico de fallos en bomba centrífuga

Centrándonos en la segunda aplicación en bomba centrífuga de agua, el objetivo principal ha sido determinar si con el audio como fuente de información se es capaz de distinguir entre los diferentes fallos de la bomba centrífuga. Puesto que la señal de audio se usa poco en el diagnóstico de fallos en bombas centrífugas, la mayoría de características se extraen de la señal de vibración. Una aportación de la presente Tesis es la aplicación de características usadas para señales de vibración en la señal de audio. En el capítulo 5 de la presente Tesis se explican las características extraídas. Parte de esta aportación está publicada en una conferencia [52].

Aportación original 6: propuesta de 31 medidas nuevas para el diagnóstico de fallos en bomba centrífuga (señales de audio y vibración)

También en la aplicación de la bomba centrífuga se ha contribuido con nuevas características extraídas tanto de la señal de vibración como de la señal de audio. Estas características son las siguientes: energías de la transformada *wavelet packet* (7 características), energías cepstrales (12 características), relación de armónico ruido cepstral (1 característica), energía de ruido cepstral (1 característica), relación armónico

ruido frecuencial (2 características), energía de ruido frecuencial (1 característica), medidas no lineales (7 características). Parte de estas contribuciones han sido publicadas en conferencias [51], [52]. En el capítulo 5 se detallan las medidas aportadas.

Aportación original 7: evaluación de las medidas en señales de audio para el diagnóstico de fallos en bomba centrífuga

La capacidad para discriminar entre diferentes estados de la maquinaria (sin fallo y con diferentes tipos de fallos) de las características extraídas se ha evaluado usando dos clasificadores, uno basado en redes neuronales y otro basado en máquinas de soporte vectorial de mínimos cuadrados (LS-SVM). Los resultados de la evaluación de las características usando la señal de audio son muy satisfactorios, llegándose a tasas de acierto del 96.53% en la discriminación entre 8 estados (estado normal de funcionamiento y 7 estados de fallo) usando sólo 7 características seleccionadas y de 88.29% en la discriminación entre 17 estados (estado normal y 10 estados de fallo en los que se separan fallos por severidades) usando 16 características seleccionadas.

También en el capítulo 5 se describe la evaluación de las medidas y los resultados obtenidos en dicha evaluación tanto para las señales de audio como para las señales de vibración por sensor individual.

Aportación original 8: estudio de la fusión de señales de audio y vibración en el diagnóstico de fallos en bomba centrífuga

Finalmente se ha realizado un estudio de la fusión de las señales de audio y vibración para determinar si su unión mejora el diagnóstico de fallos en la aplicación e bomba

centrífuga. Los resultados obtenidos son satisfactorios llegándose a aumentar la tasa de acierto en el diagnóstico del fallo hasta un 100%. En el capítulo 6 se explican las técnicas de fusión usadas y se muestran los resultados obtenidos.

Por último, y como ya se comentó en la introducción, durante el transcurso de la presente Tesis la doctoranda siguió con la investigación en señales de voz. En esta área se realizan las siguientes aportaciones:

Aportación original 9 (voz): propuesta de características basadas en dinámica no lineal para la detección de patologías laríngeas del sistema fonador

Se proponen una serie de características basadas en dinámica no lineal (teoría del caos) para la detección de patologías del sistema fonador usando la señal de voz. Fruto de este estudio se genera un artículo en revista de índica de impacto [53].

Aportación original 10 (voz): propuesta de características basadas en dinámica no lineal y de medidas de complejidad para la detección de emociones a través de la señal de voz

Se proponen una serie de características basadas en dinámica no lineal, así como medidas de complejidad para la discriminación de diferentes estados de emoción usando la señal de voz. Se genera de este trabajo dos artículos en revistas con índice de impacto [54], [55].

En el anexo de la Tesis se hace un resumen de ambos trabajos en voz, explicando la metodología usada, las características extraídas y los resultados obtenidos. Se debe mencionar que parte de las medidas propuestas en voz también han sido propuestas en esta Tesis para el diagnóstico de fallos en bombas centrífugas.

6 Conclusiones

El objetivo de la presente Tesis es mejorar la tasa de acierto en los sistemas de monitorización del estado de la máquina en diagnóstico e identificación (severidad del fallo) de fallos usando señales de audio y vibración y centrándonos en dos aplicaciones (cojinetes y bombas centrífugas) con especial énfasis en la etapa de extracción de características y en el uso de señales de audio como fuente de información. Basándonos en la investigación realizada en las dos áreas de aplicación de la Tesis, cojinetes y bombas centrífugas, y en los resultados obtenidos podemos concluir que tanto el uso de audio como fuente de información como el uso de técnicas no lineales a la hora de extraer características mejora la tasa de éxito en las dos aplicaciones en las que se ha centrado la Tesis: cojinetes y bombas centrífugas.

En la aplicación de cojinetes se han usado señales de vibración como fuente de información puesto que se han usado bases de datos públicas disponibles en Internet con muestras de cojinetes funcionando en estado normal y con fallos puntuales en las diferentes partes de los cojinetes. Se han propuesto dos métodos basados en técnicas no lineales para el diagnóstico de fallos en la cara externa, en la cara interna y en los elementos rodante de cojinetes y para la identificación de fallos en la cara externa y en la interna. Con el segundo método propuesto se ha generado un índice que sigue de forma monótona la degradación de un cojinete con fallo normal a fallo en la cara externa. Los métodos propuestos se han comparado con métodos de la literatura y los resultados obtenidos han sido satisfactorios, mejorando los resultados. Además, en el segundo método propuesto se ha realizado un estudio de la robustez del algoritmo frente a ruido Gaussiana. El estudio demuestra que el algoritmo propuesto presenta más

robustez al ruido blanco Gaussiano que los métodos de la literatura con los que se ha comparado. Por lo tanto se puede concluir que el uso de técnicas no lineales para el diagnóstico e identificación de fallos en cojinetes es una línea de investigación prometedora.

La aplicación de la bomba centrífuga se ha usado para explorar el uso de la señal de audio en el diagnóstico de fallos de bombas centrífugas. La monitorización de maquinaria en general, y en particular la referida a bombas de agua y a cojinetes, utiliza en la mayoría de los casos la señal de vibración como fuente de información. El uso de audio (rango de frecuencias [0-20kHz]) ha sido menos explorado, por esto en la presente Tesis nos hemos centrado en su estudio. Para ello se necesita obtener una base de datos de audio obtenida de una bomba centrífuga. Puesto que no hay ninguna disponible, se ha generado una base de datos propia en la que se adquieren señales de audio y vibración de forma simultánea de una bomba centrífuga funcionando con normalidad y a la que se generan diferentes tipos de fallos. Un conjunto de características del estado del arte de diagnóstico de fallos en bombas centrífuga se extraen de las señales de vibración obtenidas y se aplican también a las señales de audio. También se proponen un conjunto de 31 nuevas medidas extraídas en el dominio de la frecuencia, en el dominio de los cepstrum y en el dominio no lineal. Se realiza una selección de características y luego se evalúan por sensor con dos clasificadores. Los resultados muestran tasas de acierto altas y bastante similares en sensores de audio y de vibración. Se obtienen tasas de éxito del 99.82% y del 99.59% para los sensores de audio y del 99.91% y 99.59% para los sensores de vibración en el caso de discriminar entre 8 estados de la bomba centrífuga. En el caso de discriminar entre 17 estados se obtienen tasas de éxito del 87.48% y 94.23% para los sensores de audio y del 86.71% y

87.30% para los sensores de vibración. De los resultados obtenidos, se puede concluir que el audio puede ser usado como fuente de información en el diagnóstico de fallos de la bomba centrífuga utilizada. De todas formas, es necesario realizar más investigación al respecto con diferentes bombas centrífugas.

En la Tesis también se ha realizado un estudio de la combinación de las señales de audio y vibración obtenidas en la bomba centrífuga para determinar si la fusión de la información de ambas señales mejora la tasa de acierto. Las tasas de éxito se incrementaron significativamente a la hora de fusionar un sensor de audio y otro de vibración en el caso de discriminar entre 17 estados de la bomba centrífuga. En este caso se logró una tasa de acierto del 99.55%, bastante superior a los 94.93% obtenidos por uno de los sensores de audio. En el caso de discriminar entre 8 condiciones de la bomba centrífuga, se llegaron a obtener tasas del 100% a la hora de fusionar un sensor de audio y otro de vibración. De los resultados del estudio de la fusión se puede concluir que si bien los resultados individuales por sensor son buenos, la fusión aumenta la tasa de acierto. Este aumento es especialmente evidente en el caso del diagnóstico de 17 condiciones de la bomba centrífuga.

7 Referencias

[1] Vilela, R.M., Metrôlho, J. C., & Cardoso, J. C. (2004, May). Machine and insdustrial monitorization system by analysis of acoustic signatures. In *Electrotechnical Conference, 2004. MELECON 2004. Proceedings of the 12th IEEE Mediterranean* (Vol. 1, pp. 277-279). IEEE.

[2] Jardine, A. K., Lin, D., & Banjevic, D. (2006). A review on machinery diagnostics and prognostics implementing condition-based maintenance. *Mechanical systems and signal processing*, *20*(7), 1483-1510.

[3] Vachtsevanos, G., Lewis, F. L., Roemer, M., Hess, A. & Wu, B. Intelligent Fault Diagnosis and Prognosis for Engineering Systems, 1st ed. Hoboken, New Jersey: John Wiley & Sons, Inc., 2006.

[4] Paltridge, B. (2002). Thesis and dissertation writing: an examination of published advice and actual practice. *English for Scientific Purposes*, *21*(2), 125–143.

[5] Baydar, N., & Ball, A. (2003). Detection of gear failures via vibration and acoustic signals using wavelet transform. *Mechanical Systems and Signal Processing*, *17*(4), 787-804.

[6] Bell, R.N., McWilliams, D.W., O'Donnell, P., Singh, C., & Wells, S. J. (1985). Report of large motor reliability survey of industrial and commercial installations Part I and II. *IEEE Transactions on Industry Applications*, *21*(4), 853-872.

[7] Immovilli, F., Bellini, A., Rubini, R., & Tassoni, C. (2010). Diagnosis of bearing faults in induction machines by vibration or current signals: A critical comparison. *IEEE Transactions on Industry Applications*, *46*(4), 1350-1359.

[8] Samanta, B., Al-Balushi, K. R., & Al-Araimi, S. A. (2006). Artificial neural networks and genetic algorithm for bearing fault detection. *Soft Computing*, *10*(3), 264-271.

[9] McFadden, P. D., & Smith, J. D. (1984). Vibration monitoring of rolling element bearings by the high-frequency resonance technique—a review. *Tribology international*, *17*(1), 3-10.

[10] Choi, Y. C., & Kim, Y. H. (2007). Fault detection in a ball bearing system using minimum variance cepstrum. *Measurement Science and Technology*, *18*(5), 1433.

[11] Zhang, Y., & Randall, R. B. (2009). Rolling element bearing fault diagnosis based on the combination of genetic algorithms and fast kurtogram.*Mechanical Systems and Signal Processing*, *23*(5), 1509-1517.

[12] Antoni, J., Randall, R. B. (2006). The spectral kurtosis: application to the vibratory surveillance and diagnostics of rotating machines. *Mechanical Syst. and Signal Process.*, *20*, 308-331.

[13] Wang, D., Peter, W. T., & Tsui, K. L. (2013). An enhanced Kurtogram method for fault diagnosis of rolling element bearings. *Mechanical Systems and Signal Processing*, 35(1), 176-199.

[14] Peng, Z. K., Peter, W. T., & Chu, F. L. (2005). A comparison study of improved Hilbert–Huang transform and wavelet transform: application to fault diagnosis for rolling bearing. *Mechanical systems and signal processing*, *19*(5), 974-988.

[15] Ali, J. B., Fnaiech, N., Saidi, L., Chebel-Morello, B., & Fnaiech, F. (2015). Application of empirical mode decomposition and artificial neural network for automatic bearing fault diagnosis based on vibration signals. *Applied Acoustics*, 89, 16-27.

[16] Yang, D. M., Stronach, A. F., MacConnell, P., & Penman, J. (2002). Third-order spectral techniques for the diagnosis of motor bearing condition using artificial neural networks. *Mechanical systems and signal processing*, *16*(2), 391-411.

[17] Wang, W. J., Wu, Z. T., & Chen, J. (2001). Fault identification in rotating machinery using the correlation dimension and bispectra. *Nonlinear Dynamics*, *25*(4), 383-393.

[18] Shibata, K., Takahashi, A., & Shirai, T. (2000). Fault diagnosis of rotating machinery through visualisation of sound signals. *Mechanical Systems and Signal Processing*, *14*(2), 229-241.

[19] Cudina, M. (2003). Detection of cavitation phenomenon in a centrifugal pump using audible sound. *Mechanical Systems and Signal Processing 17*(6), 1335–1347.

[20] Singh, V., Meena, N. (2009, January). Engine Fault Diagnosis using DTW, MFCC and FFT. In *Proc. of the 1st Int. Conf. on Intelligent Human Computer Interaction*, (pp. 83-94).

[21] Mansoor, A. B., Ahmed, H., Mahmood, Z. (2009, February). Design and Development of an Automated Acoustic based Jet Engine Performance Evaluator. In *Proc. of the IEEE Int. Conf. on Industrial Technol.* (pp. 1-4).

[22] Wu, J. -D., Chuang, C. -Q. (2005). Fault diagnosis of internal combustion engines using visual dot patterns of acoustic and vibration signals. *NDT&E Int.*, *38*, 605-614.

[23] Al Thobiani, A., Gu, F., & Ball, A. (2010 June 22-24). The monitoring of cavitation in centrifugal pumps based on the analysis of vibro-acoustic measurements. In *CM 2010 and MFPT 2010*, UK.

[24] Al-Hashmi, S.A. (2012, September 23-26). Spectrum Analysis of Acoustic Signals for Cavitation Detection. In *2012 IEEE Symposium on Industrial Electronics and Applications (ISIEA2012)*, Bandung, Indonesia.

[25] Saeid Farokhzad, H.A., (2013). Acoustic Based Cavitation Detection of Centrifugal Pump by Neural Network. *Journal of Mechanical Engineering and Technology*, *1*(1), 1-5.

[26] Al-Hashmi, S.A. (2013, October). Statistical analysis of acoustic signal for cavitation detection. *International Journal of Emerging Technology and Advanced Engineering*, *3*(4).

[27] Benko, U., Petrovcic, J., Juricic, D., Tavcar, J., Rejec, J. (2005). An approach to fault diagnosis of vacuum cleaner motors based on sound analysis. *Mechanical Syst. and Signal Process.*, *19*, 427-445.

[28] Janjarasjitt, S., Ocak, H., Loparo, K. A. (2008). Bearing condition diagnosis and prognosis using applied nonlinear dynamical analysis of machine vibration signal. *J. of Sound and Vibration*, *317*, 112-126.

[29] Devi, S., Siva, L., Shanker N. R., & Prabakaran, K. (2010). A Comparative Study between Vibration and Acoustic Signals in HTC Cooling Pump and Chilling Pump. *Int. J. of Eng. and Technol.*, *2*.

[30] Case Western Bearing Data Center, http://csegroups.case.edu/bearingdatacenter/home. Última visita: Noviembre 2014.

[31] http://qsun.eng.ua.edu/cpw_web_new/intro.htm. Última visita: Enero 2014

[32] Lee, J., Qiu, H., Yu, G., Lin, J., & Rexnord Technical Services (2007). Bearing Data Set. IMS, University of Cincinnati. NASA Ames Prognostics Data Repository, [http://ti.arc.nasa.gov/project/prognostic-data-repository], NASA Ames, Moffett Field, CA."

[33] Webpage Explore the World of Piping http://www.wermac.org/equipment/pumps_general.html. Last visited: 19 November 2014

[34] "Pump Principles Manual: global training education and development program" eds. Chesterton.

[35] Zhao, X., Zuo, M. J., & Patel, T. H. (2012). Generating an indicator for pump impeller damage using half and full spectra, fuzzy preference-based rough sets and PCA. *Measurement Science and Technology*, *23*(4), 045607.

[36] Zhao, X. M., Hu, Q. H., Lei, Y. G., & Zuo, M. J. (2010). Vibration-based fault diagnosis of slurry pump impellers using neighbourhood rough set models.*Proceedings of the Institution of Mechanical Engineers, Part C: Journal of Mechanical Engineering Science*, *224*(4), 995-1006.

[37] Samanta, B., Al-Balushi, K. R., & Al-Araimi, S. A. (2006). Artificial neural networks and genetic algorithm for bearing fault detection. *Soft Computing*, *10*(3), 264-271.

[38] Randall, R. B. (2004). State of the art in monitoring rotating machinery-part 1. *Sound and vibration*, *38*(3), 14-21.

[39] McFadden, P. D., & Smith, J. D. (1984). Vibration monitoring of rolling element bearings by the high-frequency resonance technique—a review. *Tribology international*, *17*(1), 3-10.

[40] Kaiser, JF., On a simple algorithm to calculate the energy of a signal. In: *International conference on acoustics, speech, and signal processing*; 1990. p. 381–384.

[41] Li, H., Fu, L., & Zhang, Y. (2009, April). Bearing faults diagnosis based on teager energy operator demodulation technique. In *IEEE International Conference on Measuring Technology and Mechatronics Automation (ICMTMA'09)*. (Vol. 1, pp. 594-597).

[42] Al-Ghamd, A. M., & Mba, D. (2006). A comparative experimental study on the use of acoustic emission and vibration analysis for bearing defect identification and estimation of defect size. *Mechanical systems and signal processing*, *20*(7), 1537-1571.

[43] Yan, R., & Gao, R. X. (2004). Complexity as a measure for machine health evaluation. *Instrumentation and Measurement, IEEE Transactions on*, *53*(4), 1327-1334.

[44] Pudil, P., Novovičová, J., & Kittler, J. (1994). Floating search methods in feature selection. *Pattern Recognition Letters*, *15*(11), 1119-1125.

[45] Kuncheva, L. I. (2004). Combining pattern classifiers: methods and algorithms. John Wiley & Sons.

[46] Henríquez, P., Alonso, J. B., Ferrer, M. A., & Travieso, C. M. (2014). Review of automatic fault diagnosis systems using audio and vibration signals. *IEEE Transactions on Systems, Man, and Cybernetics: Systems*, *44*(5), 642-652.

[47] Henríquez, P., Alonso, J. B., Ferrer, M. A., & Travieso, C. M. (2013). Application of the Teager–Kaiser energy operator in bearing fault diagnosis. *ISA transactions*, *52*(2), 278-284.

[48] Henríquez, P., Alonso, J. B., Ferrer, M. A., Travieso, C. M. (2011, May-June). Application of Higher Order Statistics of Teager-Kaiser Energy Transformed Vibration Signal for Bearing Fault Diagnosis. In *Proc. of the 24th Int. Congress on Condition Monitoring and Diagnostics Engineering Management* (pp. 265-274), Stavanger, Norway.

[49] Henríquez, P., White, P., Alonso, J. B., Ferrer. M. A. (2011, October). Application of Teager-Kaiser Energy Operator to the Analysis of Degradation of a Helicopter Input Pinion Bearing. In *Proc. of the International Conference Surveillance 6* (pp. 265-274), University of Technology of Compiègne, France.

[50] Henríquez, P., Alonso, J. B., Ferrer, M. A., Travieso, C. M. (2014, September). Degradation assessment in bearings with outer race fault. In *27th International Congress of Condition Monitoring and Diagnostic Engineering Management*, Brisbane, Australia.

[51] Henríquez, P.; Alonso, J. B.; Ferrer, M. A.; Travieso, C. M.; Gómez, G. (2012). Fault diagnosis using audio and vibration signals in a circulating pump. *Journal of Physics: Conference Series 25th Int. Congress on Condition Monitoring and Diagnostic Engineering*, *364*, 012135.

[52] Henríquez, P.; Alonso, J. B.; Ferrer, M. A.; Travieso, C. M. (2014). Application of complexity measures to pump fault diagnosis. In *27th Int. Congress on Condition Monitoring and Diagnostic Engineering*, Brisbane, Australia.

[53] Henríquez, P., Alonso, J. B., Ferrer, M., Travieso, C. M., Godino-Llorente, J., & Díaz-de-María, F. (2009). Characterization of healthy and pathological voice through measures based on nonlinear dynamics. *IEEE Transactions on Audio, Speech, and Language Processing*, *17*(6), 1186-1195.

[54] Henríquez, P., Alonso, J. B., Ferrer, M. A., Travieso, C. M., & Orozco-Arroyave, J. R. (2013). Global Selection of Features for Nonlinear Dynamics Characterization of Emotional Speech. *Cognitive Computation*, *5*(4), 517-525.

[55] Henríquez, P., Alonso, J. B., Ferrer, M. A., Travieso, C. M., Orozo-Arroyave, J. R. (2014). Nonlinear Dynamics Characterization of Emotional Speech. *Neurocomputing*, *132*, 126-135.